

https://dspace.org/

Improving batch reactors using attainable regions: Towards automated construction of the attainable region and its application to batch reactors

Ming, David

2015-05-12
http://hdl.handle.net/10539/17709

Downloaded from a DSpace repository. https://dspace.org/

IMPROVING BATCH REACTORS USING ATTAINABLE REGIONS: TOWARDS AUTOMATED CONSTRUCTION OF THE ATTAINABLE REGION AND ITS APPLICATION TO BATCH REACTORS

David Ming

A thesis submitted to the Faculty of Engineering and the Built Environment, University of the Witwatersrand, Johannesburg, in fulfillment of the requirements for the degree of Doctor of Philosophy in Engineering.

Johannesburg, 2014

Declaration

I declare that this thesis is my own unaided work. It is being submitted for the degree Doctor of Philosophy in Engineering to the University of the Witwatersrand, Johannesburg. It has not been submitted before for any degree or examination to any other university.

_____

David Ming

_____ day of _____ year _____

Abstract

The Attainable Region is the set of all achievable states, for all possible reactor configurations, obtained by reaction and mixing alone. It is a geometric method that is effective in addressing problems found in reactor network synthesis. For this reason, Attainable Region theory assists towards a better understanding of systems of complex reaction networks and the issues encountered by these systems.

This thesis aims to address two areas in Attainable Region theory:

1. To help improve the design and operation of batch reactors using Attainable Regions.

2. To further advance knowledge and understanding of efficient Attainable Region construction methods.

Using fundamental concepts of mixing and attainability established by Attainable Region theory, a graphical method of identifying opportunities for improving the production rate from batch reactors is first presented. It is found that by modifying the initial concentration of the batch, overall production performance may be improved. This may be achieved in practice by retaining a fraction of the final product volume and mixing with fresh feed material for subsequent cycles. This result is counter-intuitive to the normal method of batch operation. Bypassing of feed may also be used to improve production rate for exit concentrations not associated with the optimal concentration. The graphical approach also allows optimisation of batches where only experimental data are given.

An improved method of candidate Attainable Region construction, based on an existing bounding hyperplanes approach is then presented. The method uses a plane rotation about existing extreme points to eliminate unachievable regions from an initial bounding set. The algorithm is shown to be faster and has been extended to include construction of candidate Attainable Regions involving non-isothermal kinetics in concentration and concentration-time space.

With the ideas obtained above, the application of Attainable Regions to batch reactor configurations is finally presented. It is shown that with the appropriate transformation, results developed from a continuous Attainable Region may be used to form a related batch structure. Thus, improvement of batch reactor structures is also possible using Attainable Regions. Validation of candidate Attainable Regions is carried out with the construction algorithm developed in this work.

To my parents
Chuck and Loraine

To Michelle

Acknowledgements

I would like to thank my supervisors, Professor David Glasser and Professor Diane Hildebrandt, for their knowledge, encouragement and guidance over the years. I know that many students tend to thank their supervisors at the end of a good research meeting. I am still not sure how many of those supervisors acknowledge the statement and follow up with a thank you of their own. I have enjoyed working with both of you very much.

I would also like to thank Professor Benjamin Glasser for acting as my surrogate supervisor and mentor during the final stages of this work. You were never too shy to 'crack the whip' to ensure that I kept going, but you always did it in a polite way. I am grateful for your guidance and knowledge as well. Thank you.

I would like to thank the University of the Witwatersrand, the National Research Foundation and the Centre of Materials and Process Synthesis (currently known as MaPS) for their support.

Contents

Declaration i
Abstract ii
Acknowledgements iv
List of figures x
List of tables xi
Nomenclature xiii

1 Introduction and literature review **1**
1.1 Introduction 1
1.2 Literature review 3
1.2.1 The Attainable Region (AR) 3
1.2.2 Batch optimisation 11
1.3 Motivation 18
1.3.1 AR construction algorithms 18
1.3.2 Batch reactors 19
1.4 Conclusion and scope of this work 20
1.5 Copyright permissions 21

2 Preliminaries **28**
2.1 The Attainable Region 28
2.2 Concentration, mixing and reaction 28
2.2.1 Concentration 28
2.2.2 Mixing 29
2.2.3 Concavities and mixing 30
2.2.4 Convex Hulls 31
2.2.5 Rate vectors and rate fields 32
2.3 Fundamental reactor types 32
2.3.1 The Plug Flow Reactor (PFR) 32
2.3.2 The Continuously-Stirred Tank Reactor (CSTR) 34
2.3.3 The Differential Side-stream Reactor (DSR) 35
2.4 Higher dimensional considerations 37
2.4.1 Dimension of the AR 37
2.4.2 Stoichiometric subspace 37

2.4.3 PFRs on the AR boundary . . . 38
2.4.4 Connectors and critical reactors . . . 39
2.4.5 Simplifications for $\mathbb{R}^3$ . . . 43
2.5 AR construction guidelines . . . 44
2.5.1 General procedure for constructing the AR . . . 44
2.5.2 Remarks . . . 47
2.6 On non-isothermal and heterogeneous systems . . . 47
2.6.1 Variable density systems . . . 47
2.6.2 Temperature and other parameters . . . 50
2.7 Conclusion . . . 51

3 Graphically improving batch production rate 53
3.1 Introduction . . . 53
3.2 Standard batch operation . . . 54
3.2.1 Problem formulation . . . 54
3.2.2 Initial observations and modifications . . . 56
3.3 Improving production rate . . . 58
3.3.1 Improvement 1: Partial emptying and filling . . . 58
3.3.2 Improvement 2: Improving production rates for other exit concentrations . . . 62
3.3.3 Experimental data . . . 64
3.3.4 Method . . . 65
3.4 Examples . . . 66
3.4.1 Hydrolysis of propylene oxide . . . 66
3.4.2 Penicillin production . . . 68
3.4.3 Lysine fermentation . . . 71
3.5 Further remarks . . . 73
3.5.1 Transfer time . . . 73
3.5.2 Fed-batch operation . . . 75
3.5.3 Improving production rate for $c_i > c_i^{\text{opt}}$ . . . 76
3.6 Conclusion . . . 77

4 AR construction using rotated bounding hyperplanes 81
4.1 Introduction . . . 81
4.2 Mathematical preliminaries . . . 82
4.2.1 Hyperplanes . . . 82
4.2.2 Orthogonal and tangent vectors . . . 83
4.2.3 Extreme points . . . 83
4.2.4 Facets and edges . . . 84
4.2.5 Vertex and facet enumeration . . . 84
4.2.6 Stoichiometric constraints . . . 84

4.3 AR construction via hyperplanes . . . 85
4.3.1 The method of bounding hyperplanes . . . 85
4.3.2 A revised method of AR construction . . . 88
4.4 Examples . . . 91
4.4.1 Isothermal constructions . . . 91
4.4.2 Temperature dependent kinetics . . . 96
4.4.3 Unbounded construction . . . 99
4.5 Example of numerical sufficiency . . . 100
4.6 Remarks . . . 104
4.6.1 Introduction . . . 104
4.6.2 Rotations in $\mathbb{R}^n$ . . . 104
4.6.3 Additional mathematical details . . . 105
4.6.4 n-dimensional rotations . . . 107
4.6.5 Proposed method . . . 108
4.6.6 Difficulties and unknowns . . . 111
4.7 Conclusion . . . 113

5 Applying AR theory to batch reactors 117
5.1 Introduction . . . 117
5.2 AR overview . . . 118
5.2.1 AR construction from three fundamental reactor types . . . 118
5.2.2 Necessary conditions of the AR . . . 120
5.2.3 Dimensional considerations . . . 121
5.3 Batch and continuous similarities . . . 122
5.3.1 The standard batch . . . 123
5.3.2 Fed-batch reaction . . . 123
5.4 Examples . . . 129
5.4.1 2D autocatalytic reaction . . . 129
5.4.2 3D van de Vusse kinetics . . . 142
5.4.3 Residence time example . . . 155
5.5 Conclusions . . . 160

6 Conclusions and future research 169
6.1 Conclusions . . . 169
6.2 Future research . . . 175

A Batch production rate 180
A.1 The effect of transfer time on batch production rate . . . 180

B Bounding hyperplanes 182
B.1 A worked example . . . 182
B.2 Stoichiometric subspace calculation . . . 187

B.2.1 Example: Methane steam reforming 190

List of Figures

1.2.1 Geometric representation CSTRs in the complement space 7
1.2.2 IDEAS framework 9

2.2.1 Geometric representation of concentration and mixing 30
2.2.2 Concavities and mixing 31
2.2.3 Rate field for a system of kinetics in $\mathbb{R}^2$ 33
2.3.1 Rate vectors on a PFR trajectory 34
2.3.2 Rate vectors on a CSTR locus 35
2.3.3 Schematic of DSR. 36
2.3.4 The space spanned by a rate vector and mixing vector 36
2.4.1 Connectors 42
2.4.2 Critical CSTRs 43
2.6.1 Overall viewpoint for variable density systems 48
2.6.2 Hypothetical reactor for mixing mass fractions 49

3.2.1 Standard batch production rate and graphical interpretation 55
3.2.2 Comparing production rate lines for different initial concentrations 58
3.3.1 Production rate by partial emptying and filling 60
3.3.2 Production rates for partial emptying and filling and the standard batch 62
3.3.3 Identifying opportunities for improving production rate 63
3.3.4 Improved structure for $c_i < c_i^{\text{opt}}$ 64
3.4.1 Hydrolysis of propylene oxide. 69
3.4.2 Concentration profile for penicillin production 70
3.4.3 Production of penicillin in a bio-reactor 72
3.4.4 Lysine fermentation. 74
3.5.1 Influence of transfer time on batch production rate 75
3.5.2 Possible improved structure for $c_i > c_i^{\text{opt}}$ when $\Delta t_2 = \Delta t_1/2$ 77

4.2.1 Geometric representation of vertex and facet enumeration 85
4.3.1 Eliminating unachievable space via hyperplanes 86
4.3.2 Unattainable region elimination via bounding hyperplanes 88
4.3.3 Unattainable region elimination via rotating hyperplanes 89

4.4.1 Construction comparison for van de Vusse kinetics 92
4.4.2 Construction comparison for non-linear van de Vusse kinetics . . . 94
4.4.3 Construction comparison for multiple steady states 97
4.4.4 Temperature dependent kinetics 99
4.4.5 Unbounded AR construction 100
4.5.1 Comparison of methods for hybrid AR construction. 102
4.6.1 Rotations in higher dimensions 109
4.6.2 Example of eliminations in $\mathbb{R}^3$ 112

5.3.1 Graphical interpretation for various fed-batch reactor trajectories . 124
5.3.2 Comparison between continuous and batch reactive equipment . . 129
5.4.1 Multiplicity features of the autocatalytic reaction of Brooks (1988) 131
5.4.2 CSTR loci for different feed points 132
5.4.3 AR and optimal reactor structures for the autocatalytic reaction of Brooks (1988) 133
5.4.4 Comparison of continuous and batch structures for the autocatalytic reaction in $\mathbb{R}^2$ 136
5.4.5 α policy and concentration profile for the autocatalytic system . . 139
5.4.6 DSR map for the autocatalytic system 140
5.4.7 Convex hull for CSTR-PFR reactor structure. 143
5.4.8 $\Lambda(\mathbf{C})$ as a function of CSTR residence time 145
5.4.9 Optimal reactor structures for the 3D van de Vusse system 147
5.4.10 Continuous and batch structure comparison for the van de Vusse system 150
5.4.11 Paths followed corresponding to two separate objective functions . 151
5.4.12 AR and batch structures for two different outcomes 152
5.4.13 ARs generated for the van de Vusse system compared to the open literature 154
5.4.14 Production rate profile for the autocatalytic system 156
5.4.15 AR for the autocatalytic reaction given in chapter 3 158
5.4.16 Optimal continuous and batch structures for an unbounded batch system 161

6.2.1 Hybrid AR construction 177

B.1.1 2D van de Vusse constructions 184
B.2.1 Stoichiometric subspace for the steam reforming system projected in different component spaces 193

List of Tables

3.1 Summary of batch production rate after four cycles 57
3.2 Rate constants for penicillin production. 80

4.1 Arrhenius constants for temperature dependent van de Vusse kinetics 96
4.2 Comparison of AR volumes generated by the RCC and rotated hyperplanes method for hybrid AR construction 103

5.1 Summary of fed-batch operating parameters. 128
5.2 Performance comparison for autocatalytic reaction 138
5.3 Performance summary for 3D van de Vusse kinetics 153

Nomenclature

Roman Symbols

ΔH^0_{rxn} Enthalpy of reaction

Δt^* Partial emptying and filling reaction time

Δt_0 Standard batch reaction time

$\overline{P}$ Production rate including transfer time

c^{opt} Batch exit concentration associated with ϕ^{opt}

c^{out} Batch exit concentration

Cp_i Constant pressure heat capacity of component i

E Reaction activation energy

P^* Production rate (partial emptying and filling)

P Production rate (standard batch)

R Universal gas constant

t_T Transfer time

T Reactor temperature

V_{tot} Total volume of batch reactor

c_i Concentration of component i in a mixture

F Fed-batch feeding rate

$H(\mathbf{n}, \mathbf{C_0})$ Hyperplane passing through point $\mathbf{C_0}$ on the plane

Q Volumetric flowrate

r Batch emptying and filling rate (transfer rate)

r_i Rate of reaction for component i

S Stoichiometric subspace

x Reactor conversion

Greek Symbols

α DSR feeding policy parameter OR fed-batch feeding policy parameter (F/V)

λ Mixing fraction

$\Lambda(\mathbf{C})$ Critical CSTR determinant function

ν_{ij} Stoichiometric coefficient of component i participating in reaction j

ϕ Retained volume fraction

τ Reactor residence time

ε Extent of reaction

$\varphi(\mathbf{C})$ VdelR function $\varphi(\mathbf{C}) = [\mathbf{J}(\mathbf{C})(\mathbf{C}_0 - \mathbf{C})]^{\mathrm{T}}[(\mathbf{C}_0 - \mathbf{C}) \times \mathbf{r}(\mathbf{C})]$

ξ Transfer time deviation

Vectors and Matrices

$\mathbf{A}$ Stoichiometric coefficient matrix

$\mathbf{C_f}$ Feed vector concentration

$\mathbf{C}^*$ Mixture concentration vector

$\mathbf{C}_0$ DSR side-stream concentration

$\mathbf{C}_i$ Concentration vector of stream i

$\mathbf{e}$ Orthogonal complement to the plane of rotation

$\mathbf{I}$ Identity matrix

$\mathbf{J}$ Jacobian matrix of $\mathbf{r}(\mathbf{C})$

$\mathbf{N}$ Null space of stoiciometric coefficient matrix $\mathbf{N} = \mathrm{null}\left(\mathbf{A}^{\mathrm{T}}\right)$

$\mathbf{n}$ Hyperplane normal vector

$\mathbf{P}$ Projection matrix

$\mathbf{r}(\mathbf{C})$ Rate vector evaluated at $\mathbf{C}$

$\mathbf{R}$ Rotation matrix

$\mathbf{v}$ Mixing vector

$\mathbf{z}_i$ Mass fraction vector of stream i

Chapter 1

Introduction and literature review

1.1 Introduction: optimisation in reactor design

Chemical reaction is at the heart of chemical engineering. Whereas the majority of total plant expenditure and complexity is attributed to separations operations and pre-processing, they typically exist as a consequence of reaction. Chemical reactors play a central role in the transformation of less valuable materials into products of a higher social and economic value. As a component of this transformation, reactions may also be critical in converting harmful and dangerous by-products into benign, and even potentially beneficial, side commodities. Environmental considerations further influence and, as of late, dominate decisions in process design. The manner in which materials are processed consequently influences the quality and type of waste produced, and hence it also shapes their associated environmental impact. The gasification of municipal waste into Fischer-Tropsch products and electricity (Hildebrandt et al., 2009; Metzger et al., 2012), or the production of $CaSO_4.2H_2O$ (Gypsum), a highly valuable product used in the building and construction industry, from acid mine drainage (Matlock et al., 2002) are two model examples of this. Although economic considerations justify the proper design and execution of chemical reactors, they are no longer of sole concern to the modern process engineer. Moreover, chemical reaction differentiates the chemical engineering profession from other similarly related science and engineering fields. It is not only that chemical engineers design reactors correctly for the benefit of the population, it is their responsibility to do so when they are the ones trained to carry out the task. It is for this reason that great care is taken to ensure that chemical reactors, and more generally chemical reactor *networks*, are operated as close to optimal as possible.

A large portion of chemical engineering is attributed to process optimisation, attempting to achieve the best yields in the most efficient manner possible. Optimisation is broad however, ranging in application from the traditional fields of physics

and finance (Hartmann and Rieger, 2001; Cornuejols and Tutuncu, 2007), to those found in economics and sociology (Grass et al., 2008). Many topics in optimisation can be found in the scientific literature. Within this field, a subset of work targeted specifically to the optimisation of chemical reactors can be found. Thus, although the topic of mathematical optimisation is reasonably broad, specific application to chemical reactor design and and chemical plant operation is somewhat more narrow.

Optimisation in reactors can also be difficult. Practitioners historically tend to concentrate on classic optimisation methods – a process model and objective function are formed, and then adjustments are carried out until no further improvement can be realised. This approach is generalised for many problems (and often in many fields of expertise), but may not always be well suited for the problems specifically related to reaction. The influence of multiple steady states associated with reaction kinetics and mixing introduce discontinuities in the operating model, complicating the optimisation and making interpretation difficult. If the optimisation model does not thoroughly reflect its actual physical performance, then the recommendations produced by the optimisation may be equally inaccurate. The quality of the optimisation result is hence a strong function of the quality of the model itself. Furthermore, this is also under the condition that there is good convergence to the optimisation problem. If multiple optima exist, then solutions may also be subject to uncertainty. An alternate, simpler, solution may exist for the same outcome. Thus, two common questions in optimisation arise:

1. Is the solution globally optimal?

2. Are there other solutions that achieve the same objective performance in a simpler manner?

Unless the problem is well understood, these answers are generally not easily resolved. The former could be addressed if knowledge of the *limits* of the current design are established, whereas the latter requires, to some extent, a better understanding of *optimal reactor structures*. Thus, the need to develop a method for determining 'the best' or establishing the outer most limitations of the problem (and how to get there) should first be established.

Given a set of reaction kinetics and feed conditions, there are potentially many ways in which to design a reactor that satisfies all requirements of the designer. At the very early stages of design, when there is typically more freedom at play, this period might serve to provide the largest gains in performance. However, a typical approach is to rather first choose a reactor based on operating and design constraints, and then optimise. The final design is then a direct consequence of the reactor that was chosen. Even if multiple reactors in series and parallel configurations are considered, one can always ask whether some other configuration of reactors or some other new reactor might have done better. Thus, traditional simulation and optimisation may not always be sufficient in chemical reactor design.

A different approach to optimisation, proposed by Horn (1964), was to determine all outcomes or solutions of the problem simultaneously, as a unified set. This set would contain every possible physically realisable outcome, both known and unknown. Horn termed this the *Attainable Region*. The Attainable Region thus represents the entirety of all possible combinations and their associated outcomes for a specified set of initial conditions. By acknowledging the full set of outputs for a prescribed set of initial constraints in the present, one is better placed to make more effective design decisions in the future. Although simple in concept, Horn's idea was an abstract one that required greater refinement and interpretation than what was initially proposed. This is particularly true for how all outcomes might be generated in practice, particularly for those that were yet to be imagined.

1.2 Literature review

1.2.1 The Attainable Region (AR)

Initial developments

Pioneering work by Glasser et al. (1987); Feinberg and Hildebrandt (1997); Glasser and Hildebrandt (1997) set out to provide an unambiguous definition of the AR. Viewed as a constrained geometric region in space that is chosen to appropriately characterise the nature of the system, the AR is the n-dimensional volume in which all achievable processes and their associated consequences must lie. In this work, we specifically associate the AR to be the region that all reactors and reactor networks must occupy. The boundary of the AR then acts as a border between all that is achievable to all that is not. It will be shown later that determination of the AR ultimately depends on the correct determination of its boundary.

Initial work in the area allowed for the understanding that, when reaction and mixing are the two allowable processes, it is possible to construct the AR using only combinations of three archetypal reactors – the Continuously-Stirred Tank Reactor (CSTR), the Plug Flow Reactor (PFR) and the Differential Side-stream Reactor (DSR). Glasser et al. (1987) provided several early 2D AR constructions, demonstrating the power of the AR approach to reactor synthesis. These constructions involved highly non-linear kinetics, were optimisation of a reactor network is typically difficult to perform by standard methods. For two dimensional problems, the AR can be constructed by use of only PFRs and CSTRs. In three dimensions and higher, DSRs have been shown to play an important role in the construction of the AR boundary.

Additionally, the AR constructions considered here are generally associated with the assumption that the system undergoes no change in density, and exists in a single phase. In the case of gaseous systems, the ideal gas assumption holds. Isothermal systems are also generally preferred, although many results may be generalised to

allow for the relaxing of this constraint (Feinberg and Hildebrandt, 1997; Feinberg, 1999, 2000b,a). With these assumptions in mind, under consideration of the three archetypal reactors, several important necessary conditions can be deduced. These are summarised as follows: for the Attainable Region, $\mathcal{A}$, generated by the two processes of reaction and mixing, the following properties must hold:

- $\mathcal{A}$ is a convex polytope.
- No rate vector on the boundary of $\mathcal{A}$ must point outwards.
- No rate vector in the complement of $\mathcal{A}$ when extrapolated backwards may intersect $\mathcal{A}$.
- No two points on a PFR in the complement of $\mathcal{A}$ when extrapolated may intersect $\mathcal{A}$.

Work by Feinberg and Hildebrandt (1997) laid down a mathematical framework for the study of the AR in a more formal context. The authors detailed the significance of extreme points, i.e. specific AR boundary points, and introduced key concepts and definitions. The most notable of these is the introduction of the complement principle. This allowed the authors to deduce elementary geometric properties of the AR. In turn, this provides proof that PFRs act as highways to the extreme points of the AR, and also shows how CSTRs and DSRs act as connectors to these PFR highways. Existence and uniqueness arguments of the AR were also provided. Thus, this work essentially demonstrates the necessary role that classical reactor types play in construction of the AR. There is no need to devise new reactor types in other words.

Subsequent papers by Feinberg (1999, 2000b,a), provided further mathematical and geometric properties that the AR boundary must include. The papers also detailed the type of special CSTR and DSR combinations required to achieve it, termed critical reactors. These typically included elaborate control policies underlying an exceptionally intricate and non-linear mathematical structure for which reaction and mixing processes must follow. Even under seemingly ideal settings of isothermal kinetics with only two or three species, the required control policies generally produce an irrational expression containing hundreds of terms (Feinberg, 2000b,a).

Feinberg's work introduced very specific rules by which the boundary of all ARs must follow. These constraints made it possible, at least conceptually, to predict the type of reactors that must be employed before AR construction is undertaken. This provided clues as to the behaviour of a given system of kinetics. When viewed in this manner, the work of Feinberg was the first of its kind to develop methods of reactor network behaviour and characterisation, with the ultimate goal of discovering a valid sufficiency condition. At the time of writing, the current set of AR literature still

does not contain any new substantial developments to these ideas. We still do not have a valid sufficiency condition for the AR.

Application of AR to industrial problems

AR theory has successfully been used as a tool for the determination of optimal reactor structures for a variety of industrial processes. Hildebrandt (1989) and Seodigeng (2006) both provided case studies of the industrial manufacture of ammonia using the AR. Recommended cold-shot cooling schemes utilised in industry have been shown to agree with the optimal designs found from AR analysis. Optimal reactor networks for the industrial manufacture of methanol have been investigated by Seodigeng (2006) whilst Kauchali et al. (2004) used the AR to generate candidate reactor network schemes for the water-gas-shift (WGS) reaction. Khumalo et al. (2006) investigated the applicability of attainable regions for use in comminution and the design of comminution circuits in which the particle size distribution of the milling circuit, comprised of n size classes, can be used to construct an n-dimensional attainable region. ARs associated with separations processes (Nisoli et al., 1997; Agarwal et al., 2008) have also been determined in the past. Milne (2008) provided extensive work on the application of Attainable Region theory in membrane reactors for the oxidative dehydrogenation of n-butanes.

Recently, Scott et al. (2013) applied AR analysis for the production of bioethanol from lignocellulose. Reaction kinetics for first enzymatic saccharification of cellulose and fermentation of glucose to ethanol steps are provided. These are used to construct a number of three-dimensional candidate ARs involving species yield, species conversion and reactor residence time. The authors find that optimal reactor structures involving critical DSRs, CSTRs and manifolds of PFRs are all present on the boundary. This is similar to the optimal reactor structures obtained for three-dimnensional van de Vusse kinetics. Although the findings are interesting, the specific choice of component axes used to generate the AR are questionable, for it is unclear whether the linear mixing relations, fundamental to AR construction, are enforced or not. Be that as it may, the work is nevertheless useful as it is another example demonstrating of the use of AR theory to realistic systems of industrial and economic significance.

AR construction methods

Early developments Subsequent work in the field of AR research has focused on the development of algorithms for the automatic construction of candidate ARs. Initially, these methods have focused on 'brute-force' computation – enumerating all conceivable combinations of the three reactor configurations and then checking for any expansion in the AR. One of the first algorithms of this type is that proposed by McGregor et al. (1999). It is considered essentially a direct application of the AR

necessary conditions. The method is initiated by first solving for the PFR trajectory and the CSTR locus from the feed. The convex hull of these points is then calculated. This forms the first candidate AR. From this, points on the convex hull are checked to determine whether any rate vectors point out of the region. PFR trajectories established from these points are able to extend the region. Points belonging to the PFR trajectory are checked to see if any CSTR can extend the region also. If new PFR and CSTR points are found, then they are included in the attainable set and a newer, larger, convex hull can be generated. With each new expansion, the AR necessary conditions are checked. If all points satisfy the conditions, a new candidate AR is proposed. The process is repeated until no further extension of the convex hull can be achieved. The final result is a convex attainable set satisfying all sufficiency conditions. In addition to this, the reactor structures required to build the boundary are also known.

The process of AR construction and subsequent visualisation and interpretation is a relatively straightforward exercise in 2D. For higher dimensional problems however, the construction of candidate regions is cumbersome. In $\mathbb{R}^3$, visualisation is possible but interpretation is difficult. In higher dimensions, visualisation is only possible if lower dimensional projections are taken. This is time consuming and awkward. The large number of available directions with which the region could expand also becomes increasingly problematic and computationally intensive. Direction enumeration of all states is simply not practical for higher dimensional problems.

Iso-state method The Iso-state method introduced by Rooney et al. (2000) aimed at addressing this problem by decomposing the problem into several easier 2D construction and convexification steps. By projecting the higher dimensional candidate region onto many 2D spaces, the problem of identifying possible points for further expansion is made easier. Once additional points for extension are identified, the region is expanded in the full space and the process is repeated. The method composes of four steps. The first step, much like the method of McGregor et al. (1999), begins by populating the initial set of attainable points with those generated by the PFR trajectory and CSTR locus from the feed point. Next, the n-dimensional space is 'sliced' into smaller 2D planes holding all but two compositions constant. Initial points for these subspaces are found by the intersection of points in the initial attainable set with each subspace, once all intersection points with the subspace are found, the convex hull is computed resulting in a candidate region for the subspace. The third stage of the algorithm extends each subspace by use of iso-compositional PFRs and CSTRs. These are PFRs and CSTRs that only operate within the subspace of choice. This is achieved by mixing of material from other attainable subspaces that are both obtained from the DSR. The final step utilises the newly extended points to recombine with the previous points into

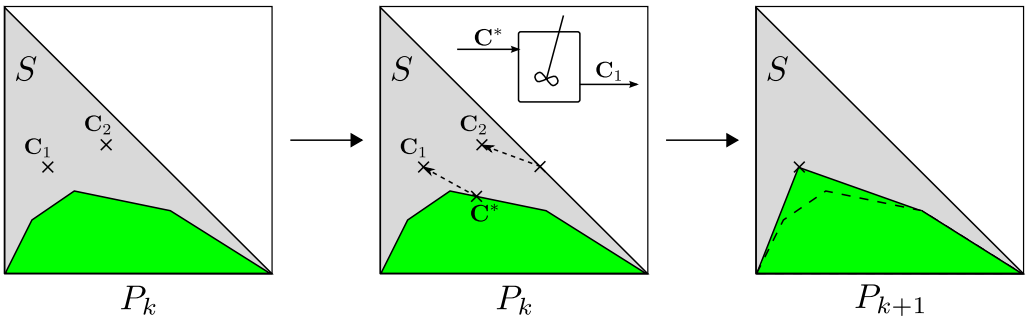


Figure 1.2.1: Geometric representation CSTRs in the complement space

the full n-dimensional space. The full set is then projected onto the 2D subspaces and new intersections with the updated set of points are found. These steps are repeated until no further extension of the region is possible.

Linear programming formulations The linear programming method proposed by Kauchali et al. (2002) is another early example of automated AR construction. The method is conceptually simple, composing of a global search in the complement of the AR for possible additional attainable points. In this way, the method can be seen as an enumeration of all possible reactor configurations for a given reaction system. The consequences of this work resulted in the derivation of stronger necessary conditions that the AR must obey. This is developed from the idea that, although single reactors may not be able to extend the AR on their own, their combinations possibly could. As with many methods, the algorithm begins by a gathering of all concentrations produced by PFRs and CSTRs. The full space in which the vector field resides is then discretised into a large number of points. Each point is then tested as a possible connector for further AR extension. This is achieved by evaluating the rate vector at each discretised point to see whether a backwards linear extrapolation intersects the current attainable set. This is represented graphically in Figure 1.2.1.

Although simple, the method is computationally intensive. Not only must single points within the space need to be considered, but also their combinations. Solution of the classic van de Vusse kinetics in 2D space for example, results in a linear programming program consisting of approximately 6×10^3 constraints in 1.1×10^6 variables using 1000 sample points. The method by which the AR is constructed using this method has initiated a new sub-category of AR construction schemes. These algorithms are more sophisticated and do not require direct enumeration of all points in space. The IDEAS algorithm by Burri et al. (2002) and Shrink-wrap method of Manousiouthakis et al. (2004) are two such examples utilising this approach.

IDEAS and Shrink-wrap methods The Infinite DimEnsionAl State-space approach (IDEAS) considers the problem of AR construction by solution of an infinite dimensional linear optimisation problem. Reactor networks are represented as the combination of two blocks, shown in Figure 1.2.2. The first, termed the reactor operator (ROP), aims to describe all actions undertaken by all reactors on process streams. The second block, referred to as the distribution network (DN), is representative of all actions undertaken by mixing, splitting, recycling and bypassing of process streams. The ROP and DN are linked together by a number of streams connecting the inlets and outlets of each block to each other as well as to themselves. This network is used as the generalised representation of an arbitrary reactor system. Both the ROP and DN blocks produce linear constraints,. These form the basis of a large linear optimisation procedure.

Construction of the AR occurs by solution of an infinite dimensional linear programming problem. Since, the solution of this kind of problem cannot be solved analytically, the authors propose an approximate solution by replacing the infinite dimensional problem with the solution of a series of finite dimensional linear problems of increasing size. It is shown that the solution of the finite problem is guaranteed to converge to the infinite dimensional case and hence this provides a means of AR construction. The results of the finite dimensional case approximate the AR arbitrarily closely. The authors were able to construct 2D ARs for the well understood van de Vusse kinetics using a number of finite approximations. Although many simple lower dimensional constructions were achievable, the IDEAS algorithm suffered from many of the challenges associated with point-sampling (linear programming) methods. A large number of number of constraints require consideration. This number increases rapidly for higher dimensional problems. Even under these circumstances however, the IDEAS formulation is a generalised and flexible framework that can be used to formulate and solve many other reactor synthesis problems that are not related to the AR.

Based on the IDEAS framework, Manousiouthakis et al. (2004) proposed a number of feasibility properties that reactor networks must obey. The properties were employed as a basis for the development of a new AR construction algorithm known as the Shrink-Wrap method. Using these ideas, the authors proposed both a necessary and sufficient condition for feasible concentrations founded on their formulations of new terms. These terms are referred to as inactive, active and isolated sub-networks. The Shrink-Wrap method begins by constructing a convex superset that is known to contain the AR. The superset is then discretised into a number of finite points. From these points, extreme points of the superset are determined by way of a convex hull algorithm. The extreme points are used as generating points from which CSTR and PFR backward trajectories can be drawn. The superset is reduced if a backward trajectory is found that does not intersect the current polytope. In this way, the method acts to trim away unachievable regions from the set. The

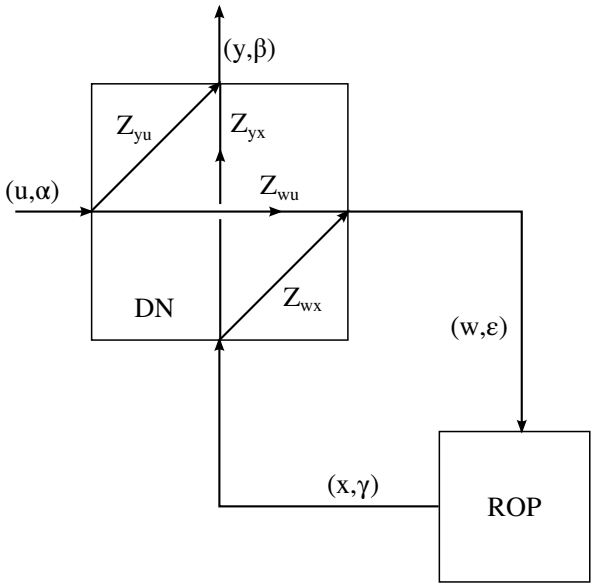


Figure 1.2.2: IDEAS framework

elimination process is repeated until CSTR and PFR backward trajectories can no longer be drawn that do not intersect the region. The candidate region is thus described by the extreme points of the reduced set. The authors also reasoned that the need for PFRs in construction of the AR are not necessary, as approximations can be achieved arbitrarily closely by a series of many small CSTRs. Again, the results of by this method appear quite favourable, with good agreement when compared to the constructions by classical methods.

Although the Shrink-Wrap method shares many of the properties found in the IDEAS approach, clear benefits with the new method are observed. Many of the intrinsic limitations associated with these methods are still apparent however, and computational effort increases rapidly with higher dimensional constructions.

Bounding hyperplanes method The method of bounding hyperplanes developed by Abraham and Feinberg (2004) approaches the construction of candidate ARs in a different manner. By first considering the stoichiometric superset that encloses the AR, the method approached construction by eliminating unattainable portions from the space. The remaining region after elimination must then be the AR. The method by which unattainable regions are eliminated is founded on the principles of a tangency condition with which all rate vectors on the boundary of the AR must support.

The use of hyperplanes is used to successively trim away regions and enclose the AR. As a result, the method of bounding hyperplanes begins first by construction of the stoichiometric superset known to contain the AR. This superset, termed the stoichiometric subspace, provides the initial bounding set of hyperplanes from which

additional bounding hyperplanes can be introduced. Corners of the polytope are calculated and used as starting points for the trimming process. At each corner of the current polytope, a new hyperplane is introduced. Its orientation is calculated from the orientation of the other hyperplanes which contribute to the corner and can be thought of as an average orientation of the hyperplanes passing through the corner point. The hyperplane is then moved into the current polytope until either a tangency point is found, or the feed vector is excluded. The hyperplane is then added to the set of bounding planes, and the corners the new polytope are determined. This process is repeated until no additional hyperplane can be added to trim away a region. The resulting region is then generally a fairly accurate approximation to the AR.

The bounding hyperplanes method is fairly robust but is computationally expensive to perform. The method has shown to be particularly effective in handling kinetics that involve multiple steady states. Construction occurs as an elimination of infeasible regions, rather than an addition of potentially feasible points. The method does not appear to scale very well with increasing dimension. A comparison of construction times for the van de Vusse problem in 2D and 3D shows that the 3D problem may take up to ten times longer to complete (Abraham, 2005). As a result, construction accuracy may suffer if higher dimensional problems are to be accomplished in reasonable time. These issues are in part due to the extra computational workload associated with the calculation of the corners in the current polytope (vertex enumeration).

Recursive constant control policy method The recursive constant control (RCC) policy algorithm developed by Seodigeng et al. (2009) is one of the most recent contributions to the field of AR construction algorithms. By exploiting the dual nature of the DSR equation and with knowledge that DSRs provide final access to the boundary of the AR (Feinberg, 2000b), candidate ARs may be constructed fairly easily in an iterative manner by use of a single reactor equation. The algorithm is particularly fast. Unlike the other methods discussed, the RCC algorithm does not appear to suffer from higher dimensional constructions in the way that discretisation-type algorithms do. This may be due to fact that the algorithm does not attempt to perform a search over the entire region. However, since the method only performs a local search, method generally does not produce the correct result for kinetics with multiple steady states. The method of construction is simple. Construction begins with the integration of the DSR equation from the feed for multiple values of the control policy parameter α. Here the value of α is fixed for a given integration and takes on values between 0 and ∞. For the range of α values chosen, a family of DSR trajectories are produced. Feed and equilibrium points are chosen as mixing points in the DSR equation. The convex hull of the points from this family is determined and this constitutes the first candidate AR approximation. The second stage of the

algorithm utilises the extreme points of the convex hull as generating points for new DSR trajectories. For each extreme point, the above procedure is repeated, with a range of constant α values chosen and their respective trajectories calculated. The points belonging to these new trajectories are then combined with the existing set of extreme points and the convex hull of the new set of points is found. The third stage further populates the region with additional DSR trajectories belonging to α values chosen to increase the number of α values in the specified range of α values. This procedure is repeated until no further growth is achieved. The convex hull resulting from this serves to represent the AR candidate.

1.2.2 Batch optimisation

Batch reactors and batch operation are common in many industries where high value, low volume products are produced. Batch reaction is also often considered to be more versatile than continuous operation, and lends itself well to small-scale work, such as that developed in experimental and piloting operations. The use of batch and semi-batch reactors thus forms an important part in the processing of many specialist chemicals, pharmaceuticals, and food-related products. For this reason, significant effort has been undertaken over the years towards the appropriate synthesis (Allgor et al., 1996; Zhang and Smith, 2004), optimisation (Levien, 1992; Vassiliadis et al., 1994) and understanding (Brooks, 1988; Bonvin, 1998; Luus and Okongwu, 1999; Puigjaner, 1999; Yi and Reklaitis, 2006) of batch processes.

It follows that a large amount of research on batch optimisation and reaction already exists, and the scope of work in this area is vast. In general, two broad areas of batch optimisation exist:

1. Batch unit optimisation, in which batch unit operations are investigated and improved. Batch reactor optimisation is accordingly a subset of this.

2. Batch *process* optimisation, in which interactions between different processing stages are analysed and improved. The entire batch plant is optimised as a whole.

The first category is concerned with the optimisation of individual batch units. This often leads to the development of kinetic and transfer models with respect to time that are then optimised, often in isolation, to the remainder of the batch plant. The optimisation of batch reactors necessarily falls within this category, although interest in this specific field is understandably still vast, due to the importance of batch reaction as a whole. Issues such as component production and yield maximisation are often areas of interest within this scope.

In contrast, batch process optimisation deals with optimisation of the entire batch plant. This includes not only the selection and integration of all batch units within the plant (mixing, reaction and separation unit operations), but also factors

related to the transfer and timing of material throughout the plant within the production campaign must be considered. Since batch equipment is far more versatile than continuous equipment, the appropriate and optimal use of batch equipment is often far more challenging, resulting a much more complex problem than the optimisation of a single batch unit operation. This requires the spatial arrangement of batch equipment on the plant floor, as well as the organisation and scheduling of batch equipment in time. Issues such as changeovers resulting from multiple products, trade-offs from multiple objectives, product order changes and demand patterns, minimising makespan (the total time for all jobs to complete), optimal allocation of resources, changeovers, inventory sizes, sanitisation, shelf-life etc. are readily encountered in a multi-product batch plants. Honkomp et al. (2000) discuss how even when mathematically sound scheduling models have been developed, the scheduler may still invest a large amount of time adjusting the model to account for unexpected details that spoil the production plan. Batch process synthesis (the *design* of batch process), may also fall within the scope of this field. Indeed, the span of batch process research is vast, covering many fields of expertise under a single branch.

Furthermore, the advancement of computer technology has allowed for a greater surge of interest in batch optimisation, where easily accessible computational power can be paired with numerical non-linear optimisation techniques. To this end, such techniques often employ traditional optimisation and optimal control methods, and are common in reactor design and modelling. Similar to that discussed in section 1.1, these works tend to focus on the optimisation of a problem given a specific model, but do not always exploit structure in a system, an approach that the AR excels in. A cursory overview of the efforts made to batch improvement is given below.

Batch process scheduling and optimisation

For the optimisation of batch processes, scheduling is fundamental to the adequate operation of the plant by optimal allocation of a fixed number of resources, over a set time from a potentially a number of desired products from a batch recipe. Different products may then be produced on common pieces of equipment, with sharing of intermediate products. Batch plants are generally classifiable into two fundamental types, based on the nature of production within the facility: multiproduct (or flow-show) problems are those belonging a production facility where all products undergo the same set of tasks in the same order (such as a conventional production line). All products must undertake the same path through the production line. The multipurpose (job-shop) representation is a generalisation of flow-shop scheduling. Here, different jobs require a different order of tasks, and so each job may undergo a different sequence within the plant. Orders may even visit the same task multiple

times(Li and Ierapetritou, 2008). The path of each product is then different to other paths for other products.

The representation of time is important in batch scheduling, as often objective functions for the plant optimisations are formulated around issues often related to makespan, tardiness, earliness, etc. The modelling of batch schedules is handled by two common approaches in time. Discrete time modelling of batches is the class of problems that attempt to divide the scheduling horizon into a discrete number of time intervals of fixed size. Tasks are then initiated and completed only at discrete points defined by the boundaries of the discretised time intervals. This simplifies the complexity of the resulting model, as only a discrete number of points and variables are considered, although this also limits the possible solution set and may also result in degenerate or infeasible solutions depending on the grid size. The accuracy and quality of solution is then strongly correlated to the number of time intervals chosen for the scheduling horizon. A further drawback of discrete time modelling is that the resulting model is typically large, encompassing a large number of variables associated with each discrete time interval. This limits the application of discrete time formulations to realistic problems. Continuous time representations aim to mitigate these issues by allowing timing decisions in the corresponding model to occur over a continuous time range. Decisions are then modelled as continuous variables indicating the exact time when tasks are completed or initiated. Typically, this results in more complex model formulations resulting from more sophisticated resource constraints(Mendez et al., 2006).

Similarly, the representation of material flows in the batch plant is handled by two common models. Network flow equations often either follow State Task Network (STN) or Resource Task Network (RTN) approaches. In STN based models, the batch plant is assumed to consume or produce materials (states) at processing nodes. The plant is then represented as a directed graph containing two distinct node types: state nodes (feed, intermediate and final products), task nodes (process operations that transform feed material into one or more output state), and arcs connecting state nodes to task nodes. This representation fits closely to that of a conventional process flow diagram. In RTN based models, the batch plant is represented as a set of nodes in which both material and processing resources such as storage are carried by the node. That is, nodes not only represent material and equipment, but also utility resources such as heating and storage. Processing and storage tasks are assumed to consume and release resources at their starting and ending times(Mendez et al., 2006). Pinto et al. (2008) provides a detailed analysis between the relative strengths of STN and RTN based models.

Furthermore, batch schedules can be distinguished based on their usage cases. Two modes are identified. Online applications refer to those that are used frequently to guide process operations over a constantly changing horizon time. In this way, online schedules are similar to plant controller problems (Honkomp et al., 2000). By

comparison, offline applications are used to make process decisions in a simulation environment in which several scenarios can be investigated and used to guide the actions of the management team.

Capon-Garcia et al. (2011) provide a complex mathematical batch scheduling model involving both economic and environmental constraints including, but not limited to, equipment changeover environmental interventions, raw material and product manufacturing environmental interventions. This leads to a multi-objective MINLP problem that provides a range of feasible solutions depending on the decision maker's criteria. Environmental assessments are mathematically formulated by use of Life Cycle Inventories (LCI), which are directly associated with the product and changeover recipes of the plant. A case study involving the manufacture of acrylic fibres in a multi-product batch plant is provided.

The area of dynamic scheduling (schedules that may be adjusted in real-time) has attracted the attention of of many batch researchers due to its practical focus on production. Scheduling of this type is often also referred to as *reactive scheduling*. Novas and Henning (2010) discuss a scheduling methodology for repair-based events. Cott and Macchietto (1989) introduce the idea of a real-time controller that measures deviations from the schedule and then forecasts the potential delays in production. Starting times for subsequent batches are then modified to minimise disruptions. Kanakamedala et al. (1994) provide a similar treatment to multipurpose batch plants based on a look-ahead heuristic that chooses alternatives which minimise impact to the rest of the schedule. Since it is a heuristic method, computation complexity may be reduced, however a completely theoretical approach may provide better solutions. A review of common reactive scheduling techniques is also discussed in (Ouelhadj and Petrovic, 2009).

Indeed, scheduling operations are broad enough to include many aspects of scheduling. These ideas may be transferred to related fields in operations research. For instance, Shah (2004) provides a general treatment for scheduling to the pharmaceuticals industry specific for supply chain modelling. The author provides an overview of challenges faced as well as describes how scheduling theory can be formulated and applied. Many of the ideas discussed in the work relate to the continuous time modelling scheduling problems utilised in batch plant scheduling models.

Similarly, Grossmann (2005) details the use of scheduling techniques to an emerging field of operations research termed *enterprise-wide optimisation* (EWO), in which optimisation of not only the plant, but more generally the entire supply chain, such as the operations of supply and distribution are included in the formulation. The author describes key challenges, such as the adequate formulation of non-linear mathematical models that describe the entire supply chain including uncertainties, the solution of these models, and the eventual implementation of the proposed solutions over a large time horizon (potentially involving many years). EWO is a new field where existing scheduling techniques and expertise may be ex-

panded into related and enterprise-centric interest areas. Wassick (2009) provides a related discussion to EWO, whereas Biegler and Zavala (2009); Grossmann (2012) propose a number of possible solution methods theories suitable for EWO problems. Varma et al. (2007) provide an interesting and extensive discussion on EWO aspects, incorporating strategic and tactical R&D management decisions into the model formulation. The authors highlight mathematical strategic and tactical enterprise models, and discuss a generalised enterprise wide network model consisting of planning and process functions. The integration of financial and operational decision models is also considered.

Li and Ierapetritou (2008) review a number of strategies for the mathematical formulation of uncertainties in the batch schedule. Whereas a number of traditional scheduling approaches adopt the view of deterministic models for their optimisation, the authors indicate how uncertainties in scheduling present different problems with their own solution strategies. Within this work, the authors describe how problems such as demand changes (rush orders), unexpected breakdowns, processing and recipe variability, and price changes might be handled. The work details how this may achieved via three distinct representations of uncertainty: placing bounds on the uncertain variables, probability distributions and fuzzy representations. Each of these is associated with a specific solution technique, although all methods often assume the form of a complex MILP or MINLP problem after reformulation.

Although scheduling problems are often solved in well developed commercial optimisation software (GAMS, AMPL, etc.), Wang et al. (1996); Chunfeng and Xin (2002); Ponsich et al. (2008a,b); Liu et al. (2010) describe various alternate methods for determining optimal batch schedules via a number of evolutionary algorithms including genetic algorithms and particle swarm optimisation.

The complexity of batch scheduling has attracted the attention of many academics over the years. Several batch process literature reviews have been produced as a result. Mendez et al. (2006) is considered the most recent contribution on the subject, discussing the issue of short-term scheduling problems in batch plants. The work provides a thorough treatment of dominant mathematical equations used to describe sequential batch and batch network plants. The authors categorise the breadth of batch scheduling problems, and discusses their solution by two worked case studies. Notably, the authors describe how scheduling problems may be formulated in different ways (through time and event representation, material balances and objective function formulations) which may make solution easier or more difficult depending on the representation adopted. Two real-world examples are given demonstrating the challenges faced by batch processes. The authors also provide a list of commercial and academic software used for short-term batch scheduling. Floudas and Lin (2004) provide an extensive comparison between continuous-time and discrete-time formulations in batch scheduling. The authors highlight the strengths and weaknesses of each approach, and also provide common mathematical formula-

tions for describing generalised batch schedules with each approach. Performance comparisons between the two are also briefly highlighted, and topics related to reactive scheduling and uncertainty are also briefly discussed. Kallrath (2002); Reklaitis (1996); Shah (1998) all provide many other excellent reviews related to aspects of batch scheduling and modellilng.

Batch reactor optimisation

Graphical methods Batch optimisation using graphical methods, particularly with regard to the problem of efficient waste-water allocation are already known. Notable contributions include (Wang and Smith, 1995b,a; Dhole et al., 1996; Hallale, 2002; El-Halwagi et al., 2003; Manan et al., 2004; Majozi et al., 2006; Chen and Lee, 2008) in which many include formulations are based upon mass transfer operations. Hallale (2002) utilises a graphical approach similar to pinch analysis in heat exchanger network synthesis for the minimisation of water in what is referred to the author as a surplus water diagram. A graphical optimisation based on dynamic programming has also been investigated by Staniskis and Levisauskas (1983), whereas several analyses using graphical methods to fermentation processes are discussed by Shioya and Dunn (1979).

O'Reilly (2002) considers a batch reactor operating under the hypothetical reaction scheme $\mathrm{I} + \mathrm{R} \rightarrow \mathrm{A} + 2\mathrm{D}$ and $\mathrm{A} + \mathrm{R} \rightarrow \mathrm{IMPS}$ in which A and D are saleable products and IMPS is a waste product. The formulation includes a detailed unsteady state mass and energy balance including aspects of mixing efficiency in the form of impeller speed, as well as heat transfer efficiency from fouling. Notably, the author describes a short-cut method for producing the results when detailed kinetic data for the reaction is not available. This is achieved using thermochemical data and a yield profile with respect to time. Solution trajectories and temperature profiles are generated using Microsoft Excel.

Optimal control theory and Pontryagin's maximum principle The application of Pontryagin's maximum principle to batch optimisation is commonly found in literature. Use of the technique, specifically to optimal batch operation in fermentation processes, has been performed by Modak et al. (1986); Modak and Lim (1989, 1992). In particular, the authors investigated general characteristics of feeding rate profiles for fed-batch operation, and later expanded the theory for two control variables (Modak et al., 1986; Modak and Lim, 1989). The problem of maximising metabolite yield and productivity in these systems was also later explored by Modak and Lim (1992). Similarly, Srinivasan and Bonvin (2003) used the maximum principle to identify conditions for optimal feed rate and temperature policies for systems of batch and fed-batch reactors with two reactions. The authors conclude that it may be difficult to find a general analytic theory for systems involving more than two reactions. Filippi-Bossy et al. (1989) considered the use of

tendency models to batch reactor optimisation. The method involved the joint use of experimental data and a suggested dynamic model to systematically improve the proposed model estimate with each successive experimental run. The authors used Pontryagin's maximum principle to calculate optimal trajectories that were used to anticipate the optimal trajectory of the next run. However, the authors noted that a priori knowledge of the reaction order was necessary, and that the success of the method relied on the accuracy of the base model. Uhlemann et al. (1994) also considered the use of tendency models and suggested that optimisation of fed-batch reactors be viewed as a two-step process first involving the determination of off-line control variables followed by an optimal control phase. Although the application of Pontryagin's maximum principle is popular in batch optimisation, the determination of optimal solutions with the technique is difficult, particularly if analytical solutions are required. Shukla and Pushpavanam (1998) observe that this may be as a result of numerical instability and a priori knowledge of the sequence of control actions for adequate convergence.

Non-linear programming methods Optimisation of batch processes by dynamic optimisation has been investigated by Dhir et al. (2000); Aziz and Mujtaba (2002). Conversion of the problem and solution via non-linear programming methods are also common (Garcia et al., 1995; Allgor and Barton, 1997), with broader formulations to include separation processes for example (Allgor and Barton, 1999). Cuthrell and Biegler (1989) used sequential quadratic programming to obtain optimal operating policies in fed-batch reactors involving discontinuous profiles. Pushpavanam et al. (1999) applied the same approach for determining optimal feeding profile, also in fermentation processes.

The use of non-linear programming methods are discussed by Allgor et al. (1999) and Allgor and Barton (1999). Cuthrell and Biegler (1989) used sequential quadratic programming to obtain optimal operating policies in fed-batch reactors involving discontinuous profiles. Pushpavanam et al. (1999) applied the same approach for determining optimal feeding profile in fermentation processes. Garcia et al. (1995) demonstrated how the optimisation of batch reactors could be achieved by converting an optimal control problem into an equivalent non-linear programming problem. The solution is then found by a generalised reduced gradient approach and a golden search method for determination of the optimal final time. The practical implementation of optimal feeding profiles in fed-batch reactors is also considered by Shukla and Pushpavanam (1998). The authors approximated optimal profiles using discrete pulses and constant flow rates over both equal and unequal sub-intervals.

The optimisation of batch processes by dynamic optimisation has been investigated by Allgor et al. (1999); Dhir et al. (2000); Aziz and Mujtaba (2002). Peters et al. (2006) considered the design of an online controller for the optimal control of batch reactors using dynamic optimisation. In this way, changes in plant dynamics

are adjusted to provide an optimal control loop without the need for offline analysis.

Stochastic optimisation methods Recently, the successful use of stochastic methods to batch optimisation has also been investigated. In particular, the use of genetic algorithms for the determination of optimal feeding profile have been investigated by Ronen et al. (2002); Sarkar and Modak (2003); Zuo and Wu (2000). Zuo and Wu (2000) in particular modelled the cultivation of biological products with hybrid neural networks and then optimised the production rate using genetic algorithms. Faber et al. (2005) utilised a simulated annealing technique to improve the convergence of dynamic optimisation methods. The method was applied to the maximisation of intermediate species concentrations. Zhang and Smith (2004) considered the determination of optimal, non-ideal batch and fed-batch systems via a superstructure approach; optimal optimisation parameters were then solved also using simulated annealing. In addition to determining optimal control policies, the statistical nature of stochastic methods also allows for the discovery of similar near-optimal control policies. Slow convergence may still be an issue with these algorithms however.

1.3 Motivation

1.3.1 AR construction algorithms

In section 1.2.1, we indicated how recent developments in AR theory have tended to focus on formulating efficient and accurate methods for numerical AR construction. The existence of these methods are important, mainly for two reasons: firstly for the advancement of fundamental AR theory, and secondly for the application these methods to modern problems.

Despite there being a large body of work on AR theory, an adequate sufficiency condition for the AR still does not exist. The application of AR theory to many problems is still subject to uncertainty. It is still not well understood whether a given region is the true AR, or only a subset of it. AR constructions are still referred to as *candidate attainable regions* as a result.

Furthermore, development of efficient AR construction methods is required because current approaches are still computationally strenuous for modern problems of interest. Constructions in four dimensions and higher are cumbersome to view and work with, and so graphical techniques are either slow or not well suited for this purpose. In this regard, the often termed ‘curse of dimensionality’ by Bellman (2010) is appropriate for AR construction schemes. Current methods often rely on a discretisation of concentration space followed by either a direct search or some variant on traditional optimisation. The successful development of faster, more efficient methods, and a better understanding of the challenges involved would allow

for more confidence in the recommendations suggested by AR algorithms.

AR construction methods therefore are necessary, not only because of the complexity of higher dimensional problems, but also because they facilitate development of conventional AR theory towards a sufficiency condition.

1.3.2 Batch reactors

Similarly, there also exists a need for improved techniques in batch *reactor* synthesis problems. Irrespective of the specific numerical technique employed, the underlying methodology to batch improvement of current methods is generally consistent. A mathematical model describing the system is formulated and then solved by adjusting operating parameters, such as feed addition rate and temperature, until an assigned performance index is optimised. Optimisation is thus carried out by determination of an optimal combination of parameters for a fixed method of batch operation. The solution to the problem is then resultant from a mathematical formulation of a non-linear optimisation problem. The success and quality of the solution is often also dependent on an initial guess, which, may be linked to one of many local optima. In order for convergence to the true global optimum to be established, one must choose a starting guess that is sufficiently close to the answer. This is common to both batch and continuous optimisation problems. Specific examples of this to reactor synthesis arise when mixtures are introduced (McGregor et al., 1999; Godorr et al., 1999). Certain objective functions may be difficult to formulate mathematically given particular time and event representations, which may lead to additional auxiliary variables and complex constraints that ultimately influences the solution and solution performance.

Often, fed-batch reactors are utilised specifically in batch reactor optimisation, as this allow for flexibility in the problem types and optimisation routines employed. Little is currently found in the scientific literature detailing how other reactor types might be employed for the improvement of batch reactors, or even how *combinations* of different reactors may be arranged together to form a complex structure that achieves the desired task. This aspect of batch reactors specifically is still missing in the field.

In this regard, further improvements might be realised by also considering *batch structure,* in a similar manner to that achieved in continuous reactors. By batch structure, we mean the specific selection and sequencing of batch reactive equipment that produces a particular output state. Once the appropriate structure is established, optimisations may be carried out in the usual manner, offering further improvement to the problem. Following from arguments related to the continuous case, the first goal in batch optimisation should be to arrive at the correct reactor structure before optimisations are performed. With this in mind, use of the AR approach to batch reactors could be helpful in providing a better understanding of

optimal batch reaction sequence.

Even as the benefits of AR theory have been clearly demonstrated with continuous reactors, the method has seen little adoption in a batch setting. In almost 40 years since its initial development, only a single paper on the application of AR theory in batch reactors (Davis et al., 2008) exists excluding this work. This is due in large part to the fact that AR theory has historically developed with continuous reaction in mind.

1.4 Conclusion and scope of this work

Earlier in section 1.2.2, we discussed how the field of batch optimisation may be categorised into two broad fields: batch unit optimisation, and batch process optimisation. In this work we will be specifically focussed on the *reactive* portion of batch processes. That is, although the breadth of batch optimisation problems is vast, encompassing many different operations and scheduling problems, the particular benefit offered by AR theory necessitates that improvements to batch processes are focussed specifically on batch reactors, and not on the entire batch plant. With the background of improvement through structure discussed, and motivation of these detailed above, this thesis aims to address two areas in AR and batch reactor theory:

1. To continue the development of robust AR construction methods: providing a deeper insight into the challenges and potential improvements of these methods.

2. Towards the improvement of batch reactors via structure: utilising the insights gained from AR theory and applying them to batch operations. In later chapters, it will be our specific aim to exploit the benefits of continuous AR results, and apply it directly to equivalent batch systems.

The AR is a powerful method that has seen little adoption other than to problems mainly posed in $\mathbb{R}^2$ and $\mathbb{R}^3$ with continuous processes in mind. Although it is currently possible to address non-adiabatic systems, unbounded constructions, comminution and basic separation operations, little work has been attempted to approach related problems in batch reactors. Most of these methods are also held back by slow construction times or limited to lower dimensions. The use of the method to a wider audience may help to spread its use to broader fields, but it is our view that the above two points limit adoption of AR methods and ideas as a generally accepted, and easily accessible theory. Further research into this theory is required in order to make it more accessible. This should be done rather with an emphasis on graphical meaning as opposed to mathematical rigour. It is the goal of this thesis to help close these two gaps. In this way, this thesis essentially communicates the ideas of alternative methods to traditional process optimisation. The emphasis in this work will be towards reactor structure, rather than on optimisation alone.

In order for this to be done, the reader should first be familiar with basic AR theory. This can be found in chapter 2, where a brief overview of the AR is discussed. From there, the benefit in exploiting reactor structure should be more apparent as a means for improvement, so that the same way of thinking can be applied to batch reactors. This is partly achieved in chapter 3, where improvements in structure ultimately bring about an improvement in production rate. In chapter 4, improvements to an existing outside-in AR construction algorithm are discussed. The direct application of AR theory to batch reactors is given treatment in chapter 5. Final conclusions and recommendations for future research are then made in chapter 6. Where appropriate, specific theory and definitions have been split into the relevant chapters and used when necessary so that the reader is not required to read this work in a linear fashion.

1.5 Copyright permissions

The majority of this work has been formed from the compilation of published work (chapters 3, 4 and 5 respectively). Copyright permissions have been granted by the publishers for these chapters as a result. The content in these chapters has been adapted for use in this thesis from their respective papers given below.

- Chapter 3: Ming, D., Hildebrandt, D., Glasser, D., 2012. A Graphical Method of Improving the Production Rate from Batch Reactors. Ind. Eng. Chem. Res. 51, 13562–13573.
- Chapter 4: Ming, D., Hildebrandt, D., Glasser, D., 2010. A revised method of attainable region construction utilizing rotated bounding hyperplanes. Ind. Eng. Chem. Res. 49, 10549–10557.
- Chapter 5: Ming, D., Glasser, D., Hildebrandt, D., 2013. Application of Attainable Region theory to batch reactors. Chem. Eng. Sci. 99, 203 – 214.

References

Abraham, T. K., 2005. Kinetic bounds on attainability in the reactor synthesis problem. Ph.D. thesis, Ohio State University, Ohio.

Abraham, T. K., Feinberg, M., 2004. Kinetic bounds on attainability in the reactor synthesis problem. Industrial & Engineering Chemistry Research 43 (2), 449–457.

Agarwal, V., Thotla, S., Mahajani, S. M., 2008. Attainable regions of reactive distillation-part i. single reactant non-azeotropic systems. Chemical Engineering Science 63 (11), 2946–2965.

Allgor, R. J., Barrera, M. D., Barton, P. I., Evans, L. B., 1996. Optimal batch process development. Computers & Chemical Engineering 20 (6-7), 885–896.

Allgor, R. J., Barton, P. I., 1997. Mixed-integer dynamic optimization. Computers & Chemical Engineering 21, Supplement (0), S451–S456.

Allgor, R. J., Barton, P. I., 9 1999. Screening models for batch process development: Part ii. case studies. Chemical Engineering Science 54 (18), 4065–4087.

Allgor, R. J., Evans, L. B., Barton, P. I., 10 1999. Screening models for batch process development: Part i. design targets for reaction/distillation networks. Chemical Engineering Science 54 (19), 4145–4164.

Aziz, N., Mujtaba, I. M., 1 2002. Optimal operation policies in batch reactors. Chemical Engineering Journal 85 (2-3), 313–325.

Bellman, R., July 2010. Dynamic Programming. Princeton Landmarks in Mathematics. Princeton University Press.

Biegler, L. T., Zavala, V. M., 2009. Large-scale nonlinear programming using ipopt: An integrating framework for enterprise-wide dynamic optimization. Computers & Chemical Engineering 33 (3), 575–582.

Bonvin, D., 1998. Optimal operation of batch reactors - a personal view. Journal of Process Control 8 (5-6), 355–368.

Brooks, B. W., 1988. Semi-batch reactors and their use for autocatalytic reactions. Chemical Engineering Science 43 (6), 1287–1290.

Burri, J. F., Wilson, S. D., Manousiouthakis, V. I., 2002. Infinite dimensional state-space approach to reactor network synthesis: Application to attainable region construction. Computers & Chemical Engineering 26 (6), 849–862.

Capon-Garcia, E., Bojarski, A. D., Espuna, A., Puigjaner, L., 2011. Multiobjective optimization of multiproduct batch plants scheduling under environmental and economic concerns. AIChE Journal 57 (10), 2766–2782.

Chen, C., Lee, J., 7 2008. A graphical technique for the design of water-using networks in batch processes. Chemical Engineering Science 63 (14), 3740–3754.

Chunfeng, W., Xin, Z., 2002. Ants foraging mechanism in the design of multiproduct batch chemical process. Industrial & Engineering Chemistry Research 41 (26), 6678–6686.

Cornuejols, G., Tutuncu, R., January 2007. Optimization Methods in Finance (Mathematics, Finance and Risk). Cambridge University Press.

Cott, B., Macchietto, S., 1989. Minimizing the effects of batch process variability using online schedule modification. Computers & Chemical Engineering 13 (1), 105–113.

Cuthrell, J. E., Biegler, L. T., 1989. Simultaneous optimization and solution methods for batch reactor control profiles. Computers & Chemical Engineering 13 (1-2), 49–62.

Davis, B. J., Taylor, L. A., Manousiouthakis, V. I., 2008. Identification of the attainable region for batch reactor networks. Industrial & Engineering Chemistry Research 47 (10), 3388–3400.

Dhir, S., Jr., K. J. M., Rhinehart, R. R., Wiesner, T., 2000. Dynamic optimization of hybridoma growth in a fed-batch bioreactor. Biotechnology and bioengineering 67 (2), 197–205.

Dhole, V. R., Ramchandani, N., Tainsh, R. A., Wasilewski, M., 1996. Make your process water pay for itself. Chemical Engineering 103 (1), 100–103.

El-Halwagi, M., Gabriel, F., Harell, D., 2003. Rigorous graphical targeting for resource conservation via material recycle/reuse networks. Industrial & Engineering Chemistry Research 42 (19), 4319–4328.

Faber, R., Jockenhovel, T., Tsatsaronis, G., 1 2005. Dynamic optimization with simulated annealing. Computers & Chemical Engineering 29 (2), 273–290.

Feinberg, M., 1999. Recent results in optimal reactor synthesis via attainable region theory. Chemical Engineering Science 54 (13-14), 2535–2543.

Feinberg, M., 2000a. Optimal reactor design from a geometric viewpoint - iii. critical cfstrs. Chemical Engineering Science 55 (17), 3553–3565.

Feinberg, M., 2000b. Optimal reactor design from a geometric viewpoint. part ii. critical sidestream reactors. Chemical Engineering Science 55 (13), 2455–2479.

Feinberg, M., Hildebrandt, D., 1997. Optimal reactor design from a geometric viewpoint- i. universal properties of the attainable region. Chemical Engineering Science 52 (10), 1637–1665.

Filippi-Bossy, C., Bordet, J., Villermaux, J., Marchal-Brassely, S., Georgakis, C., 1989. Batch reactor optimization by use of tendency models. Computers & Chemical Engineering 13 (1-2), 35–47.

Floudas, C. A., Lin, X., 2004. Continuous-time versus discrete-time approaches for scheduling of chemical processes: a review. Computers & Chemical Engineering 28 (11), 2109–2129.

Garcia, V., Cabassud, M., Lann, M. V. L., Pibouleau, L., Casamatta, G., 11 1995. Constrained optimization for fine chemical productions in batch reactors. The Chemical Engineering Journal and The Biochemical Engineering Journal 59 (3), 229–241.

Glasser, D., Hildebrandt, D., 1997. Reactor and process synthesis. Computers & Chemical Engineering 21 (Supplement 1), S775–S783.

Glasser, D., Hildebrandt, D., Crowe, C., 1987. A geometric approach to steady flow reactors: The attainable region and optimization in concentration space. Industrial & Engineering Chemistry Research 26 (9), 1803–1810.

Godorr, S., Hildebrandt, D., Glasser, D., McGregor, C., 1999. Choosing optimal control policies using the attainable region approach. Industrial & Engineering Chemistry Research 38 (3), 639–651.

Grass, D., Caulkins, J. P., Feichtinger, G., Tragler, G., Behrens, D. A., September 2008. Optimal Control of Nonlinear Processes: With Applications in Drugs, Corruption, and Terror, 1st Edition. Springer.

Grossmann, I., 2005. Enterprise-wide optimization: A new frontier in process systems engineering. AIChE Journal 51 (7), 1846–1857.

Grossmann, I. E., 2012. Advances in mathematical programming models for enterprise-wide optimization. Computers & Chemical Engineering 47 (0), 2 – 18.

Hallale, N., 9 2002. A new graphical targeting method for water minimisation. Advances in Environmental Research 6 (3), 377–390.

Hartmann, A. K., Rieger, H., September 2001. Optimization Algorithms in Physics, 1st Edition. Wiley-VCH.

Hildebrandt, D., October 1989. The attainable region generated by reaction and mixing. Ph.D. thesis, University of the Witwatersrand, Johannesburg.

Hildebrandt, D., Glasser, D., Hausberger, B., Patel, B., Glasser, B. J., 2009. Producing transportation fuels with less work. Science 323 (5922), 1680–1681.

Honkomp, S., Lombardo, S., Rosen, O., Pekny, J., 2000. The curse of reality–why process scheduling optimization problems are difficult in practice. Computers & Chemical Engineering 24 (2), 323–328.

Horn, F., 1964. Attainable and non-attainable regions in chemical reaction technique. Pergamon Press, London.

Kallrath, J., 2002. Planning and scheduling in the process industry. OR spectrum 24 (3), 219–250.

Kanakamedala, K. B., Reklaitis, G. V., Venkatasubramanian, V., 1994. Reactive schedule modification in multipurpose batch chemical plants. Industrial & Engineering Chemistry Research 33 (1), 77–90.

Kauchali, S., Hausberger, B., Hildebrandt, D., Glasser, D., Biegler, L. T., 2004. Automating reactor network synthesis: Finding a candidate attainable region for the water-gas shift (wgs) reaction. Computers & Chemical Engineering 28 (1-2), 149–160.

Kauchali, S., Rooney, W. C., Biegler, L. T., Glasser, D., Hildebrandt, D., 2002. Linear programming formulations for attainable region analysis. Chemical Engineering Science 57 (11), 2015–2028.

Khumalo, N., Glasser, D., Hildebrandt, D., Hausberger, B., Kauchali, S., 2006. The application of the attainable region analysis to comminution. Chemical Engineering Science 61 (18), 5969–5980.

Levien, K. L., 5 1992. Maximizing the product distribution in batch reactors: reactions in parallel. Chemical Engineering Science 47 (7), 1751–1760.

Li, Z., Ierapetritou, M., 2008. Process scheduling under uncertainty: Review and challenges. Computers & Chemical Engineering 32 (4), 715–727.

Liu, B., Wang, L., Liu, Y., Qian, B., Jin, Y.-H., 2010. An effective hybrid particle swarm optimization for batch scheduling of polypropylene processes. Computers & Chemical Engineering 34 (4), 518–528.

Luus, R., Okongwu, O. N., 8 1999. Towards practical optimal control of batch reactors. Chemical Engineering Journal 75 (1), 1–9.

Majozi, T., Brouckaert, C. J., Buckley, C. A., 3 2006. A graphical technique for wastewater minimisation in batch processes. Journal of environmental management 78 (4), 317–329.

Manan, Z. A., Tan, Y. L., Foo, D. C. Y., 2004. Targeting the minimum water flow rate using water cascade analysis technique. AIChE Journal 50 (12), 3169–3183.

Manousiouthakis, V. I., Justanieah, A. M., Taylor, L. A., 2004. The shrink-wrap algorithm for the construction of the attainable region: An application of the ideas framework. Computers & Chemical Engineering 28 (9), 1563–1575.

Matlock, M. M., Howerton, B. S., Atwood, D. A., 11 2002. Chemical precipitation of heavy metals from acid mine drainage. Water research 36 (19), 4757–4764.

McGregor, C., Glasser, D., Hildebrandt, D., 1999. The attainable region and pontryagin's maximum principle. Industrial & Engineering Chemistry Research 38 (3), 652–659.

Mendez, C. A., Cerda, J., Grossmann, I. E., Harjunkoski, I., Fahl, M., 2006. State-of-the-art review of optimization methods for short-term scheduling of batch processes. Computers & Chemical Engineering 30 (6-7), 913–946.

Metzger, M. J., Glasser, B. J., Patel, B., Fox, J., Sempuga, B. C., Hildebrandt, D., Glasser, D., 2012. Liquid fuels from alternative carbon sources minimizing carbon dioxide emissions. AIChE Journal.

Milne, A. D., July 2008. The application of the attainable region cocept to the oxidative dehydrogenation of n-butaes in inert porous membrane reactors. Ph.D. thesis, University of the Witwatersrand, Johannesburg.

Modak, J. M., Lim, H. C., 1989. Optimal operation of fed-batch bioreactors with two control variables. The Chemical Engineering Journal 42 (2), B15–B24.

Modak, J. M., Lim, H. C., 1992. Optimal mode of operation of bioreactor for fermentation processes. Chemical Engineering Science 47 (15-16), 3869–3884.

Modak, J. M., Lim, H. C., Tayeb, Y. J., 1986. General characteristics of optimal feed rate profile for various fed-batch fermentation processes. Biotechnology and bioengineering 28 (9), 1396–1407.

Nisoli, A., Malone, M. F., Doherty, M. F., 1997. Attainable regions for reaction with separation. AIChE Journal 43 (2), 374–386.

Novas, J. M., Henning, G. P., 2010. Reactive scheduling framework based on domain knowledge and constraint programming. Computers & Chemical Engineering 34 (12), 2129–2148.

O'Reilly, A. J., 9 2002. Batch reactor optimization, profitability vs waste minimization. Chemical engineering research & design 80 (6), 587–596.

Ouelhadj, D., Petrovic, S., 2009. A survey of dynamic scheduling in manufacturing systems. Journal of Scheduling 12 (4), 417–431.

Peters, N., Guay, M., DeHaan, D., 2006. Real-time dynamic optimization of nonlinear batch systems. Canadian Journal of Chemical Engineering 84 (3), 338–348.

Pinto, T., Barbósa-Póvoa, A. P. F., Novais, A. Q., 2008. Design of multipurpose batch plants: A comparative analysis between the stn, m-stn, and rtn representations and formulations. Industrial & Engineering Chemistry Research 47 (16), 6025–6044.

Ponsich, A., Azzaro-Pantel, C., Domenech, S., Pibouleau, L., 2008a. Constraint handling strategies in genetic algorithms application to optimal batch plant design. Chemical Engineering and Processing: Process Intensification 47 (3), 420–434.

Ponsich, A., Touche, I., Azzaro-Pantel, C., Domenech, S., Pibouleau, L., Daydé, M., et al., 2008b. A grid-based environment for multiparametric pse applications: batch plant design case study. In: VECPAR 2008: 8th International Conference High Performance Computing for Computational Science. Vol. 5336.

Puigjaner, L., 1999. Handling the increasing complexity of detailed batch process simulation and optimisation. Computers & Chemical Engineering 23 (Supplement 1), S929–S943.

Pushpavanam, S., Rao, S., Khan, I., 1999. Optimization of a biochemical fed-batch reactor using sequential quadratic programming. Industrial & Engineering Chemistry Research 38 (5), 1998–2004.

Reklaitis, G. V., 1996. Overview of scheduling and planning of batch process operations. In: Batch processing systems engineering. Springer, pp. 660–705.

Ronen, M., Shabtai, Y., Guterman, H., 2002. Optimization of feeding profile for a fed-batch bioreactor by an evolutionary algorithm. Journal of Biotechnology 97 (3), 253–263.

Rooney, W. C., Hausberger, B. P., Biegler, L. T., Glasser, D., 2000. Convex attainable region projections for reactor network synthesis. Computers & Chemical Engineering 24 (2-7), 225–229.

Sarkar, D., Modak, J. M., 2003. Optimisation of fed-batch bioreactors using genetic algorithms. Chemical Engineering Science 58 (11), 2283–2296.

Scott, F., Conejeros, R., Aroca, G., et al., 2013. Attainable region analysis for continuous production of second generation bioethanol. Biotechnology for biofuels 6 (1), 171.

Seodigeng, T., Hausberger, B., Hildebrandt, D., Glasser, D., 2009. Recursive constant control policy algorithm for attainable regions analysis. Computers & Chemical Engineering 33 (1), 309–320.

Seodigeng, T. G., January 2006. Numerical formulations for attainable region analysis. Ph.D. thesis, University of the Witwatersrand, Johannesburg.

Shah, N., 1998. Planning and scheduling-single-and multisite planning and scheduling: Current status and future challenges. In: AIChE Symposium Series. Vol. 94. New York, NY: American Institute of Chemical Engineers, 1971-c2002., pp. 75–90.

Shah, N., 2004. Pharmaceutical supply chains: key issues and strategies for optimisation. Computers & Chemical Engineering 28 (6), 929–941.

Shioya, S., Dunn, I. J., 1979. Analysis of fed-batch fermentation processes by graphical methods. Journal of Chemical Technology and Biotechnology 29 (3), 180–192.

Shukla, P. K., Pushpavanam, S., 1 1998. Optimisation of biochemical reactors – an analysis of different approximations of fed-batch operation. Chemical Engineering Science 53 (2), 341–352.

Srinivasan, B., Bonvin, D., 2003. Characterization of optimal temperature and feed-rate policies for discontinuous two-reaction systems. Industrial & Engineering Chemistry Research 42 (22), 5607–5616.

Staniskis, J., Levisauskas, D., 1983. Optimization of batch fermentation processes by graphical method. Biotechnology and bioengineering 25 (4), 985–990.

Uhlemann, J., Cabassud, M., Lann, M.-V. L., Borredon, E., Casamatta, G., 9 1994. Semi-batch reactor optimization and control for the epoxidation of furfural. Chemical Engineering Science 49 (18), 3169–3191.

Varma, V. A., Reklaitis, G. V., Blau, G., Pekny, J. F., 2007. Enterprise-wide modeling & optimizatio–an overview of emerging research challenges and opportunities. Computers & Chemical Engineering 31 (5), 692–711.

Vassiliadis, V. S., Pantelides, C. C., Sargent, R. W. H., 1994. Optimization of discrete charge batch reactors. Computers & Chemical Engineering 18 (Supplement 1), S415–S419.

Wang, C., Quan, H., Xu, X., 1996. Optimal design of multiproduct batch chemical process using genetic algorithms. Industrial & Engineering Chemistry Research 35 (10), 3560–3566.

Wang, Y., Smith, R., 1995a. Time pinch analysis. Chemical engineering research & design 73 (8), 905–914.

Wang, Y., Smith, R., 1995b. Waste-water minimization with flow-rate constraints. Chemical engineering research & design 73 (8), 889–904.

Wassick, J. M., 2009. Enterprise-wide optimization in an integrated chemical complex. Computers & Chemical Engineering 33 (12), 1950–1963.

Yi, G., Reklaitis, G. V., 2006. Optimal design of batch-storage network with uncertainty and waste treatments. AIChE Journal 52 (10), 3473–3490.

Zhang, J., Smith, R., 2004. Design and optimisation of batch and semi-batch reactors. Chemical Engineering Science 59 (2), 459–478.

Zuo, K., Wu, W. T., 2000. Semi-realtime optimization and control of a fed-batch fermentation system. Computers & Chemical Engineering 24 (2-7), 1105–1109.

Chapter 2

Preliminaries

2.1 The Attainable Region

In chapter 1, we described how the AR represents, in a geometric sense, the set of all achievable points, for all possible reactor configurations, obtained by reaction and mixing alone. The AR is commonly constructed in concentration space, although constructions involving residence time are also often found in the literature (Glasser et al., 1994; Godorr et al., 1994; Hildebrandt and Glasser, 1990; Hildebrandt et al., 1990). With the exception of unique conditions containing irregular kinetics or state vectors, the AR is typically composed of surfaces generated from reaction and mixing processes only. Reaction surfaces are the result of distinct combinations of three specific reactor types. These shall be described below. The particular combination of reactors and their arrangement with respect to one another is termed a *reactor structure*. Whereas reaction operations may be viewed to enlarge the AR, the linear nature of mixing operations ensures that any set of compositions may always be formed by a convex combination of achievable points. In this way, the AR also acts as a boundary between all that is achievable to all that is not.

In the following chapters, we discuss the nature of concentration and reaction in geometric terms. Although these discussions are best visualised in $\mathbb{R}^2$ and $\mathbb{R}^3$, the results below are still applicable in $\mathbb{R}^n$. As such, vector notation will be used throughout. All vectors are, unless specified otherwise, assumed to be column vectors.

2.2 Geometric representation of concentration, mixing and reaction

2.2.1 Concentration

Most representations of the AR are performed in concentration space, and thus an adequate understanding of the geometric properties of concentration and mixing is

important. Let us begin with a set of n components in a mixture. There may be more than one mixture present, in which case we will denote i to be the i-th mixture in the system. The molar concentrations are then given by $c_{iA}, c_{iB}, \ldots, c_{in}$. We may group the set into a n-dimensional column vector by

$$\mathbf{C}_i = \begin{bmatrix} c_{iA} \\ c_{iB} \\ \vdots \\ c_{in} \end{bmatrix}$$

and call this the *concentration vector*. $\mathbf{C}_i$ is a arranged so that the n species each represent an axis in the positive orthant in Euclidean space, and therefore any concentration in the system can be represented as a coordinate from the origin given by the zero vector. The space in which all concentrations must lie is called the concentration space, or more generally, the state space. $\mathbf{C}_i$ thus represents a unique coordinate in concentration space that may, for instance, indicate the instantaneous concentration within a reactor, or the resulting composition formed from a combination of mixing multiple effluent streams together.

2.2.2 Mixing

When two concentrations $\mathbf{C_1} = [c_{1A}, c_{1B}, \ldots, c_{1n}]^{\mathrm{T}}$ and $\mathbf{C_2} = [c_{2A}, c_{2B}, \ldots, c_{2n}]^{\mathrm{T}}$ are mixed together, we have by mass balance

$$\mathbf{C}^* = \frac{\mathrm{V}_1\mathbf{C_1} + \mathrm{V}_2\mathbf{C_2}}{\mathrm{V}_2 + \mathrm{V}_2}$$

where $\mathbf{C}^* \in \mathbb{R}^n$ is the final mixture concentration and V_1 and V_2 are the volumes of streams 1 and 2, respectively. When the substitution

$$\lambda = \mathrm{V}_2 / \left(\mathrm{V}_1 + \mathrm{V}_2\right)$$

is introduced, rearrangement of the above expression gives

$$\mathbf{C}^* = (1 - \lambda)\,\mathbf{C_1} + \lambda\mathbf{C_2} \tag{2.2.1}$$

where $0 \leq \lambda \leq 1$. This is also known as the Lever Arm Rule (Geankoplis, 1993). It is clear from eq 2.2.1 that mixing is a linear process. Geometrically, this suggests that $\mathbf{C}^*$ must lie on the straight line segment joined by $\mathbf{C_1}$ and $\mathbf{C_2}$ in concentration space. Figure 2.2.1 shows a simple representation of this for two arbitrary concentrations in $\mathbb{R}^2$.

It is assumed here that density is constant so that the total volume change remains the same. If the particular application does not admit this assumption, as in the case of gaseous or highly non ideal mixtures, then mass fractions should

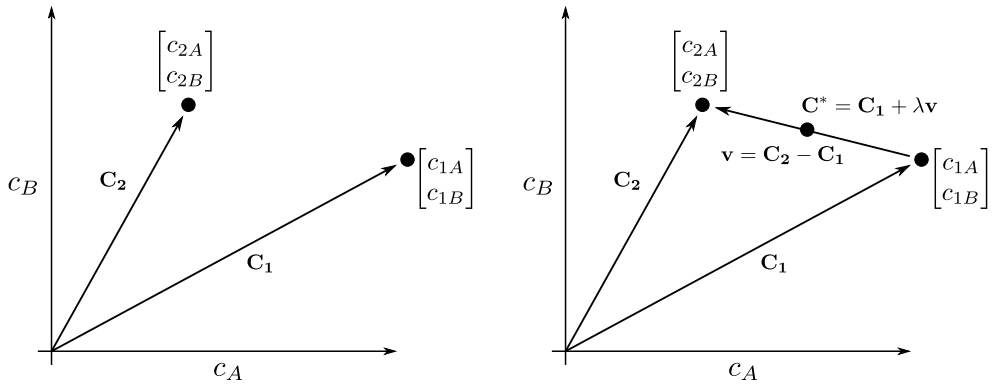


Figure 2.2.1: Geometric representation of concentration and mixing

be used in place of concentration. Mixing is therefore *always* viewed to be a linear process, and thus the above analysis is equally applicable to non-constant density systems. For the purpose of simplicity however, constant density will be assumed unless specified otherwise.

It is sometimes also convenient to define a *mixing vector* $\mathbf{v} \in \mathbb{R}^n$ as follows:

$$\mathbf{v} = \mathbf{C_2} - \mathbf{C_1} \tag{2.2.2}$$

in which case, $\mathbf{C}^*$ is then given by $\mathbf{C}^* = \mathbf{C_1} + \lambda\mathbf{v}$ which has the property that the final mixture concentration must lie on $\mathbf{v}$. The above reasoning can now be generalised to a set of k compositions $\{\mathbf{C}_1, \mathbf{C}_2, \ldots, \mathbf{C}_k\} \in \mathbb{X}$ (Feinberg and Hildebrandt, 1997). A set $\mathbb{X}$ is considered *convex* if and only if for any two points $\mathbf{C}_1, \mathbf{C}_2 \in \mathbb{X}$, the line segment $\overline{\mathbf{C}_1\mathbf{C}_2}$ is completely contained in $\mathbb{X}$. $\mathbf{C}^*$ is considered a convex combination of the set if there exists a set of k scalars $\{\lambda_1, \lambda_2 \ldots \lambda_k\}$ such that $\lambda_i \geq 0,\ i = 1, 2, \ldots, k$

$$\sum_{i=1}^{k} \lambda_i = 1$$

and

$$\mathbf{C}^* = \sum_{i=1}^{k} \lambda_i \mathbf{C}_i$$

2.2.3 Concavities and mixing

Consider the region of achievable points shown in Figure 2.2.2. The blue shaded region represents achievable points by an arbitrary set of reactors or feed points. A concavity is clearly visible, although, it does not appear to be part of the achievable set. This can be overcome by use of mixing. To see this, we join points $\mathbf{C}_1$ and $\mathbf{C}_2$ together by a straight line. In reality, this indicates that a mixture has been formed between concentrations corresponding to $\mathbf{C}_1$ and $\mathbf{C}_2$. The straight line connecting points $\mathbf{C}_1$ and $\mathbf{C}_2$ is thus also attainable now and points on the line $\overline{\mathbf{C}_1\mathbf{C}_2}$ can now

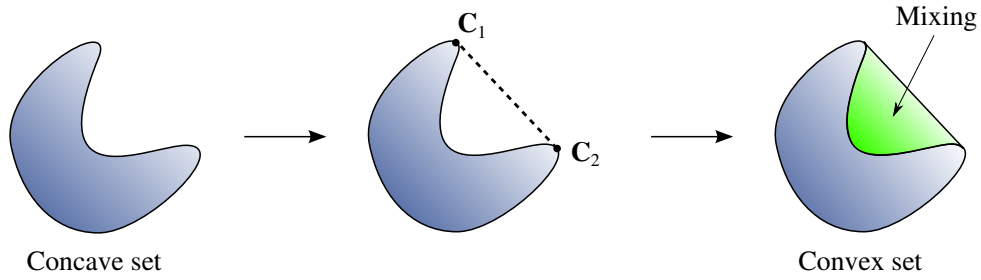


Figure 2.2.2: Concavities and mixing

be used to achieve other unattainable regions in the concavity. This establishes two important results:

1. If mixing is an allowable process, a concave set of achievable states can always be represented geometrically as a convex polytope in state space. Otherwise, mixing would be able to fill in concave regions.

2. Given a convex set of points, there are infinitely many ways in which to achieve points within the region bounded by the points. Interior points of the region may be obtained by the intersection of many states that all cross at the same point, and thus there is generally no unique combination of boundary points that can be used to achieve points located within the region.

This suggests that one need only be concerned with the boundary points of the AR, as all other points within the region may be attainable by mixing. The AR must therefore also be convex, formed from the convex hull of its boundary points. A formal definition of convex hulls is given below.

2.2.4 Convex Hulls

If $S \subset \mathbb{R}^n$ is a subset such that for any distinct pair of points $\mathbf{C_1}$, $\mathbf{C_2} \in \mathbb{R}^n$, where the line segment joining $\mathbf{C_1}$ and $\mathbf{C_2}$ is completely contained in S, then S is said to be convex. The *convex hull* of a set $S \in \mathbb{R}^n$, is the intersection of all the convex sets in $\mathbb{R}^n$ which contain S, and is denoted by conv(S). The convex hull represents the smallest convex set that contains S. Geometrically, the convex hull can be envisioned as a convex polytope in $\mathbb{R}^n$, enclosed by a finite number of hyperplanes from which the facets are composed.

The AR is thus the convex hull of the set of points that define its boundary. This is important because it means that we do not need to find all possible reactor configurations and their outcomes. The requirement is only to find the unique set of reactor structures that make up the AR boundary. It is therefore possible to form any combination of states within the region by mixing between the appropriate boundary points. The act of constructing a candidate AR is then a matter of determining the reactor structures that expand the convex hull of points. In this way, we not only

determine the set of points belonging to the AR, but we also decode the optimal structures that are used to achieve these points.

2.2.5 Rate vectors and rate fields

Consider now what occurs when, along with a set of individual species, a system of reaction kinetics is introduced. Since reaction rates typically vary for each species in a system, and since these are also commonly subject to the state of the system (temperature, pressure, composition etc.), it follows that a unique direction vector may be determined with components corresponding to the rate of formation of each species. One is therefore able to define a *rate vector.* The rate vector contains all reaction kinetics for the system under consideration. For a prescribed set of reaction kinetics and concentration vector $\mathbf{C} \in \mathbb{R}^n$, we define the rate of formation of each species i as the function $r_i(\mathbf{C})$ describing the instantaneous change of the species as a function of $\mathbf{C}$. For n components occurring in the system, n species rate expressions may be written. The rate vector may be written as follows:

$$\mathbf{r}(\mathbf{C}) = \begin{bmatrix} r_A(\mathbf{C}) \\ r_B(\mathbf{C}) \\ \vdots \\ r_n(\mathbf{C}) \end{bmatrix}$$

Here, $r_A(\mathbf{C})$ is the rate expression for component A, $r_B(\mathbf{C})$ for component B, and so on. The rate vector $\mathbf{r}(\mathbf{C})$ then, is the vector in $\mathbb{R}^n$ which describes the instantaneous change in each component at a point $\mathbf{C}$ in concentration space. Conversely, for every point in concentration space, we are able to assign a unique rate vector described by $\mathbf{r}(\mathbf{C})$. We are then able to associate a given set of reaction kinetics in terms of a uniquely defined vector field residing in $\mathbb{R}^n$.We call this the *rate field.* A rate field for a typical system is given in Figure 2.2.3.

Although many reactor types may be formed that each separately rely on $\mathbf{r}(\mathbf{C})$, movement through the rate field will be different for each type. These are described briefly below.

2.3 Fundamental reactor types

2.3.1 The Plug Flow Reactor (PFR)

The Plug Flow Reactor (PFR) belongs to the class of fundamental reactor models that exhibit no axial mixing – material is assumed to travel along the reactor's length in a differential plug, and as a result, no mixing is assumed to occur in the direction of the flow of material. For any differential slice of the PFR however, the contents of the slice is assumed to be perfectly mixed. That is, the contents is assumed to

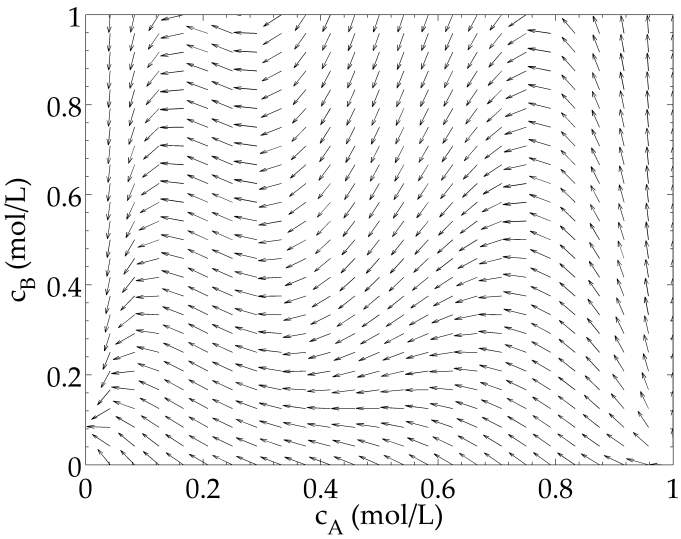


Figure 2.2.3: Rate field for a system of kinetics in $\mathbb{R}^2$

be perfectly mixed in the radial direction. For this reason the PFR is modelled, in vector form, by the following equation

$$\frac{\mathrm{d}\mathbf{C}}{\mathrm{d}\tau} = \mathbf{r}\left(\mathbf{C}\right) \tag{2.3.1}$$

Here τ is a non-negative scalar representing the PFR's residence time

$$\tau_{\mathrm{PFR}} = \mathrm{V}_{\mathrm{PFR}}/\mathrm{Q}$$

where $\mathrm{V}_{\mathrm{PFR}}$ and Q are the PFR volume and flowrate, respectively. There is a direct analogue between PFRs and batch reactors. If no material is allowed to enter a batch vessel during reaction, then the evolution of species concentrations within the batch is exactly the same as that found along the length of a PFR. The reaction time of the batch then plays the same role as residence time in a PFR. An application of this result is discussed later in chapter 5. Hence, from a modelling perspective, there is no mathematical difference between a continuous PFR and a standard batch reactor, although significant operational differences may still exist that may need to be accounted for, particularly in the context of batch process scheduling and optimisation.

The PFR equation is an ordinary differential equation (ODE), one for each component participating in the reaction, that can be solved by standard techniques, typically via numerical integration. Multiple species participating in the reaction results a system of ODEs. In order to solve the system, initial conditions and an integration time are required. These arise in the form of a PFR feed concentration and residence time, respectively. The solution of the PFR equation produces a solution trajectory; we call this a *PFR trajectory*.

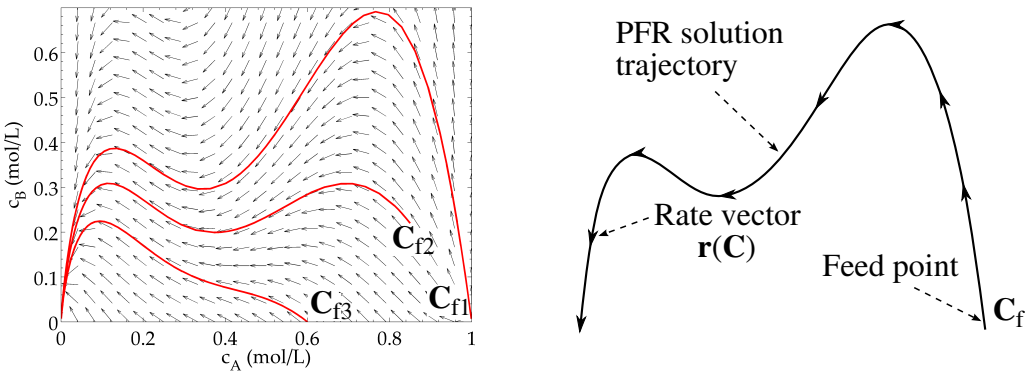


Figure 2.3.1: Rate vectors on a PFR trajectory. Rate vectors are tangent at each point on a PFR solution trajectory. This implies that PFR trajectories may never cross.

Geometrically, all rate vectors evaluated on the set of concentrations belonging to the PFR trajectory are tangent to the solution trajectory. This is clear when we keep in mind the form of eq 2.3.1. The rate of change of concentration in a PFR is equal to the rate vector evaluated at the same concentration. In practice, one is generally able to deduce the shape of all PFR trajectories for the system graphically by reviewing the direction of the rate vectors in the rate field. Furthermore, this implies that PFR trajectories can never cross – for this to occur, multiple rate vectors must be present at the intersection point (Feinberg and Hildebrandt, 1997; Hildebrandt, 1989). Figure 2.3.1 demonstrates this using the rate field supplied in Figure 2.2.3.

2.3.2 The Continuously-Stirred Tank Reactor (CSTR)

Opposite in nature to the PFR, the CSTR belongs to the class of reactors in which complete mixing is assumed. The entire vessel contents is assumed to operate at a single state so that the effluent concentration is equal to the vessel contents. The governing equation for a CSTR is hence given by mass balance over the reactor

$$\mathbf{C} - \mathbf{C_f} = \tau \mathbf{r}\left(\mathbf{C}\right) \tag{2.3.2}$$

CSTR solutions are obtained by the simultaneous solution to a system of non-linear equations. Non-linearity appears in the form of the rate expressions used for the system kinetics, and consequently the complexity of CSTR behaviour is a direct function of the complexity of the underlying kinetics. It is not uncommon to observe multiple steady states for a unique reactor volume and feed concentration. This may occur, even for relatively simple autocatalytic reactions. It is for this reason that the systematic determination of CSTR effluent concentrations is difficult, particularly if complicated kinetics are used. An example of such a reaction is shown in section

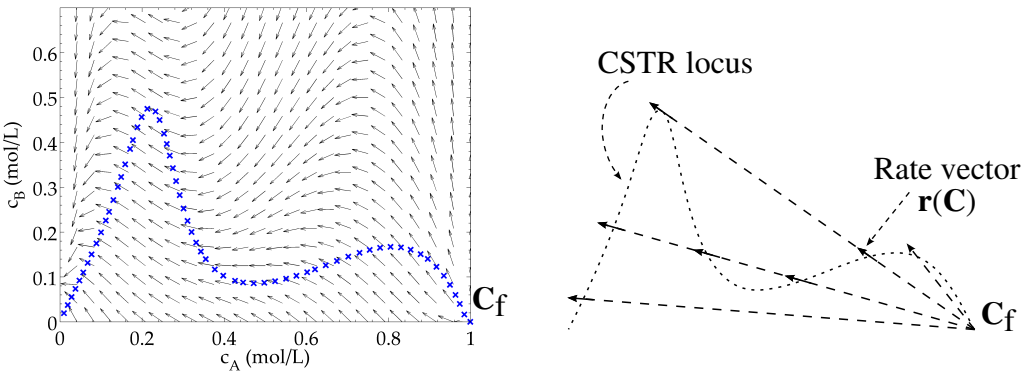


Figure 2.3.2: Rate vectors on a CSTR locus. For each point on the locus, a unique CSTR volume can be calculated. Rate vectors are co-linear with feed mixing vectors in CSTRs

5.4.1.

Solution of the CSTR equation results in a single concentration. This is in contrast to the solution trajectory obtained by the integration of the PFR equation for example. In order to generate a full set of CSTR concentrations, a range of residence times is required. The collective term for the range of CSTR solutions obtained is called a CSTR locus. A sample set of CSTR solutions for the same rate expression is given in Figure 2.3.2. These kinetics do not exhibit multiple steady states. In the case of multiple solutions, separate branches of the CSTR locus would be observed.

Geometrically, the rate vector must be co-linear with the mixing vector given by $\mathbf{v} = \mathbf{C} - \mathbf{C_f}$. This allows for a geometric method of finding CSTR solutions. The rate vectors evaluated on the CSTR locus are also shown in Figure 2.3.2. It is clear that they are collinear with the mixing vector back to the feed.

Since CSTR solutions are found at discrete points, the presence of multiple solutions in the rate expression allow for jumps and discontinuities in space. That is, CSTR solutions allow us to achieve disjoint points in space that would not be possible via continuous profiles. This presents a considerable challenge for AR construction methods, as it is generally unsafe to rely solely on continuity arguments found in traditional optimisation techniques. The presence of discontinuous regions and multiple steady states (often found in chemical engineering) thus limit the use of traditional optimisation methods, such as dynamic programming, in AR theory.

2.3.3 The Differential Side-stream Reactor (DSR)

Geometrically, the DSR is a reactor that may be viewed as a mixture between the two limiting reactor model cases described above – the CSTR represents chemical reaction in which complete mixing is observed, whereas the PFR represents reaction where no mixing is observed. Figure 2.3.3 provides a schematic of a DSR with the

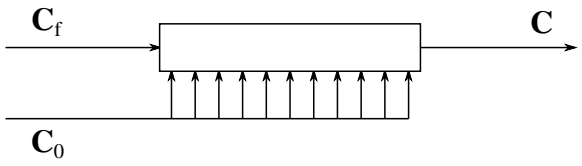


Figure 2.3.3: Schematic of DSR.

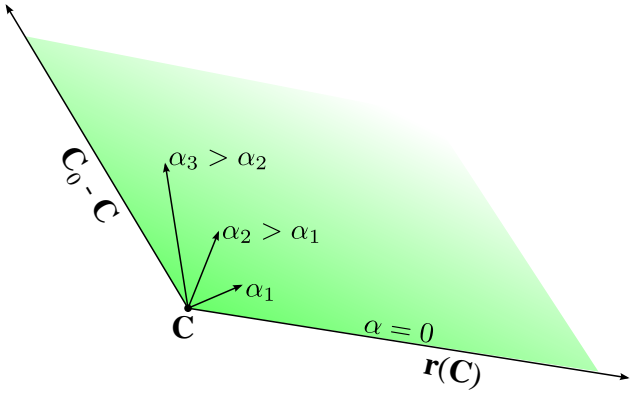


Figure 2.3.4: The space spanned by a rate vector and mixing vector. The particular DSR trajectory obtained is governed by the mixing vector and the α policy used.

feed and effluent concentrations of interest. With this in mind, the form of the DSR expression is easy to interpret. The overall change in concentration of a differential plug is expressed as a linear combination of two vectors: the reaction rate $\mathbf{r}(\mathbf{C})$, and the side-stream concentration $\mathbf{C_0}$.

$$\frac{\mathrm{d}\mathbf{C}}{\mathrm{d}\tau} = \mathbf{r}(\mathbf{C}) + \alpha(\mathbf{C_0} - \mathbf{C}) \tag{2.3.3}$$

The variable α is a control parameter that is used to adjust the relative amount of mixing by concentration $\mathbf{C_0}$ into the reactor. Furthermore, both $\mathbf{C_0}$ and α may vary along the length of the reactor. When $\alpha = 0$, we obtain the PFR equation. At equilibrium (when $\mathrm{d}\mathbf{C}/\mathrm{d}\tau = \mathbf{0}$), we obtain the CSTR equation with $\mathbf{C_0} = \mathbf{C_f}$. Integration of the DSR equation also produces a solution trajectory. We call this the DSR trajectory. In addition to requiring an initial condition and reaction time, the DSR also requires that one specify a relationship for the side-stream feeding composition and feeding policy (the α policy). In chapter 5, the apparent general purpose nature of the DSR is exploited and used to improve batch reactors.

Geometrically, the DSR must travel in a direction that is defined by the linear subspace spanned by the vector $\mathbf{r}(\mathbf{C})$ and $\mathbf{C_0}$. The duty of α is thus to determine the instantaneous direction of the DSR in space. Figure 2.3.4 gives a graphical representation of this.

By careful choice of the α policy, DSRs may be useful in helping to extend the AR in directions where both reaction and mixing are required simultaneously.

The unique α policy results in a DSR forming part of the AR boundary is called a critical α policy. DSRs are only found to play a useful role on construction of the AR boundary for three dimensions and higher. This means for 2 dimensional constructions, PFRs and CSTRs are sufficient to construct the AR.

2.4 Higher dimensional considerations

2.4.1 Dimension of the AR

Assume a system of L independent reactions is available participating amongst n components, where $L \leq n$. Although it is natural to expect the AR for the system to reside in the full concentration space $\mathbb{R}^n$, it may be shown that the AR can be viewed to lie within $\mathbb{R}^L$, a subspace of $\mathbb{R}^n$, corresponding to the number of independent reactions in the system (Feinberg and Hildebrandt, 1997). The dimension of the AR (and hence it's computation) can therefore be reduced by only considering a subset of all n components. The remaining components associated with states in the AR are then found by mass balance. That is, although it is possible to express a concentration vector $\mathbf{C} \in \mathbb{R}^n$ and rate vector $\mathbf{r}(\mathbf{C}) \in \mathbb{R}^n$ in terms of all n components participating in the system, the components are generally linearly dependent due to reaction stoichiometry. It is generally more suitable to write concentration and rate vectors in terms of only the L independent components corresponding to the independent reactions participating in the system: $\mathbf{C} \in \mathbb{R}^L$ and $\mathbf{r}(\mathbf{C}) \in \mathbb{R}^L$.

By example, consider the synthesis of ammonia from nitrogen and hydrogen $N_2 + 3H_2 \rightleftharpoons 2NH_3$. Although there are 3 components participating in the system ($n = 3$), they are all expressed in terms of a single extent of reaction. Thus, although it is possible to plot all possible concentrations for the ammonia synthesis reaction in $c_{N_2} - c_{H_2} - c_{NH_3}$ space, these points must lie on a line in $\mathbb{R}^3$ if they are to obey the reaction stoichiometry. Knowledge of the feed and effluent state for one of the components permits calculation of the other two by mass balance. The system is inherently *one-dimensional* as a result. Note that the presence of a reverse reaction does not influence the dimension of the subspace, for only *independent* reactions are required to determine the dimension of achievable states.

2.4.2 Stoichiometric subspace

Given only a system of reactions and feed point $\mathbf{C_f}$, it is possible to compute distinct bounds that enclose all possible species concentrations obeying the reaction stoichiometry and feed point. Since the AR must obey mass balance constraints and contain the feed point, it follows that these bounds must also encompass the AR. This can be done without specification of reaction kinetics, for all kinetics must also obey mass balance according to the reaction stoichiometry. Given d independent reactions occurring in n components, a *stoichiometric coefficient matrix* $\mathbf{A}$ of

size $(n \times d)$ can be formed, housing the species reaction coefficients participating in each reaction in the system

$$\mathbf{A} = \begin{bmatrix} \nu_{11} & \cdots & \nu_{d1} \\ \vdots & \ddots & \vdots \\ \nu_{1n} & \cdots & \nu_{dn} \end{bmatrix}$$

where ν_{ij} is the stoichiometric coefficient of component i participating in reaction j. It is straightforward to show how all species concentrations $\mathbf{C}$ in the system can be expressed in terms of linear combination of an initial feed vector $\mathbf{C_f}$ and the stoichiometric coefficient matrix $\mathbf{A}$

$$\mathbf{C} = \mathbf{C_f} + \mathbf{A}\varepsilon \tag{2.4.1a}$$

ε is a $(d \times 1)$ vector corresponding to each extent of reaction. Indeed, the columns of $\mathbf{A}$ correspond to the individual reactions participating in the system. The space spanned by eq 2.4.1a is hence determined by $\mathbf{A}$ offset by $\mathbf{C_f}$. Furthermore, feasible concentrations must also be non-negative

$$\mathbf{C} \geq \mathbf{0} \tag{2.4.1b}$$

Concentrations obeying eq 2.4.1a and eq 2.4.1b are said to be *stoichiometrically compatible* with the feed point $\mathbf{C_f}$. We term the space spanned by eq 2.4.1a the *stoichiometric subspace* and often denoted by the symbol S. The dimension of S is hence determined by the dimension of $\mathbf{A}$, in particular. This provides a simple way of calculating the dimension of the stoichiometric subspace since this is equivalent to finding the rank of $\mathbf{A}$, $\text{rank}\,(\mathbf{A})$. If there are d independent reactions, it follows that $\text{rank}\,(\mathbf{A}) = d$.

In section 2.4.1, we discussed how the AR exists as a subspace of $\mathbb{R}^n$. The dimension of this space is determined by the number of independent reactions present in the system. Computing the dimension of the AR is hence achieved by computation of the stoichiometric subspace, which is directly related to the number of independent reactions, from $\text{rank}\,(\mathbf{A})$. Since AR theory has typically come about from 2D constructions, the stoichiometric subspace is generally represented as a triangle. It is for this reason that the stoichiometric subspace is commonly also referred to as the *mass balance triangle*. A worked example demonstrating how to compute the stoichiometric subspace given reaction stoichiometry and a feed is given in Appendix B.2.

2.4.3 PFRs on the AR boundary

From section 2.2.3, a concave set of achievable points can always be made convex through mixing. A set $\mathbb{X}$ containing k points produced by a reactive network will

have points in or on the boundary defined by the convex hull of $\mathbb{X}$, conv $(\mathbb{X})$. If a point $\mathbf{C}_i$ satisfies the relation

$$\mathbf{C}_i = \lambda_1 \mathbf{C}_1 + \lambda_2 \mathbf{C}_2 + \cdots + \lambda_k \mathbf{C}_k$$

in which at least one of the λ's is non-negative, then $\mathbf{C}_i$ must lie on the interior of a line segment joining points in $\mathbb{X}$. Hence, $\mathbf{C}_i$ can be formed from a mixture of the boundary points in $\mathbb{X}$ given by conv $(\mathbb{X})$. It follows that if a point $\mathbf{C}_i$ can be formed from a mixture of two or more other points, then it cannot be an extreme point of conv $(\mathbb{X})$ and thus it also cannot be formed as a result of reaction. From this, we note that the extreme points of $\mathbb{X}$ are those that arise from reaction alone, for otherwise they would satisfy the above mixing relation. It follows that the boundary of the AR is generated from reaction and mixing processes only. Linear (flat) sections of the AR boundary are those resulting from mixing process whereas as convex (curved) sections of the boundary are those generated from reaction alone.

An important result of this arises in the form of theorem 1 in Feinberg and Hildebrandt (1997). Using the above result, along with the complement principle discussed in chapter 1, the theorem states that any set of extreme points disjoint from the feed are the result of the union of PFR trajectories (solutions to eq 2.3.1). Though the AR boundary may typically be composed of a complex set of multiple reactor types with intermediate mixing, the final reactor type used to achieve extreme points on the AR boundary arise from PFR trajectories *alone*. This is useful as a design guideline in reactor network synthesis problems, for terminating reactor type will always be that of a PFR.

2.4.4 Connectors and critical reactors

Connectors

Although it is known that only PFR trajectories produce extreme points on the AR boundary, other special reactor types must be employed in order to reach them. A *connector* is used in the terminology of AR theory to describe a special manifold of points residing on the AR boundary which allow for connection to the manifold of extreme PFR trajectories. In Feinberg (2000b), they are described as 'service roads' that link to PFR highways. Although a precise mathematical definition of connectors can be found in Feinberg and Hildebrandt (1997), it is sufficient for our sake to only have a qualitative understanding of their duty in the formation of the AR boundary. In simple terms, connectors are points on the AR boundary which are disjoint from the feed that originate from mixing lines. Connectors leave mixing lines to connect to PFR trajectories *smoothly*. Moreover, connectors are formed specifically from the solution of the CSTR and DSR equations only.

Critical DSRs

A DSR solution trajectory contained entirely on the AR boundary is termed a critical DSR trajectory. Critical DSR trajectories result from highly specific α feeding policies, termed *critical* α *polic*ies, that allow for traversal on the AR boundary. Critical DSR trajectories act as connectors to PFR trajectories on the boundary. In order to understand why these are special, we must understand that the AR boundary plays special physical significance in the context of achievability. By simply residing on the boundary, the corresponding reactor must be controlled in a highly specialised manner.

It is possible to compute critical α policies from this understanding using ideas from geometric control theory (Feinberg, 1999). To see this, suppose that a critical DSR trajectory is available, controlled by a critical α policy. Since it is critical, it must lie entirely on the AR boundary. Since it resides on the boundary, it borders between all achievable states to all unachievable states. If a perturbation is introduced into the control policy, then the resulting trajectory will deviate from the path prescribed by the critical trajectory. Since the trajectory is critical, this perturbation may serve only to produce a deviation *into* the AR, for else the original DSR trajectory would not be critical in the first place. We can see from this that controllability arguments dictate the form of critical DSR trajectories and hence the computation of critical α policies. Indeed, whereas we often attempt to seek completely controllable solution trajectories in practice, it is the *absence* of control that must be used as a condition for residing on the AR boundary (Feinberg, 1999). In the theory of optimal control, the resulting α policy corresponds to a singular control profile.

A condition for computing critical reactors is then possible. Since the nature of the DSR equation is inherently non-linear, the use of iterated Lie Brackets is required in order to calculate the condition. Specifically, rewriting the DSR equation in the form

$$\mathbf{f}(\mathbf{C}) = \mathbf{r}(\mathbf{C}) + \alpha \mathbf{v}(\mathbf{C})$$

where

$$\mathbf{v}(\mathbf{C}) = \mathbf{C} - \mathbf{C}_0$$

we may then define the *Lie bracket,* $\mathbf{z}^{[1]}(\mathbf{C})$, in terms of $\mathbf{f}(\mathbf{C})$ and $\mathbf{v}(\mathbf{C})$

$$\begin{aligned} \mathbf{z}^{[1]}(\mathbf{C}) &= [\mathbf{f}(\mathbf{C}), \mathbf{v}(\mathbf{C})] \\ &= \mathrm{d}\mathbf{v}(\mathbf{C})\,\mathbf{f}(\mathbf{C}) - \mathrm{d}\mathbf{f}(\mathbf{C})\,\mathbf{v}(\mathbf{C}) \end{aligned}$$

where $\mathrm{d}\mathbf{f}(\mathbf{C})$, $\mathrm{d}\mathbf{v}(\mathbf{C})$ and $\mathrm{d}\mathbf{z}^{[i]}(\mathbf{C})$ are the Jacobians of vector functions $\mathbf{f}(\mathbf{C})$, $\mathbf{v}(\mathbf{C})$ and $\mathbf{z}^{[i]}(\mathbf{C})$, respectively. From this we may define iterated Lie brackets

$$\mathbf{z}^{[2]}(\mathbf{C}) = \left[\mathbf{f}(\mathbf{C}), \mathbf{z}^{[1]}(\mathbf{C})\right]$$

$$= \quad \mathrm{d}\mathbf{z}^{[1]}(\mathbf{C})\,\mathbf{f}(\mathbf{C}) - \mathrm{d}\mathbf{f}(\mathbf{C})\,\mathbf{z}^{[1]}(\mathbf{C})$$

which may be generalised in a recursive fashion

$$\begin{aligned}\mathbf{z}^{[k]}(\mathbf{C}) &= \left[\mathbf{f}(\mathbf{C}), \mathbf{z}^{[k-1]}(\mathbf{C})\right] \\ &= \mathrm{d}\mathbf{z}^{[k-1]}(\mathbf{C})\,\mathbf{f}(\mathbf{C}) - \mathrm{d}\mathbf{f}(\mathbf{C})\,\mathbf{z}^{[k-1]}(\mathbf{C})\end{aligned}$$

It is then possible to show that for a DSR to produce effluent concentrations that reside on the AR boundary, vectors $\left\{\mathbf{f}(\mathbf{C}), \mathbf{v}(\mathbf{C}), \mathbf{z}^{[1]}(\mathbf{C}), \ldots, \mathbf{z}^{[k]}(\mathbf{C})\right\}$ must be linearly *dependent*. In practice, this is achieved by computing the determinant of the matrix whose columns are composed of the above vectors as well as vectors forming an orthogonal basis to the stoichiometric subspace S, and setting the resulting expression to zero:

$$\mathrm{Det}\left[\mathbf{f}(\mathbf{C}), \mathbf{v}(\mathbf{C}), \mathbf{z}^{[1]}(\mathbf{C}), \mathbf{z}^{[2]}, \ldots, \mathbf{z}^{[k]}, \mathbf{N}\right] = 0 \tag{2.4.2}$$

Here, $\mathbf{N}$ is a matrix containing columns orthogonal to S. Note that we only provide these definitions here for completeness. A detailed description of the procedure, with worked examples, can again be found in (Feinberg, 2000b). Even if we do not wish to know specific details of the method, it is still possible to understand the general procedure: observe that eq 2.4.2 is in fact a function of α. Solution and rearrangement of eq 2.4.2 may then be used to determine a critical α policy corresponding to a critical DSR.

An important consequence of the fact that critical DSR trajectories must lie entirely on the AR boundary is that these trajectories must then also originate on the boundary. Thus points on the true AR boundary must be used as starting points for critical DSRs. This places a large constraint on the number of possible initiating points for critical DSR trajectories. Furthermore, the side-stream concentration $\mathbf{C}_0$ is also specialised. Similar to starting points of critical trajectories, $\mathbf{C}_0$ must also be sourced from extreme points on the AR boundary. This again places a limitation on the possible side-stream concentrations used in critical DSRs, and raises questions as to how one should search for these during construction, when the full AR has not been identified yet. In practice, the value of $\mathbf{C}_0$ is often taken to be the same of the feed point $\mathbf{C}_0 = \mathbf{C}_\mathbf{f}$.

Critical CSTRs

The above control arguments may now be extended to include critical CSTRs. Suppose that a CSTR is available that produces effluent concentrations on the AR boundary (it is a critical CSTR). If a DSR is connected in series directly after the CSTR, then the DSR must also start on the AR boundary. In order for the DSR to also be critical, it's trajectory must satisfy eq 2.4.2. This provides a link for

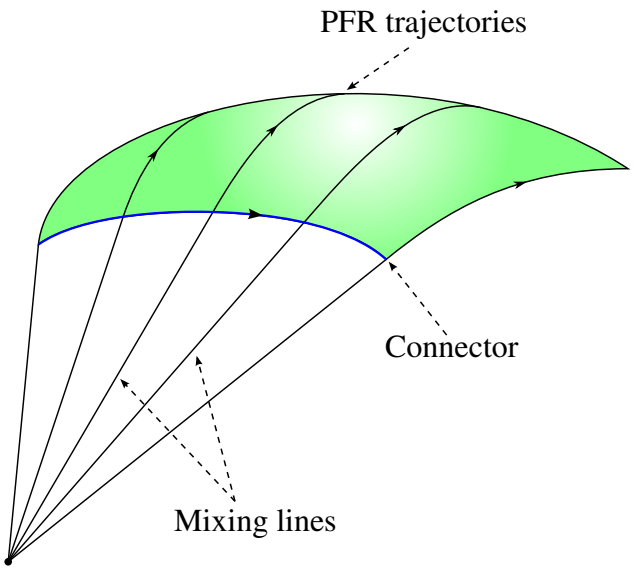


Figure 2.4.1: Connectors

how a critical CSTR condition may be calculated. Certainly, a critical CSTR must satisfy the same controllability criteria as a critical DSR, for otherwise the above arrangement would not produce concentrations on the AR boundary.

Feinberg (2000a) demonstrates how a condition similar to that given for critical DSRs may be formed. In particular, the condition for a critical CSTR also follows a determinant calculation of the following form

$$\begin{aligned} \Lambda(\mathbf{C}) &= \mathrm{Det}\left[\mathbf{v}(\mathbf{C}), \mathrm{d}\mathbf{r}(\mathbf{C})\,\mathbf{v}(\mathbf{C}), (\mathrm{d}\mathbf{r}(\mathbf{C}))^2\,\mathbf{v}(\mathbf{C}), \ldots, (\mathrm{d}\mathbf{r}(\mathbf{C}))^{k-1}\,\mathbf{v}(\mathbf{C}), \mathbf{N}\right] \\ &= 0 \end{aligned} \tag{2.4.3a}$$

substitution of the CSTR equation and rearrangement gives an equivalent expression written only in terms of $\mathbf{r}(\mathbf{C})$

$$\begin{aligned} \Lambda(\mathbf{C}) &= \mathrm{Det}\left[\mathbf{r}(\mathbf{C}), \mathrm{d}\mathbf{r}(\mathbf{C})\,\mathbf{r}(\mathbf{C}), (\mathrm{d}\mathbf{r}(\mathbf{C}))^2\,\mathbf{r}(\mathbf{C}), \ldots, (\mathrm{d}\mathbf{r}(\mathbf{C}))^{k-1}\,\mathbf{r}(\mathbf{C}), \mathbf{N}\right] \\ &= 0 \end{aligned} \tag{2.4.3b}$$

Eq 2.4.3b is particularly useful because it does not involve $\mathbf{C}_0$, which is often unknown in practice. Eq 2.4.3a describes a surface in $\mathbb{R}^n$ that critical CSTRs must satisfy. Whereas a critical DSR must adhere to eq 2.4.2 throughout its entire integration range, critical CSTR effluent compositions for the equivalent relation given by eq 2.4.3a will only be satisfied at distinct points. It is convenient then to envision the locus of CSTR points piercing the surface described by eq 2.4.3a only at distinct points. Intersection points with the surface are those that form part of the AR boundary, for these satisfy the controllability requirements of connectors. Figure 2.4.2 shows this graphically. Again, further details can be found in (Feinberg,

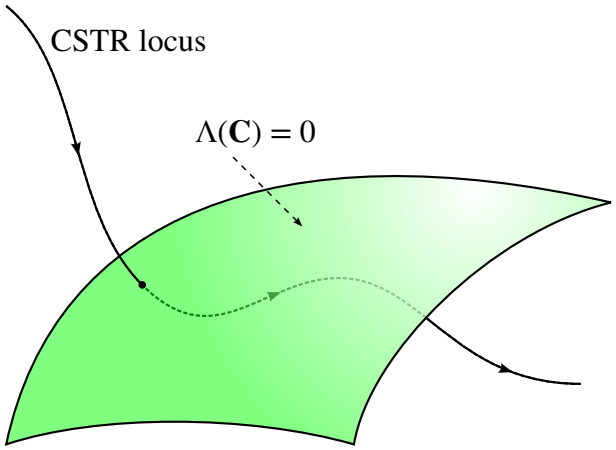


Figure 2.4.2: Critical CSTRs

2000a).

Comment Even though it is possible to compute distinct conditions for critical reactors, their analytic determination is challenging, involving determinant calculations of repeated iterated Lie Brackets formed from higher derivatives of $\mathbf{f}(\mathbf{C})$ and $\mathbf{v}(\mathbf{C})$. Although these conditions are distinct and well defined, their nature brings into the question the robustness of the rate expressions themselves employed to model the system. Indeed, for many systems of interest, analytic determination of these profiles is intractable and thus we must rely on alternate means for approximating the AR, mostly via *numerical* computation.

2.4.5 Simplifications for $\mathbb{R}^3$

In the previous section, we discussed how it is possible to determine concrete conditions for critical DSRs that may be used to synthesise an associated critical α policy. Although these conditions become increasingly complex in higher dimensions, an alternative (simpler) method for computing critical α policies exists specifically for three-dimensional systems. This is discussed in (Glasser and Hildebrandt, 1997). In particular, it can be shown that the function

$$\varphi(\mathbf{C}) = [\mathrm{d}\mathbf{r}(\mathbf{C})(\mathbf{C}_0 - \mathbf{C})]^{\mathrm{T}} [(\mathbf{C}_0 - \mathbf{C}) \times \mathbf{r}(\mathbf{C})]$$

where $\times$ is the vector cross product, satisfies conditions for a critical DSR trajectory when the value of α can be coordinated so as to maintain $\varphi(\mathbf{C}) = 0$ along the entire trajectory. This leads to the following condition

$$[\nabla\varphi(\mathbf{C})]^{\mathrm{T}} \frac{\mathrm{d}\mathbf{C}}{\mathrm{d}\tau} = 0$$

where $\nabla\varphi(\mathbf{C})$ is the gradient of the scalar function $\varphi(\mathbf{C})$, and $\mathrm{d}\mathbf{C}/\mathrm{d}\tau$ is the vector differential equation describing the DSR expression. Substituting eq 2.3.3 and further simplification leads to an explicit expression for α

$$\alpha = -\frac{[\nabla\varphi(\mathbf{C})]^{\mathrm{T}}\,\mathbf{r}(\mathbf{C})}{[\nabla\varphi(\mathbf{C})]^{\mathrm{T}}\,(\mathbf{C}_0 - \mathbf{C})} \tag{2.4.4}$$

The scalar function given by eq 2.4.4 represents a critical α policy for systems in $\mathbb{R}^3$ specifically. This result is commonly referred to as the 'VdelR' condition.

2.5 AR construction from fundamental processes

Once the fundamental process vectors of reaction and mixing are known, AR construction may begin. By optimal structures, we mean the reactor configurations that are able to expand the region of attainable points in the greatest manner possible. The convex hull of these points is then the AR. Since all interior points can be achieved by mixing, only boundary points are required to achieve all points in the region. Hence, the task of finding the AR reduces to finding the unique set of structures that form its boundary. The solution to subsequent optimisation problems thus only involves combinations of these optimal structures with mixing.

2.5.1 General procedure for constructing the AR

Unless the system kinetics under consideration is simple, AR construction is currently still not straightforward, requiring previous AR knowledge and construction experience. In general, a fair amount of time and skill is involved whenever the AR for a system is to be determined. AR practitioners often spend a large amount of time visualising and interpreting the AR boundary to identify sections for how to expand the candidate region further. Nevertheless, even if the full AR cannot be determined, it is always possible to generate a candidate region representing a large portion of the true AR. Although analytic determination of the AR is difficult, this does not prohibit the practice of a generalised, common-sense, approach to AR construction. Indeed, all constructions generally follow a similar procedure, even if the final polytope is substantially different. A typical construction procedure is provided below as a guideline for how one might generate at least a candidate AR.

Specify system kinetics and feed point (or convex hull of feed points) Since the AR is defined in terms of its kinetics and feed point, these must both be initially specified. The system of reactions must be known along with the reaction stoichiometry. Specification of the feed point is usually determined by economic or operating constraints. If there are more than one feed points available, then the convex hull of all feed points is used as the initial candidate AR.

Determine dimension of problem and (optional) stoichiometric subspace. From the reaction stoichiometry and feed point, it is possible to compute the dimension of the problem by calculating the rank of the stoichiometric coefficient matrix **A**. This determines the complexity of the solution procedure: 2D problems will not require DSRs or the calculation of critical reactors, 3D problems may exploit the 'VdelR' condition of section 2.4.5 to determine critical α policies easier, and higher dimensional problems will need to be visualised as projections onto different component spaces in $\mathbb{R}^2$ and $\mathbb{R}^3$.

It is also advantageous to compute the stoichiometric subspace from the reaction stoichiometry and feed point. This establishes limits in space in which the AR is known to reside that may guide the search for other reactor structures that extend the region.

Generate PFR trajectories and CSTR locus from the feed The simplest method for expanding the initial set of achievable concentrations is to determine the PFR trajectory and CSTR locus from the feed points. Solving the PFR is determined by integration of a system of ordinary differential equations whereas the CSTR locus involves the solution of a system on non-linear equations. Depending on the complexity of the rate expressions, multiple CSTR steady-states may exist that will also need to be accounted for. Otherwise, the full set of achievable concentrations may not be discovered. Under certain reactions, the PFR trajectory may be completely convex, indicating that a PFR from the feed is the optimal reactor structure. In this case, construction may be terminated here as the convex hull of the PFR trajectory corresponds to the true AR. This situation, although seemingly rare, is observed for linear kinetics (Glasser and Horn, 1980).

Every point on the CSTR locus may be used as an initiating point for a PFR trajectory. From section 2.4.3, it is known that PFR trajectories make up the final extreme points of the AR and therefore it is sensible to always include PFRs as the final reactor type. Thus PFR trajectories may be generated from all CSTR points. Once this has been achieved, the convex hull associated with the PFR trajectories and CSTR from the feed may be computed with a standard convex hull algorithm. The resulting polytope generally constitutes a reasonable first approximation to the AR.

Inspect the boundary for expansion The convex polytope resulting from PFR trajectories and CSTR points may now be checked for possible extensions. For two-dimensional systems, it is convenient to plot the rate field and overlay it onto the region. In this way, we are able to visually inspect the candidate region for any possible rate vectors pointing out of the boundary. For higher dimensions, it may be possible to visualise sections of the boundary and plot rate vectors in a similar manner, however manipulation, visualisation and interpretation of the data

is inherently more complex. Nevertheless, if rate vectors on the boundary can be found that point out of the region, then the region may be extended further with PFR trajectories from those particular boundary points. If it is difficult to inspect rate vectors on the boundary, then an attempt should be made to expand the region by use of DSR trajectories.

Compute the critical α policy For systems involving three or more independent reactions, the AR boundary may be composed of reactor structures containing critical DSRs. The guidelines discussed in section 2.4.4 may be followed to compute critical α policies that may form part of the AR boundary. These expressions involve the evaluation and solution of iterated Lie brackets which, depending on the complexity of the rate expression and dimension of the system, may allow for an analytic expression for the critical α policy. For systems specifically cast in $\mathbb{R}^3$, the critical α policy may be determined by use of the 'VdelR' condition instead. The particular expression obtained for α will depend on the side-stream composition $\mathbf{C}_0$ specified. As already mentioned, $\mathbf{C}_0$ must originate from a point on the true AR boundary which may be difficult to know seeing as this precludes determination of the AR. In practice we often use $\mathbf{C}_0 = \mathbf{C_f}$.

Once an expression for the critical α policy has been found, it can be substituted into the DSR expression and integrated given an appropriate initial condition. Initial points of integration for critical DSR trajectories are again constrained to lie on the true AR boundary, which is unknown up to this point. The feed set and equilibrium points from the CSTR locus and PFR trajectories are typically utilised in practice.

Compute the critical CSTR surface $\Lambda(\mathbf{C}) = 0$ Connectors on the AR boundary might also arise from critical CSTR effluent compositions. Thus, determination of the critical CSTR surface described by $\Lambda(\mathbf{C}) = 0$ may also help to expand the region. Eq 2.4.3b can be solved and plotted resulting in a surface in $\mathbb{R}^n$. Eq 2.4.3b is often employed over eq 2.4.3a seeing as it does not involve specification of $\mathbf{C}_0$, which is also unknown. CSTR solutions that intersect the surface generated by eq 2.4.3b are then critical CSTR solutions.

PFR trajectories from critical reactor solutions PFRs initiated from the critical reactor effluent concentrations are special as these form part of the true AR boundary. The resulting region generated by computing the convex hull of all points generate up to this point represents a good approximation to the AR. Depending on whether the above steps are followed to completion, there may still exist points that could expand the region further - often regions are obtained that satisfy all AR properties but which are not the true AR dues to multiple CSTR steady-states. Again, analytic determination of the AR is often difficult, requiring many visualisation and boundary interpretation steps in order to obtain a sense of

whether the candidate region is complete.

2.5.2 Remarks

We can see that although it is possible produce a candidate AR analytically, it's determination requires a large amount of time and calculation. The need for automated AR construction methods is necessary, particularly for higher dimensional problems. In theory, once numerical AR construction is complete, the optimal reactor structures can also be found by back calculation. In practice however, AR construction will often only provide the region. The optimal structure will not be known in this case. AR construction methods usually fall into one of two categories.

1. Inside-out methods attempt to construct the AR from the feed point and grow the set of attainable points outwards. Once these points have been found, the optimal reactor structures are also known.

2. Outside-in methods begin by enclosing the AR within a larger region and then removing unattainable regions. Outside-in methods are generally more robust and are able to handle complex kinetics easier. These methods do not provide the reactor structures however.

Thus, even though the AR serves to determine the optimal reactor structures for a given system, construction is usually done through geometric interpretation of the fundamental process and not through an actual simulation of proposed optimal reactors. It is generally difficult to relate these properties back to a physical reactor structure. This is different to if AR construction is determined via the analytic guidelines described above, in which the region and optimal reactor structure is generated simultaneously. Nevertheless, even if the optimal reactor is unknown, or if the structure is completely impractical, the AR still provides the absolute limits of achievability. Knowledge of these limits allows for the establishment of performance benchmarks that can be used compare our current designs with.

2.6 On non-isothermal and heterogeneous systems

Although the AR has historically been developed with continuous, isothermal, constant density systems in mind, it is possible to relax these constraints.

2.6.1 Variable density systems

Notation

When density is not constant, the linear mixing laws developed in section 2.2.3 in terms of concentration are no longer applicable. Many reactions of industrial importance occur in the gas phase, or amongst heterogeneous reaction environments.

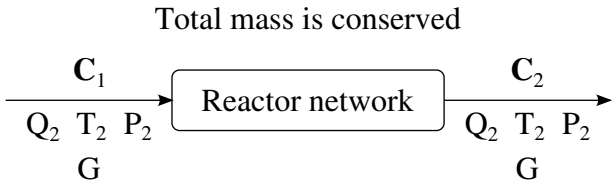


Figure 2.6.1: Overall viewpoint for variable density systems

In these situations, it is no longer possible to generate the AR in concentration space. AR theory may still be utilised for these systems, however certain necessary transformations must be undertaken in order to honour the linear mixing property that underpins the convex nature of candidate ARs. Rather than use concentrations, we must use mass fractions instead.

Consider Figure 2.6.1 which represents the overall reactor network for a variable density system. A stream containing n components is fed into a reactor network at a total volumetric flow rate of Q_1. The effluent stream leaving the network is at a total volumetric flow rate Q_2. Since the system is no longer assumed to obey the constant density assumption, $\mathrm{Q}_1 \neq \mathrm{Q}_2$. We use the symbol G to signify the total mass flow rate of a stream, whereas g_i signifies the component mass flow rate of i within a mixture. The total mass flow rate is then found as the sum of all component mass flows in the stream:

$$\mathrm{G} = \sum_{i=1}^{n} \mathrm{g}_i$$

Since mass is always conserved, the total mass flow of material in stream in Figure 2.6.1 is equal to the total mass flow in stream 2, or $\mathrm{G}_1 = \mathrm{G}_2 = \mathrm{G}$.

Mass fraction vector z

The mass fraction of component i, z_i, in a stream with a total mass flow G is defined as

$$z_i = \mathrm{g}_i/\mathrm{G}$$

z_i may be similarly defined for batch systems in terms of the mass of component i, m_i, and the total mass of the system, m_{tot}:

$$z_i = m_i/m_{\mathrm{tot}}$$

if n components are present in the system, then n mass fractions exist. Only $n-1$ mass fractions are independent, since all mass fractions in the system must sum to unity

$$\sum_{i=1}^{n} z_i = 1$$

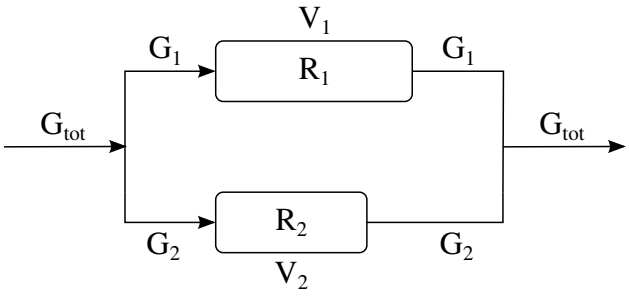


Figure 2.6.2: Hypothetical reactor for mixing mass fractions

The mass fraction vector, $\mathbf{z}$, is then defined in a similar manner to the concentration vector $\mathbf{C}$ as follows

$$\mathbf{z} = [z_1,\, z_2, \ldots,\, z_n]^{\mathrm{T}}$$

For any mixture containing n species, we may associate the mixture with a mass fraction vector $\mathbf{z}$. From a geometric viewpoint, $\mathbf{z}$ is the vector in $\mathbb{R}^n$ mass fraction space associated with a unique magnitude and direction.

Mixing

Similar to section 2.2.3, suppose that two streams with total masses G_1 and G_2 are brought into contact with each other, as given in Figure 2.6.2. The compositions of mixtures 1 and 2 may be expressed in terms of mass fraction vectors $\mathbf{z}_1$and $\mathbf{z}_2$, respectively. The total mass of the mixture is then $\mathrm{G}_{\mathrm{tot}} = \mathrm{G}_1 + \mathrm{G}_2$ and it is possible to write each species as the sum of each mixture in the following way

$$\mathbf{z}^* \mathrm{G}_{\mathrm{tot}} = \mathbf{z}_1 \mathrm{G}_1 + \mathbf{z}_2 \mathrm{G}_2$$

Dividing through by $\mathrm{G}_{\mathrm{tot}}$ and making the substitution $\lambda = \mathrm{G}_1/\mathrm{G}_{\mathrm{tot}}$ then gives

$$\mathbf{z}^* = \lambda \mathbf{z}_1 + (1 - \lambda)\, \mathbf{z}_2$$

which is identical in form to eq 2.2.1. Observe that this expression does not rely on the constant density assumption and thus it is useful for variable density systems. ARs are then generated in mass fraction space as opposed to concentration space. It can be shown how molar quantities, such as moles, concentration and mole fraction, may all be written as functions involving the species mass fractions and molar masses. In the case of concentration, an appropriate equation of state must be employed to relate the system density to composition, often in terms of process variables such as reactor temperature and pressure. Analogous quantities for residence time may also be developed involving mass fractions as well.

2.6.2 Temperature and other parameters

Although variable density systems may be accommodated for by use of mass fractions, the nonlinear nature of the energy balance means that analytically expressing temperature in terms of concentration generally does not result in a linear expression. Unless simplifying assumptions can be made, this means that temperature does not generally obey a linear mixing law. It it hence generally not possible to construct an AR with temperature as one of the axes. We are hence forced to incorporate temperature via a different route. If the system is non-isothermal, the general approach is to express the kinetics in terms of a temperature parameter. We may hence rewrite the rate vector to be a function of both the concentration vector $\mathbf{C}$ and the system temperature T, as $\mathbf{r}(\mathbf{C}, \mathrm{T})$. If the energy balance allows for the determination of T in terms of concentration, an expression of the form $\mathrm{T} = \mathrm{T}(\mathbf{C})$ is available. This may be substituted into the rate expression with the overall effect of creating a newer (more complex) rate expression incorporating temperature $\mathbf{r}(\mathbf{C}, \mathrm{T}(\mathbf{C})) = \mathbf{r}(\mathbf{C})$. AR generation then follows a conventional construction procedure. Substitutions of this type are common when the kinetics are expressed in an Arrhenius form, by example. An example of this is shown in chapter 3.

If temperature cannot be isolated and expressed in this way, then it is still possible to incorporate temperature by treating T as an extra control parameter in the rate field over a temperature range. For non-isothermal systems, every point i in concentration space may take on a range of temperature values T_i specified by the designer $\mathrm{T}_{\min} \leq \mathrm{T}_i \leq \mathrm{T}_{\max}$. Hence, the resulting rate vector is spanned by the values of T_i and the geometric interpretation follows a situation similar to that of Figure 2.3.4. Optimal control strategies may then be developed that seek to determine the optimal temperature profile that traverses the AR boundary (Godorr et al., 1994, 1999). In this way, heating and cooling equipment may also be incorporated into the AR construction, with optimal reactor networks incorporating external heating or cooling (Nicol et al., 1997, 2001).

This methodology is applicable to any kinetics in which the particular process variable can be parametrised in this manner. As such, heterogeneous/catalytic systems might be incorporated in this way, although this has not been attempted currently. Catalytic systems that follow the pseudo homogeneous and pseudo steady-state assumptions are treated much like the temperature case: developing a suitable rate expression involving interphase transport directly into the kinetics (even if the underlying rate expression may be rather complex). In the situation that the kinetics do not allow for this (where mass transfer may limit the reaction rate), then the rate vector may again be expressed in terms of the spatial concentration vector and a local mass transfer gradient at that point. The solution might then follow a similar procedure to that for concentration.

2.7 Conclusion

In this chapter, we reviewed some of the basic theory associated with Attainable Regions. We saw that by interpretation of the basic processes of reaction and mixing, one is able to construct a region in space that represents the attainable set of outcomes from a given reactor structure. This is the true benefit of the AR. The AR not only allows one to gain more information into the limits of achievability, the reactor structure associated with this limit can also be determined at the same time. Optimisation of the problem is carried out first by determining the best structure in this sense. This is often overlooked as most optimisations rely on the improvement of a object function based on a *fixed* structure.

The idea of mixing will come up often in this text, and it is important to mention it here. Mixing allows one to fill in concavities in concentration space and turn curved line segments into filled areas or regions. When concavities are present, mixing also allows us to obtain new concentrations or states by mixing between two concave points. These points might then foreseeably be used as starting points from which new structures could be formed. Again, the use of mixing allows one to exploit the inherent structure of the problem and improve the performance of the system. This is only generally observed when there is a nonlinearity (specifically a concavity) in the solution trajectory. In the next chapter this idea will be used and applied to a common production problem in a batch environment. Specifically, this will entail improving the production rate of a batch reactor by mixing feed material with final product.

References

Feinberg, M., 1999. Recent results in optimal reactor synthesis via attainable region theory. Chemical Engineering Science 54 (13-14), 2535–2543.

Feinberg, M., 2000a. Optimal reactor design from a geometric viewpoint - iii. critical cfstrs. Chemical Engineering Science 55 (17), 3553–3565.

Feinberg, M., 2000b. Optimal reactor design from a geometric viewpoint. part ii. critical sidestream reactors. Chemical Engineering Science 55 (13), 2455–2479.

Feinberg, M., Hildebrandt, D., 1997. Optimal reactor design from a geometric viewpoint- i. universal properties of the attainable region. Chemical Engineering Science 52 (10), 1637–1665.

Geankoplis, C. J., March 1993. Transport Processes and Unit Operations, 3rd Edition. Prentice Hall PTR.

Glasser, D., Hildebrandt, D., 1997. Reactor and process synthesis. Computers & Chemical Engineering 21 (Supplement 1), S775–S783.

Glasser, D., Hildebrandt, D., Godorr, S., 1994. The attainable region for segregated,

maximum mixed, and other reactor models. Industrial & Engineering Chemistry Research 33 (5), 1136–1144.

Glasser, D., Horn, F., 1980. The response of linear cascades to variations of holding times. Chemical Engineering Science 35 (11), 2281–2285.

Godorr, S., Hildebrandt, D., Glasser, D., McGregor, C., 1999. Choosing optimal control policies using the attainable region approach. Industrial & Engineering Chemistry Research 38 (3), 639–651.

Godorr, S. A., Hildebrandt, D., Glasser, D., 1994. The attainable region for systems with mixing and multiple-rate processes: finding optimal reactor structures. The Chemical Engineering Journal and The Biochemical Engineering Journal 54 (3), 175–186.

Hildebrandt, D., October 1989. The attainable region generated by reaction and mixing. Ph.D. thesis, University of the Witwatersrand, Johannesburg.

Hildebrandt, D., Glasser, D., 1990. The attainable region and optimal reactor structures. Chemical Engineering Science 45 (8), 2161–2168.

Hildebrandt, D., Glasser, D., Crowe, C. M., 1990. Geometry of the attainable region generated by reaction and mixing: With and without constraints. Industrial & Engineering Chemistry Research 29 (1), 49–58.

Nicol, W., Hernier, M., Hildebrant, D., Glasser, D., 2001. The attainable region and process synthesis: Reaction systems with external cooling and heating. the effect of relative cost of reactor volume to heat exchange area on the optimal process layout. Chemical Engineering Science 56 (1), 173–191.

Nicol, W., Hildebrandt, D., Glasser, D., 1997. Process synthesis for reaction systems with cooling via finding the attainable region. Computers & Chemical Engineering 21 (Supplement 1), S35–S40.

Chapter 3

Graphically improving batch production rate

The following chapter has been adapted from published work with permission. The associated paper is (Ming, D., Hildebrandt, D., Glasser, D., 2012. A Graphical Method of Improving the Production Rate from Batch Reactors. Ind. Eng. Chem. Res. 51, 13562–13573.) Copyright (2012) American Chemical Society. D. Ming (the present author) compiled the manuscript and contributed to the ideas in this work. D. Hildebrandt and D. Glasser supervised this work.

3.1 Introduction

In this work, we shall be concerned with graphically identifying opportunities for improvement, particularly through batch structure. Although similar aims have been developed in the past, these techniques are often complex and mathematical in nature (such as superstructure approaches), which make it difficult for someone without the appropriate knowledge or resources to carry out. The work described here then, may be viewed to fit within the larger framework of batch process synthesis as a dedicated graphical approach to the improvement of batch reactors. In particular, we shall be concerned with maximising the production rate for a desired final product concentration. We will aim to demonstrate, that by graphical interpretation of the reaction profile, opportunities for improving production rate may be identified.

The organisation of the chapter is as follows: discussion of the method will be given by way of an illustrative example, beginning in section 3.2, and followed on in section 3.3. Examples demonstrating the technique are then provided in section 3.4. Remarks regarding operational considerations are given in section 3.5, before conclusions are provided in section 3.6. We shall summarise important results and observations throughout the discussion when appropriate.

3.2 Standard batch operation

3.2.1 Problem formulation

We begin our discussion with the following autocatalytic reaction

$$\mathrm{A} + \mathrm{B} \rightarrow 2\mathrm{B}$$

For convenience, we shall assume constant density and isothermal operation so that the change in the concentration of component B, c_{B}, under standard batch operation is modelled by

$$\frac{\mathrm{d}c_{\mathrm{B}}}{\mathrm{dt}} = r_{\mathrm{B}} \tag{3.2.1}$$

By standard batch operation, we mean that an empty reactor vessel is charged with feed material of concentration c_i^0 and filled to a volume $\mathrm{V_{tot}}$. The vessel is then given time $\Delta \mathrm{t}_0$ to react, after which, the entire contents are removed thus ending the batch cycle. The corresponding final concentration is denoted by c_i. The next cycle is again charged with feed material, and the procedure is repeated until a desired total amount of product is produced. Note that no restriction regarding operating variables such as temperature, pressure and density are made in our interpretation of the standard batch. In this example, the rate of formation of component B, r_{B}, is second order overall and expressed in terms of both components

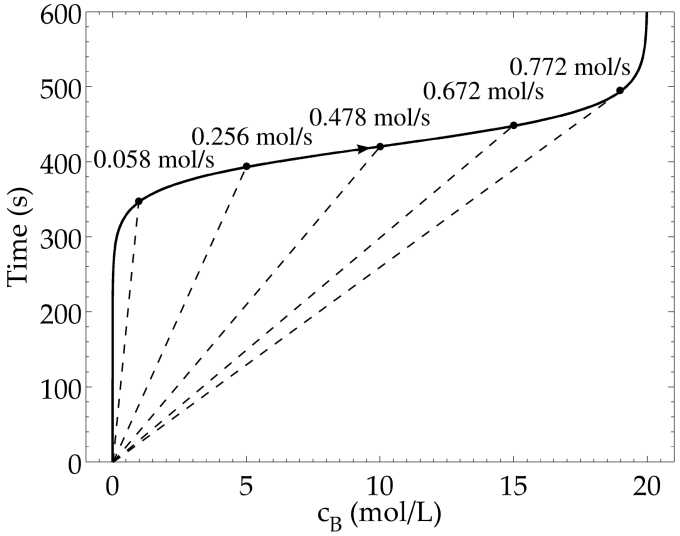
$$r_{\mathrm{B}} = k c_{\mathrm{A}}^0 \left(1 - x\right) \left(c_{\mathrm{B}}^0 + c_{\mathrm{A}}^0 x\right)$$

Concentrations are expressed in terms of the conversion of reaction, x, such that x may take on values between 0 (no reaction) and 1 (complete reaction). The rate constant is given as $k = 2 \times 10^{-3}\,\mathrm{L}/\left(\mathrm{mol} \cdot \mathrm{s}\right)$. Initial concentrations are specified as $c_{\mathrm{A}}^0 = 20\,\mathrm{mol/L}$ and $c_{\mathrm{B}}^0 = 1 \times 10^{-6}\,\mathrm{mol/L}$ respectively and $\mathrm{V_{tot}} = 20\,\mathrm{L}$. Integration of eq 3.2.1 produces the profile in Figure 3.2.1a in c_{B}–time space. Similar to the residence time AR plots highlighted in the chapter 2, batch reaction time is placed on the y-axis. Note that the shape of the profile is attributed to the rise and fall of the reaction rate, as a quadratic function of x.

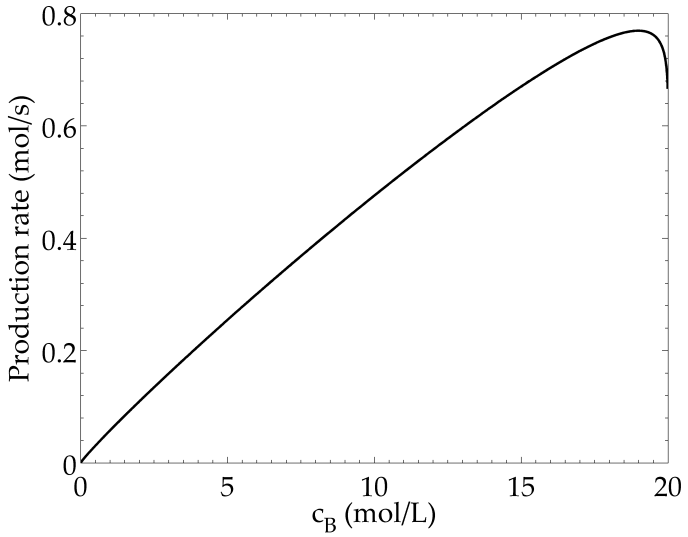
The production rate, P, for a single batch cycle is then defined as follows

$$\mathrm{P} = \frac{\mathrm{V_{tot}} \left(c_{\mathrm{B}} - c_{\mathrm{B}}^0\right)}{\Delta \mathrm{t}_0} \tag{3.2.2}$$

where $\Delta \mathrm{t}_0 = \mathrm{t}\left(c_{\mathrm{B}}\right) - \mathrm{t}\left(c_{\mathrm{B}}^0\right)$. Although batch reactors do not operate continuously, it is still possible to determine the rate of production over the entire batch period involving multiple reaction cycles. We assume that the time taken to empty and fill the vessel is small in relation to the reaction time, and so the entire cycle period is made up exclusively by the reaction time. This assumption can be relaxed without significant modification to the proposed method, or the results (see section 3.5). The



(a) Graphical interpretation of production rates, achieved in the standard batch, for different exit concentrations. Specifying a final concentration results in a unique line gradient and production rate (given here by the dotted lines). The solid curve is the batch profile obtained by integration of the batch equation for the system specified.



(b) Production rate in the standard batch as a function of product concentration. A single maximum of ~ 0.78 mol/s is observed. This is achievable by operating the reactor at an exit concentration of ~ 19 mol/L.

Figure 3.2.1: Standard batch production rate and graphical interpretation

overall production rate for a standard batch over multiple cycles is thus identical to the production rate for a single batch reaction.

Figure 3.2.1a also shows the production rate for various exit conditions marked off as coordinate points. When the two points are joined, the gradient of the straight line segment is $m = \mathrm{t}_0/\left(c_\mathrm{B} - c_\mathrm{B}^0\right)$ and, according to eq 3.2.2, is proportional to the inverse of the production rate $\mathrm{P} = \mathrm{V}_\mathrm{tot}/m$. The rate of production is therefore at its highest when the gradient of the line is minimised.

Observation 1: Production rate can be associated with a straight line in concentration – time space. This value is highest when the gradient of the line is minimised.

3.2.2 Initial observations and modifications

Let us observe the effect of mixing product with feed for subsequent cycles. The following conditions will be assumed for purposes of illustration:

- The exit concentration of component B is fixed at $c_\mathrm{B} = 19.0\,\mathrm{mol/L}$.
- The starting mixture concentration of component B is $c_\mathrm{B}^* = 1.5\,\mathrm{mol/L}$. By mass balance, it is found that ∼7.89 % of the product volume must be retained in order to achieve the desired mixture concentration. The corresponding concentration of component A is then calculated to be 18.5 mol/L accordingly. The corresponding reaction time for the new initial condition is then 136 s.

The order of tasks is then as follows:

1. Run a standard batch with initial concentrations of $c_\mathrm{A}^0 = 20\,\mathrm{mol/L}$ and $c_\mathrm{B}^0 = 1 \times 10^{-6}\,\mathrm{mol/L}$ until the concentration of B is $c_\mathrm{B} = 19.0\,\mathrm{mol/L}$. Using Figure 3.2.1a or solving eq 3.2.1 directly, the reaction time for this cycle is found to be $\sim 492\,\mathrm{s}$.
2. Empty the contents of the vessel but retain 7.89% of the volume for the next cycle. If the vessel volume is 20 L, then approximately 1.578 L of product is held back; the remaining 18.422 L may then be transferred as product. Since 18.422 L of product is transferred, 350.018 mol of B is produced in the cycle.
3. Refill the vessel again to 20 L with fresh feed. That is, since 1.578 L of the vessel is already taken by the previous product, only 18.422 L of the feed is required. By mass balance, the concentrations of A and B in the vessel after filling are then $c_\mathrm{A}^* = 18.5\,\mathrm{mol/L}$ and $c_\mathrm{B}^* = 1.5\,\mathrm{mol/L}$, respectively.
4. Run the second cycle until the concentration of B again reaches $c_\mathrm{B} = 19.0\,\mathrm{mol/L}$. Since the starting concentration in this cycle differs to the first, the reaction time to reach final product is also different. Again, eq 3.2.1 can be solved giving a reaction time of 136 s for the second cycle.

Table 3.1: Production rate with mixing after four cycles for an exit concentration of $c_B = 19.0\,\text{mol/L}$ and 7.89 % of product retained for mixing. For each successive batch, the production rate is improved. By comparison, the production rate in the standard batch for the same exit concentration is fixed at $0.772\,\text{mol/s}$.

	Production per cycle (mol)					
Stages	i	ii	iii	iv	Total time (s)	Overall production rate (mol/s)
1	380	-	-	-	492	0.772
2	350.018	380	-	-	628	1.16
3	350.018	350.018	380	-	764	1.41
4	350.018	350.018	350.018	380	900	1.59

5. Repeat steps 2 to 4 until the desired amount of product is reached.

Table 3.1 summarises the results for four successive batches using this approach.

Notice that even though the amount of product produced per cycle is less (350.018 mol for 7.89% retained, as opposed to 380 mol for the full volume), the reaction times per cycle are decreased as a result of the different starting concentration. After sufficiently many batches, the effect of the first and last batch on the overall production rate is small, and hence the average production rate is influenced by the intermediate cycles, which for the specific scenario here is given by $\text{P}^* = 350.018/136\,\text{mol/s}$. We can then determine the limiting production rate after many batches as that given by the intermediate cycles. This production rate may also be represented graphically on the concentration profile. The final concentration is the same as that previously, however the initial point is modified to a new point on the profile, which is a function of the retained fraction. The straight line joining these two points in c-t space thus represents the steady state production rate for the retained case.

The gradient of the new line is shallower than the original, which by eq 3.2.2, indicates a higher production rate. By graphical interpretation, maximising the production rate for a specified exit concentration on the curve indicates searching for the starting concentration on the profile that is associated with the straight line having minimal gradient.

Inasmuch as the production rate for the standard batch can be expressed in terms of a line gradient, P^* is also expressible in this manner

$$\text{P}^* = \frac{\text{V}_{\text{tot}}}{m^*}$$

where $m^* = \Delta\text{t}^* / (c_i - c_i^*)$. The relative gain in production rate is thus also given in terms of line gradients by $(\text{P}^*/\text{P}) = (m/m^*)$. Thus, the results of this example indicate that the production rate in a standard batch may be improved by retaining

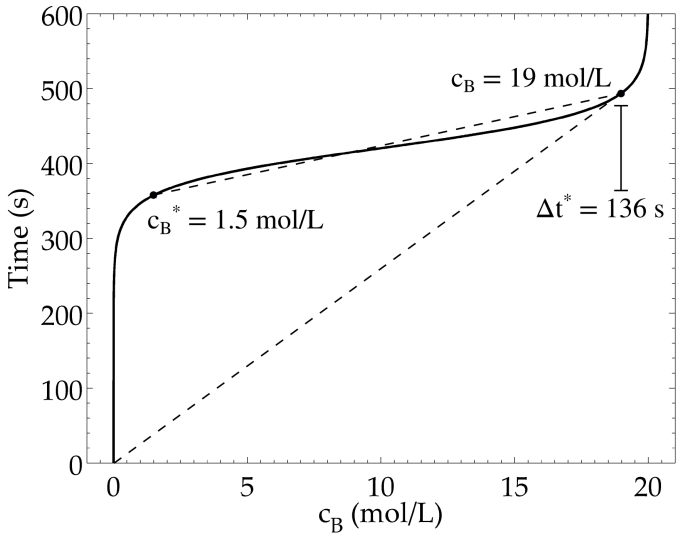


Figure 3.2.2: Comparing production rate lines for different initial concentrations

product. Intuitively, it is expected that if too much product is retained, then the reduction in time achieved may not be sufficient to overcome the loss of product that must be reserved, and production rate may drop as a result. For certain kinetics however, a drop in production rate is guaranteed for any amount of product retained. These factors are discussed below.

3.3 Improving production rate

3.3.1 Improvement 1: Partial emptying and filling

The results of section 3.2.2 are constructive in suggesting that improvements in production rate are feasible by use of a partial emptying and filling regime. Let us generalise the method for a component i by introducing preliminary notation. We begin by defining ϕ as the fraction of the total tank volume, $\mathrm{V_{tot}}$, that is retained in the batch cycle

$$\phi = \frac{\mathrm{V_{retained}}}{\mathrm{V_{tot}}}$$

The resulting (mixed) concentration, c_i^*, is then given by a linear mixing law

$$c_i^* = \phi c_i + (1 - \phi)\, c_i^0 \tag{3.3.1}$$

We have already observed that the production rate corresponding to partial emptying and filling, $\mathrm{P^*}$, approaches a limiting value after sufficiently many cycles. The average production rate over all cycles is then given by the production rate of the intermediate cycle

$$\mathrm{P^*} = \frac{\mathrm{V_{tot}}\,(c_i - c_i^*)}{\Delta \mathrm{t^*}} \tag{3.3.2a}$$

or

$$\mathrm{P}^* = \frac{(1-\phi)\,\mathrm{V_{tot}}\left(c_i - c_i^0\right)}{\Delta \mathrm{t}^*} \tag{3.3.2b}$$

where time $\Delta \mathrm{t}^*$ is the reaction time achieved from a batch concentration having been partially mixed with a fraction of the product volume, that is,

$$\Delta \mathrm{t}^* = \mathrm{t}\left(c_i\right) - \mathrm{t}\left(c_i^*\right)$$

$\mathrm{t}\left(c_i\right)$ and $\mathrm{t}\left(c_i^*\right)$ are the corresponding times on the batch profile where the concentration in the batch is equal to c_i and c_i^*, respectively. Whereas the production rate in eq 3.2.2 achieves a larger amount of product per cycle, it does so in a time equal to $\Delta \mathrm{t}_0$ given by initial and terminal concentrations

$$\Delta \mathrm{t}_0 = \mathrm{t}\left(c_i\right) - \mathrm{t}\left(c_i^0\right)$$

The production rate using partial filling, by comparison, may be achieved in a reaction time of $\Delta \mathrm{t}^*$ instead.

Using the batch profile

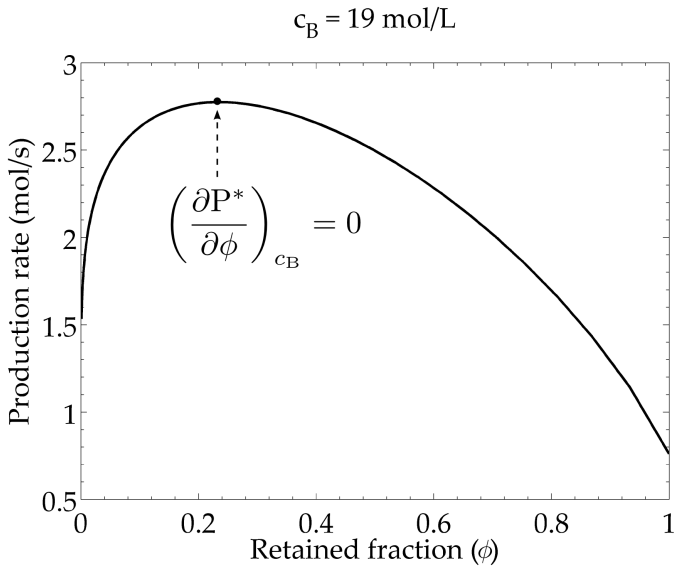
The production rate by partial emptying and filling is completely defined by specifying c_i^0, c_i and ϕ. As in section 3.3, this may be accomplished by generating the batch profile belonging to c_i^* and then obtaining $\Delta \mathrm{t}^*$ from the resulting curve. Observe however, that the profile belonging to c_i^* already exists as a section of the original batch curve – from eq 3.3.1, c_i^* must lie between c_i^0 and c_i by mass balance, and thus c_i^* represents an achievable state in the standard batch, after time $\Delta \mathrm{t}_0 - \Delta \mathrm{t}^*$. Therefore, the production rate with partial emptying and filing is equivalent to finding line gradients joining the two points on the original batch profile, however with respect to points c_i and c_i^*.

Observation 2: Only a single batch profile is needed in order to carry out computations involving partial emptying and filling.

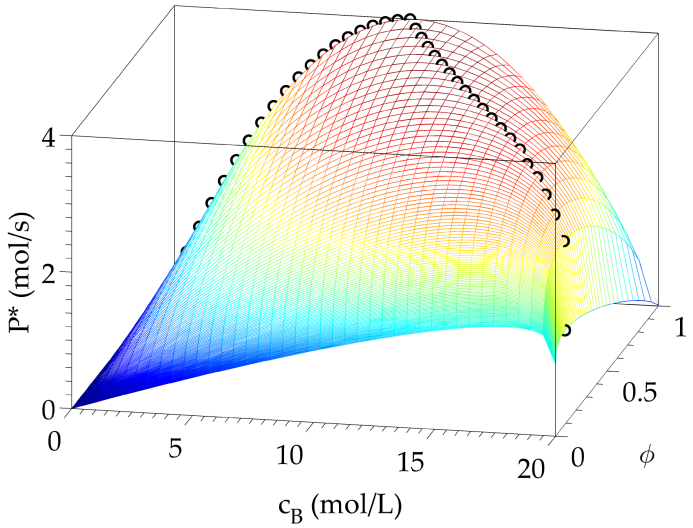
Optimising retained fraction

Production rate corresponding to partial emptying and filling is maximised by optimising eq 3.3.2b. Note that unlike eq 3.2.2, eq 3.3.2b is dependent on two parameters: the species exit concentration as well as the retained fraction. Plotting eq 3.3.2b as a function of ϕ for a fixed value of c_i produces a curve that may be used to find the optimal value of ϕ that maximises P^* for the c_i specified. Figure 3.3.1a demonstrates this for the autocatalytic system for an exit concentration of $c_\mathrm{B} = 19\,\mathrm{mol/L}$. Indeed, a surface can be constructed showing the influence of both c_i and ϕ on P^*; this is shown in Figure 3.3.1b.

There are hence two optima that we are generally interested in:



(a) Production rate as a function of ϕ for an arbitrary exit concentration



(b) Influence of production rate on exit concentration and ϕ

Figure 3.3.1: Production rate by partial emptying and filling

1. The global optimum, associated with the unique point on the surface with largest value of P^*. The global maximum is then found by determining specific values for both ϕ *and* c_i.

2. The maximum production rate achieved for a user-specified exit concentration. This value of P^* is given by an optimal retained fraction ϕ^{opt} that maximises P^* for a given value of c_i. In general, an optimal ϕ profile may then be determined that specifies the required retained fraction for maximum production at any value of c_i. This equivalent to taking a projection of Figure 3.3.1b onto the $c_i - \phi$ plane and marking off points in the space that correspond to the peaks of the surface. Figure 3.3.1b, these are shown as unfilled circles.

Limitations on ϕ

Although it is physically possible for ϕ take on any value between 0 and 1, it is unreasonable to retain particularly large fractions – in practice, c_i^* will be very close to c_i, and therefore Δt^* will be short. Consequently, many more emptying and filling operations may be required for a given desired amount of product. For values close to unity, the analysis would suggest running the reaction continuously. Even though this may be possible, our intention here will be focused towards batch improvement only.

Accordingly, Figure 3.3.2 shows the production rate as a function of final exit concentration for different (optimal) retained tank volume fractions. The value of ϕ corresponding to highest production rate is calculated by optimising the curve obtained in $P^* - \phi$ space for a fixed value of c_B (similar to Figure 3.3.1a) and repeated over the entire concentration range (refer to Figure 3.3.1b). Figure 3.3.2 is slightly different due to the fact that a constraint on ϕ is enforced. That is, a maximum retained fraction of 50% is used. Geometrically, this is equivalent to slicing the surface in Figure 3.3.1b at the $\phi = 0.5$ plane and only considering the constrained section when determining optimal ϕ and P^* pairs.

Compared to the standard batch, the production rate from partial emptying and filling achieves a larger value throughout the entire effluent concentration range. The optimal ϕ profile consists of an initial segment at which ϕ is maintained at a maximum value of 50 %, followed by a varying profile higher than approximately 14.9 mol/L.

Graphically identifying opportunities for improvement

If the gradient belonging to P^* is smaller than that of P, an opportunity exists for improving the production rate by partial emptying and filling. This only occurs when there is a concavity in the batch profile. If the batch profile is convex however, the gradient of the intermediate production line will be steeper than that of the fresh feed, and no improvement is expected by partial emptying and filling. Finally,

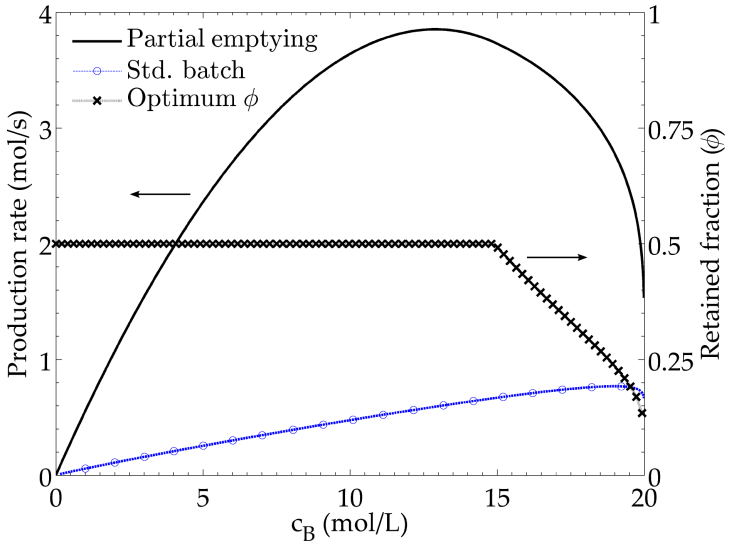


Figure 3.3.2: Comparison of production rates for partial emptying and filling (solid line), and the standard batch (−o−); the associated optimal ϕ profile (-×-) has also been plotted for bounds $0\% \leq \phi \leq 50\%$. The production rate by partial emptying is significantly higher than what is available from the standard batch production rate ($\phi = 0.0$) by the appropriate choice of ϕ value.

if the batch profile is linear, the production rate by both methods is expected to be equal, although emptying and filling may favour standard batch operation. This is summarised in Figure 3.3.3.

Observation 3: If the batch profile contains a concavity, then production rate can be improved by partial emptying and filling.

3.3.2 Improvement 2: Improving production rates for other exit concentrations

In addition to providing recommendations for when opportunities for improvement exist, Figure 3.3.2 also offers insight into identification of an optimal sequence of operation, or structure; such insight may be difficult to achieve by ordinary optimisation methods alone. Note also that this procedure is equally applicable to the standard batch, but we shall remain with partial emptying for illustration.

To begin, observe that a maximum production rate of $\sim 3.85\,\text{mol/s}$ is achieved by partial emptying and filling, corresponding to a $50\,\%$ retained volume fraction. Although it is clear from the graph that this production rate is obtained for a distinct (optimal) exit concentration c_i, our motivation here is to show how the batch structure may be modified to improve production rate for concentrations different to c_i^{opt}. In particular, our approach will be to utilise the maximum production rate

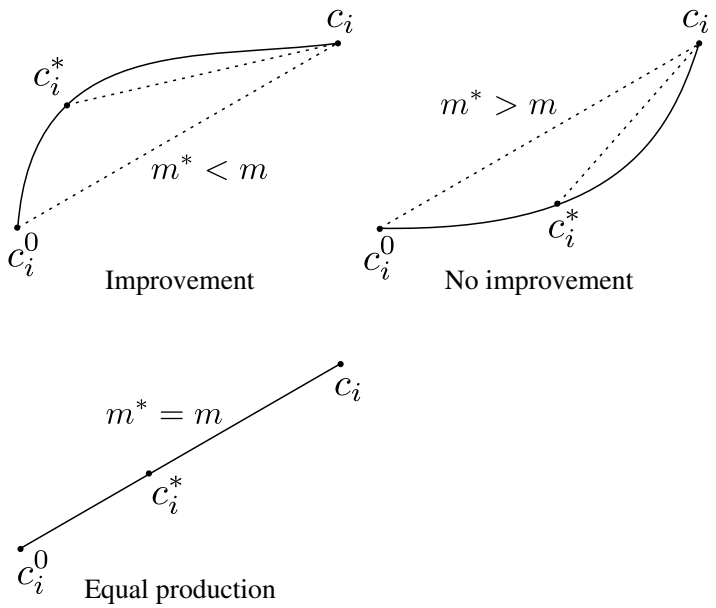


Figure 3.3.3: Identifying opportunities for improving production rate can be done by graphically inspecting the shape of the batch profile in concentration–time space. Improvements are possible when there is a concavity in the profile, as the line gradient associated with the production rate is smaller than the standard batch production rate. If the batch profile is linear, then production rate is identical by either method.

achieved at c_i^{opt} to increase the product output for different exit concentrations, denoted here by c_i.

Improving production rate for $c_i < c_i^{\text{opt}}$

We can obtain maximum production rate for all product concentrations lower than c_i^{opt} by way of a bypass. To see this, observe that if a fraction of the feed is held back from reaction and, instead, used to mix with final product after the reaction, arbitrary desired mixture compositions can be achieved by varying the relative amounts of feed and reactor product. If the time for mixing operations is assumed to be small, then additional volume may be added at no cost resulting in an increase in production rate for a given vessel volume. Alternatively, a smaller reactor volume could be used to obtain the same production rate. Therefore, it is possible to achieve the highest production rate of 3.85 mol/s for $c_i < c_i^{\text{opt}}$ by first splitting the feed into two volumes:

1. Reacting one of the volumes to an exit concentration beyond c_i to c_i^{opt} instead to achieve the highest production rate.

2. Then mixing the remaining fraction of feed material afterwards, so that the resulting mixture is at the desired final concentration c_i.

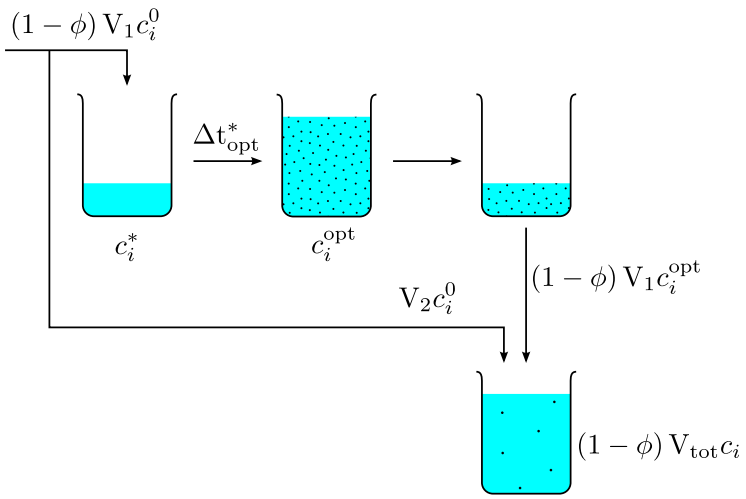


Figure 3.3.4: Improved structure for $c_i < c_i^{\mathrm{opt}}$. Maximum production rate is achievable by bypassing feed and operating at the optimal exit concentration rather than at the desired exit concentration.

Hence, the optimal structure is a batch reactor with partial emptying and filling operated at c_i^{opt} followed by mixing with fresh feed in bypass.

Observation 4: Maximum production rate can be achieved for all concentrations lower than the exit concentration corresponding to maximum production rate by bypassing a fraction of the feed and mixing it with product at the end of the cycle.

Improving production rate for $c_i > c_i^{\mathrm{opt}}$

Improving production rate for product concentrations larger than c_i^{opt} is more involved, and has been left out of the discussion for brevity. For a full development of the procedure, the reader is referred to 3.5.3. In summary, improvements are achievable by again splitting the reaction into two stages, and running multiple reactors in parallel in staggered cycles.

3.3.3 Experimental data

Note that the above example has been handled by a reaction rate expressed in functional form. This has made computation of the standard batch profile straightforward. Observe, though, that the above methodology remains unchanged even for batch profiles generated by experiment. Thus, an advantage of the graphical approach is that it may also be used for situations in when experimental data is available. Once the concentration profile has been determined, it may be inspected for concavities to identify opportunities for improving production rate, after which, line gradients and retained fractions can be computed. This provides the designer

quantitative information regarding the potential improvement in the system over the standard batch without the need for a detailed model, or before a detailed model has been developed.

Remark

Since line gradients and optimal retained fractions are directly determined by points on the concentration profile, the quality of the recommendations is influenced significantly by the quality of the experimentally measured data. The resulting production rate calculations may be adversely affected by 'noisy' data, in which sudden and steep changes in the gradient of the measured data are observed over time. In practice, when experimentally measured data are used with the method, an approximating function is employed to provide smoothed approximations of the data, suitable for gradient calculations. In this work, cubic spline interpolation is used when the method is operated on experimental data. Production rates and retained fractions are then calculated based on the cubic spline interpolant of the data. This allows for both a slightly more smoothed data set, as well as prediction of production rates for points that are not given at the discrete points of measurement obtained during experiment.

Observation 5: Calculations can be performed in the absence of a detailed model since only points from the batch profile are required.

A note should be made regarding the production of undesired products. If we run the reactor at conditions that are optimal for the production rate of the desired component, then we may also incur the risk of overproducing undesired species as well. In this case, there may be benefit to measuring the concentrations of both species so that two separate batch profiles can be obtained. It is easy then to compute production rates for both species to determine the best compromise between the two. Bypassing feed may also give a more favourable concentration in undesired components if we can afford to run the reactor at lower product concentrations. Nevertheless, it may be more practical to change operating variables such as the operating temperature to control the reactions for example. Again, benefit may be found from using these methods as a simple method of improving the production rate for a specific purity constraint, and then using traditional optimisation for further improvement.

3.3.4 Method

In order to generate the optimal P* and ϕ profiles in Figure 3.3.2, the following procedure is followed:

1. Generate the concentration profile (concentration versus time plot) for the species of interest. This may be achieved with a kinetic model by integrat-

ing the batch equation using the available reaction kinetics. Otherwise, the concentration profile is obtained from experimentally measured data.

2. For each concentration c_i in the measured concentration range, an optimal value of ϕ exists that maximises P*. In order to find the optimal value of ϕ, a curve, such as that given in Figure 3.3.1a, must be optimised for each value of c_i:

   (a) This is achieved by performing a constrained optimisation – maximising eq 3.3.2b for the value of c_i specified, bounded by $0 \leq \phi \leq \phi_{\max}$, where $\phi_{\max}$ is the maximum allowed retained fraction per cycle. If a standardised optimisation routine is employed for the optimisation, then interpolation may be required. In general, we aim to find the ϕ profile corresponding to following condition

   $$\left(\frac{\partial \mathrm{P}^*}{\partial \phi}\right)_{c_i} = 0$$

   where P* is given by eq 3.3.2b. The value of $\Delta \mathrm{t}^*$ used in eq 3.3.2b is determined by interpolating the concentration profile to find $\mathrm{t}\,(c_i)$ and $\mathrm{t}\,(c_i^*)$.

   (b) Record the value of ϕ and P* obtained from the optimisation.

3. Repeat step 2 until all points in the concentration profile have been calculated. The set of ϕ's and P*'s corresponding to each value of c_i on the concentration profile are thus the optimal retained fraction and partial emptying production rate, respectively.

The procedure described above only requires concentration and time data and is easily programmed on a computer as a compact function. Optimisations required in point 2(a) above may still be carried out numerically with experimental data if interpolation of the data (with a suitable interpolating function) is used.

3.4 Examples

3.4.1 Hydrolysis of propylene oxide

The production of propylene glycol is produced by the hydrolysis of propylene oxide in the following reaction (Fogler, 2006)

$$\begin{aligned} \mathrm{CH_2OCHCH_3} + \mathrm{H_2O} &\rightarrow \mathrm{CH_2OCHOHCH_3} \\ \mathrm{A} + \mathrm{D} &\rightarrow \mathrm{B} \end{aligned}$$

The rate of formation is first order and given by

$$r_{\mathrm{A}} = -kc_{\mathrm{A}}$$

with rate constant (in hr^{-1})

$$\begin{aligned} k &= A_0 \exp\left(-\frac{\mathrm{E}}{\mathrm{RT}}\right) \\ &= 16.96 \times 10^{12} \exp\left(-\frac{32400}{\mathrm{RT}}\right) \end{aligned}$$

where E, R and T are the activation energy, universal gas constant and temperature, respectively. The reaction is performed adiabatically in a batch reactor, so that the temperature expression (measured in Kelvin) is given in terms of conversion of reaction, x, as

$$\begin{aligned} \mathrm{T} &= \mathrm{T}_0 + \left(\frac{-\triangle \mathrm{H}^0_{\mathrm{rxn}}}{\sum \nu_j \mathrm{Cp}_j}\right) x \\ &= 515 + 90.1x \end{aligned} \tag{3.4.1}$$

We find that the rate expression is a concave function with respect to x. Observe that since the system is adiabatic, the temperature is linear with respect to conversion and therefore obeys linear mixing laws. To see this, notice that eq 3.3.1 may be adapted to express the conversion of a mixture as a linear combination of two arbitrary initial and final conversions, x_1 and x_2

$$x^* = \phi x_2 + (1-\phi)\, x_1$$

The energy balance may be invoked by substitution of eq 3.4.1 into the above expression

$$\mathrm{T}^* = \phi \mathrm{T}_2 + (1-\phi)\, \mathrm{T}_1$$

Therefore, a given conversion (and corresponding temperature) may be achieved from a single batch reaction in the usual manner, or from two separate batches (and thus two separate final temperatures) which, once mixed in the appropriate proportions, obtains the same final temperature. Hence, temperature in the batch reactor will be the same, irrespective of whether conversion is obtained by mixing product with feed, reacting feed, or a combination of the two.

For this example, $c^0_{\mathrm{A}} = 20.0\,\mathrm{mol/L}$, $c^0_{\mathrm{B}} = 0.0\,\mathrm{mol/L}$, and $\mathrm{V}_{\mathrm{tot}} = 1.0\,\mathrm{L}$. The resulting batch profile is then given by Figure 3.4.1a, and a noticeable concavity is observed. In order to identify whether any opportunities for improvement are indeed available, a comparison between the production rates for the standard batch and partial emptying and filling are given in Figure 3.4.1b. For both methods, production rate increases with increasing conversion until $\sim$90 %, where a sharp

decline in productivity is observed. Figure 3.4.1b shows several improvements over the standard batch:

- Partial emptying and filling allows for a higher production rate, although, the largest gains are achieved by operating at high conversions. In particular, the highest production rate achievable by the standard batch is $\sim 0.006\,\text{mol/s}$ near $x = 92\,\%$, whereas the maximum production rate corresponding to partial emptying and filling is $\sim 0.01367\,\text{mol/s}$ (an approximate $220\,\%$ improvement). The corresponding optimum ϕ profile (-×-) is flat throughout the entire conversion range and operates at the highest acceptable limit of $50\,\%$. Thus, for all exit conversions, it is beneficial to retain product.

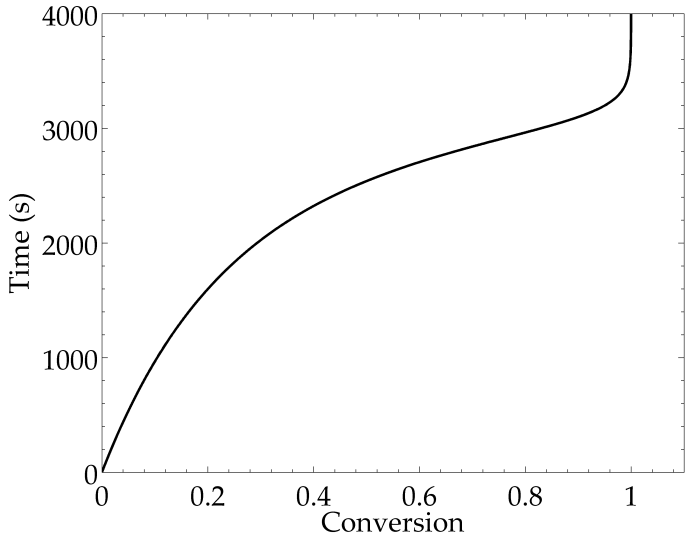
- By operating at $92\,\%$ conversion and bypassing feed in the appropriate amounts, maximum production rate is achieved for $x \leq 92\,\%$ conversion. Thus maximum production rate is possible for almost the entire conversion range by use of a bypass. Even though there exists an optimal ϕ profile, further improvement is achievable.

Observe that the suggested production rate profiles for partial emptying could be achieved by standard optimisation using ϕ a control variable. However, it is simple to check beforehand whether optimisation is at all required by visual inspection of the batch profile.

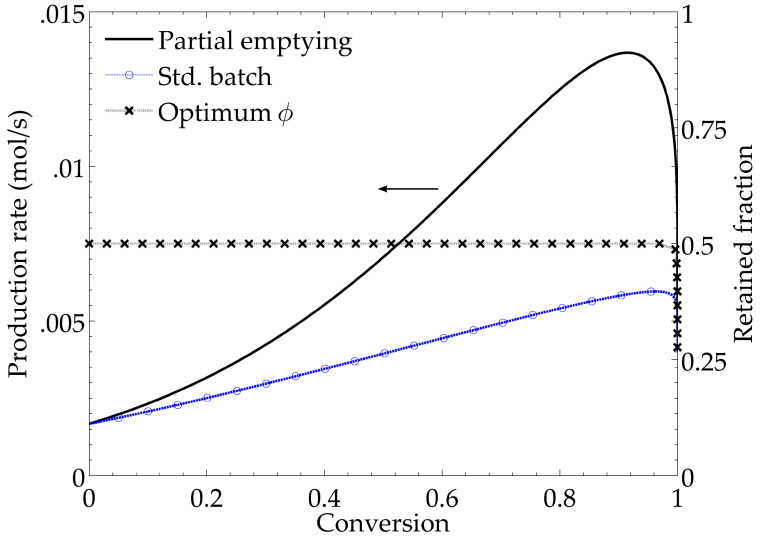
3.4.2 Penicillin production

Up to this point, the examples used have been performed using a mathematical model describing the kinetics. Calculation of production rate was convenient as a result, although, this could have been handled by a standard optimisation method. Consider then the production of penicillin in a bio-reactor. The kinetics are complex and thus measured data obtained from an experimental run is initially available, given in Figure 3.4.2. Fermentation was carried out in a 30 L fermenter over a period of 216 h at a constant temperature of 295 K. The data was generated from the work of Constantinides et al. (1970). In addition to this, Constantinides et al. (1970) also provided a model with the measured data. Although it is possible to obtain the profiles using the model alone, they are not needed to carry out the computations and thus the kinetics are not given here. That is, results from the model are overlaid on the experimental points for comparison only; the actual expressions may be found at the end of the chapter however.

Figure 3.4.3 shows the results generated from the fermentation. The solid lines in all figures correspond to the model suggested by Constantinides et al. (1970) for the same data set. A 20 h lag in penicillin concentration indicates that no product is produced initially and a concavity in the concentration profile is clearly noticeable,



(a) Batch profile for the hydrolysis of propylene oxide.



(b) Production rate comparison for propylene oxide. The production rate by partial emptying (black solid line) may be improved significantly for all conversions by operating at the maximum retained volume fraction, seen here by the constant optimum ϕ profile (-×-). The gain in production rate by mixing over the standard batch increases with higher conversions.

Figure 3.4.1: Hydrolysis of propylene oxide.

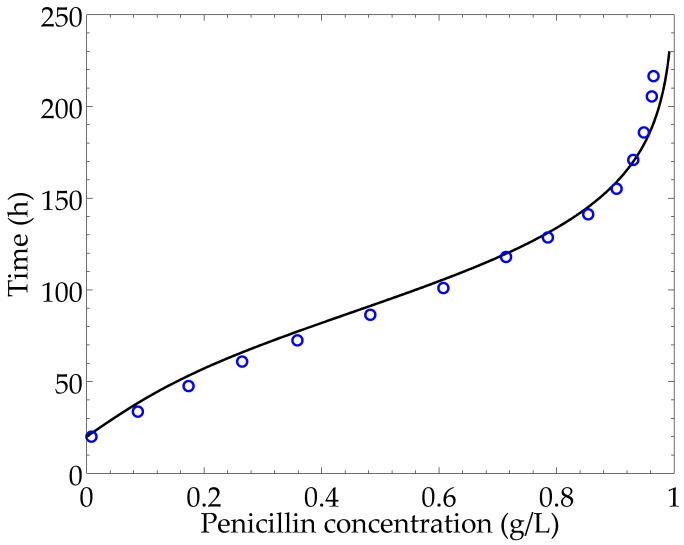


Figure 3.4.2: Concentration profile for penicillin production. No penicillin is produced in the first 20 h of operation.

although there is in fact a small, approximately linear section, up to 0.03 g/L. Due to the concavity, production rate is expected to be improved by retaining product.

The data were therefore used to compute the production rates of both the standard batch and partial emptying and filling; this is given in Figure 3.4.3a. Throughout the entire concentration range, the production rate by partial emptying is larger than the standard batch. In particular, this value is ~ 8.7 mg/h at maximum production rate compared to ~ 6.0 mg/h for the standard batch. The corresponding retained fractions generated using the experimental points are also shown in Figure 3.4.3b. As discussed above, there is a small linear section in the profile near the start and thus the optimum ϕ profile initially shows a section where no product is retained. For exit concentrations less than approximately 7 g/L, the profile is flat. This suggests that production rate is maximised by retaining as much product as possible. For product concentrations beyond this value, the optimum retained fraction follows a varying profile that steadily decreases to 0 %. Again, the curve calculated from the rate expressions is fairly close to the experimental points. Partial emptying and filling allows one to eliminate the initial 20 h lag phase, and thus production rate is larger when compared to the standard batch. For this reason, it is recommended that at least trace amounts of product be retained.

It is interesting to note that these recommendations are what are done in practice. It is common in biological reactions to recycle a fraction of cells from the product to allow sufficient time for cells to reproduce, and to minimise washout (Crueger and Crueger, 1984). Fed-batch operation is also a common method of improving production rate in practice and could be used to achieve an intermediate concentration within the batch. In this regard, the results of the graphical analysis

suggest that there is a benefit in retaining product for all effluent concentrations. This information could be used in follow-up experiments, with the results used together with further optimisation when more detailed results are available.

3.4.3 Lysine fermentation

As a counterexample, the production of lysine will be used to demonstrate a set of reaction kinetics in which mixing is not a suitable method of improving the production rate. Again, this is achieved by graphical inspection of the batch profile and so recognising improvements are easily identified. The evolution of biomass c_{X}, substrate c_{S} and product c_{P} are given by the system of equations (Pushpavanam et al., 1999).

$$\begin{aligned}\frac{\mathrm{d}c_{\mathrm{X}}}{\mathrm{dt}} &= \mu c_{\mathrm{X}} \\ \frac{\mathrm{d}c_{\mathrm{S}}}{\mathrm{dt}} &= -\sigma c_{\mathrm{X}} \\ \frac{\mathrm{d}c_{\mathrm{P}}}{\mathrm{dt}} &= \pi c_{\mathrm{X}}\end{aligned}$$

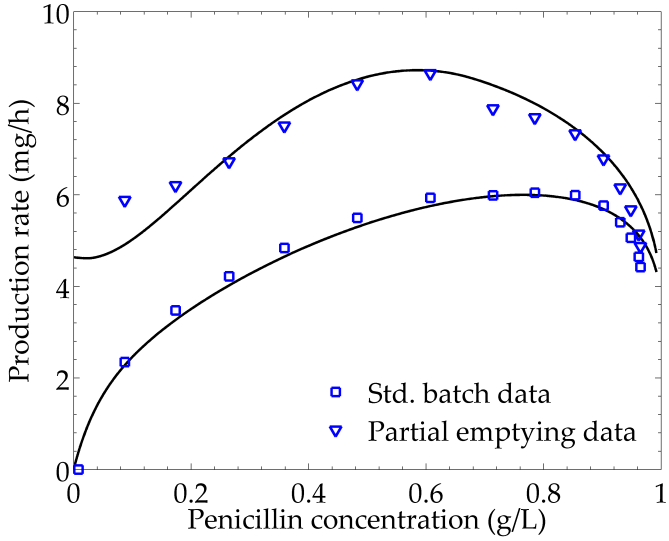
The rates of formation, with units of s^{-1}, are provided as follows:

$$\begin{aligned}\mu &= 0.125 c_{\mathrm{S}} \\ \sigma &= \frac{\mu}{0.135} \\ \pi &= -384\mu^2 + 134\mu\end{aligned}$$

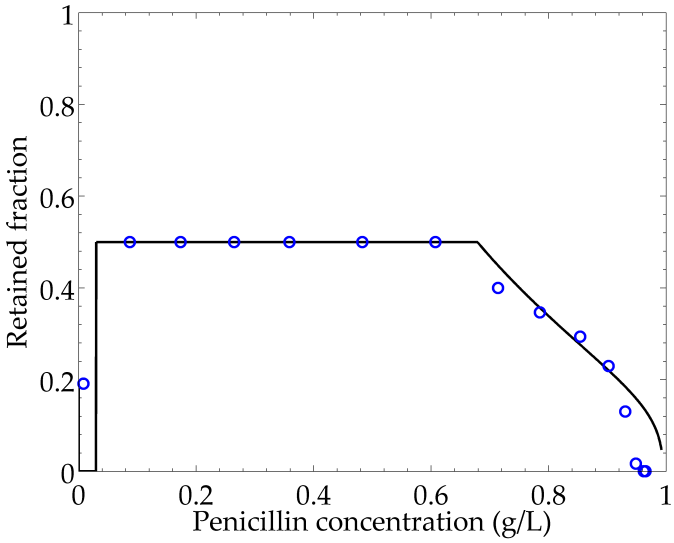
The concentrations of c_{X} and c_{P} are measured in units of g/L, whereas units for c_{S} are given in wt.%. Initial concentrations are $c_{\mathrm{X}}^0 = 0.02\,\mathrm{g/L}$, $c_{\mathrm{P}}^0 = 0.0\,\mathrm{g/L}$ and $c_{\mathrm{S}}^0 = 2.8\,\mathrm{wt.\%}$ and the fermenter volume is $\mathrm{V_{tot}} = 5\,\mathrm{L}$.

Again, it is desired to improve the production rate by partial emptying and filling. As in the previous examples, the product concentration profile in Figure 3.4.4a for the standard batch is then obtained. The reaction is found to be equilibrium limited, resulting in a final product concentration of $\sim 0.50\,\mathrm{g/L}$. The corresponding reaction time is then found to be $\sim 300\,\mathrm{s}$. The batch profile for lysine production exhibits no concavity. Indeed, a slight convex shape is observed. As a result, the production rate resulting from mixing is expected to be smaller than the standard batch.

The production rates for both the standard batch and partial emptying are thus provided by Figure 3.4.4b. It is clear that the optimal production rate achieved by the partial emptying approach is identical to the standard batch production rate. For comparison, the production rates corresponding to constant ϕ policies of 25 % (-×-) and 50 % (-o-) have also been plotted. These profiles represent the production rates obtained when the retained volume fraction is held at a constant value irrespective of the final product concentration chosen. Clearly, the rate of lysine production is



(a) The production rates predicted are in close agreement with the theory. There is benefit in retaining product as no penicillin is produced initially.



(b) Retained fractions calculated using the experimental points only are also close to the profile suggested by the theory.

Figure 3.4.3: The production of penicillin in a bio-reactor. Expected production rates are calculated using the experimental points only. Theoretical predictions are given by solid lines for comparison.

reduced for increasing retained volume fractions and hence for $0\% \leq \phi \leq 100\%$, the corresponding production rate by partial emptying is smaller than a standard batch.

It follows that there exists no opportunity for improvement by mixing for these kinetics. Although no improvement is possible, the graphical approach has still provided insight into an optimal operating policy. This is still useful in itself. $\phi = 0\%$

3.5 Further remarks

3.5.1 Transfer time

The contribution of emptying and filling times, or transfer time, may be accounted for by the addition of extra terms in the production rate equations. In general, this quantity must be added to each cycle, and as a result, may be regarded as constant. The production rate equations are then adapted as follows

$$\overline{\mathrm{P}} = \frac{\mathrm{V_{tot}}\left(c_i - c_i^0\right)}{\left(\mathrm{t_0} + \mathrm{t_T}\right)} \qquad \overline{\mathrm{P^*}} = \frac{(1-\phi)\,\mathrm{V_{tot}}\left(c_i - c_i^*\right)}{\left(\mathrm{t^*} + \mathrm{t_T^*}\right)}$$

Where $\mathrm{t_T}$ denotes transfer time. Here, use of the overbar signals that production rate under consideration of transfer time has been accounted for. Two observations can be made with respect to its inclusion:

1. Clearly, $\mathrm{t_T}$ serves to increase the gradients of the production lines, suggesting a decrease in production rate.

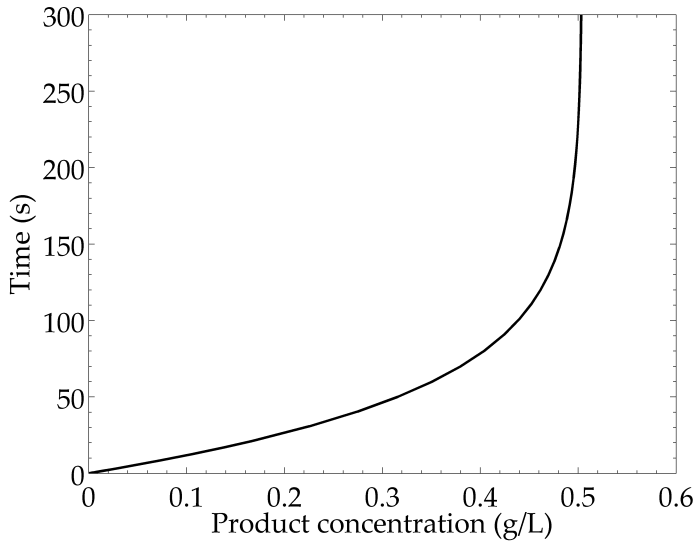
2. Since $\mathrm{t_T}$ is associated with an emptying and filling rate, given here by r, transfer time is a function of the volume transferred, and by association, ϕ. As a result, the transfer time for partial emptying and filling is smaller than the standard batch. The ratio of the production rates defined above can be written in terms of filling rate and retained fraction as follows

$$\frac{\overline{\mathrm{P^*}}}{\overline{\mathrm{P}}} = \left(\frac{\mathrm{P^*}}{\mathrm{P}}\right)\xi \tag{3.5.1}$$

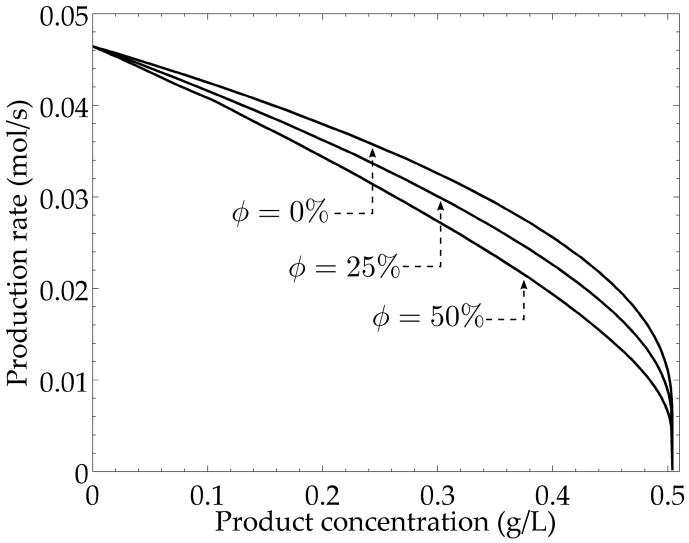
where

$$\xi = \left[\frac{r}{\mathrm{V_{tot}}} + \frac{1}{\Delta \mathrm{t_0}}\right] / \left[\frac{r}{\mathrm{V_{tot}}} + \frac{(1-\phi)}{\Delta \mathrm{t^*}}\right] \tag{3.5.2}$$

The derivation of eq 3.5.1 can be found in appendix A.1. The relative gain in production efficiency can be viewed as the product of two factors: a standard ratio of production performance where no allowance for transfer time is accounted for, multiplied by a transfer time factor. Due to the dependence on ϕ, this factor is approximately equal to unity. The relative gain in production rate therefore might not be significantly influenced by transfer time. Figure 3.5.1 provides a plot of this ratio for different filling rates.



(a) Concentration profile for lysine fermentation. The batch profile is convex throughout the entire concentration range, suggesting that no improvement is possible by way of partial emptying and filling.



(b) Production rate comparison for lysine fermentation, given by the standard batch (solid line), and constant retained volume fractions of 25 % (-×-) and 50 % (-o-). For any retained volume fraction, the associated production rate is lower than that of the standard batch.

Figure 3.4.4: Lysine fermentation.

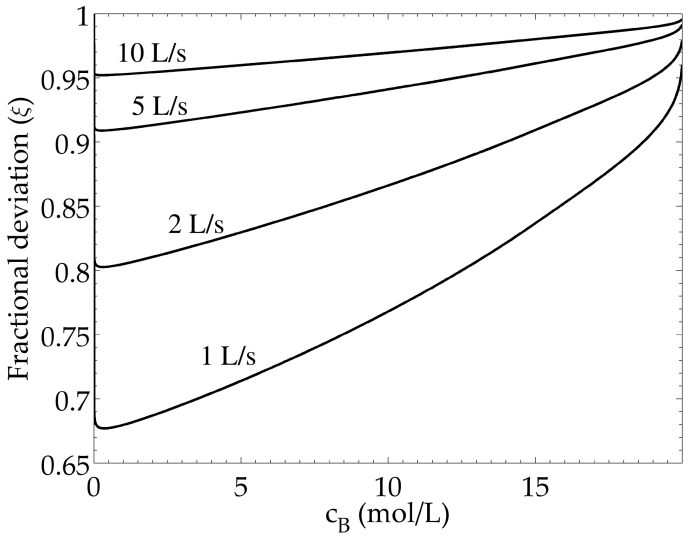


Figure 3.5.1: The ratio ξ versus exit concentration for the example problem given in section 3.2. The effect of transfer time is plotted for different filling rates r. The impact of transfer time becomes progressively smaller for higher value of r.

3.5.2 Fed-batch operation

The methods described above are also applicable to fed-batch operation. In addition to the required rates of formation for each species, a time-dependent feed rate, $F(t)$ is also specified and reactor volume also varies as a result. The production rate equations are equally valid for fed-batch operation, although $F(\mathrm{t})$ can be seen to introduce an added degree of freedom which may allow for the design of optimal feeding policies.

The initial conditions for fed-batch operation must be specified as a function of the final conditions from the previous cycle and the retained volume fraction. Therefore, since the initial concentrations are formed from a mixture of fresh feed and final product, the initial conditions are given as

$$\begin{aligned} \mathbf{C}(\mathrm{t}_0) &= \phi\mathbf{C}(\mathrm{t}_\mathrm{f}) + (1-\phi)\mathbf{C^0} \\ \mathrm{V}(\mathrm{t}_0) &= \phi\mathrm{V}(\mathrm{t}_\mathrm{f}) \end{aligned}$$

where $\mathrm{V}(\mathrm{t}_0)$ and $\mathbf{C}(\mathrm{t}_0)$ represent the initial state of the fed-batch reactor obtained by mixing with the previous batch, and may not, in general, be considered equivalent to the conditions of the first (non-mixed) batch. In particular, retained product could be stored in a separate vessel and added to the reactor in a fed-batch manner, so that mixing could be achieved through the feeding policy also. Notice that the above formulation may be solved by standard techniques such as dynamic optimisation (Dhir et al., 2000; Faber et al., 2005). Although, this is not always possible as a detailed model of the process is generally required.

3.5.3 Improving production rate for $c_i > c_i^{\text{opt}}$

For $c_i > c_i^{\text{opt}}$, the above approach in section 3.3.2 can again be modified, although further reaction steps are required in order to reach the desired final concentration. Obtaining maximum production rate for $c_i > c_i^{\text{opt}}$ may not always be realised in general, although, improvements are still possible with the appropriate modifications. By example, assume that a final product concentration of $c_i = 15.6\,\text{mol/L}$ is desired. Then the reaction can be split into two physically separate reaction stages:

1. In the first (stage A), feed material is reacted to the optimum concentration by the usual partial emptying and filling approach. The time taken to react from c_i^0 to c_i^{opt} is denoted by Δt_1. This is referred to as reactor A_1.

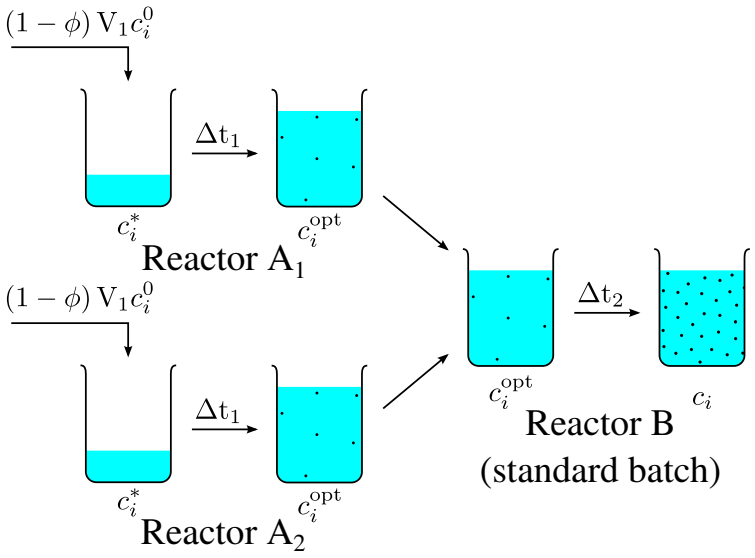
2. In the second step (stage B), product from A_1 is transferred to a standard batch stage, referred to here as reactor B, which further reacts the material to the final desired concentration. The time taken to react from c_i^{opt} to c_i is given here by Δt_2. The choice of exit concentration is chosen such that $\Delta\text{t}_2 = \frac{1}{2}\Delta\text{t}_1$.

Since reactor B is idle for half the reaction time of A_1, it can be supplied *after every cycle* if two stage A reactors are used and operated in parallel. Again, in order to ensure that production rates remain consistent and comparable, we keep the sum of volumes from all reactors, both in stages A and B, so that they are equal to the total equivalent standard batch reactor volume. Thus, for two stage A reactors, we have that $\text{V}_{\text{tot}} = 2\text{V}_1 + \left(1 - \phi^{\text{opt}}\right)\text{V}_1$, where ϕ^{opt} is the optimum retained fraction associated with stage A. V_1 can then be factorised and substituted into the production rate expression. The corresponding production rate for two stages is then $\left[\left(1 - \phi^{\text{opt}}\right)\text{V}_1\left(c_i - c_i^0\right)\right] / \left[\frac{1}{2}\Delta t_1\right]$ which gives $3.728\,\text{mol/s}$. We can generalise this for N stage A reactors to give

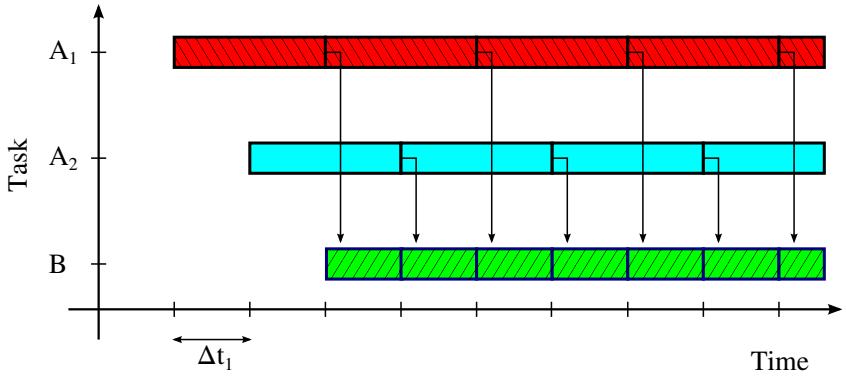
$$\begin{aligned}\text{P} &= \frac{\left(1 - \phi^{\text{opt}}\right)\text{V}_1\left(c_i - c_i^0\right)}{\frac{1}{N}\Delta\text{t}_1} \\ &= \frac{N\left(1 - \phi^{\text{opt}}\right)\text{V}_{\text{tot}}\left(c_i - c_i^0\right)}{\left(N + 1 - \phi^{\text{opt}}\right)\Delta\text{t}_1}\end{aligned}$$

The improved batch structure is thus two reactors operated in parallel in staggered cycles followed by a standard batch. Furthermore, note that for $c_i > c_i^{\text{opt}}$, multiple reactors are required. A similar rearrangement can be performed for when $\text{t}_2 > \text{t}_1$. In this case, multiple reactors for stage B and a single reactor for stage A would be required.

It may be difficult to have prior knowledge of a single (maximum) production rate that could be used to improve the productivity of other final concentrations. It is also not always clear that batch structure may change depending on the desired final concentration. The graphical method presented here provides insight into identifying opportunities for improvement in batch structure.



(a) Physical arrangement



(b) Gantt chart demonstrating reaction sequence for $c_i > c_i^{opt}$

Figure 3.5.2: Possible improved structure for $c_i > c_i^{opt}$ when $\Delta t_2 = \Delta t_1/2$. Production rate can be improved by use of a partial emptying and a standard batch stage. Reactors A_1 and A_2 are staggered so that reactor B is fed after every cycle of Δt_2.

3.6 Conclusion

This chapter presented a graphical method for identifying opportunities that improve the production rate in batch reactors. This approach is also used as a basis for the development of a simple modification to standard batch operation given as follows: a standard batch profile in concentration–time space is generated or obtained from experimental data, and straight line segments are joined between the initial and final conditions within the reactor on the curve. In this way, production rate is inversely proportional to the gradient of the line and thus the method provides a quick means of interpreting the performance by inspection of the shape of the batch profile. Identifying conditions associated with high production rate involves locating the starting and ending points that generate the shallowest gradient. For a fixed exit concentration, optimum initial concentrations within the reactor may

be determined by locating the point associated with smallest slope. This suggests that the standard batch cycle can be improved by changing the initial conditions to produce more favourable gradients. It also follows that production rate can be improved when the batch profile contains concavities, and hence it is easy to determine these opportunities by graphical inspection.

From this, it can be shown that instead of withdrawing the full product volume from the reactor at the end of each cycle, it is potentially more advantageous to retain a fraction of the product volume and mix with fresh feed in the following cycle. This may appear to be counter-intuitive to the normal method of batch operation. The graphical approach also provides a better understanding into identification of improved batch structures. In particular, the batch procedure may change depending on the desired final product concentration. For all concentrations less than the optimal concentration, maximum production rate is achievable by bypassing a fraction of the feed and mixing afterwards. For concentrations greater than the optimum, further improvements may be achieved by distributing feed over multiple reactors operating in parallel in staggered cycles.

Several industrial examples were demonstrated to improve over the standard batch when concavities in the batch profile were observed. For lysine production however, no improvement was achieved. Inasmuch as these cases have not shown any enhancement in production efficiency, the graphical approach still provides relevant information regarding the nature of the kinetics, and therefore allows for screening of potentially productive batch structures before more complex optimisations are undertaken. Subsequent optimisation may also be easier if an appropriate structure is used in the optimisation model.

Consideration of how the production rate equations may be further applied for non-standard batch operation was also briefly discussed. The method is equally valid for fed-batch operation and no alteration to the equations is required. Furthermore, the added flexibility of fed-batch operation provides opportunities to tailor production performance by variation of the feed policy.

The graphical methods described here are simple enough that they may be performed by those who do not have the required knowledge or resources to carry out traditional optimisations. Additionally, this approach may also be used as a shortcut method before more sophisticated techniques are employed. Considering that the method only requires data points from the batch profile before meaningful information can be obtained, it is possible to use these methods on experimental data in the absence of a detailed model, or before a model has been developed. Although this could be viewed as an optimisation of the initial condition with splitting and mixing constraints, identifying these opportunities are not always apparent from the equations alone. The ideas presented here have come about from an understanding that structure is an important component to the overall performance of a system. The need for simple graphical methods is therefore incredibly useful, even in modern

day design we believe.

With this in mind, AR theory might be viewed to address both of these aspects: AR theory is geometric in nature, and thus interpretation of the boundary structures is simpler when compared to standard optimisation methods. Additionally, knowledge of the optimal structure can also be gained by the approach. Many of the ideas presented in this chapter have been established on concepts originating from traditional (continuous) AR theory. It is not unreasonable, then, for one to seek ways in which the desirable properties of the AR approach can be employed in batch. At present however, current AR construction methods are slow, and so there is an equally pressing need to develop better methods for their construction. In the next chapter, we will address this issue directly and tackle the problem of automated AR construction. An existing automated construction method is discussed and then modified to form a new version. The end goal in mind will be towards developing a faster construction method that may be used for more complex kinetics.

Kinetics for penicillin production

In this chapter, we demonstrate how the batch profile may be used to determine an optimal value for the retained fraction (ϕ). Due to the graphical nature of the technique, no additional information is required in order to carry out the analysis. In section 3.4.2, the example of penicillin production using a batch profile, generated entirely from experimental data, is given and used to demonstrate the usefulness of the method. Predictions derived from the experimental data provided are then compared to theoretical predictions. The theoretical basis for these predictions is developed from kinetics for penicillin growth and provided in a functional form. These kinetics are only included to demonstrate that the method has no reliance on any other information other than that given in the experimental data. The actual expressions for the kinetics are given here now for comparison and completeness. The rate of cell growth, c_{X}, and penicillin, c_{P}, are taken from Constantinides et al. (1970) and given as follows

$$\begin{aligned} \frac{\mathrm{d}c_{\mathrm{X}}}{\mathrm{dt}} &= b_1 c_{\mathrm{X}} \left(1 - \frac{c_{\mathrm{X}}}{b_2}\right) \\ \frac{\mathrm{d}c_{\mathrm{P}}}{\mathrm{dt}} &= b_3 c_{\mathrm{X}} - b_4 c_{\mathrm{P}} \end{aligned}$$

Rate constants are given in Table 3.2. In the original paper, the concentration of cell mass and penicillin are converted into non-dimensional form. The model is thus independent of the units specified for both species concentrations used in the experiment.

Initial concentrations are hence specified as $c_{\mathrm{X}}^0 = 5.0$ and $c_{\mathrm{P}}^0 = 0.0$. Integration of the equations is performed in the usual manner with the initial conditions provided.

Table 3.2: Rate constants for penicillin production.

b_1	b_2	b_3	b_4
0.04079	43.33	9.269	0.04008

The resulting solution trajectory is subsequently given in Figure 3.4.2.

References

Constantinides, A., Spencer, J. L., Gaden, E. L., 1970. Optimization of batch fermentation processes. i. development of mathematical models for batch penicillin fermentations. Biotechnology and bioengineering 12 (5), 803–830.

Crueger, W., Crueger, A., 1984. A Textbook of Industrial Microbiology. Sinauer Associates Inc.

Dhir, S., Jr., K. J. M., Rhinehart, R. R., Wiesner, T., 2000. Dynamic optimization of hybridoma growth in a fed-batch bioreactor. Biotechnology and bioengineering 67 (2), 197–205.

Faber, R., Jockenhovel, T., Tsatsaronis, G., 1 2005. Dynamic optimization with simulated annealing. Computers & Chemical Engineering 29 (2), 273–290.

Fogler, H. S., 2006. Elements of Chemical Reaction Engineering. Prentice Hall, Ch. 9, pp. 526, 595.

Pushpavanam, S., Rao, S., Khan, I., 1999. Optimization of a biochemical fed-batch reactor using sequential quadratic programming. Industrial & Engineering Chemistry Research 38 (5), 1998–2004.

Chapter 4

AR construction using rotated bounding hyperplanes

The following chapter has been adapted from published work with permission. The associated paper is (Ming, D., Hildebrandt, D., Glasser, D., 2010. A revised method of attainable region construction utilizing rotated bounding hyperplanes. Ind. Eng. Chem. Res. 49, 10549–10557.) Copyright (2010) American Chemical Society. D. Ming (the present author) compiled the manuscript and contributed to the ideas in this work. D. Hildebrandt and D. Glasser supervised this work.

4.1 Introduction

For the past three decades, knowledge of the Attainable Region (AR) has allowed one to approach the problem of optimal reactor network design from a geometric viewpoint. Originally introduced by F.J.M Horn in 1967 (Horn, 1964) but later pioneered by the work of Glasser et al. (1987), Hildebrandt (1989) and Hildebrandt and Glasser (1990), Feinberg and Hildebrandt (1997) and Feinberg (2000b,a), the AR has addressed the problem of optimal reactor design by determining *all* possible outputs for a given set of feed conditions, reaction kinetics and operating constraints. In doing so, the AR approach has allowed for the solution of a large variety of reactor network synthesis and optimisation problems.

In chapter 2, we discuss how many of the most recent developments in the field have focused toward the advancement of algorithms for the automatic construction of candidate ARs. Current methods of construction fall into two categories:

1. Methods which attempt to generate the AR from a known starting feed condition and grow the region outwards (Rooney et al., 2000; Kauchali et al., 2002; Seodigeng et al., 2009), referred to as inside-out methods.

2. Methods that compute an initial (and possibly large) superset in which the AR is known to reside, and then progressively shrink the region inwards (Burri

et al., 2002; Manousiouthakis et al., 2004; Abraham and Feinberg, 2004), referred to here as outside-in methods.

In this chapter, we shall be concerned with a variation of an existing outside-in algorithm originally developed by Abraham and Feinberg (Abraham and Feinberg, 2004). This procedure constructs candidate regions using a large number of bounding hyperplanes. Our chief objective will be to first present the necessary changes made to the original method, and then demonstrate its application to problems in concentration and concentration-time space, particularly in $\mathbb{R}^2$. We aim to show that by a change in hyperplane placement, AR construction efficiency may be improved by a significant margin. We shall only be concerned with the construction of candidate ARs in which density and, unless specified otherwise, temperature may be assumed constant. As in chapter 2, this allows us to assert special geometric characteristics of the process of mixing and hence the shape of the AR boundary.

Sections 4.2.1 to 4.2.6 provide the necessary mathematical background and general results required for the proper understanding of the modified algorithm. Sections 4.3.1 and 4.3.2 introduce the reader to the original and modified construction methods respectively. The main motivations for improvement are also discussed at the end of section 4.3.2. Section 4.4 provides several examples for classical isothermal problems as well as non-standard problems that have not been implemented by the original bounding hyperplanes algorithm. These examples allow for the determination of the AR for a wider variety of systems and kinetics. Section 4.4.1, in particular, provides a comparison between the two approaches. Finally, section 4.6 provides several remarks regarding higher dimensional constructions before concluding remarks are supplied in section 4.7.

4.2 Mathematical preliminaries

In chapter 2, an overview of the geometric nature of concentration and mixing is provided. These properties are then used to define the AR by exploiting the convex nature of mixing in conjunction with the use of three fundamental reactor types. The AR construction algorithm outlined next relies on a basic understanding of hyperplanes, as well as the geometric constituents (facets, edges, vertices) that are formed when multiple hyperplanes are arranged in space to form a convex polytope. Definitions and brief descriptions for these are also given below.

4.2.1 Hyperplanes

A *hyperplane* $H(\mathbf{n}, \mathbf{C_0})$ is defined as one that obeys the following equation

$$H(\mathbf{n}, \mathbf{C_0}) = \left\{ \mathbf{C} \in \mathbb{R}^n : \mathbf{n^T} (\mathbf{C} - \mathbf{C_0}) = \mathbf{0} \right\} \tag{4.2.1}$$

where vectors $\mathbf{C}$ and $\mathbf{C}_0$ are points lying in $H(\mathbf{n}, \mathbf{C_0})$ and where $\mathbf{n}$ is a vector orthogonal to $(\mathbf{C} - \mathbf{C}_0)$. A hyperplane separates a space $\mathbb{R}^n$ into two *half-spaces*. The positive and negative closed half spaces are defined by

$$\begin{aligned} H^{\geq} &= \left\{\mathbf{C} \in \mathbb{R}^n : \mathbf{n^T}(\mathbf{C} - \mathbf{C_0}) \geq \mathbf{0}\right\} \\ H^{\leq} &= \left\{\mathbf{C} \in \mathbb{R}^n : \mathbf{n^T}(\mathbf{C} - \mathbf{C_0}) \leq \mathbf{0}\right\} \end{aligned} \tag{4.2.2}$$

and similarly for the open half spaces

$$\begin{aligned} H^{>} &= \left\{\mathbf{C} \in \mathbb{R}^n : \mathbf{n^T}(\mathbf{C} - \mathbf{C_0}) > \mathbf{0}\right\} \\ H^{<} &= \left\{\mathbf{C} \in \mathbb{R}^n : \mathbf{n^T}(\mathbf{C} - \mathbf{C_0}) < \mathbf{0}\right\} \end{aligned} \tag{4.2.3}$$

Clearly, $\mathbf{n}$ forms an orthogonal subspace to $H(\mathbf{n}, \mathbf{C_0})$ and may be used as a test for tangency to the plane.

4.2.2 Orthogonal and tangent vectors

The inner product of two vectors $\mathbf{x}$, $\mathbf{y}$ may be defined by the following relation

$$\mathbf{x}^{\mathrm{T}}\mathbf{y} = \|\mathbf{x}\| \, \|\mathbf{y}\| \cos(\theta)$$

where θ is the angle between $\mathbf{x}$ and $\mathbf{y}$. This relation may be used to signal when the two vectors are orthogonal ($\cos(\theta) = 0$) or tangent ($|\cos(\theta)| = 1$) to one another. Hence, $\mathbf{x}$ and $\mathbf{y}$ are orthogonal, if there is at least one non-zero element in $\mathbf{x}$ and $\mathbf{y}$ and where

$$\mathbf{x}^{\mathrm{T}}\mathbf{y} = \mathbf{0} \tag{4.2.4}$$

where $\mathbf{0}$ is the zero vector. Similarly, $\mathbf{x}$ and $\mathbf{y}$ are tangent if

$$\mathbf{x}^{\mathrm{T}}\mathbf{y} = \|\mathbf{x}\| \, \|\mathbf{y}\| \tag{4.2.5}$$

where $\|\mathbf{x}\|$ and $\|\mathbf{y}\|$ represent the magnitudes of $\mathbf{x}$ and $\mathbf{y}$, respectively. If $\mathbf{x}$ and $\mathbf{y}$ are unit vectors, then the above reduces to

$$\mathbf{x}^{\mathrm{T}}\mathbf{y} = 1$$

4.2.3 Extreme points

A point $\mathbf{x} \in \mathbb{R}^n$ is an extreme point if it is a vertex of the convex hull. Extreme points may not lie in the interior of the convex hull, nor in the interior of the line segment bounding the facets of the convex polytope.

4.2.4 Facets and edges

A hyperplane is said to a *n-face* or *n-facet* of the convex polytope conv(P), if n linearly independent points in P lie on $H(\mathbf{n}, \mathbf{C_0})$. An *n-edge* of the convex polytope conv(P) is one which contains $n-1$ linearly independent points that make up the n-face (Chand and Kapur, 1970).

4.2.5 Vertex and facet enumeration

A convex polyhedron P in $\mathbb{R}^n$ may be described independently both in terms of its vertices, and in terms of its facets. P is said to be given in the vertex representation (the V-representation), when the polytope is described in terms of a collection of vertices. Similarly, the same polyhedron is said to given in the hyperplane representation (the H-representation) when the polytope is described by a collection of hyperplane constraints of the following form:

$$\mathbf{Ax} \geq \mathbf{b}$$

Notice that imposing non-negativity constraints on the component concentrations is equivalent to expressing the system in the above form. The *vertex enumeration problem* constitutes finding the vertices (corners) of P when P is described by the H-representation. Conversely, the *facet enumeration problem* arises when P is described by the V-representation and we wish to determine the associated hyperplane constraints in H-representation. We have already encountered the facet enumeration problem on numerous occasions, disguised under the form of the convex hull of a set of points. Vertex and facet enumeration are, in the sense of convex optimization, dual problems. Solution of the one automatically results in solution of the other. It is clear that computing the convex hull of a set of points is equivalent to solving the facet enumeration problem for a given convex polytope describing a set of achievable states in state space. Similarly, computing the extreme points of the stoichiometric subspace is equivalent to finding the intersection points that produce feasible vertices from a system of inequality constraints; we are in fact solving the vertex enumeration problem. Figure 4.2.1 gives a visual representation of the two problems.

4.2.6 Stoichiometric constraints

Given a system of chemical reactions and associated kinetics and feed point, we aim to determine the limits to which a given concentration may be achieved by stoichiometry alone. Knowledge of an upper bound on attainability allows one to establish that the AR will lie in a smaller subspace in $\mathbb{R}^n$ (Feinberg, 2000b). Clearly, non-negativity constraints restrict the subspace to lie within the positive orthant in $\mathbb{R}^n$. From chapter 2, it is simple to show that tighter bounds on attainability may be

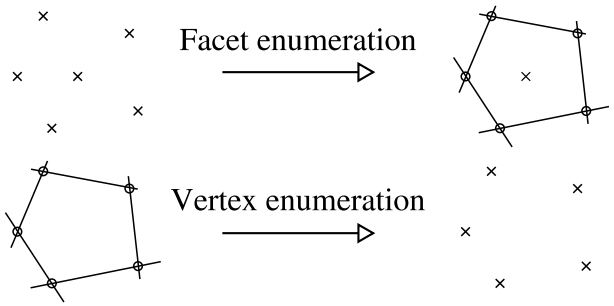


Figure 4.2.1: Geometric representation of vertex and facet enumeration

established through mass balance constraints via the stoichiometric subspace S. We provide a fuller description of the method in appendix B.2 together with a worked example. Nevertheless, knowledge and calculation of stoichiometric subspace forms the basis of the method of bounding hyperplanes (Abraham and Feinberg, 2004), as will be discussed next.

4.3 AR construction via hyperplanes

4.3.1 The method of bounding hyperplanes

Removing unachievable points

The original method of bounding hyperplanes is an AR construction technique that utilises the successive addition of bounding hyperplanes to eliminate unattainable regions from the stoichiometric subspace S. With each successive iteration, unattainable regions (regions that form part of the stoichiometric subspace but that are physically unachievable through any conceivable reactor network), are cut away from the space. Repeated removal of unachievable states produces a tighter bounding set of achievable points in the space. Hyperplanes are orientated such that division of the two regions results in one of the two halves containing only unachievable concentrations.

This is feasible because it is possible to form a condition that guarantees the denial of achievability. This is done utilizing a proof from Abraham and Feinberg (2004). Hence points on the separated half space must be checked for denial of achievability relative to the current hyperplane. Abraham and Feinberg (2004) demonstrate that if a rate vector $\mathbf{r}(\mathbf{C}_i)$ evaluated at a point $\mathbf{C}_i$ on a hyperplane points into the hyperplane, then $\mathbf{C}_i$ is not achievable. The method of bounding hyperplanes thus utilizes this condition to eliminate these points in a systematic manner. This is achieved by successively introducing hyperplanes at different positions and orientations in space in an attempt to identify all unachievable concentrations in the stoichiometric subspace. By moving hyperplanes inwards starting from the

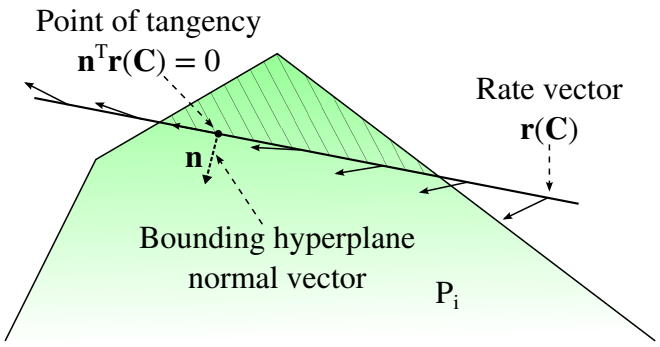


Figure 4.3.1: Eliminating unachievable space via hyperplanes. Hyperplanes are moved into the current polytope until tangency between $\mathbf{r}(\mathbf{C})$ and $\mathbf{n}$ is observed.

extreme points of the polytope, we ensure that only unachievable states are removed from the space.

Figure 4.3.1 demonstrates this graphically for a regionP_i. Three distinct classes of rate vectors, relative to the bounding hyperplane, may be distinguished from Figure 4.3.1:

1. Rate vectors that point into the hyperplane. These rate vectors satisfy the condition $\mathbf{n^T r}(\mathbf{C}) > \mathbf{0}$. These points are unachievable according to Abraham and Feinberg (2004).

2. Rate vectors evaluated with respect to the hyperplane normal satisfy the condition $\mathbf{n^T r}(\mathbf{C}) < \mathbf{0}$. We can make no assumption about the attainability of these points (provided they lie within the current polytope).

3. Rate vectors tangent to the hyperplane. These satisfy the condition $\mathbf{n^T r}(\mathbf{C}) = \mathbf{0}$. Points that satisfy this condition may or may not be achievable.

Stopping criteria

In practice, a hyperplane is moved into the current polytope at discrete steps in the opposite direction of the hyperplane normal. Further movement into the region is possible as long as the following stopping conditions are not encountered:

1. The hyperplane does not exclude any feed points. Feed points are by definition attainable and thus these points must be included in the current polytope.

2. The hyperplane does not exclude any equilibrium points. Similar to feed points, equilibrium points are also attainable (in the limit of infinite residence time) and thus must also be included.

3. The hyperplane does not exclude any rate vectors which are tangent to the hyperplane normal. That is, concentrations satisfying the condition $\mathbf{n^T r}(\mathbf{C}) \leq \mathbf{0}$ must be retained.

Notice that no assumption is made about the attainability of points whose rate vectors point out of or are tangent to the hyperplane. It is not possible to discern from the condition and so points satisfying $\mathbf{n^T r}(\mathbf{C}) \leq \mathbf{0}$ cannot be exclude them from the region on this basis alone.

The method

We only present a generalised description of the method. Once a hyperplane with the above orientation is achieved, the portion of the current bounded region lying on the negative half space of the hyperplane is discarded and the newly introduced hyperplane is added to the current set of constraints forming the bounding set. Repeated stages of refinement transform the original stoichiometric subspace into a smaller convex polytope containing only those output compositions achievable through reaction and mixing (the AR).

The algorithm begins with initialisation of stoichiometric constraints. These constraints are in the form of a list of hyperplanes constraints that define a bounded region in concentration space (the H-representation). Figure 4.3.2 demonstrates the general geometric action of the bounding hyperplanes algorithm. The region defined by the initial set of hyperplanes represents the stoichiometric subspace S. New hyperplanes are then introduced at the vertices (corners) of S and eliminations are carried out. Newly introduced hyperplanes are moved into S until one of the above conditions are met. At this point, the region has been refined by the entry of additional constraints. The extreme points of the resulting polytope are calculated and the process is repeated for the new region. That is, the current polytope is transformed into the V-representation with the new hyperplane via vertex enumeration.

The process may now be repeated. Additional hyperplanes are introduced and eliminations continue until no further hyperplane can be added without violation of the above conditions to within a specified tolerance. The convex polytope resulting from the bounding process represents the set of achievable concentrations through reaction and mixing, and is an approximation to the AR as a result.

The bounding hyperplanes method is found to be a robust AR construction technique, and is particularly successful in constructions belonging to kinetics involving multiple steady states. This success is, above all, a consequence of its approach to infeasible region elimination rather than feasible region addition. What is unclear from the above description though is the large overhead involved for intermediate computations between trimming stages. These stages add to the total construction time and make the algorithm uncompetitive for the construction of simpler kinetics. A modification to the above technique is presented below that aims to maintain the virtues of infeasible region elimination whilst reducing the volume of unnecessary intermediate computations.

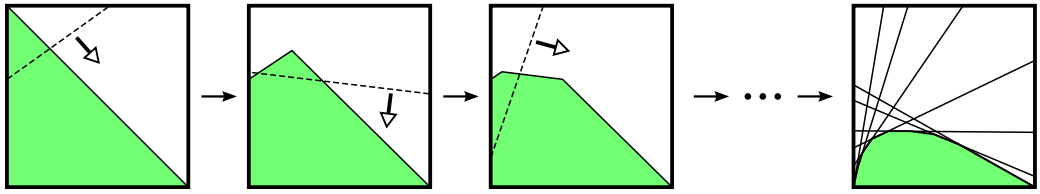


Figure 4.3.2: Unattainable region elimination via bounding hyperplanes. At each iteration a hyperplane is introduced at the corner of the current polytope. The plane is moved into the region until either a tangent rate vector is found, or feed or equilibrium points are excluded. After each hyperplane addition, the bounded region is smaller than the last and represents a more accurate approximation of the AR. This algorithm requires computation of the polytope vertices (vertex enumeration).

4.3.2 A revised method of AR construction

As in section 4.3.1, description of the revised method is facilitated by consultation of Figure 4.3.3, in which a general schematic of the construction process is shown. The original method of bounding hyperplanes seeks to eliminate unattainable regions by introducing a new hyperplane at a corner of the polytope. These hyperplanes have a fixed orientation, calculated as a weighted average of the hyperplane that shape the corner. The hyperplane is then moved into the current bounding set until rate vectors evaluated on the plane are either tangent or point out of the plane. In this way, eliminations can be viewed as a translation through space with fixed orientation. An alternative method of eliminations is possible, however. The idea is presented as follows:

Rather than fixing the hyperplane orientation and moving it about through space, fix the hyperplane position and vary its orientation.

This is done through a rotation about an existing edge of the current polytope. Existing extreme points of the polytope generated from previous iterations may then be used as edges from which new hyperplanes may be introduced and rotated about. New extreme points to the AR may be combined with existing ones obtained from previous iterations. The polytope describing the region is then built facet-by-facet. The revised method is hence given as follows

1. Compute the stoichiometric subspace S. S can be converted into a list of hyperplane constraints. These hyperplanes are calculated by the methods described above for the determination of S, and are specific to the reaction stoichiometry under consideration and feed vector $\mathbf{C_f}$.

2. Determine the hyperplane that passes through the feed point $\mathbf{C_f}$. This is the first hyperplane to be considered for rotation. The feed point will also act as the edge about which the first hyperplane is to be rotated.

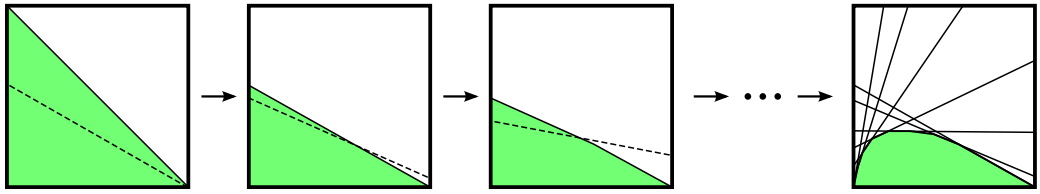


Figure 4.3.3: Unattainable region elimination via rotating hyperplanes. In this instance, hyperplanes are rotated about an edge making up the current polytope. Vertex enumeration is not required with this method.

3. Using the known extreme point, rotate the chosen hyperplane by a small angle θ. If it is found that any feed or equilibrium points lie outside of the current feasible region due to the new rotation, then unrotate and stop. Output the list of extreme points and terminate the algorithm.

4. Discretise concentrations lying on the plane.

   (a) For each discretised point $\mathbf{C}_i$, compute $\mathbf{n}^{\mathrm{T}}\mathbf{r}\left(\mathbf{C}_i\right)$

      i. If $\mathbf{n}^{\mathrm{T}}\mathbf{r}\left(\mathbf{C}_i\right) \leq \mathbf{0}$, then condition 1 is no longer satisfied and a tangent point has been found. Record this concentration $\mathbf{C}_i$.

      ii. Unrotate the hyperplane back to its previous position.

      iii. In addition to this, unrotate the vector $(\mathbf{C}_0 - \mathbf{C}_i)$ by angle θ used above. This is done so that the extreme point found in step a.i) maintains its position on the newly unrotated hyperplane. Record this rotated $\mathbf{C}_i$ and go to 6.

5. If all discretised points in the list have been considered and it is found that none of these points satisfy the tangency condition, then the current hyperplane orientation may be rotated into the polytope further. Hence return to 3.

6. Combine the new rotated hyperplane with the current list of hyperplanes currently bounding the region. Add the newest extreme point found in 4(a)iii to the current list of extreme points. Go to 3.

Rotations are achieved by the use of a rotation matrix $\mathbf{R} \in \mathbb{R}^n$. The direction of rotation is chosen such that rotations bring about a reduction in the size of the resulting polytope. Rotations performed in the special two dimensional setting are particularly simple to compute, involving a single matrix multiplication. In addition to this, there is only one plane through which rotations may occur, and the edges rotated about are single points.

Motivation for rotations

The benefit afforded by rotations as opposed to translations through space is subtle, and only arises upon implementation of the two methods. The former undergoes

two computationally intensive, yet entirely necessary, stages.

1. The first, which is common to both approaches, is the act of hyperplane discretisation (computing distinct points lying on the hyperplane and then checking the rate vector at each point). Since a hyperplane represents an $n-1$ dimensional subspace in $\mathbb{R}^n$, hyperplane discretisation may be viewed as a computational process of degree $n-1$. Adopting Big-O notation, the number of floating point operations (flops) for such a process is proportional to approximately $O(\mathrm{M}^{n-1})$, where M is the number of discretised points for each axis in space and n is the dimension of the computational space (the dimension of S).

2. The second intensive computation is altogether suppressed during the early stages of refinement but quickly emerges as the number of bounding hyperplanes increases throughout construction. In order for new hyperplanes to be introduced, we must know the locations of the extreme points of the polytope, defined by the current list of hyperplanes. That is, for each iteration of the elimination process, the vertex enumeration problem must be solved. This is a non-trivial problem, particularly for higher dimensional spaces involving many hyperplanes. A brute-force implementation can be achieved by computing the intersection of each plane with every other hyperplane in the region: Given L hyperplanes in $\mathbb{R}^n$, brute-force computation results in at most $L!/\left[n!\,(L-n)!\right]$ total intersections that must be calculated, and hence this method is not recommended. More efficient methods exist that solve the problem in polynomial time (Dyer, 1983), potentially alleviating part of the computational burden, although a vertex enumeration step is nevertheless required in order for eliminations to be carried out.

   A final consideration is the issue of redundant hyperplanes, that is, hyperplanes that play no useful role in defining the feasible region. It is wise to exclude these from the set of bounding constraints as quickly as possible though, as the numbers of redundant hyperplanes can quickly outnumber the number of useful planes describing the feasible region. This ultimately affects the vertex enumeration step in an undesirable manner. As a result, the additional expense of redundant hyperplane removal contributes further to the total computation time of the bounding process.

The benefit of utilising hyperplane rotations as opposed to translations is that the former does not require the enumeration of vertices (point 2). As a result, the costly exercise of redundant hyperplane removal and vertex enumeration stages may be avoided. This is accomplished by the addition policy of the revised method. Since rotations are done about existing, known attainable points, the hyperplane tangency condition guarantees that the new extreme point found is (in $\mathbb{R}^2$) attainable by CSTR from eq 2.3.2. Hence, at every stage of construction, boundary points of the

AR are found, and intermediate points never enter the problem. The enumeration of vertices is still an unnecessary computation however. We refer the reader to section 4.6 for a discussion on how constructions might be carried out in higher dimensions.

Although it is the aim to achieve candidate AR constructions via an elimination of unachievable space, this can be carried in a number of ways. The use of hyperplane rotations is one such method which is, in principle, no different to the method of bounding hyperplanes – both methods ultimately rely on the tangency condition with the rate vector, as discussed above. However, the use of rotations is observed to be faster in practice. We demonstrate this with a number of examples below.

4.4 Examples

4.4.1 Isothermal constructions

van de Vusse kinetics

We now demonstrate how the method of bounding hyperplanes may be improved by plane rotations for various examples. In all the examples presented, we have assumed that the systems are operated isothermally and under constant density. Although we shall later present an example in which the isothermal assumption is relaxed, we honour this restriction for purposes of comparison to the original method.

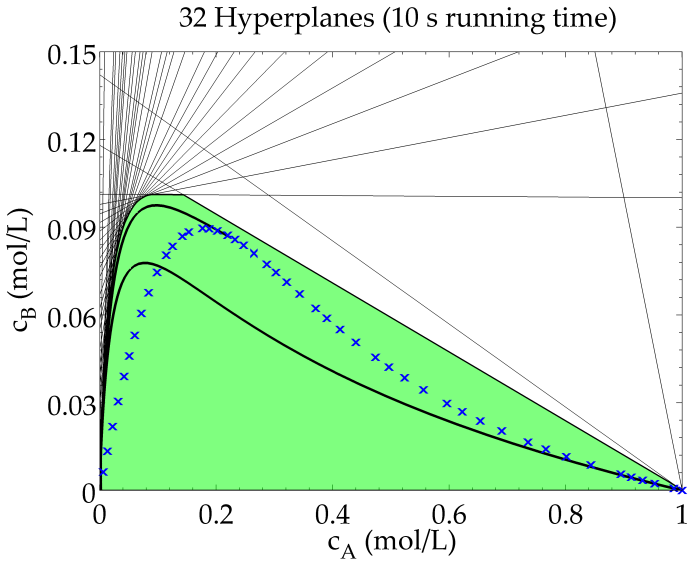
We begin with the well understood van de Vusse reaction scheme. The system is given by the following set of reactions:

$$\begin{aligned} \mathrm{A} &\underset{k_2}{\overset{k_1}{\rightleftharpoons}} \mathrm{B} \overset{k_3}{\rightarrow} \mathrm{C} \\ 2\mathrm{A} &\underset{k_4}{\rightarrow} \mathrm{D} \end{aligned} \tag{4.4.1}$$

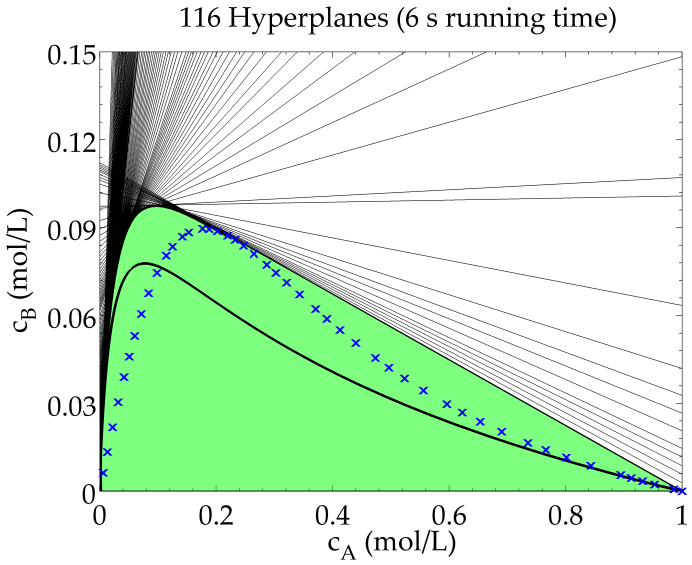
Several variations of the above kinetics exist but only the simplest scenario is presented here, that is a 2D system in $c_A - c_B$ space with mass action kinetics given by the following constants $k_1 = 1.0$, $k_2 = 0.0$, $k_3 = 1.0$ and $k_4 = 20.0$, such that

$$\mathbf{r}(\mathbf{C}) = \begin{bmatrix} -k_1 c_{\mathrm{A}} + k_2 c_{\mathrm{B}} - 2k_4 c_{\mathrm{A}}^2 \\ k_1 c_{\mathrm{A}} - k_2 c_{\mathrm{B}} - k_3 c_{\mathrm{B}} \end{bmatrix}$$

The AR is then found to be produced by a CSTR followed in series by a PFR. Unfortunately this arrangement cannot be established by the algorithm, but has been included to demonstrate the accuracy to which constructions may agree with their theoretical predictions. A worked example for the first iteration of this problem can be found in appendix B.1. Here, the reader will find details discussing the necessary set-up steps required before the algorithm can be initialised. The results of the construction are given by Figure 4.4.1 below where a comparison is made between the original (translated) and revised (rotated) methods.



(a) Bounding hyperplanes.



(b) Rotated hyperplanes.

Figure 4.4.1: A comparison of construction methods carried out for van de Vusse kinetics. The CSTR locus (×) and PFR trajectories (-o-) have also been drawn.

The total running time for the original method took 10 seconds and is bounded by 32 hyperplanes. The shape of the boundary produced by the original method agrees with the analytical solution although a distinct difference between the two is noticeable near the CSTR-PFR junction. In particular, the maximum concentration of component B is overestimated slightly with the original method. The results achieved with the revised approach by comparison are in close agreement with the theory. The time taken to construct the new region took 6 seconds and is constructed with 116 hyperplanes. Although running time is of a similar order to the former, the region is assembled with a significantly larger number of hyperplanes, allowing for a more precise bound to be established.

The results highlight an important consideration associated with both methods. That is, there is no claim that the resulting polytope obtained from construction is indeed the true AR. Rather, the results provide an upper bound on kinetic attainability. Certainly there is evidence to suggest that in the limit as more hyperplanes are used to bound the region, we approach the true AR boundary, however the regions obtained by either method are necessarily always larger than the true solution. If both an inside-out and outside-in method are available, then comparison between the two candidate ARs may allow for the determination of the true AR boundary. If the results of the two do not correspond, then a closer bound on the true boundary is reached as we know that the true region must lie between the two constructions.

Complex van de Vusse kinetics

Next we study a fairly artificial example, one in which highly non-linear behaviour is observed. This may be produced by the following rates of formation

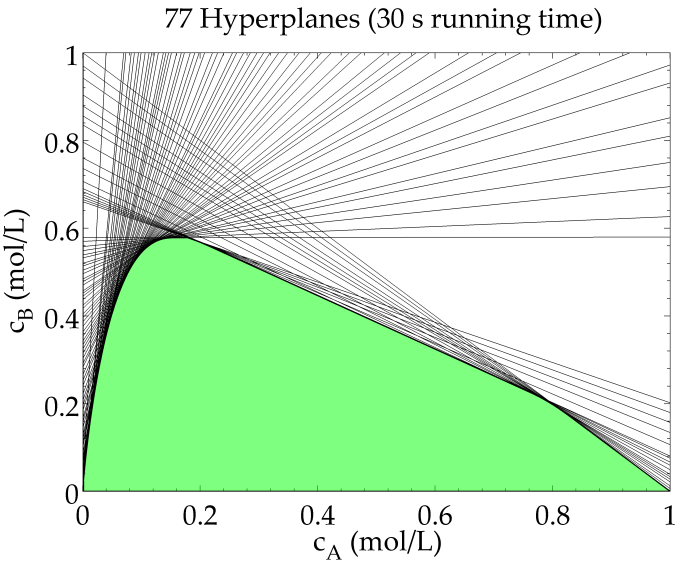
$$\begin{aligned} r_{\mathrm{A}}(\mathbf{C}) &= \mathrm{f}(c_{\mathrm{A}})^2 + c_{\mathrm{A}} c_{\mathrm{B}} \frac{\mathrm{d}\mathrm{f}(c_{\mathrm{A}})}{\mathrm{d}c_{\mathrm{A}}} \\ r_{\mathrm{B}}(\mathbf{C}) &= c_{\mathrm{A}} \mathrm{f}(c_{\mathrm{A}}) \end{aligned}$$

where

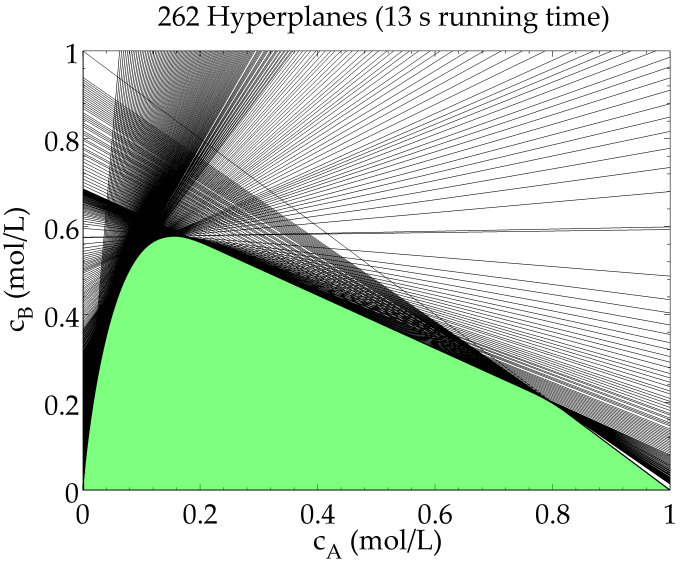
$$\mathrm{f}(c_{\mathrm{A}}) = 6c_{\mathrm{A}}^6 - 6c_{\mathrm{A}}^5 + 9c_{\mathrm{A}}^4 - 16c_{\mathrm{A}}^3 + 9c_{\mathrm{A}}^2 - 2c_{\mathrm{A}}$$

The reaction scheme is identical to the one posed for regular van de Vusse kinetics by eq 4.4.1, although the actual rate expressions are more complicated now. A PFR trajectory associated with the kinetics given above show multiple concavities, indicating that both reaction and mixing processes will feature prominently in the formation of the AR boundary. Indeed, it is found that for a feed concentration of $\mathbf{C_f} = [1, 0]^{\mathrm{T}}$, the AR is constructed from a four reactor series network of CSTR-PFR-CSTR-PFR (Glasser et al., 1987). Figure 4.4.2 provides results obtained from both methods of construction.

Once again, both the original and revised methods allow for an accurate approximation of the AR boundary, even for highly non-linear kinetics. The efficiency by



(a) Bounding hyperplanes.



(b) Rotated hyperplanes.

Figure 4.4.2: Construction comparison for non-linear van de Vusse kinetics

which constructions are carried out differ greatly between the two nevertheless. 77 hyperplanes have been used to construct the AR by the original method in a time of 30 seconds and agree favourably with the results obtained from the new approach. The latter is produced with over three times as many hyperplanes and is accomplished in a significantly shorter time. Hence, in a period of 13 seconds, the method of rotations has allowed for the introduction of 262 hyperplanes producing a tightly bound region. For this example, the use of either method requires the introduction of a rather large number of hyperplanes in order for an adequate approximation of the AR to be made. Multiple curved and straight line segments are noticeable on the boundary and it is apparent how curvature is approximated with many hyperplanes. Hence it can be expected that the most gains in calculation time may be associated with boundaries having high curvature. We next examine a situation in which this is not the case in the next example.

Multiple steady states

Hence, we now compare constructions for an example where multiple steady states allow for the occurrence of discontinuous regions to be observed from within the stoichiometric subspace. The reaction system is given by the following rates of formation

$$\begin{aligned} r_{\mathrm{A}}(\mathbf{C}) &= -k_1\left[c_{\mathrm{A}} + \frac{b\left(c_{\mathrm{A}}c_{\mathrm{B}}\right)^2}{1+k_2 c_{\mathrm{A}}c_{\mathrm{B}}^2} + ac_{\mathrm{A}}\right] \\ r_{\mathrm{B}}(\mathbf{C}) &= k_1\left[c_{\mathrm{A}} + \frac{b\left(c_{\mathrm{A}}c_{\mathrm{B}}\right)^2}{1+k_2 c_{\mathrm{A}}c_{\mathrm{B}}^2}\right] \end{aligned}$$

with $k_1 = 1\times10^{-3}\,\mathrm{min}^{-1}$, $k_2 = 40\,\mathrm{L}^3/\mathrm{mol}^3$, $a = 100$ and $b = 1\times10^4\,\mathrm{L}^3/\mathrm{mol}^3$. We shall again assume that a single feed stream exists, with pure A such that the feed stream concentration vector is $\mathbf{C_f} = [1,\,0]^{\mathrm{T}}$. A plot of the CSTR locus identifies two separate branches that exist for the specified feed concentration. It is possible, using standard techniques (Glasser et al., 1987), to show that a CSTR followed by a PFR is required in order to obtain the AR associated with the kinetics provided. The results are given by Figure 4.4.3. The candidate AR found indicates a maximum achievable c_{B} concentration of approximately 0.61 mol/L.

For comparison, the CSTR locus of $\times$'s corresponding to the feed concentration has been plotted. The second branch is an isola and it is apparent from the constructions the significant contribution it provides in the full range of total achievable concentrations. Kinetics involving multiple steady states are particularly difficult to construct and are most likely to cause differences between constructions of inside-out and outside-in methods. Candidate AR construction via inside-out methods requires knowledge of multiple steady states, as the discovery of only partial convex regions may result if knowledge of their existence is unknown. Prior knowledge of

this behaviour is often difficult to predict however. Indeed, behaviour in isothermal reactions may vary considerably, even for noticeably similar kinetics (Schlosser and Feinberg, 1994). These situations occur frequently in adiabatic reactions unfortunately (Hildebrandt, 1989) and thus there is a need to develop techniques that are able to handle these systems.

Both methods produce an accurate bound on the set of all attainable concentrations despite the fact that there exists irregular areas formed by the isola. The AR exhibits minimal curvature, that is, the PFR trajectories vary somewhat linearly near the AR boundary. This allows for a rather simply shaped triangular region that is easily approximated using a small number of bounding hyperplanes. As a result, the associated construction times and candidate regions produced by both methods are fairly competitive and little benefit is obtained with the use of plane rotations rather than translations. Consequently, the AR constructed by the original approach is approximated by 16 hyperplanes and was achieved in a time of 16 seconds whilst the revised method bounds the same region in a time of 4 seconds with 18 hyperplanes. Nevertheless, we notice that even for kinetics in which the AR may be approximated well with few hyperplanes, opportunities for improvement still exist. Although such examples exhibit minimal overhead involved in vertex enumeration, we find that rotations allow for more appropriate placement of hyperplanes in space and offer a more efficient means of candidate AR boundary construction.

4.4.2 Temperature dependent kinetics

Let us know consider an example in which the isothermal constraint is no longer required. The system of reactions we consider here again take the form of the familiar van de Vusse kinetics, however we shall now allow the rate constants to be of the Arrhenius form (Godorr et al., 1999)

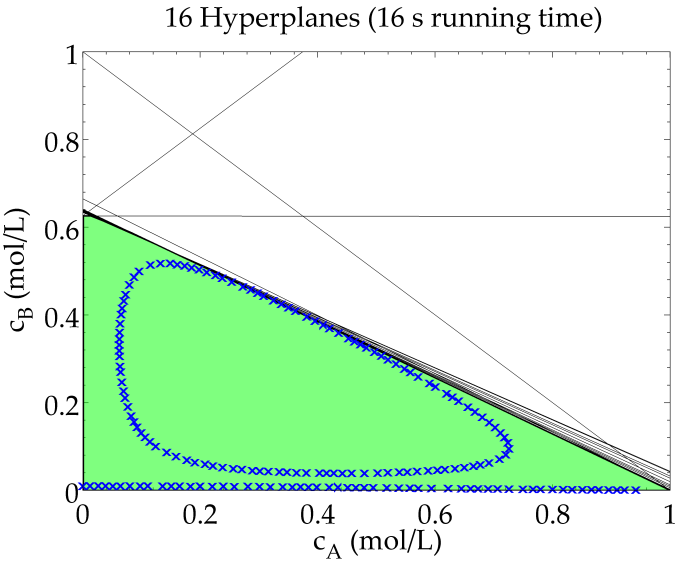
$$k_i\left(\mathrm{T}\right) = k_i^0 \exp\left(-\frac{\mathrm{E}_i}{\mathrm{RT}}\right) \tag{4.4.2}$$

The values for k_i^0 and E_i for each component are given below

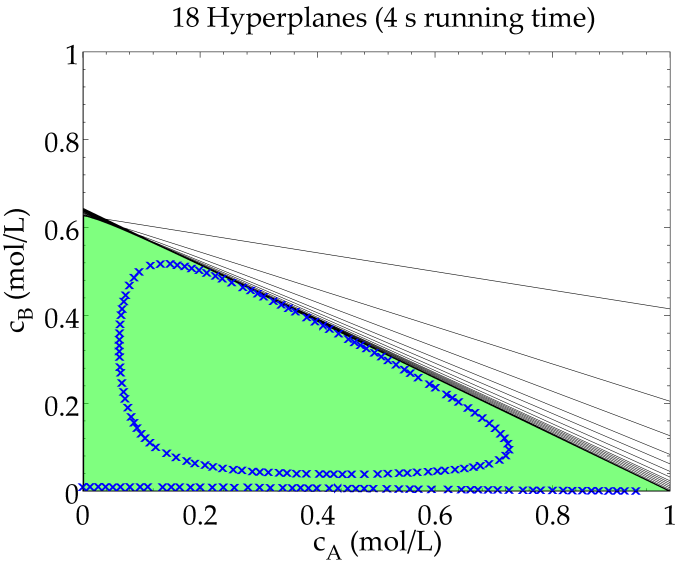
Table 4.1: Arrhenius constants for temperature dependent van de Vusse kinetics

i	$k_i\left(\frac{\mathrm{mol}}{\mathrm{L\cdot min}}\right)$	$\frac{\mathrm{E}_i}{\mathrm{R}}\left(\mathrm{K}\right)$
k_1	4	500
k_2	1.5	800
k_3	6	0
k_4	0	0

As a result, the rate vector is no longer a sole function of $\mathbf{C}$ and is now also



(a) Bounding hyperplanes.



(b) Rotated hyperplanes.

Figure 4.4.3: AR construction with multiple steady states. $\times$ represent the CSTR locus for the feed concentration

temperature dependent

$$\mathbf{r}\left(\mathbf{C}, \mathrm{T}\right) = \begin{bmatrix} -k_1\left(\mathrm{T}\right) c_{\mathrm{A}} - 2k_4\left(\mathrm{T}\right) c_{\mathrm{A}}^2 \\ k_1\left(\mathrm{T}\right) c_{\mathrm{A}} - k_3\left(\mathrm{T}\right) c_{\mathrm{B}} \end{bmatrix}$$

It is now possible to vary the direction in which the rate vector points by a variation in temperature. Hence, for every point in concentration space, the rate vector is allowed to take on multiple directions depending on the temperature at which it is evaluated at. The handling of temperature dependent kinetics is a fairly straight forward modification to the standard approach discussed in section 4.4.1 above. Instead of checking for a single tangent rate vector at a concentration residing on the plane, we now check for a range of rate vectors. This range corresponds to the range of allowable temperatures specified between given operating temperature limits. Much in the same way that a grid is generated in concentration space for calculation of discretised points on the plane, points in temperature space between the maximum and minimum permissible temperature limits are now also determined. Then, for each valid concentration generated on the plane, the range of rate vectors between the operating limits are all evaluated for tangency.

Figure 4.4.4 shows the results of the construction for the non-isothermal case operating between a temperature interval of 300 K to 1000 K. In order to maintain a path on the boundary of the AR, the temperature profile would need to follow the one suggested in Figure 4.4.4. It can be seen that the temperature profile declines rapidly over a small c_{A} concentration range from approximately 0.25 mol/L to 0.18 mol/L. The optimum recommended operating temperature profile is in agreement with the recommendation suggested by (Godorr et al., 1999). Construction time took significantly longer for this case, totalling 479 seconds. This is largely due to a fine grid of 500 points used between the temperature interval and small rotation angle of 1×10^{-4} radians. The boundary is composed of 150 hyperplanes.

AR boundaries corresponding to isothermal operation at the minimum and maximum allowed operating temperature are also provided in Figure 4.4.4. Hence the AR resulting from a design in which the operating temperature is maintained at 1000 K allows for a large portion of the total optimal set of concentrations to be achieved. This is expected as the optimal temperature profile suggests that, for the c_{A} range of approximately 1 mol/L to 0.25 mol/L, the temperature which extends the region the most is one that is maintained at its maximum value. A design using only the lower temperature of 300 K on the other hand results in a region which is noticeably smaller between the entire c_{A} range. What is apparent nevertheless is that isothermal designs maintained at either temperature do not result in an AR which is considered optimal, as a small range of concentrations near $c_{\mathrm{A}} = 0.1$ mol/L to $c_{\mathrm{A}} = 0.0$ mol/L exist that are only achieved by a varying temperature profile.

Determination of the optimal profile is easily handled by this approach, as no

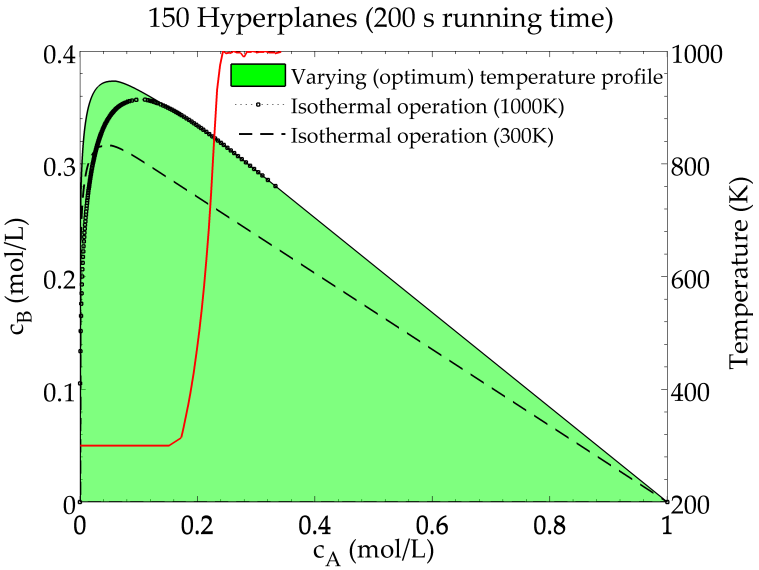


Figure 4.4.4: Temperature dependent kinetics. The ARs constructed for isothermal operation at the two operating limits are both smaller than the one obtained by the optimal temperature profile.

other modifications to the underlying elimination method need to be changed. Constructions for non-isothermal kinetics allow for inclusion of many more reactor optimisation problems, and ones which are much more likely to occur in reality when used with mass fractions described earlier.

4.4.3 Unbounded construction

Finally we consider finding the AR for the case when we wish to determine the smallest reactor volume. These examples are common in the design of batch processes (Nicol et al., 2001). We consider an AR construction in concentration-residence time space where the resulting feasible region is unbounded. The reaction is assumed to be an adiabatic decomposition under constant pressure. The rate of formation is again assumed to follow the Arrhenius form

$$r\left(c\right) = ck_1 \exp\left(\frac{-4000}{\mathrm{T}\left(c\right)}\right) - \left(1-c\right) k_2 \exp\left(\frac{-8000}{\mathrm{T}\left(c\right)}\right)$$

where c is concentration and $k_1 = 5 \times 10^5$ and $k_2 = 5 \times 10^8$. For simplicity, we assume constant specific heat and heat of reaction, the temperature for the process is then

$$\mathrm{T}\left(c\right) = \mathrm{T}_\mathrm{b}^0 + \mathrm{T}_\mathrm{ad}\left(1-c\right)$$

where $\mathrm{T}_\mathrm{b}^0 = 300\,\mathrm{K}$ and $\mathrm{T}_\mathrm{ad} = 200\,\mathrm{K}$. In this space, the rate vector is given as

$$\mathbf{r}\left(c\right) = \begin{bmatrix} r\left(c\right) \\ 1 \end{bmatrix}$$

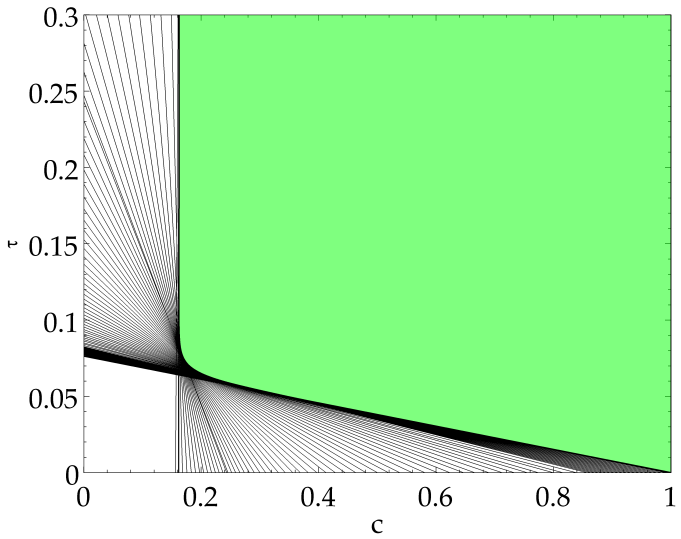


Figure 4.4.5: Unbounded AR construction

We specify that the feed stream does not contain any products so that $c = 1$ and construct the unbounded region in the same manner as in the previous examples. The only additional alteration required is the direction of rotation. Seeing as equilibrium is achieved as residence time is increased, we now specify that hyperplanes must be rotated in a clockwise direction in order for the region to be bounded correctly. The results of the construction are provided by Figure 4.4.5. For the specified rate a minimum residence time of approximately 0.09, at which minimum $c = 0.16$ has been reached. The region is defined by 78 hyperplanes and took 43 seconds to construct.

Construction of the AR face by face presents unique opportunities for the construction of a special class of convex polytope, that being unbounded polytopes. Elimination via a rotation implies no dependence or knowledge of all existing corners to the current polytope, and hence reliance on a closed polytope is not a requirement. Constructions of these types are unique to the revised method and are unachievable by the regular method. Both the original and revised bounding hyperplane algorithms were programmed in C++ using Microsoft Visual Studio 2008. The computations for all examples discussed were carried out on an Intel Core i3-530 processor (2.93 GHz) and 4 GB RAM (DDR3 1600) under Windows 7 64-bit Edition.

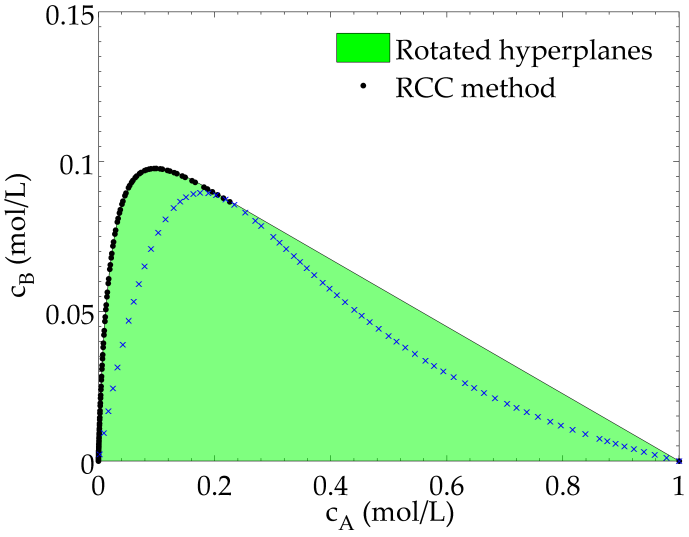
4.5 Example of numerical sufficiency: Comparison to an inside-out method

Although the rotated hyperplanes method has shown to generate regions consistent with the method of bounding hyperplanes, uncertainties still remain in the resulting

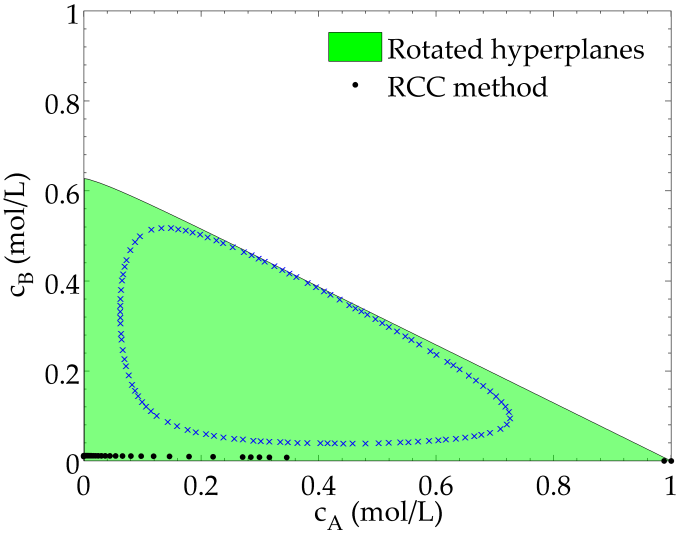
constructions. Due to the elimination nature of the hyperplanes method, one can only guarantee the removal of unachievable points; the remaining region may still contain unachievable states. The true AR must then reside as a subspace within the candidate region generated by the method, and only in the case that all unachievable points are removed is the true AR obtained. Similarly, inside-out methods achieve AR construction via the addition of regions that are guaranteed to be achievable. The resulting region is then an approximation of the true AR only if all achievable points have been identified during the construction process. This is of course a non-trivial task if multiple steady-states exist in the system. A discrepancy exists between both construction procedures as a result.

Observe however that if both approaches are combined, this gives way to a more robust procedure for computing candidate ARs. Agreement in shape and size between the two methods signals, at least numerically, for when the true AR might be found. Although significant advancement in the field may still be needed in terms of developing a theoretical sufficiency condition for the AR, combining both inside-out and outside-in construction approaches provides an avenue for numerical sufficiency. It should be recognised that there exists a rich field of literature exists for a similar problem encountered in global optimisation. Specifically, the idea of spatial branch and bound methods in global optimisation bears resemblance to the idea presented here. Lower and upper estimate bounds on the optimisation solution are generated and then refined to obtain a globally optimal solution (Land and Doig, 1960; Tawarmalani and Sahinidis, 2004). Convergence to the global optimum is achieved when the lower and upper bounds meet.Clausen (1999) provides a readable introduction to branch and bound techniques in optimisation, whereas the application of branch and bound techniques to chemical reactor networks are discussed by Ryoo and Sahinidis (1995); Smith (1996); Smith and Pantelides (1999).

In Figure 4.5.1a, we demonstrate this idea with the 2D van de Vusse and Isola examples from section 4.4.1. The rotated hyperplanes method is used as the outside-in part of the construction, whereas the inside-out portion is carried out using the Recursive Constant Control policy method of Seodigeng et al. (2009); Seodigeng (2006). The RCC method is chosen as it is found to be particularly flexible in terms it's construction types, it is simple to program, and is generally considered to be a fast candidate AR construction method. In Figure 4.5.1a, the results of both constructions are compared and overlaid onto the same plot for the van de Vusse system. The shaded region is that belonging to the rotated hyperplanes construction, whereas the boundary corresponding to filled circles are those obtained from the RCC method. The CSTR locus is also shown for comparison. Notice that there is close agreement between the two methods, even though each method has generated the region from two independent construction approaches. This provides a strong indication that the region in Figure 4.5.1a is the true AR, barring minor numerical differences.



(a) 2D van de Vusse kinetics



(b) Isola kinetics

Figure 4.5.1: Comparison of methods for hybrid AR construction.

Table 4.2: Comparison of AR volumes generated by the RCC and rotated hyperplanes method for hybrid AR construction

System	RCC volume	Rotated hyperplanes volume	% Similarity
2D van de Vusse	0.0532	0.0533	99.8%
Isola	0.0010	0.3207	0.312%

Figure 4.5.1b, by comparison, demonstrates the construction results from both techniques for the isola example. Unlike the van de Vusse example, there is a clear difference between the region obtained by the hyperplanes method and the RCC method. Whereas the hyperplanes method produces the larger region including the isola, the inside-out nature of the RCC method does not successfully identify the isola. This is because the RCC method relies on continuity information, in the form of integrating the DSR equation for many constant α values; the method has no inherent knowledge of the existence of multiple steady states outside of the localised region that the DSR expression operates in the lower portion of the space. In this example, there is a clear discrepancy in results between the two methods. Thus, use of both inside-out and outside in methods in a combined analysis provides proof when there is agreement between the two, and signals for further work when there is a significant difference in results.

The AR volume may be used as a numerical measure from which the two methods may be compared against. The AR volume is always positive and is maximised corresponding to the true AR. The region becomes smaller with outside-in methods and larger with inside-out methods. Table 4.2 shows the AR volumes corresponding to both methods for the examples considered. The % similarity column is calculated as the ratio of volumes obtained by the RCC and rotated hyperplanes method, repsectively. In the case of the van de Vusse example, the volumes are in very close agreement. Indeed, the RCC volume is 99.8% the volume of the hyperplanes approach. There is still a difference in calculated volumes, due to the numerical nature of each approach, however the two produce effectively the same region to within the numerical tolerances specified. On the other hand, the RCC volume for the isola example is 0.312% of the rotated hyperplanes method. This is due, of course, to the existence of the large isola which is only identified by the hyperplanes method. Even if the isola had not been known, this result is still useful as it indicates that there may be irregular behaviour (multiple steady-states) in the system which requires further investigation.

4.6 Remarks on higher dimensional construction

4.6.1 Introduction

Constructions in $\mathbb{R}^n$ are currently not yet fully developed, however several ideas are provided below for how they might be carried out. The expected complications involved in generalised n-dimensional constructions are also discussed. In order to extend the method of rotation to higher dimensions, we must first have an understanding of how these may be generalised, in spaces that cannot be easily visualised. First, a generalised description of rotations is discussed which describes how this is achieved in $\mathbb{R}^n$. Next, supporting mathematical details are given, followed by a proposed method for extension to higher dimensions. A brief discussion on the potential difficulties and uncertainties with the approach is then supplied at the end.

4.6.2 Rotations in $\mathbb{R}^n$

Facets and ridges

Before a generalised discussion can be done, a basic understanding of the facets and ridges, associated with an n-dimensional convex polytope, must be known. We symbolise the convex polytope associated with the a candidate AR construction by conv($\mathbb{X}$). From section 4.2.4, a facet of conv($\mathbb{X}$) is a collection of extreme points such that n linearly independent points in conv($\mathbb{X}$) lie on a hyperplane $H(\mathbf{n}, \mathbf{C}_0)$ residing in $\mathbb{R}^n$. A facet is hence a $(n-1)$-dimensional polytope in $\mathbb{R}^n$ and a subspace of conv($\mathbb{X}$) – two vertices define a facet in $\mathbb{R}^2$, three in $\mathbb{R}^3$, and so on.

Ridges (edges) of conv($\mathbb{X}$) are similar in structure to facets. Indeed, a ridge is composed of vertices from a facet and hence it is a linear subspace of a facet. Specifically, $n-1$ linearly independent points of a facet create a ridge. A ridge is hence a $(n-2)$-dimensional polytope, and for any facet containing n vertices, there are $n-1$ ridges that are associated with it. The intersection of two facets creates a ridge. This is show in Figure 4.6.1a for two and three dimensions. A distinction is made between ridges and edges since edges are generally viewed with specific reference to three dimensions, whereas ridges are generalised for all dimensions.

General understanding

Rotations in higher dimensions are more challenging than those cast in $\mathbb{R}^2$ alone. This originates primarily from the fact there are more ways in which to rotate a plane in higher dimensional space. By example, in $\mathbb{R}^3$ there are three principle axis that a hyperplane can be rotated about (the standard basis involving x, y and z axes are an example of this). In general, there are $\binom{n}{2}$ principle axes in $\mathbb{R}^n$ and thus rotations in higher dimensions are not uniquely defined (Aguilera and Perez-Aguila, 2004). Moreover, the view of rotations in $\mathbb{R}^2$ and $\mathbb{R}^3$ can be misleading. That is,

rotations are often viewed to occur about an axis of rotation (a one-dimensional subspace of $\mathbb{R}^n$). From the previous statements, simply fixing the dimension for rotation only reduces the number of degrees of freedom for rotation by one, but for spaces greater than three, there are more principle axes from which rotations may still occur. Hence the understanding of rotations to occur about an axis of rotation (an edge) is only convenient for systems in $\mathbb{R}^3$.

Instead, it is better to view rotations in terms of a *rotation in a plane*. Points in space are then transformed with respect to the plane of rotation and a space orthogonal to the plane. The component of the point in the orthogonal subspace is hence unchanged by the action of a rotation. Rotations are therefore still two dimensional in nature, even when considered in higher dimensions. In Figure 4.6.1b we show this for $\mathbb{R}^3$, although the method is true for all dimensions.

We can generalise the idea of an edge and instead view rotations to occur about a ridge. Since a ridge is a $n-2$ dimensional subspace of $\mathbb{R}^n$, this leaves a two dimensional subspace about which points may be rotated in. Rotation are then not arbitrary, but rather are aligned with ridges from existing facets.

4.6.3 Additional mathematical details

Change of basis

A vector $\mathbf{x}$ viewed under one coordinate system can be written with respect to another by a change of basis. That is, given an general matrix $\mathbf{A}$ containing k linearly independent vectors forming a basis

$$\mathbf{A} = [\mathbf{a}_1, \mathbf{a}_2, \ldots, \mathbf{a}_k]$$

where $k \leq n$, the matrix multiplication

$$\mathbf{A}\mathbf{y} = \mathbf{x}$$

implies that $\mathbf{x}$ can be written as a linear combination of the columns of matrix $\mathbf{A}$. Elements in $\mathbf{y}$ are then scalar 'weights' that give the relative proportions of the columns of $\mathbf{A}$ used to express $\mathbf{x}$. Vector $\mathbf{y}$ is hence a k-dimensional vector that re-expresses $\mathbf{x}$ with respect to the new basis defined by $\mathbf{A}$. Observe that $\mathbf{A}$ need not be square (the columns of $\mathbf{A}$ form a subspace of $\mathbb{R}^n$) and the columns of $\mathbf{A}$ need not be orthogonal (although it is useful is the columns of $\mathbf{A}$ form an orthonormal basis).

Rotation matrix

The rotation matrix

$$\mathbf{R} = \begin{bmatrix} \cos(\theta) & -\sin(\theta) \\ \sin(\theta) & \cos(\theta) \end{bmatrix} \tag{4.6.1}$$

rotates a vector $\mathbf{C}_i \in \mathbb{R}^2$ by an angle θ in the plane when $\mathbf{R}$ is multiplied to $\mathbf{C}_i$. It follows that a rotated vector $\mathbf{C}_i^{'} \in \mathbb{R}^2$ is given by

$$\mathbf{C}_i^{'} = \mathbf{R}\mathbf{C}_i$$

By definition, rotations preserve lengths and angles. We can see that the action of $\mathbf{R}$ might also be viewed as a change of basis in which lengths and angles are preserved.

Projections onto a plane and the orthogonal complement

Suppose that $\mathbf{A}$ is a matrix containing k linearly independent vectors in $\mathbb{R}^n$ ($\mathbf{A}$ is a matrix of size $n \times k$). An arbitrary vector $\mathbf{C}_i \in \mathbb{R}^n$ can be projected onto the subspace spanned by the columns of $\mathbf{A}$ with the following matrix

$$\mathbf{P} = \mathbf{A}\left(\mathbf{A}^{\mathrm{T}}\mathbf{A}\right)^{-1}\mathbf{A}^{\mathrm{T}}$$

We call matrix $\mathbf{P}$ the *projection matrix* and the matrix product $\mathbf{P}\mathbf{C}_i$ the *projection of* $\mathbf{C}_i$ *onto the subspace spanned by* $\mathbf{A}$. If $\mathbf{A}$ contains two linearly independent vectors ($k = 2$), the subspace spanned by $\mathbf{A}$ is a two-dimensional plane in $\mathbb{R}^n$. In general, we can express vector $\mathbf{C}_i$ as the sum of two vectors:

$$\mathbf{C}_i = \mathbf{P}\mathbf{C}_i + \mathbf{e}$$

where $\mathbf{P}\mathbf{C}_i$ is the projection of $\mathbf{C}_i$ onto a subspace, and $\mathbf{e}$ is a vector orthogonal to the subspace. Vector$\mathbf{e}$ is said to be the *orthogonal complement* of $\mathbf{C}_i$. Given $\mathbf{A}$ and $\mathbf{C}_i$, the orthogonal complement can be found by rearranging the above expression for $\mathbf{e}$

$$\begin{aligned} \mathbf{e} &= \mathbf{C}_i - \mathbf{P}\mathbf{C}_i \\ &= (\mathbf{I} - \mathbf{P})\,\mathbf{C}_i \end{aligned} \tag{4.6.2}$$

where $\mathbf{I}$ is the identity matrix. Observe that if the columns of $\mathbf{A}$ form an orthonormal basis, then the projection matrix $\mathbf{P}$ may be simplified:

$$\mathbf{P} = \mathbf{A}\mathbf{A}^{\mathrm{T}}$$

since

$$\mathbf{A}^{\mathrm{T}}\mathbf{A} = \mathbf{I} \tag{4.6.3}$$

if $\mathbf{A}$ is an orthogonal matrix.

4.6.4 n-dimensional rotations

Now that the necessary mathematical details have been discussed, it is simple to understand how rotations of a point about an n-dimensional ridge may occur. It is useful to refer to Figure 4.6.1b in the following description. Since it is known that rotations occur in a plane, we can project a state vector $\mathbf{C}_1$ onto a plane of rotation using a projection matrix $\mathbf{P}$ given two vectors that span a two-dimensional plane in $\mathbb{R}^n$. Suppose that a matrix $\mathbf{A}$ is available containing two vectors $\mathbf{a}_1$ and $\mathbf{a}_2$. The plane spanned by $\mathbf{a}_1$ and $\mathbf{a}_2$ may also be used as a plane of rotation. Assume furthermore that $\mathbf{a}_1$ and $\mathbf{a}_2$ form an orthonormal basis. The vector $\mathbf{A}^{\mathrm{T}}\mathbf{C}_1$ is hence a change of basis relative to $\mathbf{A}$. The projection of $\mathbf{C}_1$ onto the plane is hence given by

$$\mathbf{P}\mathbf{C}_1 = \mathbf{A}\left(\mathbf{A}^{\mathrm{T}}\mathbf{A}\right)^{-1}\mathbf{A}^{\mathrm{T}}\mathbf{C}_1$$

We wish to rotate only the component of $\mathbf{C}_1$ that lies in the plane using the 2×2 rotation matrix $\mathbf{R}$. Hence, we must first express $\mathbf{P}\mathbf{C}_1$ in terms of the columns of $\mathbf{A}$ by a change of basis and then multiply this by $\mathbf{R}$. The change of basis relative to the plane spanned by $\mathbf{A}$ is given by

$$\mathbf{A}\mathbf{y} = \mathbf{P}\mathbf{C}_1$$

in which $\mathbf{y}$ is a vector describing $\mathbf{P}\mathbf{C}_1$ relative to the columns of $\mathbf{A}$ ($\mathbf{y}$ is a 2×1 vector if $\mathbf{A}$ is a $n \times 2$ matrix). Multiplying both sides by $\mathbf{A}^{\mathrm{T}}$ and expressing for $\mathbf{y}$ gives

$$\begin{aligned} \mathbf{y} &= \left(\mathbf{A}^{\mathrm{T}}\mathbf{A}\right)^{-1}\mathbf{A}^{\mathrm{T}}\mathbf{A}\left(\mathbf{A}^{\mathrm{T}}\mathbf{A}\right)^{-1}\mathbf{A}^{\mathrm{T}}\mathbf{C}_1 \\ &= \left(\mathbf{A}^{\mathrm{T}}\mathbf{A}\right)^{-1}\mathbf{A}^{\mathrm{T}}\mathbf{C}_1 \end{aligned} \tag{4.6.4}$$

A rotation of $\mathbf{y}$ in the two-dimensional plane may be achieved using the 2×2 rotation matrix given by eq 4.6.1. $\mathbf{R}\mathbf{y}$ is hence the vector $\mathbf{P}\mathbf{C}_1$, rotated in the plane spanned by $\mathbf{A}$, by an angle θ, expressed with respect to the plane basis vectors. Expressing the rotated vector relative to the standard coordinates is done by another change of basis $\mathbf{A}\left(\mathbf{R}\mathbf{y}\right)$, that is

$$\mathbf{P}\mathbf{C}_2 = \mathbf{A}\left(\mathbf{R}\mathbf{y}\right)$$

Substitution of eq 4.6.4 gives

$$\mathbf{P}\mathbf{C}_2 = \mathbf{A}\mathbf{R}\left(\mathbf{A}^{\mathrm{T}}\mathbf{A}\right)^{-1}\mathbf{A}^{\mathrm{T}}\mathbf{C}_1$$

This gives the component of $\mathbf{C}_1$ rotated in the plane. To obtain the final rotated vector, the orthogonal complement that is unchanged by rotation must be added

back to $\mathbf{PC}_2$. Hence

$$\begin{aligned}\mathbf{C}_2 &= \mathbf{PC}_2 + \mathbf{e} \\ &= \mathbf{AR}\left(\mathbf{A}^{\mathrm{T}}\mathbf{A}\right)^{-1}\mathbf{A}^{\mathrm{T}}\mathbf{C}_1 + (\mathbf{I}-\mathbf{P})\,\mathbf{C}_1 \\ &= \left(\mathbf{ARA}^{\mathrm{T}} + \mathbf{I} - \mathbf{P}\right)\mathbf{C}_1\end{aligned}$$

which is obtained by use of eq 4.6.2 and eq 4.6.3.

Procedure

The method of rotations described above is feasible because rotations are uniquely defined in n-dimensional space when they occur about a ridge. A ridge is an $(n-2)$-dimensional subspace that can be found directly from the facets of the current polytope during construction. In general, point $\mathbf{C}_1$ is a point on the current hyperplane that is to be rotated and point $\mathbf{C}_2$ is the final rotated point. The columns spanned by $\mathbf{A}$ act as the actual 2D subspace in which $\mathbf{C}_1$ is rotated in. The above procedure relies on the knowledge of matrix $\mathbf{A}$, however this not a concern in practice because it is possible to define $\mathbf{A}$ in terms of a ridge of the current polytope. In this sense, a ridge is a $n \times (n-2)$ matrix $\mathbf{E}$ with columns given by linear combination of the vertices of a n-dimensional facet. Finding a space orthogonal to the ridge is achieved by computing the nullspace of the matrix transpose of $\mathbf{E}$. The ridge about which points are rotated forms the orthogonal complement that is unaffected by rotation. Thus we have

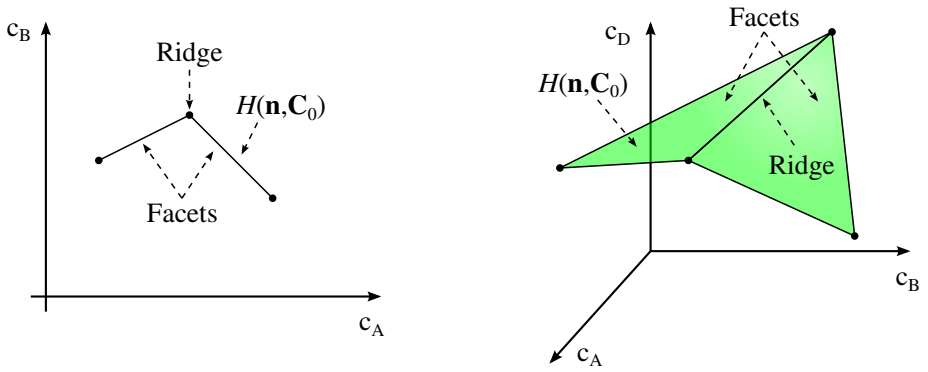
$$\mathbf{A} = \mathrm{null}\left(\mathbf{E}^{\mathrm{T}}\right)$$

Linear combinations of the columns in $\mathbf{E}$ give rise to the orthogonal vector $\mathbf{e}$, used in eq 4.6.2. In practice, if a method such as Gram–Schmidt orthogonalisation or QR decomposition is applied when computing $\mathrm{null}\left(\mathbf{E}^{\mathrm{T}}\right)$ as well, then the columns of $\mathbf{A}$ form an orthonormal basis. This simplifies rotation calculations, in the form of matrix inversions, greatly.

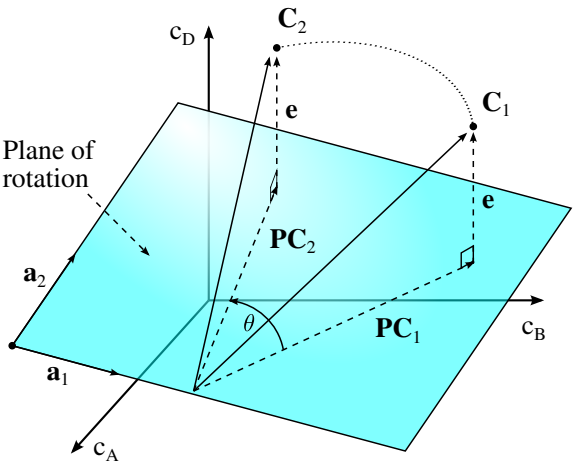
4.6.5 Proposed method

AR construction is conceptually identical when extended to higher dimensions. We aim to enclose the AR within a large region P_0, and then seek to successively eliminate unattainable regions by the introduction of additional bounding hyperplanes, specifically through rotations. Initially P_0 is given by the stoichiometric subspace S. P_0 is reduced to a smaller polytope P_r by r trimming stages. P_r is therefore a closer bound on all attainable concentrations. Construction of P_r occurs facet-by-facet, utilising existing hyperplanes and ridges about which new hyperplanes may be introduced and rotated from.

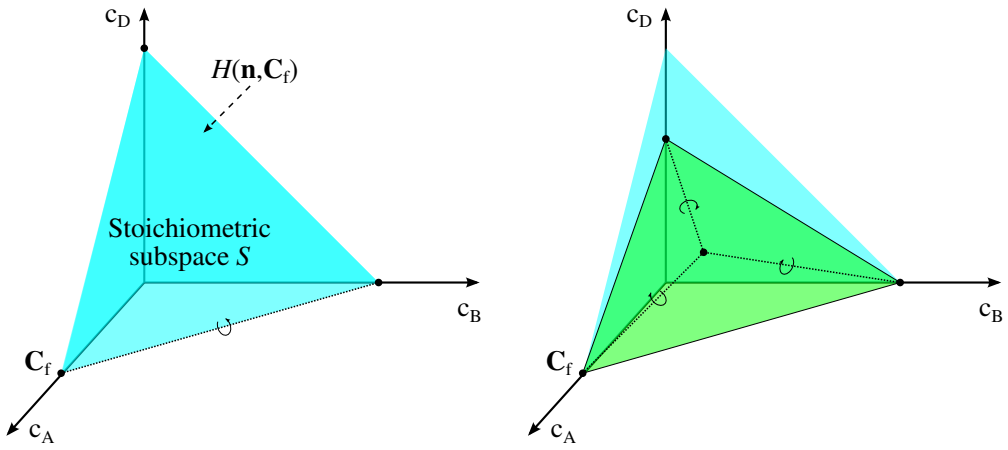
Construction begins by determination of the stoichiometric subspace S in the usual manner. This produces the largest convex polytope belonging to the system



(a) Facets and ridges in $\mathbb{R}^2$ and $\mathbb{R}^3$



(b) Rotation in a plane



(c) Initiating rotations

Figure 4.6.1: Rotations in higher dimensions

under consideration, and is the simplest approximation of the AR (S represents all concentrations satisfying mass balance constraints). The extreme points belonging to S are determined so that the facets and ridges associated with the region may be constructed. The orientation of a facet in $\mathbb{R}^n$ provides an initial orientation of the new bounding plane, whilst the ridges of the face provide an orthogonal space about which rotations may be achieved.

Additional hyperplanes are aligned to an existing facet and rotated around the ridges associated with the facet. For a problem residing in $\mathbb{R}^d$ then, d points must be known before a facet may be determined. It follows that d possible edges belonging to the face may be chosen for rotations.

The first elimination stage begins by identifying a face passing through the feed point $\mathbf{C}_\mathrm{f}$ which is used to orientate the first bounding hyperplane. The hyperplane is rotated until a tangent rate vector lying in $H(\mathbf{n}, \mathbf{C_f})$ is found, at which point the position in space is recorded and a new face is constructed from the remaining $d-1$ points. In general, hyperplane discretisation and tangency evaluation are easily extended to higher dimensions. These functions of the elimination step follow until one of the stopping criteria detailed in section 4.3.1 are met. Creating of a new facet establishes an orientation for the next hyperplane rotation, whilst a new rotation edge is obtained from the establishment of further edges belonging to the new facet. This is shown in Figure 4.6.1c. The identification of a new vertex in the plane allows for the introduction of additional ridges connected to that point. A choice must be made as to which ridge to utilise next for subsequent rotations, and also a direction of rotation must be specified. These decisions must also take into consideration the following movement criteria:

1. Rotations must not exclude feed or equilibrium points.

2. Rotations may not result in an *increase* in the size of the feasible region.

After each successive elimination steps, a new facet, or potentially many facets, of a smaller convex polytope is determined. Nevertheless, selection criteria must be made established to determine which facet to rotate next. Construction continues until no further rotations are achievable to within a specified tolerance.

Initially, only feed points are known to be achievable and construction of the first face is determined by computing the initial extreme points of S. From section 4.3.1, the tangency condition exists only to remove unattainable states from the region; there is no assumption that the tangent point is achievable. Therefore, tangent points that are found from rotations may not, in general, be satisfied by eq 2.3.2. These points may not be physically achievable in a steady state reactor network as a consequence. Be that as is may, so long as it is possible to continue introducing hyperplanes and rotating them into the region, then unachievable states can be removed from the the set. In Figure 4.6.2, we demonstrate this with a sample polytope. The region shown in Figure 4.6.2a represents an intermediate polytope

generated after an arbitrary number of eliminations have already been carried out. The facets of the polytope thus represent hyperplanes that have already been rotated into the region and stopped due to a tangent point found relative to the hyperplane. Also shown in Figure 4.6.2a is a new hyperplane that is to be rotated into the region. Points on the plane are displayed as blue $\times$'s. A ridge associated with the current facet is chosen to act as the space to rotate about. In Figure 4.6.2b we show the rotation of a plane into the region. The hyperplane is moved in until a tangent point is found. Hence, even though the original facet is positioned in space due to a previous elimination step, rotation with respect to a different ridge brings about further eliminations. Rotation of the plane about the new ridge has excluded a small set of vertices fro the previous step – relative to the new hyperplane, these concentrations are not achievable. In Figure 4.6.2c, we show the polytope obtained after the rotated hyperplane has been appended to the current set of hyperplane constraints. Notice that new vertices (and hence new facets and ridges) have been created by the hyperplane. Additional rotations may now be carried out. After each step, the introduction of new points serves to break ties with the original extreme points. Eventually, a stage in construction is reached where the edges of the current face are no longer composed of the extreme points of the original face. These may then be removed from the feasible set. Eliminations of this form continue until no further rotations can be carried out. The remaining region serves as an approximation of the AR relative to the numerical tolerance specified.

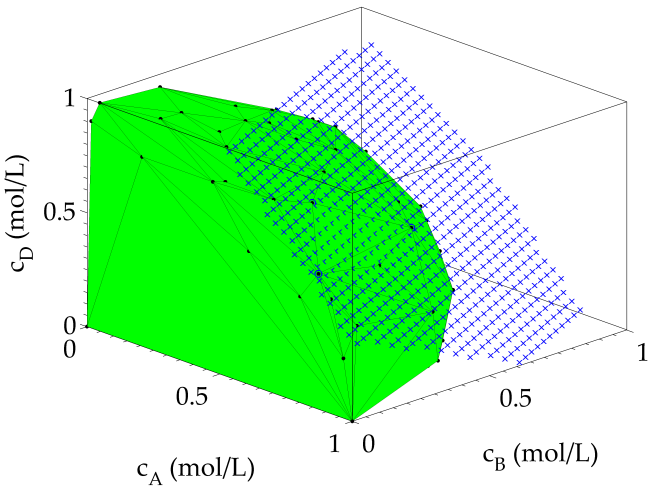
4.6.6 Difficulties and unknowns

Uncertainties

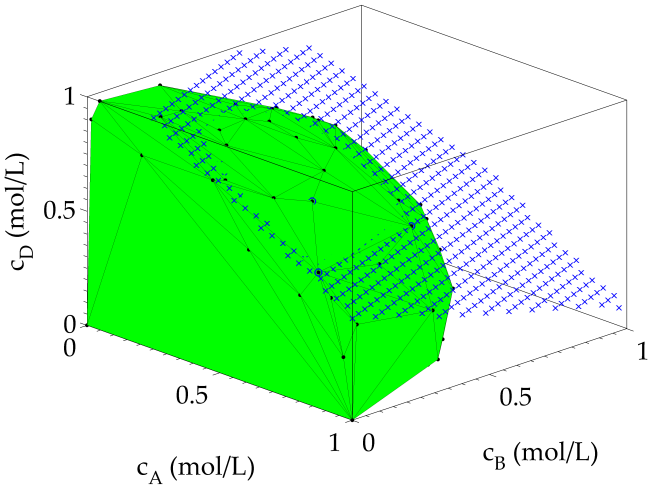
Uncertainty still remains as to whether eliminations in the manner described above in fact converge to the true AR (these topics are an active area of discussion at present). Nevertheless, the polytope resulting from this method must always enclose the true AR and will always be smaller than the initial stoichiometric subspace. This in itself is useful in establishing bounds on the attainability of a system.

The special setting of $\mathbb{R}^2$ allows construction to occur on an ordered (Hamiltonian) path – each extreme point discovered is visited exactly once. Higher dimensional constructions are not generally ordered along such a path however, and a systematic method must be developed for how new vertices are chosen to carry out further rotation steps. Indeed, higher dimensional rotations allow for extra freedom in movement. In general, three choices must be made before rotations can be carried out:

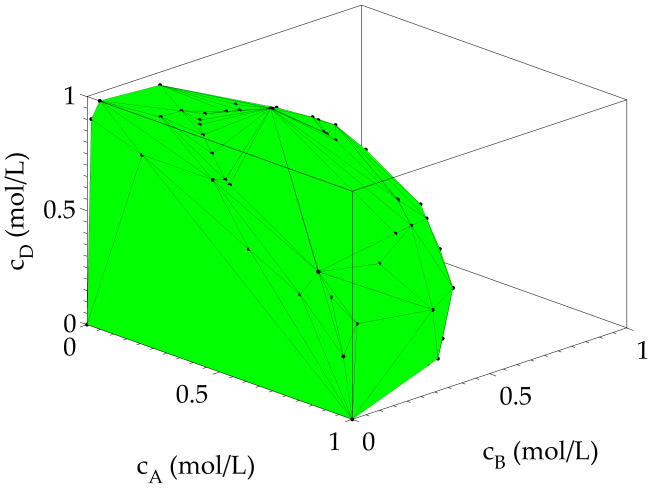
1. Choosing which facet to rotate on the current polytope
2. Once done, choosing a ridge of the facet about which to rotate
3. Choosing a direction of rotation and step size that achieves optimal elimination



(a) Initial orientation



(b) Rotation



(c) Resulting region following elimination

Figure 4.6.2: Example of eliminations in $\mathbb{R}^3$

An approach that incorporates these decisions in a systematic manner has yet to be developed. Strategies for selecting facets/ridges/rotations that achieve the largest eliminations efficiently are can be formulated, and these may be guided more by empirical data (gained during construction) rather than from a purely theoretical basis at the beginning. Certainly, so long as rotations allow for further elimination of unachievable states, there are many equally valid approaches to achieve this. The strategy chosen may come about from a range of possible methods that are picked based on the current state of construction.

Difficulties

Additional computational overheads are involved with higher dimensions that do not arise in two dimensions. These arise mainly from the bookkeeping of facets and ridges used in the decision making process for how to rotate additional hyperplanes. Additionally, constructions in higher dimensions demand larger data requirements, which places a greater strain on the computing resources available. For instance, Abraham and Feinberg (2004); Abraham (2005) discuss how the number of hyperplanes required for adequate AR approximation increases rapidly with increasing dimension. The need to discretise and evaluate points on a higher dimensional hyperplane comes with greater computational time to approximate regions appropriately.

Hence, rotations in higher dimensions may not be as competitive when considered with competing algorithms. However, much like how a robust ODE integration scheme may employ a range of methods for different problem types, the same could be envisioned for AR construction - we may wish to treat elimination via rotations as a suitable 2D scheme, employed in an intermediate step or special selection case of a grander AR construction algorithm incorporating many other methods as well.

4.7 Conclusion

Originally proposed for bounded isothermal constructions in concentration space, the method of bounding hyperplanes (Abraham and Feinberg, 2004) has proven to be a robust method of AR construction. This is particularly apparent for the determination of degenerate kinetics when multiple CSTR steady states are present. However, constructions performed in this way are hindered by computational complexities that become ever more apparent with an increasing number of hyperplanes. It is found that the cost of hyperplane discretisation, extreme point enumeration and redundant hyperplane removal are computationally demanding stages in the original method that otherwise hinder a rather novel construction technique. A revised algorithm sharing many of the positive attributes linked with the original has been presented and shown to construct regions that agree with the constructions of other authors (Feinberg and Hildebrandt, 1997; Glasser et al., 1987; Hildebrandt, 1989;

Seodigeng et al., 2009; Abraham and Feinberg, 2004; Godorr et al., 1999).

In much the same way as its predecessor, the method relies on the successive addition of bounding hyperplanes to separate a region (containing both achievable and unachievable parts) into two half spaces, such that one half contains unattainable concentrations only. Orientation of the cutting plane has been revised to allow for a rotation about an axis, rather than a fixed orientation and translation through space. This allows for the same trimming mechanism found desirable in the original approach, whilst simultaneously eliminating the need for vertex enumeration and redundant hyperplane removal after the introduction of each elimination stage. The method demonstrates an improvement in both running time and construction accuracy when compared to the original for the same problem, however the most gains are observed for kinetics where the AR boundary is composed of many hyperplanes. This might arise when curvature is introduced by PFR solution trajectories for example. These situations involve a large overhead in costly vertex enumeration stages. Construction via rotations of a plane has allowed for the approximation of unbounded ARs in concentration–time space. The method has also been extended to allow for determination of non-isothermal ARs and shown to agree with the regions obtained via traditional methods. Extension of the method for the inclusion of these cases has allowed for the determination of a rather more broad set of reactor network optimisation problems that occur frequently in many common reactor designs.

A discussion of how the algorithm may be extended to n-dimensions was also presented. The ideas that characterise construction in $\mathbb{R}^2$ take on familiar roles in $\mathbb{R}^n$. Extreme points of existing facets provide starting orientations (positions in space) whilst the edges of the same facet provide an edge about which the bounding plane may be rotated. Eliminations performed in this way allow for the creation of new facets and edges, about which new hyperplanes may be introduced and rotated to further advance the elimination process. Higher dimensional constructions are not as simple to perform as those determined in two dimensions unfortunately. Discussions as to how these methods may be improved are still actively being investigated. This is in part due to the need for additional bookkeeping of facets and edges, but chiefly due to tangent points that are not generally guaranteed to be achievable.

Nevertheless, the performance gain and extended flexibility afforded by non-isothermal and unbounded constructions can now be used in a wider range of reactor network problems. It has already been discussed previously how the AR has observed a small adoption in batch. In the next chapter, we will provide simple transformation guidelines for converting continuous reactor structures, used in traditional AR theory, so that they may be applied to batch directly. We will apply the method described in this chapter to assist in determining the correct AR boundary belonging to a particular set of kinetics in which multiple steady states occur. These kinetics would otherwise be difficult for traditional inside-out AR construction schemes to

perform. As a result, direct application of the transformation rules from continuous to batch may result in sub-optimal results if the incorrect boundary structure is employed. The rotated hyperplanes construction method developed in this chapter thus provides a sanity check on the AR. This allows for greater confidence in the recommendations that are obtained from it.

References

Abraham, T. K., 2005. Kinetic bounds on attainability in the reactor synthesis problem. Ph.D. thesis, Ohio State University, Ohio.

Abraham, T. K., Feinberg, M., 2004. Kinetic bounds on attainability in the reactor synthesis problem. Industrial & Engineering Chemistry Research 43 (2), 449–457.

Aguilera, A., Perez-Aguila, R., 2004. General n-dimensional rotations. International Conference in Central Europe on Computer Graphics, Visualization and Computer Vision.

Burri, J. F., Wilson, S. D., Manousiouthakis, V. I., 2002. Infinite dimensional state-space approach to reactor network synthesis: Application to attainable region construction. Computers & Chemical Engineering 26 (6), 849–862.

Chand, D. R., Kapur, S. S., 1970. Algorithm for convex polytopes. J Ass Comput Mach 17 (1), 78–86.

Clausen, J., 1999. Branch and bound algorithms-principles and examples. Department of Computer Science, University of Copenhagen, 1–30.

Dyer, M. E., 1983. Complexity of vertex enumeration methods. Mathematics of Operations Research 8 (3), 381–402.

Feinberg, M., 2000a. Optimal reactor design from a geometric viewpoint - iii. critical cfstrs. Chemical Engineering Science 55 (17), 3553–3565.

Feinberg, M., 2000b. Optimal reactor design from a geometric viewpoint. part ii. critical sidestream reactors. Chemical Engineering Science 55 (13), 2455–2479.

Feinberg, M., Hildebrandt, D., 1997. Optimal reactor design from a geometric viewpoint- i. universal properties of the attainable region. Chemical Engineering Science 52 (10), 1637–1665.

Glasser, D., Hildebrandt, D., Crowe, C., 1987. A geometric approach to steady flow reactors: The attainable region and optimization in concentration space. Industrial & Engineering Chemistry Research 26 (9), 1803–1810.

Godorr, S., Hildebrandt, D., Glasser, D., McGregor, C., 1999. Choosing optimal control policies using the attainable region approach. Industrial & Engineering Chemistry Research 38 (3), 639–651.

Hildebrandt, D., October 1989. The attainable region generated by reaction and mixing. Ph.D. thesis, University of the Witwatersrand, Johannesburg.

Hildebrandt, D., Glasser, D., 1990. The attainable region and optimal reactor structures. Chemical Engineering Science 45 (8), 2161–2168.

Horn, F., 1964. Attainable and non-attainable regions in chemical reaction technique. Pergamon Press, London.

Kauchali, S., Rooney, W. C., Biegler, L. T., Glasser, D., Hildebrandt, D., 2002. Linear programming formulations for attainable region analysis. Chemical Engineering Science 57 (11), 2015–2028.

Land, A. H., Doig, A. G., 1960. An automatic method of solving discrete programming problems. Econometrica: Journal of the Econometric Society, 497–520.

Manousiouthakis, V. I., Justanieah, A. M., Taylor, L. A., 2004. The shrink-wrap algorithm for the construction of the attainable region: An application of the ideas framework. Computers & Chemical Engineering 28 (9), 1563–1575.

Nicol, W., Hernier, M., Hildebrant, D., Glasser, D., 2001. The attainable region and process synthesis: Reaction systems with external cooling and heating. the effect of relative cost of reactor volume to heat exchange area on the optimal process layout. Chemical Engineering Science 56 (1), 173–191.

Rooney, W. C., Hausberger, B. P., Biegler, L. T., Glasser, D., 2000. Convex attainable region projections for reactor network synthesis. Computers & Chemical Engineering 24 (2-7), 225–229.

Ryoo, H. S., Sahinidis, N. V., 1995. Global optimization of nonconvex nlps and minlps with applications in process design. Computers & Chemical Engineering 19 (5), 551–566.

Schlosser, P. M., Feinberg, M., 1994. A theory of multiple steady states in isothermal homogeneous cfstrs with many reactions. Chemical Engineering Science 49 (11), 1749–1767.

Seodigeng, T., Hausberger, B., Hildebrandt, D., Glasser, D., 2009. Recursive constant control policy algorithm for attainable regions analysis. Computers & Chemical Engineering 33 (1), 309–320.

Seodigeng, T. G., January 2006. Numerical formulations for attainable region analysis. Ph.D. thesis, University of the Witwatersrand, Johannesburg.

Smith, E. M., Pantelides, C. C., 1999. A symbolic reformulation/spatial branch-and-bound algorithm for the global optimisation of nonconvex minlps. Computers & Chemical Engineering 23 (4), 457–478.

Smith, E. M. d. B., 1996. On the optimal design of continuous processes. Ph.D. thesis, Imperial College London (University of London).

Tawarmalani, M., Sahinidis, N. V., 2004. Global optimization of mixed-integer nonlinear programs: A theoretical and computational study. Mathematical programming 99 (3), 563–591.

Chapter 5

Applying AR theory to batch reactors

The following chapter has been adapted from published work with permission. The associated paper is (Ming, D., Glasser, D., Hildebrandt, D., 2013. Application of Attainable Region theory to batch reactors. Chem. Eng. Sci. 99, 203 – 214.) Copyright (2013) Elsevier. D. Ming (the present author) compiled the manuscript and contributed to the ideas in this work. D. Hildebrandt and D. Glasser supervised this work.

5.1 Introduction

The problem of determining optimal operating policies in batch operations is a popular one, and has been given a great deal of attention in the literature, particularly due to the importance of batch reaction in a large number of industrially relevant processes. Batch reactors are used extensively in the production of a variety of pharmaceutical (Davies and Gloor, 1971) and biological (Cheong et al., 2007; Modak and Lim, 1992; Najafpour et al., 2004; Senthuran et al., 1997) products, as well as in the waste water (Woolard and Irvine, 1995; Zwiener et al., 2002) and polymerisation (Zeman and Amundson, 1965) industries, and are typically considered to be rather more versatile than that of equivalent continuous processes (Bonvin, 1998). Batch reactors also find use in the small-scale production of highly specialised products, negating the benefit otherwise obtained by large-scale production. Moreover, batch reaction may be the only viable method of producing certain products, such as when experimental work is performed at lab-scale and pilot-scale.

It follows that optimisation plays an important function in the design and operation of these processes. Much attention has been placed on the development of methods that seek to improve batch performance, particularly with regards to the determination of optimal operating conditions and scheduling strategies. Although research into determining efficient batch structures exists (Allgor et al., 1996; Aziz

and Mujtaba, 2002; Capon-Garcia et al., 2011; Mendez et al., 2006), a brief search of the current literature would suggest that this area may not appear to be as popular as traditional batch optimisation. Even then, current methods for determining optimal batch structures often rely on traditional optimisation methods (Allgor et al., 1996, 1999; Allgor and Barton, 1999).

For the past two decades, the papers of Feinberg and Hildebrandt (1997); Feinberg (1999, 2000b,a); Glasser et al. (1987); Glasser and Hildebrandt (1997) have motivated the use of a novel method of identifying optimal reactor configurations, termed Attainable Region (AR) analysis. Determination of optimal reactor structures using the AR is unique since synthesis is achieved via a geometric interpretation of reactor configurations. This approach has shown to be an effective alternative method to optimal reactor synthesis, particularly with regard to systems involving multiple side reactions or reactions with complicated kinetics. Nearly all applications of the AR have been performed on continuous reactors however; the single paper of Davis et al. (2008) currently remains the only use of AR theory to batch systems.

Our aim in this work will thus be towards improving batch reactor structures with specific use of the AR and the associated benefits of this approach. This is done as follows: for a given set of feed conditions and kinetics, a candidate AR may be generated and interpreted, initially, in the form of a continuous reactor structure. Once generated, the appropriate conversions to the batch setting may be performed, providing an equivalent recommended batch reactor structure. A key objective in this work has been towards reusing the results and insight discovered from a continuous AR structure, such that the same outputs might be obtained with an equivalent batch system.

We will begin by first providing a brief overview of AR theory, and drawing a relevant set of results associated with continuous equipment; this is done in section 5.2. Section 5.3 investigates how equivalent structures in batch may be derived from continuous equipment. The correct choice and exact combination of continuous equipment is guided by AR analysis, and thus the development of the AR is central to the approach presented in this work. Finally, examples and concluding remarks are given in sections 5.4 and 5.5 respectively.

5.2 Overview of AR theory in continuous equipment

5.2.1 AR construction from three fundamental reactor types

The purpose of this section will be towards providing a brief overview of AR theory for continuous equipment. The results obtained will allow for the development of optimal batch structures. The geometric nature of AR theory has been discussed in numerous papers before Davis et al. (2008); Feinberg and Hildebrandt (1997);

Feinberg (1999, 2000a,b); Glasser et al. (1987); Glasser and Hildebrandt (1997); Godorr et al. (1994, 1999); Hildebrandt and Glasser (1990); Hildebrandt et al. (1990); Khumalo et al. (2006); Nicol et al. (1997, 2001); Nisoli et al. (1997), and only a brief overview of the theory shall be provided here as a result.

Certain common aspects relating to reaction and mixing were also given treatment in chapter 2, and so they are not discussed here either. We do however, wish to repeat certain concepts relating to fundamental reactor types. This will be done so that comparisons from continuous to batch can be performed directly without the reader needing to constantly refer back to chapter 2. We shall thus begin with a basic review of fundamental reactor types, after which, important properties of the AR boundary will be discussed.

Plug Flow Reactor (PFR)

It may be shown that no more than three fundamental reactor types, together with mixing between structures, are needed to construct the AR (Feinberg and Hildebrandt, 1997). These are the plug flow reactor (PFR), the continuously stirred tank reactor (CSTR) and the differential side-stream reactor (DSR). PFRs are defined by the following expression

$$\frac{\mathrm{d}\mathbf{C}}{\mathrm{d}\tau} = \mathbf{r}\left(\mathbf{C}\right) \tag{5.2.1}$$

Geometrically, the set of concentrations achieved by integration of eq 5.2.1 produces a solution trajectory in concentration space. All rate vectors evaluated along this trajectory are tangent to it, and thus PFR solutions move along in the direction of the vector field. It is shown (Feinberg and Hildebrandt, 1997) that PFR trajectories serve to act as highways to which the final most states of the AR boundary are achieved and therefore they assume an important role in the overall optimal AR structure. In view of this, we find that optimal AR structures usually terminate in a PFR. PFRs allow one to traverse along the outer most extremities of the AR boundary, and as a result, play an integral role in optimal AR structures. A collection of PFR trajectories that form part of the AR boundary is often termed a *manifold* (Feinberg and Hildebrandt, 1997).

Continuously-Stirred Tank Reactor (CSTR)

The CSTR is one in which the reactor contents is assumed to be perfectly mixed, and therefore the exit stream of a CSTR is assumed to be identical to that found inside the reactor. The defining equation is given as

$$\mathbf{C} = \mathbf{C_f} + \tau\mathbf{r}\left(\mathbf{C}\right) \tag{5.2.2}$$

CSTRs possess a unique geometric interpretation. If the mixing vector is taken as $\mathbf{C} - \mathbf{C_f}$, then clearly the set of concentrations satisfying eq 5.2.2 must be those points which are collinear to $\mathbf{r}(\mathbf{C})$. Whereas trajectories corresponding to the PFR are obtained by integration of eq 5.2.1, the locus of points associated with the CSTR are generally found by the solution of a system of non-linear equations. The CSTR therefore operates on discrete points in space, and hence there exists an opportunity for jumps and discontinuities to also occur as a result. Interpretation of CSTR behaviour in this manner allows for a convenient geometric method for the determination of CSTR solutions. This is useful for systems involving multiple steady states. *Critical CSTR* points are those which reside on the AR boundary.

Differential Side-stream Reactor (DSR)

A DSR may be viewed as a PFR with side-stream addition along its length. The rate of material addition, α, as well as the concentration of the side-stream, $\mathbf{C}_0$, are allowed to vary along the reactor length. We will assume that $\mathbf{C}_0$ remains at a fixed value in this work however.

$$\frac{\mathrm{d}\mathbf{C}}{\mathrm{d}\tau} = \mathbf{r}(\mathbf{C}) + \alpha(\mathbf{C})(\mathbf{C}_0 - \mathbf{C}) \tag{5.2.3}$$

where $0 \leq \alpha \leq \infty$. Geometrically, the rate of formation of species achieved in a DSR is determined by the rate of reaction and the mixing vector $(\mathbf{C}_0 - \mathbf{C})$. The resultant vector is then a linear combination of the two, and the net direction must therefore lie within the space spanned by $\mathbf{r}(\mathbf{C})$ and $(\mathbf{C}_0 - \mathbf{C})$. The overall direction may be steered between the two by appropriate manipulation of the α parameter, and consequently, its magnitude must be varied in a manner that produces a trajectory that is able to maximise the set of achievable concentrations. The unique α policy that allows the DSR trajectory to traverse along the AR boundary is termed a *critical α policy*, whilst the DSR corresponding to this policy is termed a *critical DSR*.

Construction of the AR using structures containing DSRs is only useful for systems involving three or more independent reactions, and thus it is sufficient to describe the AR, involving two or one independent reactions, with combinations of PFRs and CSTRs only. It follows that systems with two simultaneous competing reactions may be solved without the use of DSRs.

5.2.2 Necessary conditions of the AR

From the above discussion, it is possible to establish a set of necessary conditions that the AR must satisfy (Glasser et al., 1987; Glasser and Hildebrandt, 1997); these are:

- The AR must contain the feed – The feed point is attainable, and therefore it

must be contained with the set of all achievable points.

- The AR must be convex – A set of achievable points that is not convex can always be made convex by mixing. Mixing can fill in concave regions and spaces between two separate, yet achievable, regions.
- All rate vectors on the boundary of the AR must point into, or be tangent, to the AR – A PFR may be used to extend the region otherwise.
- All rate vectors (or linear combinations of rate vectors) located in the compliment of the AR may not be extended backwards to intersect the boundary – A CSTR may be used to achieve the given point and therefore extend the region otherwise.

Currently, there exists no sufficiency condition for the AR. Regions that are produced that satisfy the above necessary conditions are therefore termed *candidate attainable regions*. A number of AR construction methods, suitable for implementation on computer, have been devised. The interested reader should refer to the works of Rooney et al. (2000); Burri et al. (2002); Kauchali et al. (2002); Abraham and Feinberg (2004); Manousiouthakis et al. (2004); Zhou and Manousiouthakis (2006); Seodigeng et al. (2009); Ming et al. (2010) for further details.

5.2.3 Dimensional considerations

Dimension of the AR

Although it is natural to describe the dimension of the AR in terms of the total number of species in the system, these are generally not independent, and hence this approach may be unnecessary. Feinberg (2000b,a) demonstrated that it is usually possible to recast the AR in a lower dimensional subspace in $\mathbb{R}^L$. Here, L is the number of linearly independent reactions taking part in the system. In addition to this, given an initial feed concentration and system stoichiometry, the set of attainable compositions achieved by reaction and mixing may not violate the conservation of mass. The AR must therefore be bounded by stoichiometric constraints. This region is termed the *stoichiometric subspace*. We denote by S the set of concentrations stoichiometrically compatible with the feed.

Maximum number of parallel structures

There also exists an upper bound on the maximum number of parallel structures required by the AR in order to achieve a given state. These bounds hold for both within the AR, and on its boundary (Feinberg, 2000b), and are a consequence of Carathéodory's theorem. The results are summarised below for an AR constructed in $\mathbb{R}^n$:

- The maximum number of parallel structures required to achieve any concentration within the interior of the region is n.
- If concentrations on the boundary are to be achieved, the number of parallel structures is, at most, equal to $n - 1$.

It follows that the maximum number of parallel structures is equal to the number of independent reactions in the system. Although it is generally not possible to determine, a priori, the number or sequence of reactor units that make up a branch of an optimal AR structure, it is still feasible to obtain an upper bound on the maximum number of unique parallel structures required by the system. Unless the objective function intersects the AR boundary at multiple points, it is generally not a requirement that all optimal reactor structures be used in the optimisation. This result shall become more meaningful in the examples that are to follow.

5.3 Similarities between batch and continuous reactive equipment

A note on continuous and batch operation

In the upcoming discussion, we will want to show how the states realized in the three fundamental continuous reactors used in AR theory can be achieved by batch equipment. Moreover, we would like to demonstrate that the necessary transformations from continuous to batch can be used in conjunction with the AR to help guide the design of optimal batch structures. Before we begin our discussion on the similarities between batch and continuous reactors however, we would like to highlight a clear difference between the two operating regimes.

Thus, even though we wish to show that it is possible to attain steady state *concentrations* in a batch, it is not assumed that steady state itself can ever be attained. By the very nature of batch processes, this is clearly not possible. Hence, our outlook here will not be of the view that batch reactors, specifically fed-batch reactors, can ever be operated in any particular way that is able to reach steady state. We would, however, like to demonstrate that it is still possible to achieve the specific concentration associated with that steady state. Certainly, this will require a special operating regime to achieve (which shall be detailed in the following sections), but this will always be with the idea that the reactor is operated under batch conditions - that is, with a distinct cycle time in which the state variables of the batch reactor (volume, concentration, etc.) do, in fact, vary for the duration of this period. With this in mind, let us begin our discussion starting with the simplest of cases.

5.3.1 The standard batch

By standard batch, we have in mind a batch reactor where there is no inflow or outflow of material during the reaction period. The reactor contents are well mixed, although, the concentration of species evolves with respect to time. Given an initial concentration of species, the concentration profile within a standard batch reactor may be determined by integration of the appropriate rate expression. Thus, we have for the standard batch

$$\frac{\mathrm{d}\mathbf{C}}{\mathrm{dt}} = \mathbf{r}\left(\mathbf{C}\right) \tag{5.3.1}$$

Thus, the solution trajectory obtained by integration of eq 5.3.1 is identical to that obtained by integration of eq 5.2.1 for the same initial conditions - the initial concentration of the standard batch at $\mathrm{t} = 0$ is identical to the feed concentration in a PFR at $\tau = 0$. The reaction time of the batch replaces residence time of the PFR as the integration parameter in this regard. As a result, optimal reactor structures where PFRs form the boundary of the AR may be achieved in batch processes by running a standard batch reactor with the appropriate reaction time.

5.3.2 Fed-batch reaction

Fed-batch or semi-batch reactors are reactors that allow the feeding of additional material into the reaction vessel during the reaction period, and may be used to bias the selectivity of components in competing reactions. Assume that a fed-batch reactor is available with a side-stream volumetric feed rate of F (F has units of [volume]/[time]) and a side-stream concentration of $\mathbf{C}_0$. It is assumed that F varies with respect to time whereas the side-stream feed concentration, $\mathbf{C}_0$, is constant. A molar balance for component i over the fed-batch with respect to time results in the following differential equation

$$\frac{\mathrm{d}n_i}{\mathrm{dt}} = \mathrm{V}\left(\mathrm{t}\right) r_i\left(\mathbf{C}\right) + \mathrm{F}\left(\mathrm{t}\right) c_i^0$$

where n_i, $r_i\left(\mathbf{C}\right)$ and c_i^0 are the moles of i in the reactor, species rate function and side-stream concentration of component i, respectively, ,and $\mathrm{V}\left(\mathrm{t}\right)$ is the current volume of the reactor. Expressing n_i in terms of c_i by $n_i = c_i \mathrm{V}\left(\mathrm{t}\right)$gives

$$c_i \frac{\mathrm{dV}}{\mathrm{dt}} + \mathrm{V}\left(\mathrm{t}\right) \frac{\mathrm{d}c_i}{\mathrm{dt}} = \mathrm{V}\left(\mathrm{t}\right) r_i\left(\mathbf{C}\right) + \mathrm{F}\left(\mathrm{t}\right) c_i^0$$

and recognising that a volume balance over the fed-batch

$$\frac{\mathrm{dV}}{\mathrm{dt}} = \mathrm{F}\left(\mathrm{t}\right)$$

this results in

$$\frac{\mathrm{d}c_i}{\mathrm{dt}} = r_i\left(\mathbf{C}\right) + \left[\frac{\mathrm{F}\left(\mathrm{t}\right)}{\mathrm{V}\left(\mathrm{t}\right)}\right]\left(c_i^0 - c_i\right)$$

This may be written for each component in the system. The general *vector* form of the fed-batch reactor is thus given as follows

$$\begin{aligned} \frac{\mathrm{d}\mathbf{C}}{\mathrm{dt}} &= \mathbf{r}(\mathbf{C}) + \left[\frac{\mathrm{F}(\mathrm{t})}{\mathrm{V}(\mathrm{t})}\right](\mathbf{C}_0 - \mathbf{C}) \\ &= \mathbf{r}(\mathbf{C}) + \alpha(\mathbf{C}_0 - \mathbf{C}) \end{aligned} \tag{5.3.2}$$

Where $\alpha = \mathrm{F}(\mathrm{t})/\mathrm{V}(\mathrm{t})$. Note that eq 5.3.2 is obtained when density and the side-stream concentration $\mathbf{C}_0$ are assumed constant. Such an assumption makes no difference to the final result however (Feinberg, 2000b).

The properties of fed-batch reactors are such that they may assume several functions corresponding to the continuous equipment in section 5.2.1. This is more easily understood by way of an illustrative example. Consider then Figure 5.3.1, which represents a hypothetical scenario for a number of fed-batch trajectories that have been plotted in concentration space. We assume that each trajectory is obtained by the integration of eq 5.3.2 for a unique α policy. The feed conditions for each are the same and given here by point O, that is, point O represents $\mathbf{C_f}$. The behaviour for each policy is then given as follows:

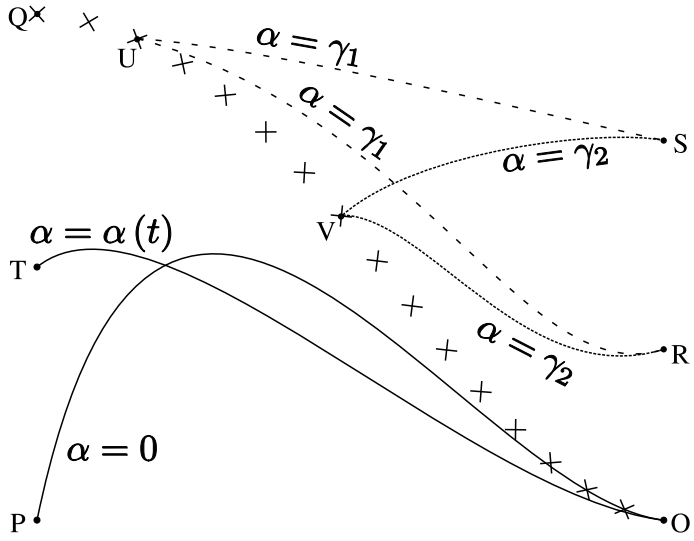


Figure 5.3.1: Graphical interpretation for various fed-batch reactor trajectories.

Case 1: $\alpha = 0$ **(A PFR)**

The solid curve OP is that of a solution trajectory corresponding to a fed-batch reactor when $\alpha = 0$. Point P is therefore the equilibrium point. Clearly, the form of the fed-batch for this situation reduces to that of eq 5.3.1 for the standard batch, and thus PQ is also a solution for a PFR with feed composition given by point O. The analogy between standard batch reaction and PFRs has already been discussed above, and therefore this case will not be considered further.

Case 2: $\alpha = \alpha\left(\mathbf{C}\left(t\right)\right)$ **(A DSR)**

The most familiar method of operation is one in which the feed addition policy is adjusted throughout the reaction period. Hence, consider now the case when α is given by a varying profile. Again, eq 5.3.2 may be integrated if an initial condition, side-stream composition (given by $\mathbf{C}_0$) and α policy are supplied. The curve OT is representative of such a solution where point T is the equilibrium point for this trajectory. Observe once more that the form of the fed-batch equation is identical to eq 5.2.3 for the DSR, and identical behaviour may be achieved in the batch by appropriate interpretation of the α variable as a result.

The set of concentrations belonging to the trajectory OT is thus equivalent to that obtained in a DSR with feed composition equal to point O, and side-stream composition given by $\mathbf{C}_0$ (not shown in the figure). With similar reasoning to the standard batch/PFR analogy, residence time in the DSR is replaced by reaction time in the fed-batch. The value of α in the DSR represents the feed rate with respect to DSR length, whereas in the batch, $\alpha = \mathrm{F/V}$ (the ratio of side-stream addition feed rate to reactor volume). $\mathrm{F}\left(t\right)$ and $\mathrm{V}\left(t\right)$ are determined by integration of the α policy with respect to time and the differential expression for the volume change, usually given by $\mathrm{dV/dt} = \mathrm{F}\left(t\right)$. Nevertheless, notice that there is a direct analogue between fed-batch reactors with varying α policies and DSRs. AR boundary structures that contain DSR segments are thus easily convertible to an equivalent fed-batch system as a result.

Case 3: $\alpha = \text{constant}$ **(A CSTR)**

Consider now the particular case when α is maintained at a constant value throughout the reaction period. Again, if an initial condition and fed-batch addition composition are specified, eq 5.3.2 can be integrated for any arbitrary reaction time. The pair of curves represented by RU and SU are representative solutions for when α is kept at a constant value of γ_1, whereas the pair RV and SV is that which is obtained when α is kept at a different value given by γ_2. Clearly, RU and RV share the same initial point, given by point R, and points SU and SV share the same initial condition given by S. For $\alpha = \gamma_1$, the fed-batch trajectories both terminate at point U, even though the starting conditions differ, the same behaviour is observed for $\alpha = \gamma_2$. All trajectories however (RU, SU, RV and SV), are fed with material of concentration given by point O.

For a sufficiently long reaction time, the concentration of species within the vessel approaches equilibrium, and eq 5.3.2 reduces to

$$\mathbf{0} = \mathbf{r}\left(\mathbf{C}\right) + \alpha\left(\mathbf{C_0} - \mathbf{C}\right) \tag{5.3.3}$$

End points U and V therefore represent equilibrium points in the fed-batch for a

constant α policy, and are thus also solutions to eq 5.3.3. For all values of α in the range $0 < \alpha < \infty$, integration of eq 5.3.2 to equilibrium may be carried out with the fed-batch feed concentration $\mathbf{C}_0$ set at point O. The locus of ($\times$) given by the curve OVUQ represents the set of equilibrium concentrations achieved in the system as a result.

Clearly, equilibrium concentrations for the fed-batch are equivalent to CSTR concentrations when the CSTR feed composition, $\mathbf{C_f}$, is equal to point O. This may be more easily seen by comparing eq 5.3.3 to the form of the CSTR expression given by eq 5.2.2. The value of α at equilibrium is thus related to the CSTR residence time by

$$\alpha = \frac{1}{\tau_{\text{CSTR}}} \qquad \text{at equilibrium}$$

It follows that all values of α in the range $0 \leq \alpha \leq \infty$ for fed-batch reactors operating at equilibrium correspond to the set of CSTRs with residence times between the range $\infty \leq \tau_{\text{CSTR}} \leq 0$.

The curve OVUQ in Figure 5.3.1 also corresponds to solutions for a CSTR (with feed point O), and therefore curve OVUQ is also representative of a CSTR locus. CSTR compositions can thus be obtained in a batch by operating a fed-batch reactor at its equilibrium concentration. The particular equilibrium point is defined by the specific constant α value chosen, which corresponds to a particular CSTR solution with residence time given by $\tau = 1/\alpha$.

Several observations may be noted for the constant α fed-batch reactor with relation to a CSTR:

1. Initial conditions

   Notice that the equilibrium point in the fed-batch is defined by the value of α and the fed-batch feed concentration, and is not a function of the initial condition at t = 0. The choice of initial condition may still be somewhat constrained, as certain specific instances prevent the designer from choosing the starting point in a completely arbitrary manner. Details of these are discussed under point 3.

   It follows that equivalent CSTR behaviour may only be achieved in the fed-batch at equilibrium, and therefore, in order to obtain CSTR concentrations in a batch system, the reactor must be initiated *at the equilibrium condition*s. In practice, this may be achieved by several methods:

   - Initially run a small CSTR at the appropriate residence time to produce the desired equilibrium composition. Then transfer the contents of the CSTR into a fed-batch.
   - Begin at a condition sufficiently close to the desired CSTR concentration so that equilibrium may be approached during the reaction period.

- Artificially form the desired CSTR concentration by combining pure chemicals in the appropriate amounts to achieve the correct equilibrium composition.

Irrespective of the method employed, this procedure need only be carried out once at the beginning of the first batch cycle. Once product of the correct CSTR composition is produced, a portion may be used to seed further fed-batch cycles; the sequence is self-sustaining as a result.

2. Initial volume

   At equilibrium, the concentration of species within the vessel is maintained at a constant value of $\mathbf{C}$ throughout the entire reaction period. Reactor volume therefore varies without a change in concentration in this instance.

   In order to achieve a production rate comparable to that of an equivalent CSTR, the correct initial volume of material must be chosen. The final batch volume must allow for an additional small volume V_0 for seeding of subsequent batches. Therefore, the final volume produced in the batch at $t = \tau_{CSTR}$ must be equal to the equivalent CSTR volume (V_{CSTR}) and the initial volume required for successive batches (V_0). We thus have

$$\frac{dV}{dt} = \alpha V$$

   with boundary conditions given by

$$V(t_0) = V_0 \qquad \text{and} \qquad V(\tau_{CSTR}) = V_0 + V_{CSTR}$$

3. Multiple steady states

   Multiple steady states are often observed in CSTRs (Gray and Scott, 1983, 1984; Schlosser and Feinberg, 1994). Indeed, even for fairly simple chemistry, there may exist opportunities to operate at more than one steady state for a given feed composition and residence time. To this end, fed-batch reactors may exhibit the same behaviour for an equivalent fixed α policy and side-stream feed composition. Thus, care must be taken in the choice of equilibrium concentration applied, as rather different outcomes in performance may arise, even when the correct optimal structure belonging to the AR is enforced.

4. Dynamic behaviour of DSRs and fed-batch reactors

   Observe that the system of differential equations described by eq 5.3.2 contains equilibrium points associated with solutions to eq 5.3.3. These points, often termed fixed points, are time-independent solutions that provide meaningful information into the dynamical behaviour of the system. The stability of fixed points is often distinguished by examination of the eigenvalues of the

Table 5.1: Summary of fed-batch operating parameters.

Continuous structure	PFR	DSR	CSTR
Initial condition	$\mathbf{C}(0) = \mathbf{C_f}$	$\mathbf{C}(0) = \mathbf{C_f}$	$\mathbf{C}(0) = \mathbf{C}_{\mathrm{CSTR}}$
α policy	$\alpha = 0$	$\alpha = \alpha(t)$	$\alpha =$ constant
Side-stream composition	$\mathbf{0}$	$\mathbf{C}_0$	$\mathbf{C_f}$
Volume	$V =$ constant	$V(t) = F(t)/\alpha(t)$	$V(t) = F(t)/\alpha$
Reaction time	$t_f = \tau_{\mathrm{PFR}}$	$t_f = \tau_{\mathrm{DSR}}$	$t_f =$ free

Jacobian matrix of the system (Strogatz, 2001). These are classified as either stable, if all real parts of the eigenvalues are negative, or unstable, if at least one eigenvalue has a positive real part, or if there are multiple zero eigenvalues. The stability and position of the fixed points in state space influence the dynamical behaviour of the system, and thus also influence the choice of initial condition – nodes associated with unstable equilibrium points may exhibit chaotic behaviour and unstable operation. Furthermore, depending upon the feed condition and kinetics specified, multiple steady states may arise, and thus the stability of each equilibrium point should be considered in turn. Again, the initial condition of the fed-batch should be considered carefully to ensure that the desired equivalent CSTR behaviour is maintained.

5. Solution

   It is evident that CSTR solutions may be obtained in a fed-batch reactor by use of a constant α fed-batch, however the method of obtaining these solutions is different. A CSTR solution is obtained by solving a system of non-linear equations, in the form of the vector CSTR equation. Hence, a non-linear solver such as Newton's method must be employed. Graphically, a CSTR effluent concentration is collinear with the rate vector. By comparison, the same concentration is obtained in a fed-batch by integrating eq 5.3.2 to equilibrium. Hence the solution obtained is via the numerical integration of an ordinary differential equation, such as with a Runge-Kutta method. Graphically, the same concentration corresponds to a point in concentration space where the $d\mathbf{C}/dt$ term in eq 5.3.2 is the zero vector in the vector field described by eq 5.3.2.

A comparison between continuous and batch equipment is given in Figure 5.3.2, with defining parameters required by the fed-batch reactor summarised in Table 5.1. These serve as a convenient point of reference for the examples below.

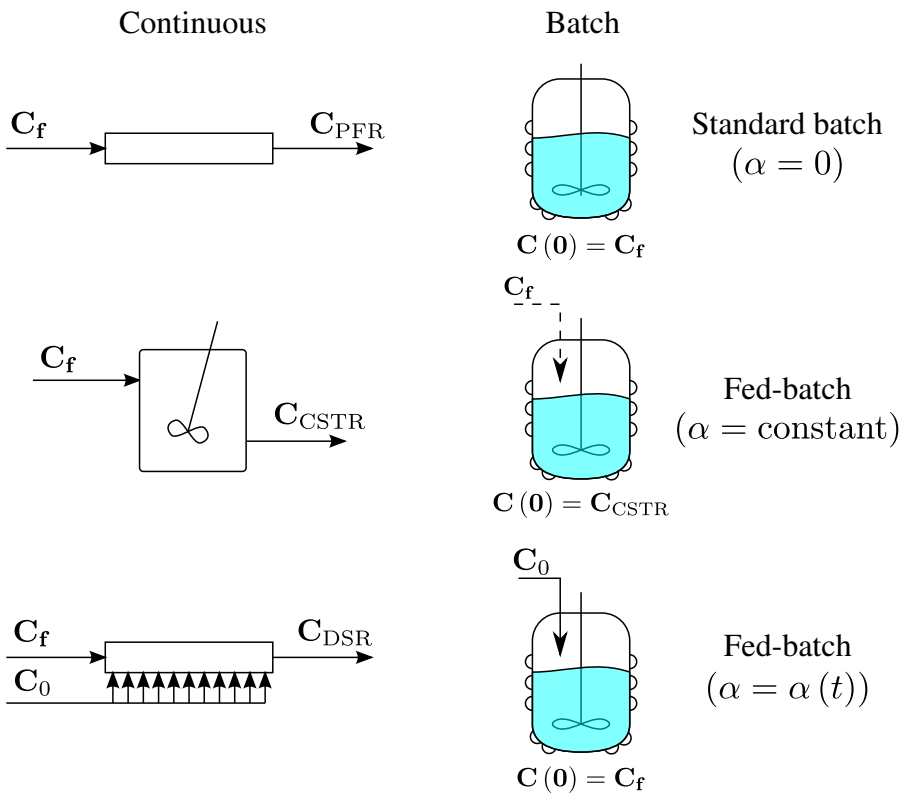


Figure 5.3.2: Comparison between continuous and batch reactive equipment. All three continuous reactors required to form the AR boundary may be likened to an equivalent batch structure.

5.4 Examples

5.4.1 2D autocatalytic reaction

System kinetics and feed point specification

Consider the following autocatalytic system(Brooks, 1988)

$$\begin{aligned} \mathrm{A} + 2\mathrm{B} &\xrightarrow[k_1]{} 3\mathrm{B} \\ \mathrm{B} &\xrightarrow[k_2]{} \mathrm{C} \end{aligned}$$

with rate constants $k_1 = 1\,\mathrm{L}^2/\left(\mathrm{mol}^3\mathrm{h}\right)$ and $k_2 = 1\,\mathrm{h}^{-1}$. A reaction of this type is found to be of interest in a number of applications including the production of industrial chemicals (Maestri and Rota, 2007; Xu et al., 2014), crystallisation reactions (Subotic, 1989; Kondepudi and Asakura, 2001) and biological systems (Putot et al., 2002; Watzky et al., 2008).

From section 5.2, the system contains two independent reactions and hence the entire system can be constructed in $\mathbb{R}^2$ alone. The resulting rate vector is then

expressed in terms of components A and B, and given by the following kinetics

$$\mathbf{r}(\mathbf{C}) = \begin{bmatrix} r_{\mathrm{A}}(\mathbf{C}) \\ r_{\mathrm{B}}(\mathbf{C}) \end{bmatrix} = \begin{bmatrix} -k_1 c_{\mathrm{A}} c_{\mathrm{B}}^2 \\ k_1 c_{\mathrm{A}} c_{\mathrm{B}}^2 - k_2 c_{\mathrm{B}} \end{bmatrix}$$

The objective here will be towards finding the appropriate batch sequence that maximises the concentration of component B in a batch cycle. This shall be achieved by first constructing the AR for a continuous system, and then carrying out the necessary conversions to establish an optimal batch structure. Brooks (1988) notes two observations of particular interest:

1. Multiple steady states are achievable depending on the feed concentration specified. In particular, this occurs when $c_{\mathrm{A}}^0 > 1 > c_{\mathrm{B}}^0$.

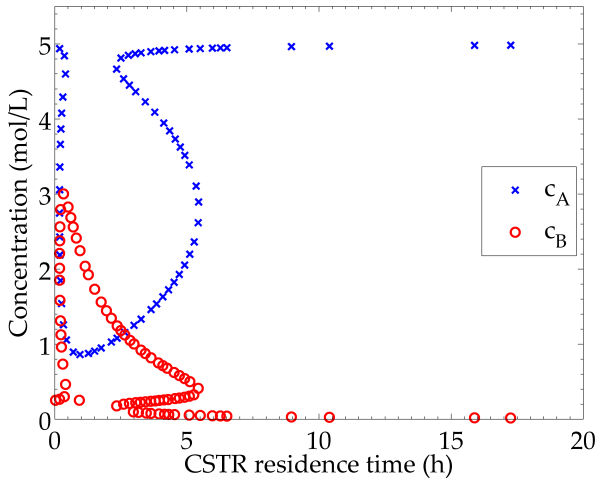
2. A higher concentration in B may be obtained if a period of standard batch reaction is employed directly after the initial fed-batch period.

The resulting maximum concentration achieved is then found to be larger than both a standard batch or fed-batch operation alone. The above recommendations correspond to those obtained by AR analysis also. To see this, we begin by first computing the AR for a specified feed condition. A composition of $\mathbf{C_f} = [5.0,\, 0.25]^{\mathrm{T}}$ has been chosen here so that it is consistent with the condition $c_{\mathrm{A}}^0 > 1 > c_{\mathrm{B}}^0$, and as a result, the system is expected to contain multiple steady states according to Brooks (1988).

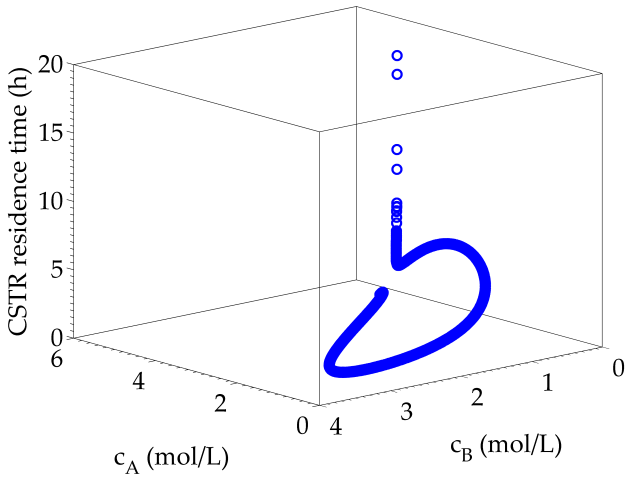
Multiplicity features

Solving the CSTR equation using $\mathbf{C_f} = [5.0,\, 0.25]^{\mathrm{T}}$ and plotting the resulting concentrations as functions of CSTR residence time demonstrates the existence of multiple steady states in the system. The residence times corresponding to these points are easily computed from eq 5.2.2, and shown in Figure 5.4.1a along with supplementary plots demonstrating the multiplicity features of the system. Indeed, it is clear that for the specified feed point, multiple CSTR effluent concentrations are available for specific residence time ranges - from Figure 5.4.1a, it appears that values of τ other than those in the range of $\sim 1.0\,\mathrm{h} \leq \tau \leq \sim 2.2\,\mathrm{h}$ produce multiple steady states. Knowledge of these residence times is important as a CSTR solution operating on the AR boundary corresponding may be associated with other points in space sharing the same residence time.

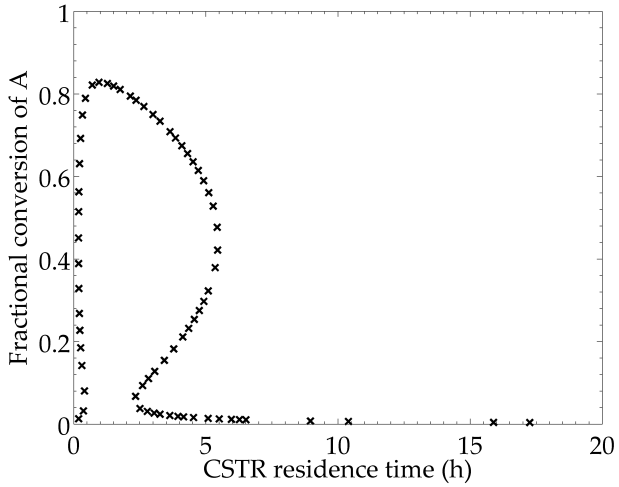
We highlighted previously that multiple steady states are only produced for specific values of the initial species concentrations feeding the CSTR. Figure 5.4.2 demonstrates the effect that the feed point plays in the existence of multiple steady states by plotting nine different feed points and their associated CSTR loci in $c_{\mathrm{A}} - c_{\mathrm{B}}$ space. These plots are inspired from similar work by Balakotaiah and Luss (1982, 1983, 1984). Feed points are given by the filled triangles whereas the CSTR locus in



(a) Concentration profiles for A and B.



(b) Concentration profile in $\mathbb{R}^3$



(c) Multiple conversions of A are possible in the system.

Figure 5.4.1: Multiplicity features of the autocatalytic reaction of Brooks (1988)

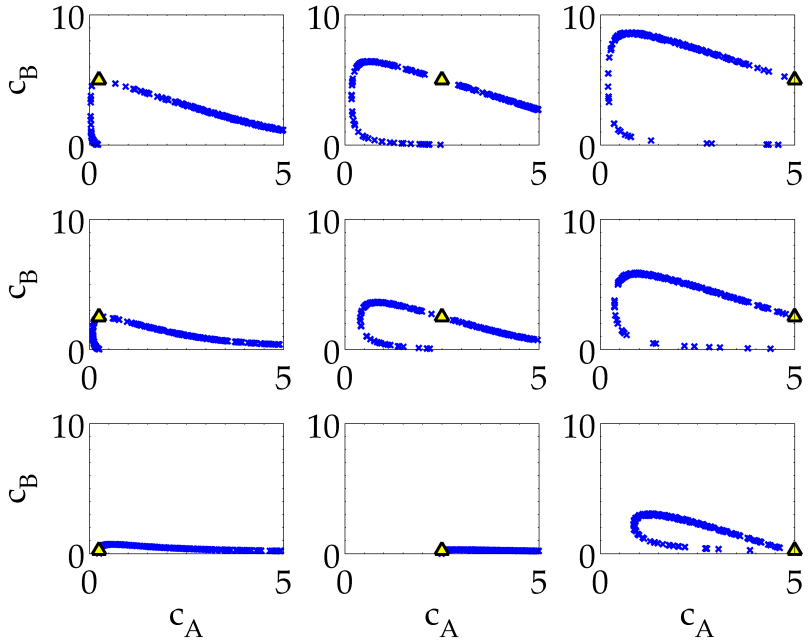


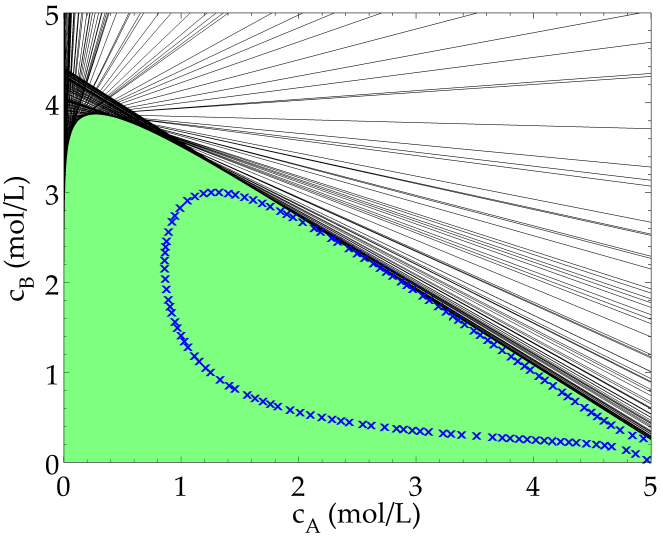
Figure 5.4.2: CSTR loci for different feed points

each sub-figure is denoted by ×'s. The species feed concentrations for components A and B are chosen at three distinct points, namely 0.25 mol/L, 1.0 mol/L and 5.0 mol/L for each axis respectively. Observe that irregularities in the shape of the locus are observed as the value of c_A is increased and the value of c_B is decreased, which corresponds to Brooks (1988).

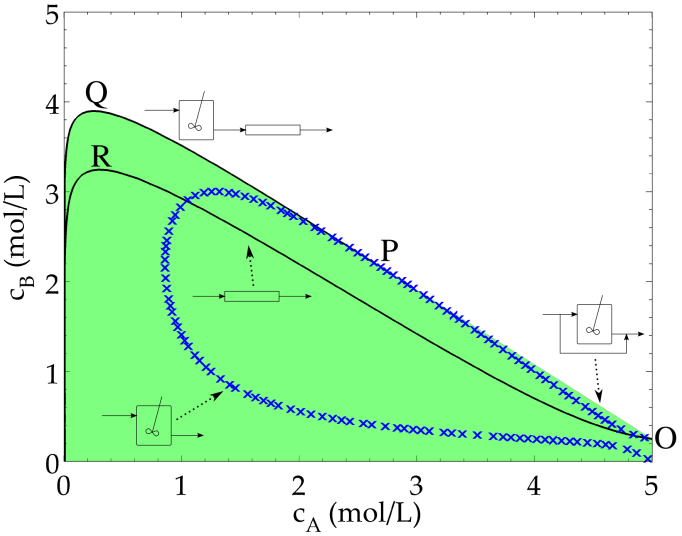
AR generation and optimal reactor structure

Seeing as the particular feed condition is expected to exhibit irregular behaviour, it is sensible to begin by choosing an AR construction technique capable of handling such kinetics. An outside-in method is a preferred method in this instance, and so either the bounding hyperplanes or rotated hyperplanes algorithm may be utilised. In this instance, we elect the rotated hyperplanes method as constructions are generally performed quicker.

Consequently, Figure 5.4.3a shows the resulting output from running the rotated hyperplanes algorithm for the system of reactions described above together with the particular feed point associated with multiple steady state behaviour. The hyperplanes have been included in the plot to indicate how they have been orientated in space to define the AR. We find that there is a maximum concentration of approximately 3.9 mol/L in B can be achieved in the system with the specific feed. The locus of CSTR points (×) belonging to the feed point for the system is overlaid for comparison. The CSTR locus is of particular interest, as it forms an almost completely closed loop within the space.



(a) AR construction from the rotated bounding hyperplanes method developed in chapter 4. The CSTR locus (×) belonging to the feed point has also been overlaid.



(b) PFR trajectories (–) and the CSTR locus (×) for the autocatalytic reaction given by Brooks (1988). A feed vector of $[5.0, 0.25]^{\mathrm{T}}$ has been used. The CSTR locus produces a separate region is space that may be used to achieve higher concentrations of component B. Point R corresponds to the point of maximum B for a PFR whereas Q is obtained by a CSTR-PFR structure that is part of the AR boundary.

Figure 5.4.3: AR and optimal reactor structures for the autocatalytic reaction of Brooks (1988)

In Figure 5.4.3b optimal reactor structures, corresponding to interesting sections of the AR, are shown. The PFR trajectory and CSTR locus beginning at the feed point have been plotted. Figure 5.4.3b also establishes all physically realisable concentrations achieved by mixing and reaction; that is, the shaded region represents the AR for the chosen feed point. This is obtained by computing the convex hull of all points resulting from a CSTR with feed concentration (point O), followed by a PFR to equilibrium. The CSTR-PFR sequence is thus the optimal reactor structure for the proposed AR. It follows that this is the only structure required in order to achieve all other physically realisable concentrations in the space. Of particular interest is point P, which provides the unique CSTR concentration that, when followed by a PFR, maximises the concentration of component B in the system; this occurs at point Q ($c_{\mathrm{B}} \sim 3.9\,\mathrm{mol/L}$). The corresponding CSTR residence time is then found to be $0.18367\,\mathrm{h}$ accordingly. Point P therefore corresponds to a critical CSTR point. All concentrations on the line segment OP are thus obtained by a CSTR with bypass of a portion of the feed. These results are in agreement with those suggested by Brooks (1988) for the batch case, where it is observed that a higher concentration in component B may be achieved if a standard batch is employed directly after the fed-batch period. This is displayed in the figure by the PFR trajectory PQ. Point R by comparison, is the point of maximum B for a single PFR initiated at the feed composition found at point O.

Nomenclature adopted by Brooks

Brooks (1988) discusses a strategy for reaction by initiating the cycle in fed-batch operation, and then terminating the cycle by charging the vessel with the remainder of feeding material in the form of a final feeding 'plug'. This converts the fed-batch into a standard batch, creating a fed-batch to standard batch reactor structure similar to the that obtained by AR analysis. When this is performed, Brooks (1988) notes that the concentration of B is higher than if standard batch operation is employed for the entire reaction cycle.

In order for comparisons to be made with the current work, a consistent set of quantities for concentration and reaction time need to be established. Brooks (1988) works with dimensionless concentrations in the form

$$x = \left(\frac{k_1}{k_2}\right)^{1/2} c_{\mathrm{A}} \qquad y = \left(\frac{k_1}{k_2}\right)^{1/2} c_{\mathrm{B}}$$

Note that $x = c_{\mathrm{A}}$ and $y = c_{\mathrm{B}}$ when $k_1 = 1\,\mathrm{L}^2/\left(\mathrm{mol}^3\mathrm{h}\right)$ and $k_2 = 1\,\mathrm{hr}^{-1}$, as is the case here. Brooks (1988) also assumes the fed-batch is operated under a constant feeding rate (F = const). A volume balance over a fed-batch assuming constant density gives

$$\frac{\mathrm{dV}}{\mathrm{dt}} = \mathrm{F}$$

which, upon integration, gives an expression for V in terms of F and reaction time t

$$\mathrm{V}(\mathrm{t}) = \mathrm{V}_0 + \mathrm{Ft}$$

V_0 is the initial volume of the fed-batch. To find an expression for residence time τ comparable with the current results, we invoke the definition of residence time using the total reactor volume and feeding rate. Rearrangement gives

$$\begin{aligned} \tau &= \mathrm{V/F} \\ &= \frac{\mathrm{V}_0}{\mathrm{F}} + \mathrm{t} \end{aligned}$$

This is a linear function in terms of residence time. The inverse of this is hence the equivalent expression for α

$$\alpha = \frac{1}{\mathrm{V}_0/\mathrm{F} + \mathrm{t}}$$

Brooks (1988) provides a dimensionless residence time, given by

$$\mathit{\Gamma} = k_2 \left(\frac{\mathrm{V}_0}{\mathrm{F}} + \mathrm{t} \right)$$

The author also assumes $\mathrm{V}_0 = 0\,\mathrm{L}$. We have a one-to-one relation for residence time and reaction time in the fed-batch

$$\mathit{\Gamma} = \tau = \mathrm{t} \qquad \text{and} \qquad \alpha = 1/\mathrm{t} \tag{5.4.1}$$

Dimensionless concentration profiles for x and y in terms of $\mathit{\Gamma}$ are then given in (Brooks, 1988). The above transformations are utilised in order to compare the results presented here with the literature, which is discussed next.

Conversion from continuous to batch

Once the AR and its associated continuous structure have been formed, the task of converting to an equivalent batch system is straightforward. The CSTR-PFR structure required for continuous reaction is interpreted as follows:

1. A fed-batch reactor with constant α policy for the CSTR portion of the structure

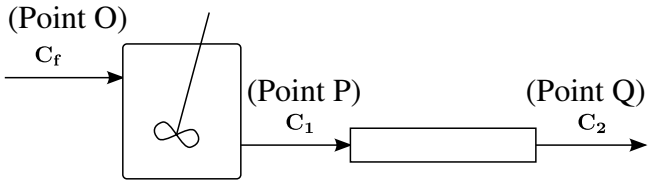
2. Followed by a period of standard batch reaction for the PFR.

The distinct value for α is given by the associated residence time and equilibrium concentration of the CSTR. Hence, for a residence time of $0.18367\,\mathrm{h}$, $\alpha = 1/0.18367\,\mathrm{h}^{-1}$. Prior to performing the reaction however, the desired concentration at point P must first be prepared. This is carried out using the suggested procedures discussed in section 5.3.2. Since concentrations within the vessel do not vary with time during the

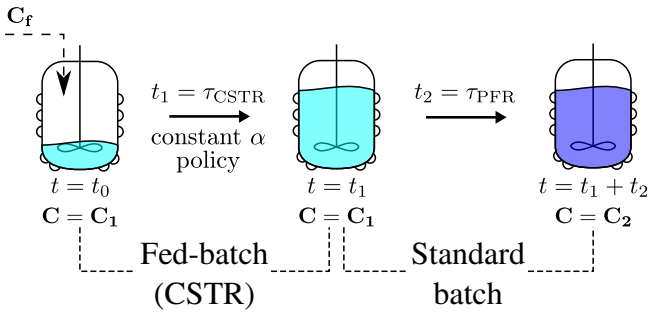
fed-batch portion of the cycle, reaction time is somewhat arbitrary, although, it is clear that the rate of filling (governed by the value of α) and the final desired volume are important parameters when deciding on the reaction time. We have used the familiar boundary condition when $t = \tau_{CSTR}$, $V = V_{CSTR} + V_0$ as in section 5.3.2.

For the standard batch component of this structure, reaction time is determined by the residence time of the PFR. It is found that a PFR residence time of 0.2140 h is required in order to react from point P to point Q and therefore the same period is required by the standard batch. Reaction time is determined directly by the residence time of the PFR in this case.

Conversion from a continuous structure to an equivalent batch structure is now complete. The resulting sequence of batch operations is given by Figure 5.4.4.



(a) Recommended continuous structure. A CSTR from the feed (point O) followed by a PFR.



(b) Batch structure. The cycle begins with a constant α fed-batch period initiated at the critical CSTR effluent composition (given by point P), followed by a standard batch period.

Figure 5.4.4: Comparison of continuous (a) and batch (b) structures for the autocatalytic reaction in $\mathbb{R}^2$. Only a single structure is required for this system. Notice that the structure terminates with a PFR in the continuous case, and a standard batch period for the batch. This is in agreement with the suggested final batch period recommended by Brooks (1988).

It is also possible to operate the entire sequence within a single reaction vessel. By comparison, an equivalent approach would be difficult to achieve in a single continuous reactor. Hence, from an initial volume and CSTR concentration, the cycle might begin, say, with a period of fed-batch operation and allow for the reaction to proceed until the desired product volume has been obtained. Batch reaction could then be initiated afterwards by terminating the side-stream feed to the reactor. The

α policy and concentration profile of component B for this process is given by Figure 5.4.5a and 5.4.5b respectively. The recommended α policy is fairly simple in this instance, and involves a period of constant side-stream addition for approximately 0.2 h, followed immediately by a longer period with no additional side-stream feeding (the point of maximum B occurs at $\mathrm{t} = 0.3977\,\mathrm{h}$). The total cycle time is then $\tau_{\mathrm{CSTR}} + \tau_{\mathrm{PFR}}$. The equivalent α policy for the recommendations by Brooks (1988) are shown in Figure 5.4.5a. Whereas the value of α is constant in this work, that of Brooks (1988) is a non-linear function given by $\alpha = 1/\mathrm{t}$ from eq 5.4.1.

Results and comparison to literature

The concentration profiles belonging to Brooks (1988) are given by unfilled circles. The sudden decline and subsequent rise in c_{B} at $\mathrm{t} = 3\,\mathrm{h}$ corresponds to the period when the fed-bath period is terminated and the standard batch is initiated. Notice that the fed-batch to standard batch sequence is identical in structure this work, however the maximum concentration of B is only slightly larger than the standard batch (3.43 mol/L compared to 3.24 mol/L), whereas that given by the AR is larger 3.90 mol/L then both.

The concentration profile corresponding to a standard batch for the same feed point is provided for comparison. It is observed that a higher concentration is achieved in the fed-batch when compared to the standard batch. Moreover, the time required to achieve maximum concentration in the standard batch is noticeably longer when compared to that of the fed-batch-standard batch sequence (2.128 h compared to 0.3977 h); the production rate of the recommended structure is approximately five times faster compared to the standard batch as a result. The maximum value corresponding to point Q is that belonging to the AR boundary, and a higher value in c_{B} is not possible with a change the side-stream or feed point concentration. Both the maximum concentration of B and optimal batch structure have been identified via AR theory.

Hansen et al. (1993) also studied the above reaction and investigated the optimal feeding profile for the generalised reaction

$$\begin{aligned} \mathrm{A} + n\mathrm{B} &\rightarrow (n+1)\,\mathrm{B} \\ m\mathrm{B} &\rightarrow \mathrm{C} \end{aligned}$$

The above is identical to the system considered here when $n = 2$ and $m = 1$. The authors employ Pontryagin's maximum principle and solve for optimality conditions to find singular arcs in the feeding profile. Specifically, a final time-independent performance measure of maximum concentration of B is used in the analysis. Hansen et al. (1993) investigate the case when $n = 2$ and $m = 1$ and compute optimal feeding trajectories for the same feed point used here. Noticeably, the authors state that

Table 5.2: Performance comparison for autocatalytic reaction

Author	Max c_B obtained	Optimal structure	Methodology/Reason
Brooks (1988)	3.4 mol/L	Decreasing α policy fed-batch followed by standard batch (constant F).	Exploiting structure of fed-batch equations. Observed higher concentrations when standard batch is employed directly afterwards.
Hansen et al. (1993)	3.89 mol/L	Singular control (increasing F policy) fed-batch followed by standard batch.	Pontryagin's maximum principle. Structure from switching policy of optimality conditions.
Present work	3.90 mol/L	Constant α policy fed-batch followed by standard batch.	Attainable Region analysis. Structure from AR construction.

1. The optimal profile is composed of a combination of singular and non-singular profiles in the feeding policy.

2. The switching sequence for the feeding profile is

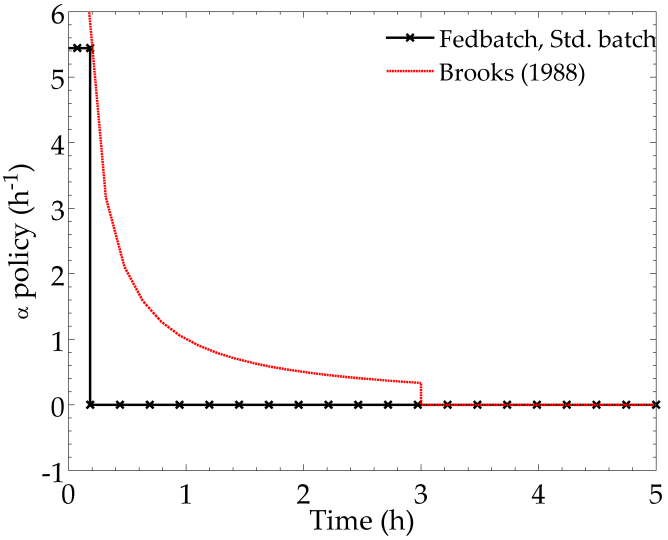
   (a) first a period of fed-batch reaction, corresponding to a singular feeding rate belonging to the optimality condition

   (b) followed by a period of batch operation.

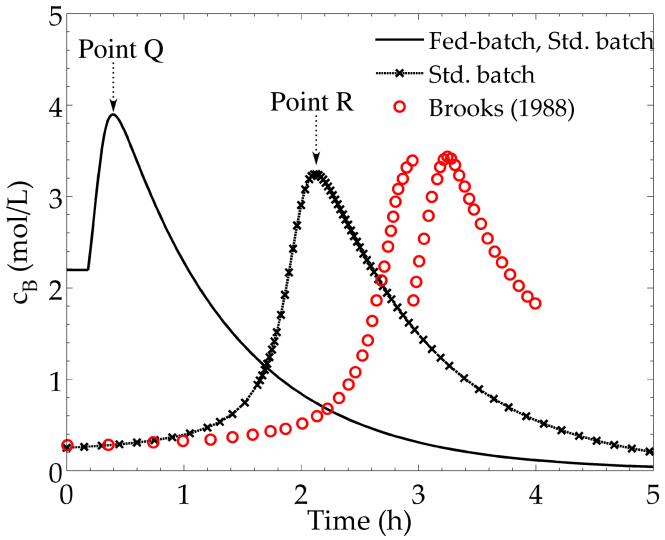
Hansen et al. (1993) also note that, typically, a non-singular arc is used to bring the conditions to the singular point, at which time singular control takes over. A final batch period is used afterwards to reach the performance index. This describes a reaction sequence identical to that suggested by the AR construction. Notice that in the case of AR analysis, the singular point is identified as point P on the AR boundary in Figure 5.4.3b (the critical CSTR point). The period of batch operation following this singular point corresponds to the PFR trajectory from the critical CSTR point and thus both methods are in agreement with one another even though the recommendations have come about from two independent theories.

Solution of the optimal control problem by Hansen et al. (1993) corresponds to a single point on the AR boundary. Hence, points on the AR boundary can be found from optimal control arguments, but many different optimisations must be solved in order to generate the AR boundary. Table 5.2 summarises the performance achieved by the different methods.

The correct sequencing and timing of individual batch operations is important,



(a) α policy for the combined fed-batch to standard batch system. The profile is composed of two sections, a constant value ($\alpha = 1/0.18367\,\mathrm{h}^{-1}$) corresponding to the critical CSTR portion of the structure, and a period of no filling ($\alpha = 0$) corresponding to the final PFR section.



(b) Concentration of component B achieved by the batch cycle obtained from the AR compared to that achieved by a standard batch initiated at the feed concentration. The initial constant concentration profile for the fed-batch corresponds to the CSTR concentration given by the continuous AR structure. The reaction time for the AR structure is shorter and achieves a higher concentration in B compared to the standard batch.

Figure 5.4.5: Recommended α policy (a) and associated concentration profile of component B (b) for the autocatalytic system.

and reaction time is a central parameter in this regard. In contrast to batch equipment, continuous structures require the adequate ordering of equipment through *space*. Hence for continuous equipment, reactor volume (or residence time) is the important parameter.

Stability and dynamic behaviour

The appropriate choice of initial condition for the CSTR concentration is an important consideration when dealing with the dynamic behaviour of both continuous and batch operation. To see this, consider again the CSTR locus given in Figure 5.4.6.

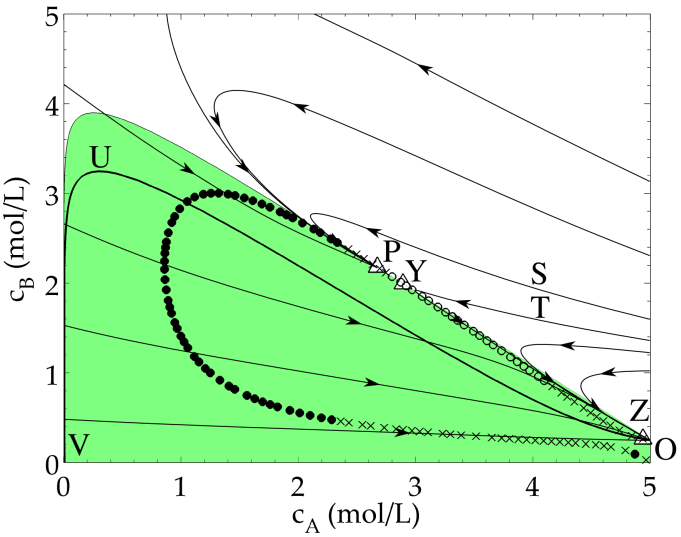


Figure 5.4.6: DSR map for the autocatalytic system generated for an α value corresponding to the critical CSTR residence time ($\alpha = 1/0.18367\,\mathrm{h}^{-1}$). Three equilibrium points associated with this value of α are observed (given by white triangles). Points P and Z lie on the CSTR locus representing stable nodes ($\times$). Equilibrium point Y lies on the section of the locus associated with unstable nodes (unfilled circles). The solid circles are locus points associated with a stable focus. The trajectory ZUV is obtained by a PFR initiated with a concentration from equilibrium point Z.

As in Figure 5.4.3b, the AR and CSTR concentrations have been plotted in $c_\mathrm{A} - c_\mathrm{B}$ space. The graph also shows points on the locus corresponding to solutions to eq 5.2.2 for when $\tau = 0.18367\,\mathrm{h}$ (the CSTR residence time associated with the critical CSTR), given here by points P, Y and Z. Note that points O and P are the same point as those given in Figure 5.4.3b. DSR trajectories corresponding to this residence time for a variety of feed points have also been plotted, allowing for the determination of the DSR map for the specified α in space – for each value of α specified, a unique DSR map may be generated, providing information regarding the dynamic behaviour of DSRs in space. The path traced out by the CSTR locus therefore represents the set of equilibrium points achieved by the DSR for various values of α. Points P, Y and Z are thus also the distinct equilibrium points associated

with the unique fed-batch reactor for when $\alpha = 1/0.18367\,\mathrm{h}^{-1}$.

The CSTR locus is represented differently in this figure. Here, it is generated by examination of the eigenvalues corresponding to the Jacobian matrix, $\mathbf{J}$, for this system

$$\mathbf{J} = \begin{bmatrix} -\alpha - k_1 c_\mathrm{B}^2 & -2k_1 c_\mathrm{A} c_\mathrm{B} \\ k_1 c_\mathrm{B}^2 & -\alpha + 2k_1 c_\mathrm{A} c_\mathrm{B} - k_2 \end{bmatrix}$$

The CSTR locus may be classified according to the following three stability criteria

1. Sections of the locus displayed by filled circles are those which represent a stable focus (complex eigenvalues, negative real part).

2. Crosses indicate stable nodes (real eigenvalues both negative in sign).

3. Unfilled circles correspond to saddle points (real eigenvalues, differing in sign).

Notice that points P and Z lie on sections of the locus that are stable, and are therefore stable equilibrium points, whereas point Y is a saddle point. It is clear from the figure that depending on the initial concentration chosen for a fed-batch, one may achieve significantly different outcomes. Although three fed-batch equilibrium solutions exist for the intended residence time, only two are physically realisable.

If an initial concentration equal to point S is chosen, then the fed-batch trajectory follows the curve SP and the equilibrium point achieved is that of point P (the critical CSTR point for the AR). Accordingly, a period of standard batch operation following from point P results in the full set of concentrations achieved corresponding to the AR. By comparison, if an initial concentration equal to point T is used instead, then the fed-batch trajectory follows curve TYZ. For this initial condition, the trajectory begins at point T, approaches unstable node Y, and then diverges sharply towards stable node Z. Point Z is thus the equilibrium point for the initial concentration given by point T and corresponds to an alternate CSTR solution for the chosen residence time. Consequently, a period of standard batch operation following from point Z results in the smaller achievable region instead, given by curve ZUV. The set of achievable concentrations obtained by this outcome is noticeably smaller than that given by the full AR. This is in effect despite selecting conditions that correspond to the correct, and optimal, CSTR-PFR structure for identical residence times. If the feed point were to be used as the initial concentration for this problem, then the fed-batch would have converged to the incorrect equilibrium concentration, and the actual product achieved by the batch sequence would differ to that suggested by the continuous structure. Again, care must be taken when selecting the initial condition for constant α fed-batch operations. Although it may seem convenient to use the feed concentration for example, multiple steady states and instability might interfere with the fed-batch equilibrium achieved, even for situations in which the structure has been determined correctly.

5.4.2 3D van de Vusse kinetics

System specification

Next, we shall examine the nature of the optimal batch structure for the well-known van de Vusse reaction scheme. Consideration of this system will demonstrate the role that DSRs, and by extension, the role that fed-batch reactors with varying α policies play in the formation the AR boundary. The system is composed of three independent reactions, that is,

$$\mathrm{A} \overset{k_1}{\rightarrow} \mathrm{B} \overset{k_2}{\rightarrow} \mathrm{C}$$
$$2\mathrm{A} \underset{k_3}{\rightarrow} \mathrm{D}$$

Although four species are present, only three are independent, as the fourth may be determined by mass balance. The rate expression follows mass-action kinetics and may be written in terms of components A and B by the following rate vector

$$\mathbf{r}(\mathbf{C}) = \begin{bmatrix} -k_1 c_\mathrm{A} - 2k_3 c_\mathrm{A}^2 \\ k_1 c_\mathrm{A} - k_2 c_\mathrm{B} \\ k_3 c_\mathrm{A}^2 \end{bmatrix}$$

The associated rate constants are then given as $k_1 = 1\,\mathrm{h}^{-1}$, $k_2 = 1\,\mathrm{h}^{-1}$, $k_3 = 10\,\mathrm{L}/(\mathrm{mol}\cdot\mathrm{h})$. Historically, the associated AR has been determined in $c_\mathrm{A} - c_\mathrm{B} - c_\mathrm{D}$ space, so that the concentration vector may be expressed as $\mathbf{C} = [c_\mathrm{A},\, c_\mathrm{B},\, c_\mathrm{D}]^\mathrm{T}$. We specify that the feed is pure in component A, in which case $\mathbf{C_f} = [1,\, 0,\, 0]^\mathrm{T}$.

Construction of the AR for the above problem has been discussed in previous work, and the optimal structure is well understood (Hildebrandt and Glasser, 1990; Feinberg and Hildebrandt, 1997). As a result, we are able to utilise the previously developed results and apply them here with very little added effort, so that the development of an equivalent batch structure may be carried out. A brief summary of the construction procedure for the system is provided below for completeness.

Optimal continuous structure

Only the feed point is achievable initially. As with many AR construction problems, it is most natural to begin by considering single reactor structures that expand the initial set of achievable points from the feed. The simplest method of achieving this is by computing the PFR trajectory and CSTR locus from $\mathbf{C_f}$. This is equivalent to the procedure performed for the 2D van de Vusse system in chapter 5.

PFRs and CSTR locus from the feed PFRs make up the final approach to the extremities of the AR boundary and thus it is helpful to include PFR segments as the final reactor to all structures. In effect, we wish to generate the convex

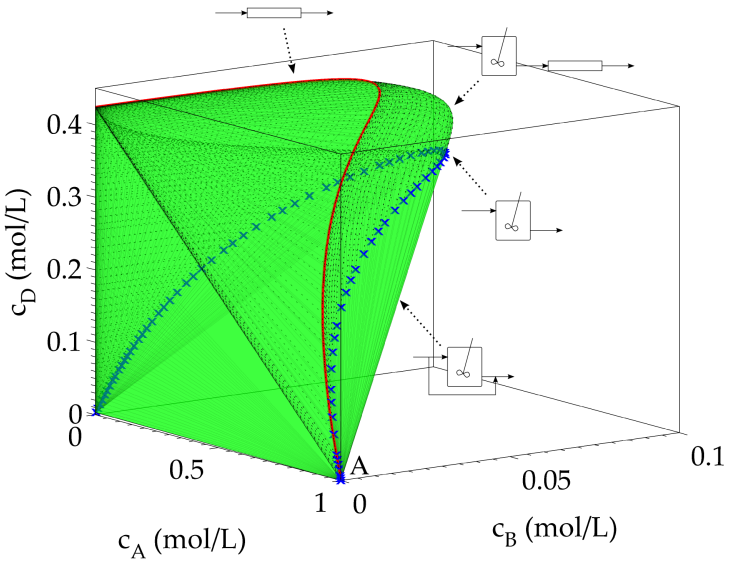


Figure 5.4.7: Convex hull of the CSTR-PFR reactor structure from the feed. Note that this is not the full AR for the 3D van de Vusse system.

hull for a CSTR followed by a PFR in series from the feed point. This is achieved algorithmically by first solving the CSTR equation and generating a CSTR locus that may be used as feed points for PFR trajectories. CSTR effluent concentrations act as initial conditions for the PFR integration. For N CSTR points generated in the locus, N PFR trajectories may be computed. These points are then appended to the existing set of achievable concentrations and the convex hull for the larger set may again be computed. The results of which are shown in Figure 5.4.7.

The region generated represents a significant portion of the true AR, although it is incomplete(Feinberg and Hildebrandt, 1997). Structures involving critical CSTRs and DSRs are still missing. Ideas developed in chapter 2 are used next to expand the region.

Critical CSTRs It is conceptually and computationally easier to begin expansion of the region by consideration of critical CSTRs first. This is initiated by computing the controllability conditions for a critical CSTR, as discussed in chapter 2. Note that determining the behaviour of critical CSTRs and DSRs requires that the full dimension of the system (that is, all components as opposed a subset) be considered - to compute the determinant function, $\Lambda(\mathbf{C})$, for this system (see chapter 2), a rate vector containing the total number of components present in the system must be considered. Therefore a four component variant of the rate vector given above is utilized, rather than the typical three component rate vector given above. The original rate vector is hence augmented with the rate expression corresponding to component C in the system, and the following rate vector is obtained:

$$\mathbf{r}^{\#}(\mathbf{C}) = [r_{\mathrm{A}}(\mathbf{C}), r_{\mathrm{B}}(\mathbf{C}), r_{\mathrm{C}}(\mathbf{C}), r_{\mathrm{D}}(\mathbf{C})]^{\mathrm{T}}$$

$$= \begin{bmatrix} -k_1 c_{\mathrm{A}} - 2k_3 c_{\mathrm{A}}^2 \\ k_1 c_{\mathrm{A}} - k_2 c_{\mathrm{B}} \\ k_2 c_{\mathrm{B}} \\ k_3 c_{\mathrm{A}}^2 \end{bmatrix}$$

We use rate vector $\mathbf{r}^{\#}(\mathbf{C})$ to differentiate it from the standard rate vector $\mathbf{r}(\mathbf{C})$ containing only 3 components. Similarly, the Jacobian matrix, $\mathbf{J}^{\#}(\mathbf{C})$, corresponding to $\mathbf{r}'(\mathbf{C})$ may be computed

$$\mathbf{J}^{\#}(\mathbf{C}) = \begin{bmatrix} -k_1 - 4k_3 c_{\mathrm{A}} & 0 & 0 & 0 \\ k_1 & -k_2 & 0 & 0 \\ 0 & k_2 & 0 & 0 \\ 2k_3 c_{\mathrm{A}} & 0 & 0 & 0 \end{bmatrix}$$

Thus for the van de Vusse system, the determinant function is given by:

$$\Lambda(\mathbf{C}) = -3.5 c_{\mathrm{A}}^3 k_2 k_3 (2c_{\mathrm{A}} k_3 + k_1) \left(2c_{\mathrm{A}}^2 k_1 k_3 - 4c_{\mathrm{A}} c_{\mathrm{B}} k_2 k_3 - c_{\mathrm{A}} k_1 k_2 - c_{\mathrm{B}} k_1 k_2 + c_{\mathrm{B}} k_2^2\right)$$

The level sets of function $\Lambda(\mathbf{C})$ describe surfaces in $\mathbb{R}^3$. The particular level set when $\Lambda(\mathbf{C}) = 0$ is of interest here since critical CSTRs must satisfy this condition specifically – for a CSTR effluent concentration to exist on the AR boundary, the associated CSTR locus must intersect the surface described by $\Lambda(\mathbf{C}) = 0$. CSTR effluent concentrations may be substituted into $\Lambda(\mathbf{C})$ to determine if the point is a solution to the function. If a CSTR effluent concentration $\mathbf{C}$ is a root of $\Lambda(\mathbf{C})$, then $\mathbf{C}$ must exist on the AR boundary. Since the CSTR locus at the feed point has been solved previously, substitution of the locus values into $\Lambda(\mathbf{C})$ may be carried out in a straightforward manner. Each CSTR solution is associated with a unique residence time. It is hence sensible to graph the values of $\Lambda(\mathbf{C})$ as a function of τ. Thus, instead of computing $\Lambda(\mathbf{C})$ as a function of $\mathbf{C}$ to obtain a surface in $\mathbb{R}^3$, we plot $\Lambda(\mathbf{C}(\tau))$ versus τ, where τ is the corresponding CSTR residence time associated with $\mathbf{C}$. This produces the 2D plot, given in Figure 5.4.8.

A root of $\Lambda(\mathbf{C})$ exists time near $\tau \sim 36.7\,\mathrm{s}$ in the range of 0 to 300 s. The value of $\Lambda(\mathbf{C})$ also appears to approach zero as the value of τ is increased. This suggests that the equilibrium CSTR point is also a critical CSTR point. The curve in Figure 5.4.8 thus suggests that there are two concentrations that lie on the AR boundary. The remainder of the CSTR locus does not lie on the boundary and these concentrations are hence not optimal. PFR trajectories initiated from the CSTR locus not associated with the two critical CSTR solutions therefore also do not form part of the manifold of PFR trajectories on the true AR boundary. Other structures must therefore exist that constitute the AR boundary. The only remaining fundamental reactor structure available is the DSR.

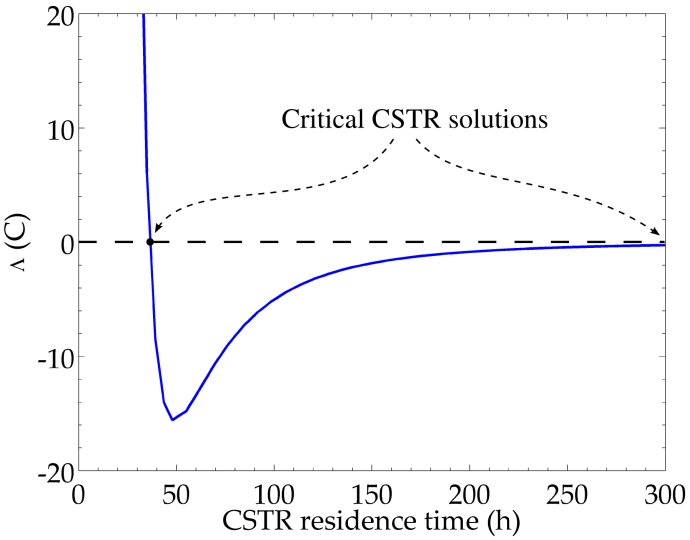


Figure 5.4.8: The determinant of the controllability matrix from section 2.4.4 as a function of CSTR residence time from the feed point. Two roots exist: one at $\tau \sim 36.7\,\mathrm{s}$ and the other at the CSTR equilibrium point.

Critical DSRs The form of the critical α policy for the DSR is generalized and therefore potentially many different α policies may be computed that all conform to the controllability criteria for critical DSRs . As noted in chapter 2, side-stream concentrations $\mathbf{C}_0$ used in a critical DSR must originate from points on the AR boundary. This assists in refining the possible concentrations available to act as side-stream compositions. Since the feed point is always specified and included on the AR boundary, we often use $\mathbf{C}_0 = \mathbf{C_f}$ for convenience.

A critical DSR profile for the system may now be computed. Since the system under investigation is a three dimensional problem, two possibilities are available for computing the critical α policy for the system:

1. The controllability criterion for the system may be applied, by computing iterated Lie brackets as in chapter 2.

2. The 'vDelR' condition, specific to three dimensional problems, also discussed in chapter 2 may also be employed.

Often for 3D problems, the second approach is quicker and so this will be done here. The condition is reproduced below

$$\varphi(\mathbf{C}) = [\mathbf{J}(\mathbf{C})(\mathbf{C}_0 - \mathbf{C})]^{\mathrm{T}} [(\mathbf{C}_0 - \mathbf{C}) \times \mathbf{r}(\mathbf{C})]$$

and

$$\alpha(\mathbf{C}) = -\frac{[\nabla\varphi(\mathbf{C})]^{\mathrm{T}} \mathbf{r}(\mathbf{C})}{[\nabla\varphi(\mathbf{C})]^{\mathrm{T}} (\mathbf{C}_0 - \mathbf{C})} \tag{5.4.2}$$

The resulting generalised expression for the van de Vusse system is too large to

display in terms of all system variables alone. Numerical values for the kinetic constants and mixing point may be substituted into eq 5.4.2 to simplify the expression slightly. The expression given in Feinberg (2000b) is then obtained.

$$\alpha\left(\mathbf{C}\right)=\frac{1}{2}\left[\frac{c_{\mathrm{A}}\left(20{c_{\mathrm{A}}}^{3}c_{\mathrm{B}}-80{c_{\mathrm{A}}}^{2}c_{\mathrm{B}}-{c_{\mathrm{A}}}^{2}+37c_{\mathrm{A}}c_{\mathrm{B}}+c_{\mathrm{A}}+2c_{\mathrm{B}}\right)}{c_{\mathrm{B}}\left({c_{\mathrm{A}}}^{2}-2c_{\mathrm{A}}+1\right)}\right] \tag{5.4.3}$$

Note that eq 5.4.3 is specific to the feed point $\mathbf{C}_0=\mathbf{C_f}=[1,\,0,\,0]^{\mathrm{T}}$ and the values of the rate constants given at the beginning of the example. If different conditions are used, eq 5.4.2 must again be employed and simplified for the new α expression.

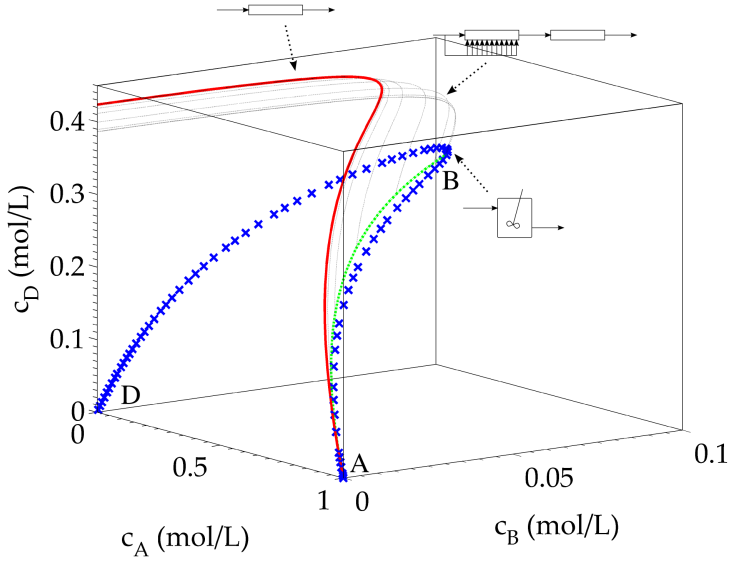
Initial conditions for the DSR are next considered. It is intuitive to initiate a DSR from the feed point. The DSR expression is thus integrated together with the critical policy provided previously to produce a DSR trajectory. We note that eq 5.4.3 is undefined at $\mathbf{C}=\mathbf{C}_0$. Hence, to initiate the integration, the initial condition for the DSR is offset slightly from feed point value. Hence, an initial condition of $\mathbf{C_f}=[0.9999,\,0.0001,\,0]^{\mathrm{T}}$ is supplied as opposed to $[1,\,0,\,0]^{\mathrm{T}}$. The DSR equation is then integrated together with eq 5.4.3 over a sufficiently long integration time. The resulting profile is given in Figure 5.4.9a. The convex hull corresponding to this candidate is not shown here so that the underlying boundary structures are more easily identified.

This produces a critical DSR trajectory in space. Note that although the DSR trajectory appears to behave in a similar fashion to the CSTR locus, the sets of concentrations produced by the two are distinct. All of the points on the critical DSR trajectory lie on the AR boundary. PFR trajectories in series with the DSR will therefore serve to fill out a manifold of extreme points on the AR boundary. These trajectories are also displayed in the figure.

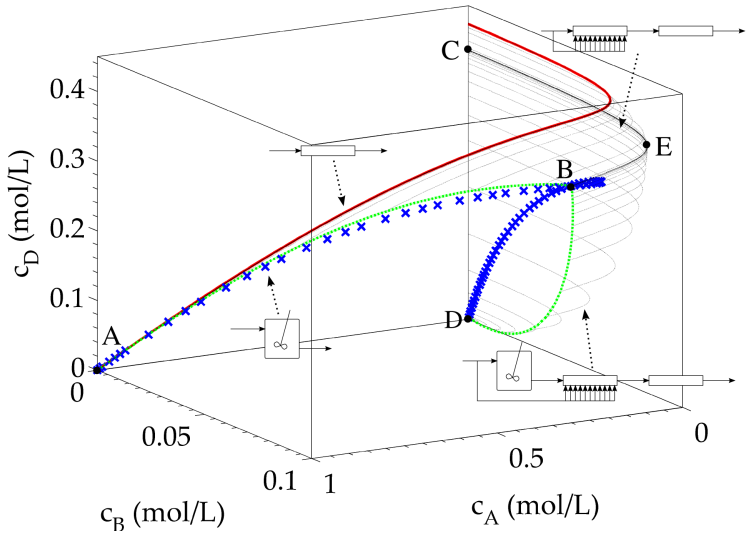
It is interesting to note that the critical DSR trajectory obtained in Figure 5.4.9a terminates at an intermediate point near CSTR locus. This is labelled as point B in Figure 5.4.9a. The second critical CSTR solution located at the equilibrium point does not appear to intersect the DSR trajectory. Since the AR boundary is composed of PFR trajectories connected by critical CSTRs and DSRs, a portion of the AR boundary is missing that joins the two critical CSTR points obtained previously together. Additional DSR structures must exist that connect the two critical points together that are not currently associated with the proposed structure.

To identify the other critical DSR, a bit of deduction is necessary: Since the feed point $\mathbf{C_f}$ has already been utilized as an initial condition to the critical DSR that passes through one of two critical CSTR points (the DSR equilibrium concentration is at the critical CSTR concentration), the only critical concentration available is that of the other critical CSTR point obtained at the CSTR equilibrium concentration.

Accordingly, to complete construction of the AR boundary, another DSR tra-



(a) Unfilled candidate region for the 3D van de Vusse system including a critical DSR trajectory from the feed point.



(b) AR for the van de Vusse system in $\mathbb{R}^3$. The mixing points for both α policies have been approximated arbitrarily closely. Mixing lines have been excluded from the construction so that the optimal continuous structures are more clearly visible. DSR trajectories are given by solid green lines, the CSTR locus from the feed point (point A) by blue circles, and PFR trajectories by dashed black lines.

Figure 5.4.9: Optimal reactor structures for the 3D van de Vusse system

jectory is initiated at the CSTR equilibrium point. When this is performed, the resulting critical DSR trajectory is different to that initiated at $\mathbf{C_f}$: the trajectory appears to connect the two critical CSTR concentrations together. This second DSR trajectory is a further connector on the AR boundary. PFR trajectories are again initiated from critical DSR trajectory to fill out the remaining bottom portion of the AR boundary. This is serves to complete construction of the AR boundary for the 3D van de Vusse system. All reactor structures forming the AR boundary is given in Figure 5.4.9b.

A summary of the optimal structures is thus given as follows:

1. Structure 1: A DSR from the feed vector (point A) to equilibrium (point B) followed by a PFR to equilibrium (point C). This fills out the first part of the AR boundary (path ABEC).

2. Structure 2: A CSTR operating at its equilibrium (point D), followed by a DSR at equilibrium (point B) and then a PFR. The unique PFR trajectory BEC that passes through point E is the point of maximum concentration in component B. This fills out the underside of the AR boundary (path DBEC).

The kinetics exhibit three independent reactions and hence, at most, two parallel reaction schemes are required to achieve all concentrations on the AR boundary. Combination of these two reactor structures alone allows for the synthesis of every possible concentration for every possible reactor configuration imaginable. A distinct choice must be made between the two depending upon the desired final state. Different optimizations may now be carried out to identify points where the AR boundary and objective function intersect. Once these intersection points have been established, the appropriate optimal reactor structures may be employed to achieve the points of interest. Notice that the above structures are consistent with what it expected from the theory discussed in chapter 2:

- The AR is convex.
- DSR trajectories and CSTR critical points form connectors to a manifold of PFR extreme points.
- The boundary of the AR is composed of straight line sections (indicating mixing) and PFR trajectories only. The final approach to all reactive portions of the boundary is achieved via a PFR.

This concludes the AR construction for the 3D van de Vusse kinetics. Notice that the inclusion of critical CSTRs and DSRs complicates construction, but these are required in order to generate the true AR.

Conversion to batch

For this example, the AR is defined by two parallel continuous structures. It follows that we require, at most, two batch structures to achieve all points on the AR boundary. Figure 5.4.10 provides the necessary conversion from continuous to batch. Again, a one-to-one correspondence between batch and continuous equipment is observed. In both cases, fed-batch reactors with varying α policies are seen to contribute significantly to the overall set of achievable concentrations.

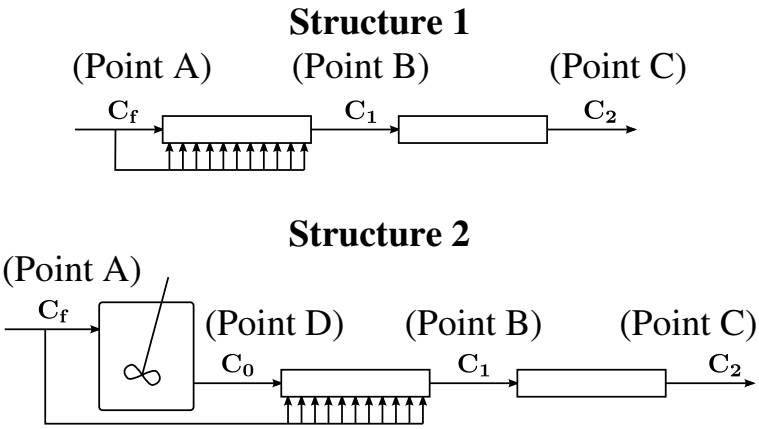
The following batch cycles are required (Figure 5.4.10b):

- For structure 1, a fed-batch reactor followed by a period of standard batch reaction. This is provided by path ABEC in Figure 5.4.9b.
- For structure 2, three distinct reaction intervals are needed, two of which are fed-batch operations. The cycle is initiated with a period of constant α, followed by a non-constant α interval, and completed with a period of standard batch reaction. This is given in Figure 5.4.9b by the path DBEC.

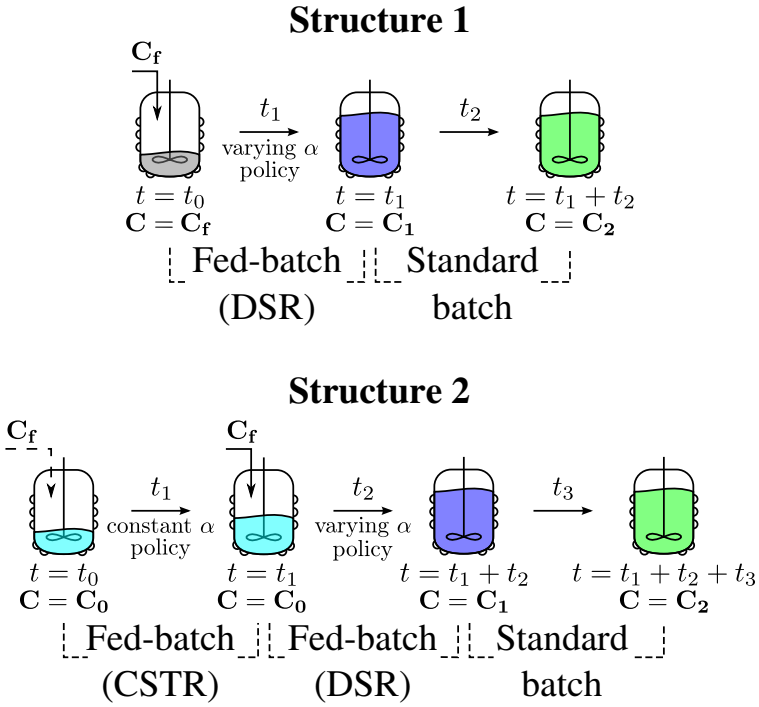
Again, as these structures are analogous to the original continuous equipment, both may be used to achieve point E. Unless one is interested in achieving concentrations along the unique PFR trajectory BC, reduced segments belonging to structures 1 and 2 such as those of AFG and DHI can be used. For concentrations occurring within the region however, combinations of these structures along with mixing between them may be used.

Effect of different objective functions

Now that the AR and its associated batch structures have been determined, optimisation for a number of scenarios may be investigated. Suppose that it is desired to achieve the maximum amount of intermediate component B. By the above discussion, both structures in Figure 5.4.10 pass through point E and therefore both may be used to achieve maximum B. Suppose, instead, that we wish to limit the formation of component D to a maximum value of 0.3 mol/L whilst still achieving maximum B. This point must lie on the intersection of the AR boundary and the plane described by $c_{\mathrm{D}} = 0.3\,\mathrm{mol/L}$; this is obtainable by structure 2 (given here by Figure 5.4.11). By comparison, assume that it is decided to find the maximum amount of B for $c_{\mathrm{D}} = 0.4\,\mathrm{mol/L}$ instead. We find that structure 1 is now required, and thus the nature of the batch cycle is different. Both of these scenarios however, are contained within the structure of the AR. The AR is composed of at most two unique structures, and as a result, *all* concentrations on the boundary may



(a) Optimal continuous structures. Structure 1 is given by a critical DSR to equilibrium (point B) followed by a PFR to point C. Structure 2 is given by a CSTR operating at the equilibrium concentration (point D), followed by a critical DSR to point B, and completed with a PFR. For both structures, the DSR side-stream composition is given by the feed point concentration.



(b) Optimal batch structures. The batch cycle for structure 1 begins with a varying α fed-batch initiated at the feed concentration and ends with a standard batch period. Structure 2 begins with a constant α fed-batch initiated at the CSTR equilibrium concentration given by point D, followed by a varying αpolicy corresponding to a critical DSR. This is terminated with a standard batch period. Similar to the continuous case, all side-stream compositions used for fed-batch operations are equal the feed point concentration.

Figure 5.4.10: Continuous (a) and batch (b) structure comparison for the van de Vusse system in $\mathbb{R}^3$.

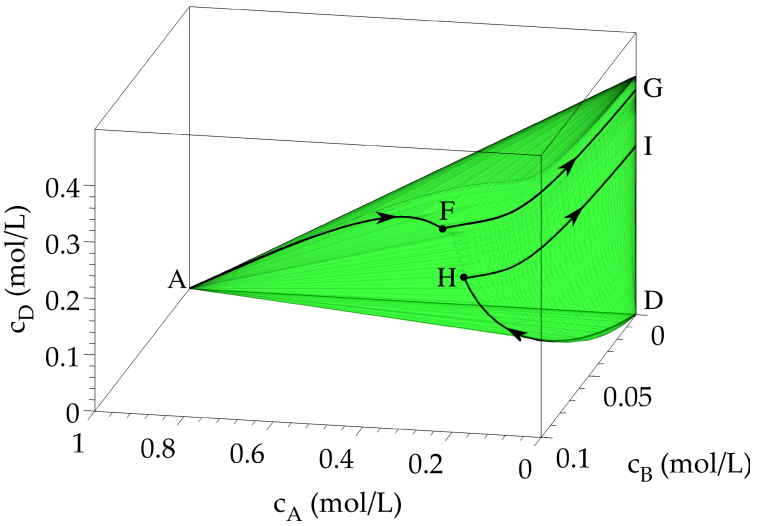
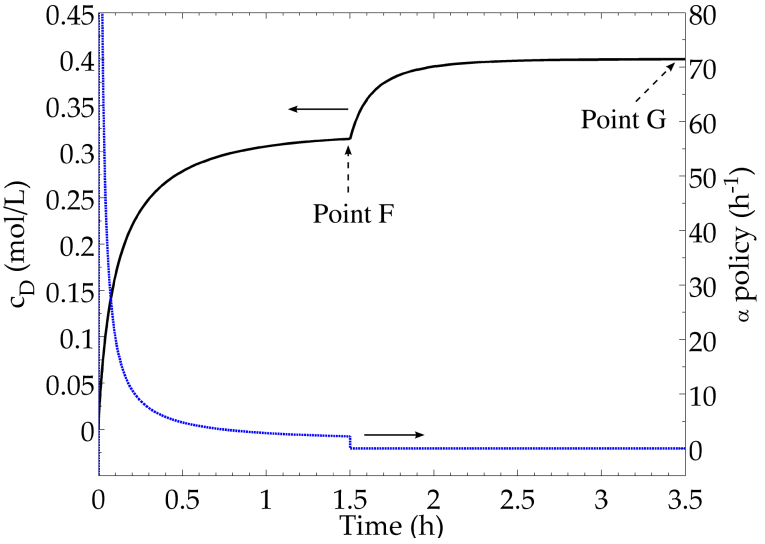


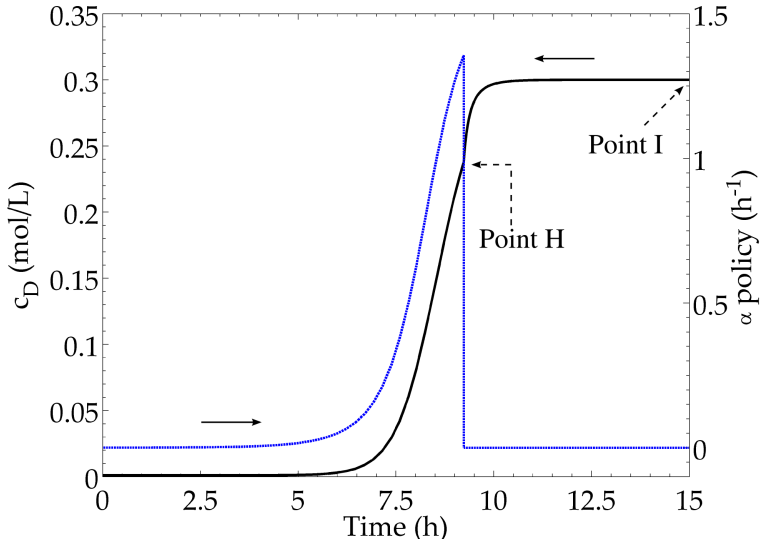
Figure 5.4.11: Example of the paths followed corresponding to two separate objective functions ($c_D = 0.3\,\text{mol/L}$ and $c_D = 0.4\,\text{mol/L}$). Path AFG corresponds to structure 1, whereas DHI corresponds to structure 2. In both cases, the structures result in a traversal on the AR boundary and not within the region. Points A and D are the same as those given in Figure 5.4.9b.

be achieved by these two structures alone together with mixing. The associated α policies and concentration profile of component D for a generalised single fed-batch configuration associated with structures 1 and 2 are given by Figures 5.4.12a and 5.4.12b respectively. For structure 1, the α policy begins with an exponential decline in side-stream addition to a time of approximately 1.536 h, followed by a period of standard batch reaction to termination. The total batch cycle time for this structure is thus 3.5 h. Theoretically, the correct α policy for this structure starts at a value of ∞, however this has been approximated by utilising a starting concentration that gives an initial value of $\alpha \sim 200\,\text{h}^{-1}$ ($\mathbf{C} = [0.9885, 0.0006, 0.0055]^{\text{T}}$). The recommended operating policy corresponding to structure 2 is slightly different when compared to that of structure 1, as it undergoes three reaction periods. The cycle begins with a fed-batch period of constant α in accordance with the equilibrium CSTR concentration given by point D. The cycle is then brought into a period of varying α, where the side-stream addition is observed to increase sharply to a maximum value of $\sim 1.356\,\text{h}^{-1}$, and then completed with a standard batch period lasting approximately 9.24 h; the total batch cycle time for this structure is thus roughly 15 h.

An observation on parallel structures should be made here with regards to the differences in operating requirements between batch and continuous equipment. If the reaction is to be performed in a continuous setting, two separate sets of equipment are required and must be run simultaneously. Compositions are then obtained by mixing the appropriate streams belonging to each structure in the appropriate



(a) α policy and associated concentration profile for structure 1 of the van de Vusse problem. The value of α decreases throughout this cycle. The size of α initially begins at a large value and drops rapidly until approximately 1.5 h (corresponding to point F). The side-stream feed is then terminated resulting in a standard batch period that ends at c_D = 0.4 mol/L.



(b) Concentration profile and α policy for structure 2 of the van de Vusse problem. For this structure, the value of α initially increases from zero to $\sim 1.3\,h^{-1}$ near a reaction time of 7.8 h (corresponding to point H). Beyond this point, the side-stream feed is again terminated resulting in a final concentration of 0.3 mol/L in component D.

Figure 5.4.12: The AR (a) and associated batch structures and α policies for two different outcomes. When it is desired to limit the amount of component D to 0.3 mol/L, structure 2 given by path DHI is used. If however, we require c_D = 0.4 mol/L, path AFG corresponding to structure 1 is employed instead.

Table 5.3: Comparison of values reported by Bikić et al. (2002) summarising the maximum c_B value achieved for the van de Vusse system by different authors.

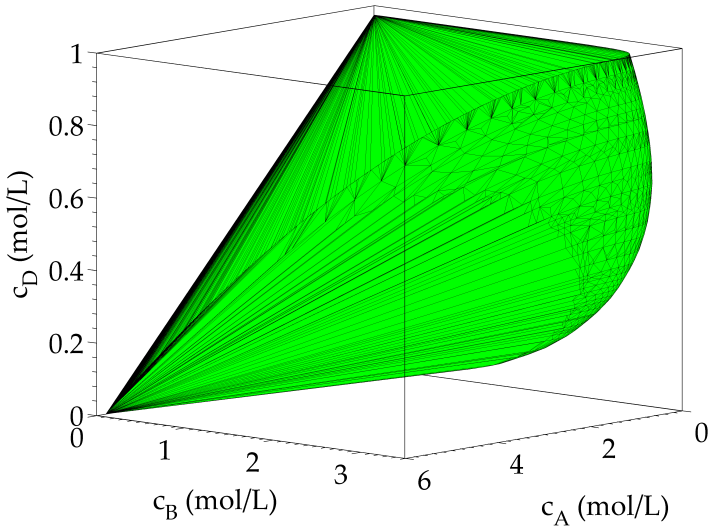
Author	c_B (mol/L)	Method
Kokossis and A. (1990)	3.6796	Optimisation of CSTR superstructure.
Chitra and Govind (1981)	3.67772	Local search for PFR, PFR with bypass and CSTR-PFR reactor structures.
Achenie and Biegler (1986)	3.6806	Gradient-based non-linear optimisation based on axial dispersion reactor (ADR).
Bikić et al. (2002)	3.6818	Analysis of optimality conditions based on PFR superstructure.
Present work	3.682	AR theory.

amounts. By comparison, if it is desired to perform the same task under batch conditions, an identical outcome may be achieved by two serial operations together with intermediate storage of material used in mixing processes. Hence, it may turn out that a single set of reactive equipment be required. Again, whereas in continuous systems one is concerned with the arrangement of equipment through space, in batch systems, one may also utilise time. The order of batch operations is important in developing an efficient reactive structure.

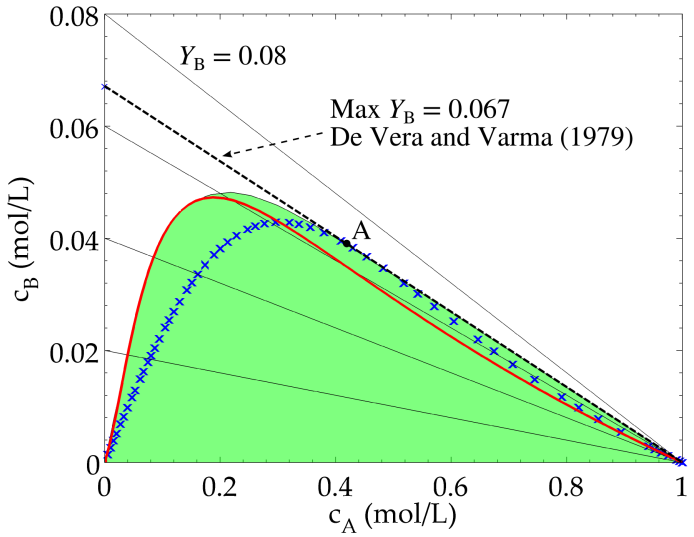
Comparison to literature

Maximum c_B The van de Vusse system has been studied extensively in the open literature and the nature of the system is hence well understood. However, many of the investigations have related to continuous reactor structures. Comparisons to batch structures are nevertheless still possible since the underlying conversions discussed in this work are founded on continuous structures. Bikić et al. (2002) provide a summary of the maximum concentration of B achieved from different investigations. These are shown in table 5.3 along with the results discussed here. Note that values reported in table 5.3 are for a feed point of $\mathbf{C_f} = [5.8,\ 0.0,\ 0.0]^{\mathrm{T}}$ and rate constants $k_1 = 10\,\mathrm{h}^{-1}$, $k_2 = 1\,\mathrm{h}^{-1}$, $k_3 = 1\,\mathrm{L}/\,(\mathrm{mol}\cdot\mathrm{h})$. Hence, the problem must be resolved for the new feed point and kinetics. The resulting region for the modified system is shown in Figure 5.4.13a. We note that even though shape of the resulting region is different to the original, the optimal rector structures remain unchanged. Hence the same transformations discussed earlier may be used to optimise equivalent batch structures.

The claimed values are all in close agreement. Notice that the values given by Bikić et al. (2002) are effectively identical to the maximum c_B value predicted by the AR within realistic numerical accuracy.



(a) AR for the 3D van de Vusse system corresponding to $\mathbf{C_f} = [5.8, 0.0, 0.0]^T$



(b) Relative yield contours for the van de Vusse system

Figure 5.4.13: ARs generated for the van de Vusse system compared to the open literature

Maximum relative yield Brooks (1990) investigated maximising the relative yield of B in a fed-batch reactor for different feed points and rate constants in the van de Vusse system. Here, the relative yield of B, Y_{B}, is defined as

$$Y_{\mathrm{B}} = c_{\mathrm{B}} / \left(c_{\mathrm{A}}^{0} - c_{\mathrm{A}}\right) \tag{5.4.4}$$

The author notes that when the ratio $(k_3/k_1)\, c_{\mathrm{A}}$ is greater than k_1/k_2, Y_{B} is larger in a constant feeding rate fed-batch compared to a standard batch. The author goes on to demonstrate the performance of the fed-batch over continuous equipment including a CSTR and PFR recycle reactor. Similar investigations for the van de Vusse system have also been carried out by Lee (1977) for a PFR with intermediate side-draw and De Vera and Varma (1979); Gillespie and Carberry (1966) for a PFR with recycle.

In Figure 5.4.13b, we plot a projection of the 3D AR onto $c_{\mathrm{A}} - c_{\mathrm{B}}$ space. The region shown in Figure 5.4.13b is obtained by generating the AR boundary for a feed point of $\mathbf{C_f} = [1,\, 0,\, 0]^{\mathrm{T}}$ and rate constants $k_1 = 1\,\mathrm{h}^{-1}$, $k_2 = 4\,\mathrm{h}^{-1}$ and $k_3 = 10\,\mathrm{L}/\left(\mathrm{mol}\cdot\mathrm{h}\right)$. This is done so that constructions are consistent with the investigations found in the literature. Since the relative yield expression in eq 5.4.4 is a function of c_{A} and c_{B}, it is possible to plot contours of relative yield for different values of Y_{B}. These are displayed as solid straight lines all passing through the feed point. Note that $Y_{\mathrm{B}} = c_{\mathrm{B}}$ when $c_{\mathrm{A}} = 0$. The values of Y_{B} for each contour is hence easily read off the graph by inspecting the point of intersection on the c_{B} axis.

Note that the point of maximum Y_{B} occurs at point A on the AR boundary in Figure 5.4.13b. Point A also corresponds to the critical CSTR point on the AR boundary. Hence, maximum relative yield is achieved in a constant α fed-batch (CSTR) operating at point. De Vera and Varma (1979) classifies $(k_3/k_1)\, c_{\mathrm{A}} - k_1/k_2$ space for the above system into four regions indicating the reactor structure that produces highest Y_{B} for each region. For the values of the rate constant specified here, a CSTR is optimal according to the authors. Thus, the recommendations generated by the AR construction agree with the suggestions by De Vera and Varma (1979).

5.4.3 Residence time example

As a final example, we would like to apply the transformation rules and apply them to problems involving residence time. As stated previously, constructions involving residence time are performed when it is desired to find the optimal reactor structure associated with smallest reactor volume. When viewed through this perspective, residence time demonstrates a similar mechanism to reaction time in batch. Therefore for an equivalent reactor volume V, flow rate Q, in the continuous setting is similar to production rate in the batch once multiplied by the concentration difference over

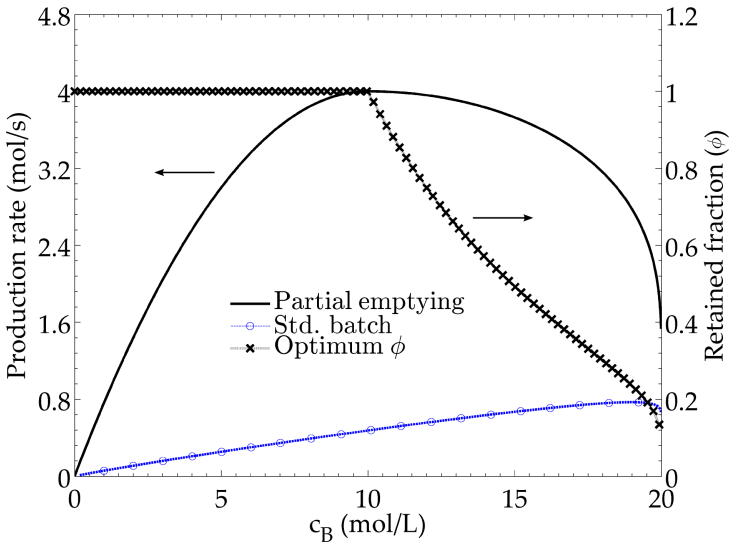


Figure 5.4.14: Production rate profile for the autocatalytic system given in chapter 3. Here, a 99% retained fraction has been employed rather than the recommended 50% given before. A maximum production rate of 4.0 mol/s is obtained at an optimal exit concentration of $c_B = 10.0$ mol/L.

the reactor.

$$Q = \frac{V}{\tau}$$

Before we begin, it would be helpful to refer back to the example problem given in chapter 3. There we posed the problem of improving the production rate for an autocatalytic system by retaining a fraction of product. A maximum retained fraction limit of 50% was enforced so that the number of emptying and filling operations could be handled to within a practical level. If however, we choose to relax this constraint, then it is possible to improve the production rate even further. Thus, when we allow for up to 99% of the reactor volume to be retained, the following profile in Figure 5.4.14 is obtained.

Although this presents a significant improvement to the production rate suggested before, however the practical implications of this approach are rather restrictive:

- To achieve the predicted 4.0 mol/s production rate, we must retain a very high fraction of product behind.
- The small fraction that does get removed must be replaced with an equally small feed volume.
- It follows that since the ratio of fresh feed to product volume will be small, reaction time is small (essentially instantaneous) and may be considered to occur due to mixing rather than reaction.
- Since reaction time is short, we must then immediately remove product and repeat the cycle once again.

In operating the reactor at such high retained volumes, it is not difficult to see that we, in essence, approximate the operation of a CSTR.

In order to investigate whether the optimal structure for maximum production might include a CSTR, we can reformulate the kinetics and view the problem in the form of a continuous AR construction in residence time space. This is performed in Figures 5.4.15b and 5.4.15a. Here, the rate vector is defined as follows

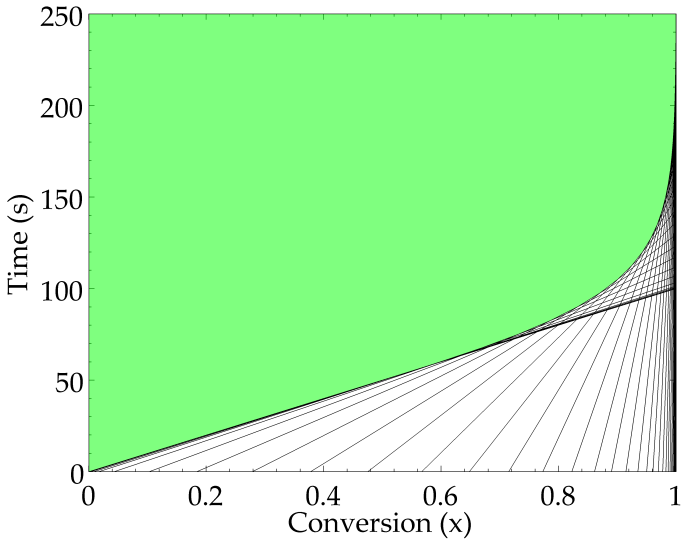
$$\mathbf{r}(\mathbf{C}) = \begin{bmatrix} k_1 c_{\mathrm{A}}^0 (1-x)\left(c_{\mathrm{B}}^0 + c_{\mathrm{A}}^0 x\right) \\ 1 \end{bmatrix}$$

We can thus view the problem stated in chapter 3 as a continuous 2D AR construction in x–τ space. In order to determine the absolute limits of achievability, regarded here in terms of minimum residence time, the AR for the associated kinetics is first generated. To obtain a better appreciation for the dynamics of the system, the AR has been generated again utilising the rotated bounding hyperplanes algorithm developed in chapter 4. Figure 5.4.15a thus shows the resulting output of the construction. We see that almost complete conversion is obtainable before a residence time of 200 s is reached. Moreover at an exit conversion of 50%, a residence time of 50 s is also achievable. In chapter 3, a 20 L reactor volume was used in the example to achieve the stated 4 mol/s production rate. For the same reactor volume and feed conditions used here, it is not difficult to show that a corresponding molar flow rate of 4 mol/s is also achieved in the continuous case. This is significant. It suggests that we are able to achieve similar performance in continuous and batch. It also suggests that the AR can be used as a method to improve batch production rate.

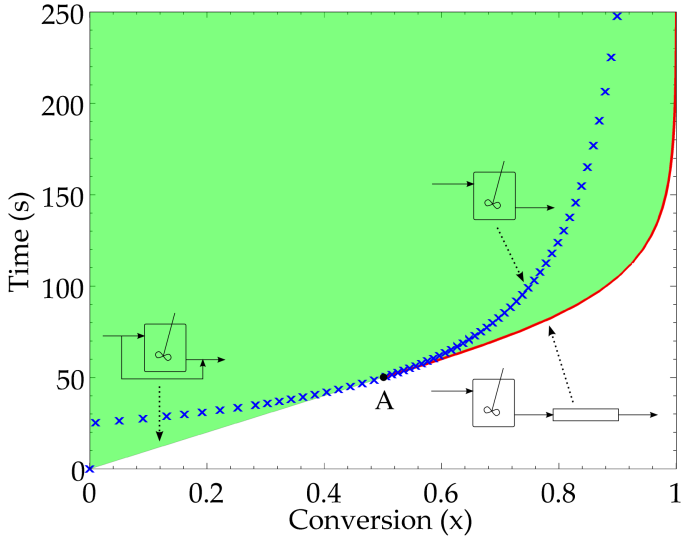
In Figure 5.4.15a, the corresponding optimal reactor structures have been overlaid on the AR. It is found that the optimal continuous structure is a CSTR followed by a PFR. This corresponds with the recommendations given in chapter 3 for the same kinetics – for exit conversions larger than 50%, the optimal structure is a CSTR followed by a PFR. Thus, the results of the AR construction appear promising. These suggest that it may also be possible to use the information gathered from continuous AR constructions in residence time space, and apply the transformations discussed in this chapter to improve problems involving batch production rate.

Batch conversion

We first approximate the behaviour of a CSTR in the usual manner: by first forming the desired CSTR effluent concentration, and then running a constant α fed-batch at the equilibrium feeding rate and feed concentration. For exit concentrations beyond this point, the side-stream may be terminated to convert the fed-batch to a standard batch. From the residence time plot, we can read off the optimal residence time directly from the graph. This corresponds to a residence time of $\tau = 50$ s. Using the equilibrium relation between DSRs and CSTRs, we calculate that $\alpha =$



(a) The resulting boundary obtained for the autocatalytic reaction given in chapter 3 using the rotated bounding hyperplanes algorithm developed in chapter 4. The results of the construction suggest that almost complete conversion is obtainable for residence times lower than 200 s.



(b) Corresponding AR in $c_B - \tau$ space (continuous reaction) for the autocatalytic reaction given in chapter 3. The optimal reactor structure for minimum residence time is a CSTR ($\times$) followed by a PFR ($-$). The CSTR exit conversion is 50% corresponding to a product concentration of $c_B = 10\,\text{mol/L}$. This concentration is associated with the optimal product exit concentration for maximum production rate in the batch example. The straight line connecting the feed point to the CSTR is a mixing line.

Figure 5.4.15: AR for the autocatalytic reaction given in chapter 3

$1/50\,\mathrm{s}^{-1}$, and thus a F/V ratio of $0.02\,\mathrm{s}^{-1}$ is required for the CSTR portion of the structure. For this example, the production rate is 4 mol/s. At an optimal exit concentration of 10 mol/L, and for a 20 L reactor volume, this indicates that a side-stream flow rate of F = 0.4 L/s is required. In this arrangement, there is no need to perform partial emptying and filling. The retention of product is fulfilled by the operation of an equivalent constant α fed-batch to keep the batch at the desired CSTR concentration.

In a similar fashion as to how we approached the problem previously, it is possible to classify our structure into three sub-categories depending on the required exit conversion: exit conversions less than 50%, exit conversion equal to 50%, end exit conversion greater than 50%. We shall discuss each of these separately below.

Production rate for $x < 50\%$:

For exit conversions less than 50% ($c_\mathrm{B} = 10.0\,\mathrm{mol/L}$), the optimal structure corresponding to smallest residence time is a CSTR with bypass of feed. Similar to chapter 3, we can achieve the maximum production rate by running a smaller reactor for a longer period past the desired exit conversion at the optimal exit conversion of 50%. This arrangement ensures that maximum production rate is achieved in the batch. It is then possible to bypass the remaining feed material directly to the product tank and mix to the desired exit conversion. The optimal batch cycle thus involves a bypass of feed material. The maximum production rate of 4 mol/s is achievable for all conversions less than 50%. Figure 5.4.16a provides a comparison between the optimal continuous and batch structures.

Production rate for $x = 50\%$:

For exit conversions equal to the optimal, maximum production rate is achieved by a CSTR alone and no bypass is required. Figure 5.4.16b shows the conversion from a continuous structure to the equivalent batch cycle. Thus, at the filling rate and reactor volume specified above, it is known that a cycle time of 50 s is achieved at 50% conversion. Alternatively, we could also consult the continuous plot provided in Figure 5.4.15b and read off the equivalent residence time for the CSTR at 50% conversion. The production rate is maximised at this point. This corresponds with the suggested production rate given in chapter 3 using partial emptying end filling with a 99% retained fraction.

Production rate for $x > 50\%$:

For desired conversions greater than 50%, the full AR structure is needed. That is, a CSTR (constant α fed-batch) to 50% followed by a PFR (standard batch). Again, note that this is similar in nature to the recommendation for exit concentrations great than the optimal in chapter 3., where the reaction was split into two reaction

steps. Instead of requiring multiple first stage reactors however, the structure can be simplified by substitution with a fed-batch reactor. Again, there is no requirement to perform partial emptying and filling, as we can convert AR structures to batch using fed-batch reactors.

It follows that in order to carry out the reaction in the shortest time, we repeat the same procedure for $x = 50\%$ and augment the cycle with a period of standard batch reaction. In practice, this may be achieved by continuing the reaction once the vessel has been filled by simply stopping additional fed-batch feed flow. Thus, we begin with a filling stage corresponding to the CSTR portion of the structure for 50s, and then terminate the side stream feeding policy ($\alpha = 0$) to simulate the PFR trajectory corresponding to the AR boundary. The duration of the standard batch will then be dependent on the exit conversion desired by the designer. Again, it is also possible to reference the AR in Figure 5.4.15b read off the required conversion and corresponding residence time. Knowledge of the reactor volume and final product concentration then allows for easy calculation of the production rate.

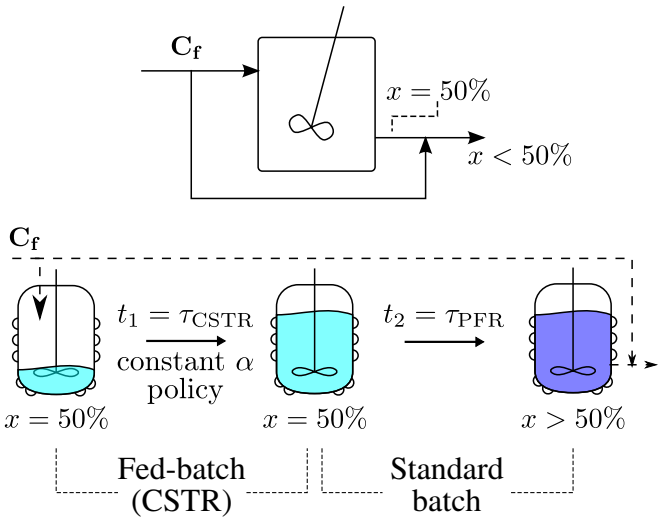
5.5 Conclusions

An important goal of this chapter has been towards developing a method for converting optimal continuous structures, obtained via conventional AR analysis, to an equivalent batch structure. Due to the one-to-one nature between continuous and batch reactor equations, it is a fairly simple task to convert continuous structures to batch. Indeed, it is possible to derive an equivalent batch structure by first computing the AR in the continuous setting, and then applying the necessary transformations to batch.

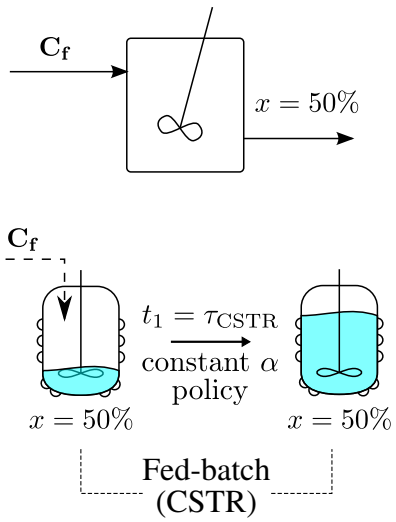
Previous work (Feinberg, 2000b) has demonstrated that three unique reactor types are needed to construct the AR, these are the PFR, DSR and CSTR. The transformations to batch for these types are as follows:

- Standard batch reactors replace PFRs. It is already well understood that standard batch reactors have identical performance to PFRs, and so they may be used in place of them in batch processes. Reaction time then replaces residence time of the PFR.

- Fed-batch reactors may be operated to function as both a DSR or CSTR depending on the α policy chosen. The variable α in this case, is the ratio of F/V, and if an expression for the α policy exists, then both the side-stream feed rate and reactor volume may be determined. Thus, if the fed-batch is operated with a varying α policy, DSR performance is obtained. If, instead, a constant α policy is employed, then CSTR behaviour is possible, although, only under the correct operating conditions.

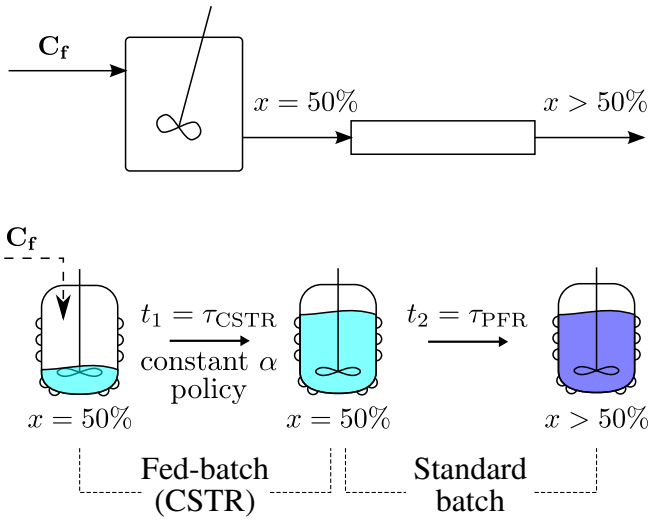


(a) Optimal structures for exit concentrations less than 50%. Maximum production rate is achievable for all conversions lower than 50%.



(b) Optimal structures for exit concentrations equal to 50%.

Figure 5.4.16: Optimal continuous and batch structures for an unbounded batch system



(c) Optimal structures for exit concentrations greater than 50%. In this instance, maximum production rate is not achieved, though this arrangement is still the optimal for smallest residence time and hence optimal for best production rate.

Figure 5.4.16: Optimal continuous and batch structures for an unbounded batch system

For each value of α, there exists an associated equilibrium concentration that must be used. Possibly many equilibrium points may be obtained for kinetics involving multiple steady states. This is related to the equivalence found between CSTRs and constant α DSRs operating at equilibrium. Constant α fed-batch reactors thus mimic CSTRs at the equilibrium point. This results in interesting operational consequences:

1. Fed-batch reactors must be initiated and operated at a concentration equal to that of the equivalent CSTR effluent composition. The concentration of species within the fed-batch is constant during this period of reaction as a result. Reaction time is also determined by the filling rate and vessel volume.

2. Various methods may be used to achieve the initial CSTR composition, although these methods may be ineffective in obtaining the desired CSTR composition if the corresponding DSR equilibrium point is unstable. In practice, if the desired CSTR point unstable, one may wish to introduce a stabilising controller to realise the desired state.

Thus, care must be taken when choosing an initial concentration for the fed-batch for converting structures containing CSTRs to an equivalent batch. It is generally not sufficient to choose an initial concentration in an arbitrary manner in the hope to reach a desired CSTR concentration. The dynamic behaviour of the system, in the form of multiple steady states and instability, may not allow one to do so. Furthermore, it might not be possible to achieve the desired CSTR concentration

if the associated equilibrium point corresponding to eq 5.3.3 proves to be unstable . At the time of writing, we have yet to encounter systems in which the desired equilibrium point belonging to a critical CSTR is also unstable, however the possibility should not be overlooked. Such a situation could prove to be troublesome for both continuous and batch structures, as both the CSTR and fed-batch may not be controllable without further work to stabilise the state. Otherwise, one would then need to work within a constrained region of the full AR utilising points that are known to be stable.

We also investigated the use of ARs constructed in residence time space as a means of improving the production rate in a batch reactor. It was observed that residence time provides a similar metric to batch reaction time. Thus, there exists a relation between the reactor volume and flow rate in a continuous setting, to an equivalent volume and production rate in a batch. However, although it is possible to mix residence time, it is not possible to achieve the same in the batch equivalent. This investigation was performed on the same worked example provided in chapter 3. We noticed that unlike the recommendations given in chapter 3, we do not need to employ a partial emptying and filling strategy to achieve maximum performance. Instead, the approach used here is to relate the optimal reactor structure associated with smallest residence time to an equivalent batch operating policy using the transformations provided in this chapter. In place of a partial emptying and filling stage followed by a standard batch, we employ a constant α fed-batch followed by a standard batch. The production rate achieved by this approach corresponds to the same volumetric flow rate in the continuous case, and so the method is consistent. It follows that AR constructions involving more than one independent reaction might also be used to improve a batch with the same kinetics and feed composition, however this has not been tested in this work.

Although the work given in chapter 3 appears to be subsumed by that given here, we note that the two methods apply to different design scenarios: The former may be employed in the absence of a kinetic model, when only experimental data are available, whereas the the latter relies on AR theory, which in turn relies on specification of a well defined rate field and feed point in order to generate the AR. It is difficult to generate a candidate region using only the results of chapter 3, even if these ideas are founded on principles in AR theory. Nevertheless, if kinetics is supplied, with the intention of improving batch production rates, then the ideas presented here are more easily generalised for many independent reactions.

Finally, although many similarities between batch equipment in time and continuous equipment in space exist, a number of differences are also noted.

1. It may be possible to achieve all concentrations belonging to the AR by a single reaction vessel in batch systems, whereas for continuous equipment, a physically separate set of reactors is required for each branch of the recom-

mended AR structure. By the same reasoning, one should also be mindful of the order that batch operations are carried out, as different batch operating policies may be required for different points desired in or on the AR boundary.

2. If a single batch reactor is employed, one may be constrained if bypass mixing with a stream downstream concentration at a future time is employed. Continuous equipment for a spatial reactor network are superior in this regard. This may also be overcome in a batch if intermediate storage is utilised for mixing with subsequent reaction stages in future cycles.

3. From general AR theory it is known that DSRs are not required for *continuous* systems involving two independent reactions. The familiar VdelR condition of chapter 2 is a consequence of this. However, since CSTRs are approximated in a batch environment by use of constant α fed-batch rectors, which are analogous to DSRs in the continuous setting, DSRs are generally still required in batch unless the optimal reactor structure for the associated 2D system is a convex PFR. Note that these fed-batch trajectories do not fulfill the same function as critical DSR trajectories, but rather they approximate CSTR concentrations. Besides critical CSTR points, these fed-batch trajectories operate inside the AR. Hence, if a particular optimisation scenario is employed in which the objective function intersects the CSTR locus at a point other than the critical CSTR point, then this may be awkward to realise with fed-batch reactors.

The above discussion suggests that improvement in batch reactors is possible by a geometric approach. Interpretation of the problem first as a continuous system allows for the determination of the AR, which provides insight into the limits of achievability for all reactor structures. This, in turn, guides the choice of reactor structure employed. Consideration of the AR thus offers a different method of potential improvement in batch reactors. The AR and its corresponding structures therefore serve the dual purpose of establishing a set of recommended reactor configurations that may be used to improve both batch and continuous equipment from a single configuration.

References

Abraham, T. K., Feinberg, M., 2004. Kinetic bounds on attainability in the reactor synthesis problem. Industrial & Engineering Chemistry Research 43 (2), 449–457.

Achenie, L. E., Biegler, L. T., 1986. Algorithmic synthesis of chemical reactor networks using mathematical programming. Industrial and Engineering Chemistry Fundamentals 25 (4), 621–627.

Allgor, R. J., Barrera, M. D., Barton, P. I., Evans, L. B., 1996. Optimal batch process development. Computers & Chemical Engineering 20 (6-7), 885–896.

Allgor, R. J., Barton, P. I., 9 1999. Screening models for batch process development: Part ii. case studies. Chemical Engineering Science 54 (18), 4065–4087.

Allgor, R. J., Evans, L. B., Barton, P. I., 10 1999. Screening models for batch process development: Part i. design targets for reaction/distillation networks. Chemical Engineering Science 54 (19), 4145–4164.

Aziz, N., Mujtaba, I. M., 1 2002. Optimal operation policies in batch reactors. Chemical Engineering Journal 85 (2-3), 313–325.

Balakotaiah, V., Luss, D., 1982. Exact steady-state multiplicity criteria for two consecutive or parallel reactions in lumped-parameter systems. Chemical Engineering Science 37 (3), 433–445.

Balakotaiah, V., Luss, D., 1983. Multiplicity features of reacting systems: dependence of the steady-states of a cstr on the residence time. Chemical Engineering Science 38 (10), 1709–1721.

Balakotaiah, V., Luss, D., 1984. Global analysis of the multiplicity features of multi-reaction lumped-parameter systems. Chemical Engineering Science 39 (5), 865–881.

Bikić, D., Butinar, B., Glavič, P., 2002. Optimal reactor systems for van de vusse reaction scheme with multicomponent feed. Computers & Chemical Engineering 26 (10), 1335–1343.

Bonvin, D., 1998. Optimal operation of batch reactors - a personal view. Journal of Process Control 8 (5-6), 355–368.

Brooks, B. W., 1988. Semi-batch reactors and their use for autocatalytic reactions. Chemical Engineering Science 43 (6), 1287–1290.

Brooks, B. W., 1990. Product yields from the van de vusse reaction scheme: use of semi-batch reactors. Chemical Engineering Science 45 (6), 1589–1594.

Burri, J. F., Wilson, S. D., Manousiouthakis, V. I., 2002. Infinite dimensional state-space approach to reactor network synthesis: Application to attainable region construction. Computers & Chemical Engineering 26 (6), 849–862.

Capon-Garcia, E., Bojarski, A. D., Espuna, A., Puigjaner, L., 2011. Multiobjective optimization of multiproduct batch plants scheduling under environmental and economic concerns. AIChE Journal 57 (10), 2766–2782.

Cheong, D.-Y., Hansen, C. L., Stevens, D. K., 2007. Production of bio-hydrogen by mesophilic anaerobic fermentation in an acid-phase sequencing batch reactor. Biotechnology and bioengineering 96 (3), 421–432.

Chitra, S. P., Govind, R., 1981. Yield optimization for complex reactor systems. Chemical Engineering Science 36 (7), 1219–1225.

Davies, W. L., Gloor, W. T., 1971. Batch production of pharmaceutical granulations in a fluidized bed i: Effects of process variables on physical properties of final granulation. Journal of pharmaceutical sciences 60 (12), 1869–1874.

Davis, B. J., Taylor, L. A., Manousiouthakis, V. I., 2008. Identification of the at-

tainable region for batch reactor networks. Industrial & Engineering Chemistry Research 47 (10), 3388–3400.

De Vera, A. L., Varma, A., 1979. Yield optimization for the van de vusse reaction. The Chemical Engineering Journal 17 (2), 163–167.

Feinberg, M., 1999. Recent results in optimal reactor synthesis via attainable region theory. Chemical Engineering Science 54 (13-14), 2535–2543.

Feinberg, M., 2000a. Optimal reactor design from a geometric viewpoint - iii. critical cfstrs. Chemical Engineering Science 55 (17), 3553–3565.

Feinberg, M., 2000b. Optimal reactor design from a geometric viewpoint. part ii. critical sidestream reactors. Chemical Engineering Science 55 (13), 2455–2479.

Feinberg, M., Hildebrandt, D., 1997. Optimal reactor design from a geometric viewpoint- i. universal properties of the attainable region. Chemical Engineering Science 52 (10), 1637–1665.

Gillespie, B., Carberry, J., 1966. Reactor yield at intermediate mixing levels–an extension of van de vusse's analysis. Chemical Engineering Science 21 (5), 472–475.

Glasser, D., Hildebrandt, D., 1997. Reactor and process synthesis. Computers & Chemical Engineering 21 (Supplement 1), S775–S783.

Glasser, D., Hildebrandt, D., Crowe, C., 1987. A geometric approach to steady flow reactors: The attainable region and optimization in concentration space. Industrial & Engineering Chemistry Research 26 (9), 1803–1810.

Godorr, S., Hildebrandt, D., Glasser, D., McGregor, C., 1999. Choosing optimal control policies using the attainable region approach. Industrial & Engineering Chemistry Research 38 (3), 639–651.

Godorr, S. A., Hildebrandt, D., Glasser, D., 1994. The attainable region for systems with mixing and multiple-rate processes: finding optimal reactor structures. The Chemical Engineering Journal and The Biochemical Engineering Journal 54 (3), 175–186.

Gray, P., Scott, S. K., 1983. Autocatalytic reactions in the isothermal, continuous stirred tank reactor : Isolas and other forms of multistability. Chemical Engineering Science 38 (1), 29–43.

Gray, P., Scott, S. K., 1984. Autocatalytic reactions in the isothermal, continuous stirred tank reactor : Oscillations and instabilities in the system a + 2b -> 3b; b -> c. Chemical Engineering Science 39 (6), 1087–1097.

Hansen, J. M., Lim, H. C., Hong, J., 1993. Optimization of autocatalytic reactions. Chemical Engineering Science 48 (13), 2375–2390.

Hildebrandt, D., Glasser, D., 1990. The attainable region and optimal reactor structures. Chemical Engineering Science 45 (8), 2161–2168.

Hildebrandt, D., Glasser, D., Crowe, C. M., 1990. Geometry of the attainable region generated by reaction and mixing: With and without constraints. Industrial & Engineering Chemistry Research 29 (1), 49–58.

Kauchali, S., Rooney, W. C., Biegler, L. T., Glasser, D., Hildebrandt, D., 2002. Linear programming formulations for attainable region analysis. Chemical Engineering Science 57 (11), 2015–2028.

Khumalo, N., Glasser, D., Hildebrandt, D., Hausberger, B., Kauchali, S., 2006. The application of the attainable region analysis to comminution. Chemical Engineering Science 61 (18), 5969–5980.

Kokossis, A. C., A., F. C., 1990. Optimization of complex reactor networks - i. isothermal operation. Chemical Engineering Science 45 (3), 595–614.

Kondepudi, D. K., Asakura, K., 2001. Chiral autocatalysis, spontaneous symmetry breaking, and stochastic behavior. Accounts of chemical research 34 (12), 946–954.

Lee, H. H., 1977. Tubular reactor with recycle from an intermediate point: yield of van de vusse's reactions. Chemical Engineering Science 32 (5), 562–563.

Maestri, F., Rota, R., 2007. Safe and productive operation of homogeneous semibatch reactors involving autocatalytic reactions with arbitrary reaction order. Industrial & Engineering Chemistry Research 46 (16), 5333–5339.

Manousiouthakis, V. I., Justanieah, A. M., Taylor, L. A., 2004. The shrink-wrap algorithm for the construction of the attainable region: An application of the ideas framework. Computers & Chemical Engineering 28 (9), 1563–1575.

Mendez, C. A., Cerda, J., Grossmann, I. E., Harjunkoski, I., Fahl, M., 2006. State-of-the-art review of optimization methods for short-term scheduling of batch processes. Computers & Chemical Engineering 30 (6-7), 913–946.

Ming, D., Hildebrandt, D., Glasser, D., 2010. A revised method of attainable region construction utilizing rotated bounding hyperplanes. Industrial & Engineering Chemistry Research 49 (21), 10549–10557.

Modak, J. M., Lim, H. C., 1992. Optimal mode of operation of bioreactor for fermentation processes. Chemical Engineering Science 47 (15-16), 3869–3884.

Najafpour, G., Younesi, H., Ismail, K. S. K., 2004. Ethanol fermentation in an immobilized cell reactor using saccharomyces cerevisiae. Bioresource technology 92 (3), 251–260.

Nicol, W., Hernier, M., Hildebrant, D., Glasser, D., 2001. The attainable region and process synthesis: Reaction systems with external cooling and heating. the effect of relative cost of reactor volume to heat exchange area on the optimal process layout. Chemical Engineering Science 56 (1), 173–191.

Nicol, W., Hildebrandt, D., Glasser, D., 1997. Process synthesis for reaction systems with cooling via finding the attainable region. Computers & Chemical Engineering 21 (Supplement 1), S35–S40.

Nisoli, A., Malone, M. F., Doherty, M. F., 1997. Attainable regions for reaction with separation. AIChE Journal 43 (2), 374–386.

Putot, A., Gallice, F., Hoff, C., Guillot, V., 2002. Thermal stability of an oligosaccharide: Autocatalytic behavior. Organic process research & development 6 (6), 901–905.

Rooney, W. C., Hausberger, B. P., Biegler, L. T., Glasser, D., 2000. Convex attainable region projections for reactor network synthesis. Computers & Chemical Engineering 24 (2-7), 225–229.

Schlosser, P. M., Feinberg, M., 1994. A theory of multiple steady states in isothermal homogeneous cfstrs with many reactions. Chemical Engineering Science 49 (11), 1749–1767.

Senthuran, A., Senthuran, V., Mattiasson, B., Kaul, R., 1997. Lactic acid fermentation in a recycle batch reactor using immobilized lactobacillus casei. Biotechnology and bioengineering 55 (6), 841–853.

Seodigeng, T., Hausberger, B., Hildebrandt, D., Glasser, D., 2009. Recursive constant control policy algorithm for attainable regions analysis. Computers & Chemical Engineering 33 (1), 309–320.

Strogatz, S. H., 2001. Nonlinear Dynamics And Chaos: With Applications To Physics, Biology, Chemistry, And Engineering. Westview Press, Ch. 5.

Subotic, B., 1989. Influence of autocatalytic nucleation on zeolite crystallization processes. In: ACS symposium series. Vol. 398. pp. 110–123.

Watzky, M. A., Morris, A. M., Ross, E. D., Finke, R. G., 2008. Fitting yeast and mammalian prion aggregation kinetic data with the finke- watzky two-step model of nucleation and autocatalytic growth. Biochemistry 47 (40), 10790–10800.

Woolard, C. R., Irvine, R. L., 1995. Treatment of hypersaline wastewater in the sequencing batch reactor. Water research 29 (4), 1159–1168.

Xu, Y., Chen, Q., Zhao, Y.-j., Lv, J., Li, Z.-h., Ma, X.-b., 2014. Autocatalytic kinetic study of dimethyl oxalate consecutive hydrolysis. Industrial & Engineering Chemistry Research 53 (11), 4207–4214.

Zeman, R. J., Amundson, N. R., 1965. Continuous polymerization models - part ii: Batch reactor polymerization. Chemical Engineering Science 20 (7), 637–664.

Zhou, W., Manousiouthakis, V. I., 2006. Non-ideal reactor network synthesis through ideas: Attainable region construction. Chemical Engineering Science 61 (21), 6936–6945.

Zwiener, C. Z., Seeger, S. S., Glauner, T. G., Frimmel, F. F., 2002. Metabolites from the biodegradation of pharmaceutical residues of ibuprofen in biofilm reactors and batch experiments. Analytical and Bioanalytical Chemistry 372 (4), 569–575.

Chapter 6

Conclusions and future research

6.1 Conclusions

Chapter 1

In chapter 1, a brief overview of chemical reactor optimisation was given, and used to provide some insight into the current landscape of reactor network optimisation. We discussed the general approach to chemical reactor design, and argued that the development of newer, more appropriate, optimisation methods may lead to better insights and ultimately improved performance in these systems. Traditional optimisation is well understood and documented, however, these methods are generalised and may not always be well suited for chemical reactor design. This is particularly evident when one surveys the current scientific literature for work performed involving multiple reactors and reactor network synthesis. The issue of mixing, in particular, allows for discontinuous jumps in space that may present difficulties for traditional optimisation methods. These approaches often rely on continuity arguments and derivative information from calculus.

Lately, emphasis has been directed towards more generalised non-linear programming methods that may be better suited for these kinds of problems. Even while these methods can be used to overcome many of the drawbacks inherent in older techniques, the model approach to improvement is still brought about in the same way as conventional optimisation. The quality of the optimisation is still often limited by the flexibility of the process model, and the appropriate choice of an initial guess still remains an important consideration. It is, however, often difficult to know before hand what points might be useful to solve the model. Thus, similar issues might still arise. The former could be addressed if a better understanding of optimal reactor structures is known, whereas the latter could be addressed if limits of achievability could be found – it is not uncommon to find methods that rely on a reactor superstructure that is sufficiently generalised enough to account for the entire behaviour of the kinetics. The reasons for choosing and designing certain

superstructures may be influenced more out of practicality rather than through a better understanding of optimal reactor structures. It follows that there is a need to discover new ways and new interpretations of these systems, in order to solve these problems better.

The AR is one type of approach to this class of problems. Unlike many of the current methods, AR theory is geometric in nature. The method has demonstrated to be a novel way of solving reactor network problems, however this has usually been in the way of simple isothermal continuous reactor problems. AR theory is therefore still rather new and further advances (both in terms of theoretical and computational aspects) must be made before wide-spread use of the method can take place. There is currently a low level of adoption of AR ideas in current reactor synthesis problems and optimisation toolkits.

In this work, we work on two issues that may be the cause of the low adoption of AR theory in practice:

1. The first is AR construction. Determining the AR is difficult. The AR is a convex polytope usually found for higher dimensional problems and complex kinetics, and thus is it difficult to both visualise and compute these regions accurately and efficiently. A large portion of recent AR research has moved away from traditional theory and directed towards the development of AR construction algorithms. Current methods either produce inaccurate results, or are computationally intensive however, and there is a need for further research in this field.

2. A second factor is the use of AR to a wider class of problems. In particular, problems in batch reactors. The AR has historically been formulated for use in continuous processes, although increasing emphasis towards biochemical and specialist applications has meant that batch reaction has played a larger role in modern process engineering. Unfortunately, this has meant that the benefits and insight into optimal reactor structure, provided by AR theory, were not carried over to batch.

It is the aim of this work to tackle these two issues in Attainable Region theory.

Chapter 2

In chapter 2, we discussed the basic methodology of the Attainable Region approach and its use as an alternate method to solving reactor network synthesis problems. An overview was provided to help explain three fundamental reactor types and their role in forming the boundary of the AR. The AR boundary is essentially the most important aspect of AR theory, and knowledge of its complete structure and how it is constructed are of great importance to us.

Factors influencing boundary construction, and the difficulties associated with current AR construction methods, were also given brief mention. Current methods of construction may not always establish both the boundary and the associated optimal reactor structure however. Nevertheless, knowledge of the AR boundary without the reactor structures used to form it is still valuable in itself, as it still allows for the limits of achievability to be determined on the system. This provides a benchmark with which current designs can be compared to.

The graphical interpretation of mixing, and its application to AR theory was also discussed. Mixing plays two useful roles. Firstly, it allows for the connection of two separate, yet achievable, points in state space. In this way, mixing permits the formation of a convex region from a set of distinct states. Secondly, mixing allows for the attainment of new states when concavities (non-linearities) are present in the system. The attainment of these new states renders starting points from which new, potentially improved structures, can be initiated from. In this sense, mixing should be viewed as an avenue for improving performance.

Chapter 3

Chapter 3 followed on from the ideas established in chapter 2 (using mixing to improve the performance of the system), and presented a graphical method of improving the production rate in a batch reactor. We find that advancements can be made when there is a concavity in the concentration profile. This suggests that, at the end of a batch cycle, it is potentially beneficial to retain product to seed subsequent cycles rather than emptying out the full product volume and starting afresh. When carried out in this manner, product volume is smaller for each cycle, but cycle time may be significantly shorter thus offsetting the loss in volume produced. The overall effect is a modified batch procedure with a average higher production rate compared to the standard batch.

This method is entirely graphical and only relies on points generated in concentration – time space. In order to carry out computations, line segments are drawn between the initial and final states in the reactor. Depending on the starting and terminating points chosen, recommendations regarding the optimal retained fraction of product can also be deduced. All of these recommendations can be summarised on a single plot of production rate and retained fraction versus desired exit concentration for the species of interest.

The strength of the approach lies in its simplicity. There is no dependence on any other data besides that provided in the batch profile. This makes it a suitable option for when practitioners are not experienced in advanced optimisation techniques but would still like to benefit from improved production performance. Moreover, the technique could also be utilised as a short-cut method of enhancement before a more sophisticated model has been formulated. This approach allows for the method to

be used even on experimental data when no model is present, or when one has not yet been developed.

In this chapter, mixing was also employed to improve production rate for situations where the desired exit concentration is different to the one associated with the optimal. For exit concentrations less dilute than the optimal concentration, maximum production rate can be achieved by running a smaller volume to the optimal concentration, and then bypassing feed to the final product tank. For exit concentrations greater than the optimal, improvements can be obtained by splitting the reaction into two steps. The first is a reaction up to the optimal concentration in a staggered configuration with an identical reactor, followed by a period of standard batch operation.

Chapter 4

Chapter 4 introduced a modified outside-in method of AR construction. This work is founded on the idea that the AR can be enclosed within a larger region containing both achievable and unachievable states. Unattainable portions are then removed from the space. It follows that the remaining region must be the AR if elimination is performed perfectly. Enclosing the AR is done using stoichiometric constraints. Due to mass balance requirements, all compositions from reactors compatible with the feed must reside in this space. Elimination of unattainable regions is then achieved by the introduction of hyperplanes that serve to trim away portions of unachievable space. The check for achievable compositions is based on a tangency condition with the hyperplane. This condition is easily implemented although it is used extensively in the method and thus contributes to a significant portion to the overall computational workload. Elimination of additional space is carried out by the introduction of more hyperplanes. Thus, the approximation of curvature and the accuracy of constructions can be made arbitrarily close with a sufficiently large number of hyperplanes. This method is particularly effective in defining regions that originate from complicated kinetics.

In the original method, addition hyperplanes are are introduced at the vertices of the current polytope. The hyperplane orientation is determined by an average of the hyperplanes that make up the vertex, and elimination is carried out by moving the hyperplane into the region with a fixed orientation. Computation of the number and position of these vertices is carried out by a separate procedure for enumerating the feasible intersections of hyperplanes that describe the region. This process is termed vertex enumeration. Vertex enumeration adds an additional cost to the overall computational requirement of the AR. This, in turn, makes the resulting algorithm fairly slow when compared to competing methods.

In the revised approach, vertex enumeration is eliminated by using hyperplanes that are allowed to swivel/rotate around the vertices of the current polytope. Elim-

ination is then carried out by a continual adjustment of the hyperplane orientation at a fixed position in space. This is in contrast to the original method that uses a varying position and a fixed orientation to carry out elimination. The costly step of vertex enumeration can be skipped resulting in a quicker method of AR construction using bounding hyperplanes.

The method was shown to be superior in three areas when compared to the original approach:

1. Speed. Constructions for example kinetics were typically twice as fast compared to the original.

2. Accuracy. Constructions appear to define curvature better for the same number of hyperplanes. Due to faster construction times, a larger number of hyperplanes can be used to define the region, giving a tighter bound on the AR.

3. Support for more AR construction types. The revised method has been modified to handle kinetics involving a control parameter, such as temperature, so that more constructions can be performed with this method. Since eliminations are conducted via rotations, there is no dependence on using closed polytopes. The method is therefore suitable for unbounded constructions in residence time space.

The revised method using rotations therefore demonstrates useful improvements over the original. Currently, the algorithm handles 2D constructions, though adaptation to higher dimensional constructions were also discussed in the chapter. The method also does not provide the optimal reactor structure. This is a common trait associated with outside-in methods.

With this in mind, these constructions still offer great insight into discovery of the true AR. Multiple steady states introduce significant challenges for inside-out methods, as these often rely on a check for the necessary conditions of the AR. Candidate regions constructed with these methods may still preserve the necessary conditions, even if only a certain branch of the set of multiple steady states are found. Construction from the compliment region (outside-in methods) thus offers a new method to check whether inside-out constructions give the true AR:

- If the regions from both methods match, then we have found the true AR. Subject to the construction algorithm employed, we may also have the optimal structure.

- If the regions do not match, then we know that there are potentially additional structures missing from the boundary. Further investigation is then required.

Thus, use of this method paired with an inside-out method may allow for the development of new 'hybrid' methods (algorithms involving both addition and elimination

of regions). These may be the best option for truly robust AR construction methods in the future.

Chapter 5

Chapter 5 discussed the idea of directly applying the AR to batch reactor structures and sequencing. This is done by converting individual reactor structures to an equivalent batch operating arrangement. Conversion is feasible due to the generalised properties of fed-batch reactors. Under the correct operating conditions, fed-batch reactors possess the ability to mirror the behaviour of each of the three fundamental reactor types used in standard AR theory. Use of intermediate storage and mixing between reaction steps then allows for the same structures found in continuous AR to be used in batch. Conversion of a conventional fed-batch to continuous reactors is obtained by noting that the ratio of fed-batch feed flow to reactor volume, F/V, results in the same form as the DSR equation. Similarly, the DSR may be operated in specific ways to achieve equivalent behaviour in a PFR and CSTR. The F/V ratio thus fulfils the same duty as the α parameter in the DSR and the two can be used interchangeably to achieve the desired continuous reactor.

It follows that conversion of the PFR to batch occurs when the F/V ratio is zero. This implies that no material is fed into the fed-batch during reaction and the resulting reactor is a standard batch. When the ratio is allowed to vary with time, then the concentration in the vessel is the same as the effluent composition obtained from a DSR of the same α profile. Conversion of CSTR behaviour to batch is slightly more involved. DSRs are able to achieve CSTR effluent concentrations only for long residence times with a constant α policy (when the DSR operates close to an equilibrium point). The resulting DSR is then maintained in an equilibrium state. CSTR concentrations in batch can therefore be accomplished by holding the ratio of F/V constant with time and initiating the fed-batch at the CSTR effluent concentration. It follows that the start-up procedure of fed-batch with CSTR behaviour should be considered carefully – this effectively requires the formation of the desired CSTR concentration by other means *before* the reactor is brought online. This, however, is only required to be performed once, and the resulting CSTR concentrations from the fed-batch can be used to seed additional cycles. In addition to this, the designer should also be mindful of the particular reaction kinetics taking part in the system. If multiple steady states are a feature of the system, the incorrect choice of CSTR solution may lead to significantly different performance. This might arise even when the correct reactor structure as been identified and implemented.

The operation of fed-batch reactors with constant feeding policies (so that the desired CSTR concentration is maintained) is therefore a strong function of the stability criteria associated with the system. Unstable nodes in the DSR topology provide clues as to how best to operate the reactor. The correct choice of initial

condition not only allows for the proper CSTR concentration to be achieved, it may also avoid the possibility of introducing states in the system that give rise to unstable behaviour. Knowledge of the system's stable CSTR nodes provide an additional use. Knowing these solutions might allow for easier control of the reaction during production cycle. In summary, conversion of AR structures to batch requires that care be taken so that the appropriate behaviour is realised.

Finally, the possibility of applying ARs generated in residence time space was investigated. We observed that although batch reaction time cannot be mixed in the same way that residence time in a continuous reactor can, it is still possible to employ the same transformation rules and convert optimal continuous reactor structures to equivalent batch structures. Whereas in continuous reaction these constructions allows one to address problems concerned with efficient use of reactor volume, in batch the same problem could be viewed to be one in which batch throughput is the desired objective. Thus, ARs generated in residence time space are useful in helping to improve problems involving batch production rate.

With this understanding in place, the possibility of using the AR to improve two separate design cases may be more viable now. From a single set of kinetics, the AR could be used to optimise for a given performance. Knowledge of the structure then allows the designer to articulate both continuous and batch reactor structures designs. Use of the AR might then permit more freedom at the early stages of conceptual design, as one does not need to commit into either a batch or continuous route.

6.2 Directions for future research

A large portion of this work has been dedicated to articulate the idea of improvements through structure, rather than through traditional optimisation alone. This is ultimately communicated via ideas founded in Attainable Region theory. Within this, two dominant themes exist throughout: the development of AR construction methods, and improving batch performance through structure obtained via AR analysis. There are still avenues for improvement in both of these areas. Some ideas for future work are provided below.

AR construction algorithms

Greater improvements to AR construction algorithms and understanding is necessary for the adequate understanding of AR theory as a whole. In particular, the search for a sufficiency condition would provide an excellent means of validation to constructions. This would also assist in removing any remaining uncertainty regarding whether a particular construction is the true AR, or whether it is only a subset of it. Although the search for a theoretical sufficiency condition must continue, greater

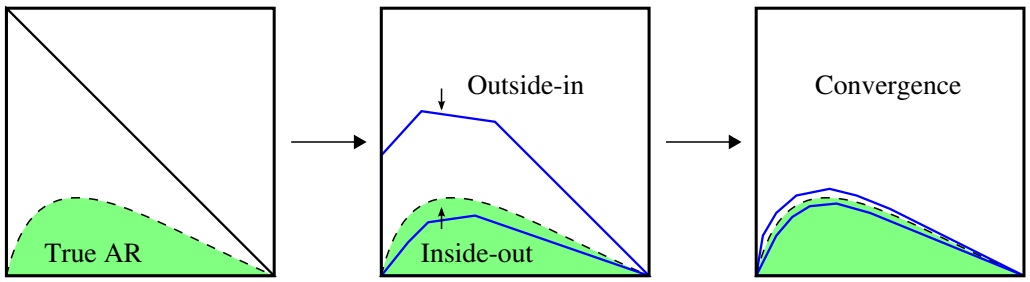
progress can be made towards a numerical sufficiency condition. Numerical sufficiency, in this sense, implies that if a region can be validated via two independent AR construction methods, then we are in a better position to show that it is the true AR. Even if the results of the constructions do not match, then this is still valuable because then it is known other, more complex, structures may not have been identified. This ultimately helps guide construction further. Automated AR construction techniques may become particularly valuable in this regard.

The development of a hybrid AR construction method, one that utilises both inside-out and outside-in steps to construct the AR, might allow for both more accurate and robust AR constructions as well as assist towards numerical methods for AR validation. Figure 6.2.1 demonstrates this geometrically. Both convergence or disagreement in constructions provides stronger numerical evidence for the existence of the true AR. Furthermore, robust numerical AR construction algorithms may be used to check AR constructions against theoretical predictions, in the form of a theoretical validation tool. There still has not yet been significant progress towards a hybrid algorithm, and work should continue in this direction, I feel. In chapter 4, we demonstrated the positive features of such a method by employing both the rotated hyperplanes and RCC method in a single analysis for a number of systems. The use of both methods, in conjunction with tracking the AR volume, provides an effective means of AR construction suitable for a large variety of constructions. What is still necessary, however, is a structured and generalised method employing these techniques (and possibly others) under a unified code base. Furthermore, both inside-out and outside-in methods are still not developed to the point that they are each capable of handling the same construction types (unbounded regions, variable density systems, non-isothermal systems, etc.); this makes combining multiple methods difficult. Nevertheless, modification of existing methods to allow for a wider variety of systems should be straightforward if the underlying concepts of each method are adequately understood.

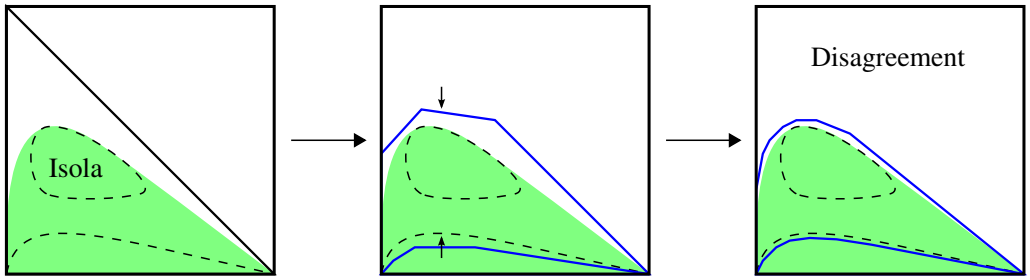
AR construction methods, on their own, must also be given further investigation. Potentially many more novel insights could be found that would assist in making AR construction both faster and more accurate. The rise of computational power, specifically in the era of parallel computation, will allow for more complicated systems to be studied. The development of these methods requires a change in thinking however, and thus either the old algorithms must be adapted, or new methods must be formulated in order to take advantage of 'wider' computational architectures.

Batch reaction

Many of the current methods in batch reactor research rely on traditional optimisation techniques. Although these methods are robust and generalised enough to tackle a large variety of problems in batch processing, there are potentially many



(a) Convergence



(b) Disagreement

Figure 6.2.1: Hybrid AR construction

other avenues for improvement that could also be utilised in conjunction with optimisation. In particular, a greater awareness of optimal structure may also lead to further improvements in designs. The techniques and recommendations developed in this work are simple enough that they can be found graphically, however this does not prevent the methods from being adapted to handle higher dimensional and more complex problems. The partial emptying and filling concept could be extended to give a more detailed treatment for how multiple reactions could be taken into account for example. Further insight and recommendations might be gained if the theory can be developed further with this in mind. This might also allow use of the approach in a more generalised fashion along with traditional batch scheduling techniques. If this is the case, then a deeper understanding of its mechanics to non-isothermal and fed-batch conditions should be undertaken. Good opportunities therefore are available for extending the method into these two areas (multiple reactions, and fed-batch operation).

The direct conversion of continuous AR structures to batch is a new research area with the potential for further development. Currently, the handling of state vectors other than concentration, and the use of control parameters such as temperature, specifically to batch ARs, have yet to be investigated. These concepts should, at least in theory, be simple extensions to the batch setting if equivalent batch analogies can be found. A somewhat more interesting case is the application of this method to residence time examples. As observed in the final example of chapter 5, it is known that residence time is analogous to reaction time in a batch. It is possible to

mix residence time, but the same clearly does not translate to batch using reaction time. Chapter 3 is dedicated to batch production rate, and so there is a connection between the simple recommendations given to the larger picture of AR residence time examples. It may turn out that when converting continuous AR structures to batch using residence time constructions, greater benefit might be obtained if flow rate and volume are considered, rather than simply residence time alone. Understanding this relation might allow for the conversion of more complicated residence time ARs to batch. Consequently, higher dimensional problems in batch could also be addressed if some of the questions posed above are given attention.

We note that along with the idea of a hybrid approach to AR construction, there also exists another hybrid approach specific to batch reactors. That is, along with the developments of AR theory to batch reactors, this methodology could also be incorporated into more generalised batch structures involving other batch processing equipment. Opportunities for further research exists that investigates improvements to batch reactors by combining AR theory concepts into batch process scheduling policies. Specifically, the AR could be combined with non-linear programming strategies and used as an initialisation for these methods – if it is known that a particular state is achievable within the reactive portion of the batch network, then this allows for rapid iteration to a final, optimal batch schedule using AR theory. It would be useful to understand, from a scheduling perspective, that, within the reactive portion of the batch plant, a specific product can be delivered within a certain quality specification (yield, waste minimisation, conversion, etc.), within a cycle time (residence time or reactor volume), under the operating constraints of the plant. Knowing this might open up further avenues for batch improvement as now the designer is knowledgeable of the absolute limits of rector section of the plant. This knowledge may be useful for highly complex batch process optimizations; AR theory helps us to understand the details inside the reactor network. The combination of ARs with generalised batch equipment is an interesting concept that has not yet been explored, but which may offer powerful insights into batch process improvements in general.

Final remarks

Although the current landscape of AR research is not vast, particularly when considered against other fields far more established (and popular) than that considered here, this should not be interpreted as a field that is by any means complete. If anything, this would suggest that the field is still in its infancy. There remains a great deal of unknown to the theories developed in AR (and yet to be developed), and their relation to a sufficiency condition. The challenges in AR stem from three main areas of concern:

1. Accurate and efficient AR construction.

2. A low adoption of the method within the process engineering community.

3. And a relatively limited theory base on what is actually known about the AR.

It is my hope that progress in AR will continue to be made with these issues in mind.

With developments of new ideas and the expansion of the profession into broader fields of work, process engineers find use working in industries that would historically not have been considered in the past. The training and methods developed in traditional areas of practice will thus need to find use under different fields of application. There exists a great need to continue developing topics in chemical engineering that can then be transferred, translated and adapted to new areas of expertise.

Appendix A

Batch production rate

A.1 The effect of transfer time on batch production rate

Expressions for the production rate of a batch reactor were defined in chapter 3 for both the standard batch as well as when a fraction of material is retained. These are repeated below as follows:

$$\mathrm{P} = \frac{\mathrm{V_{tot}}\left(c_i^{\mathrm{out}} - c_i^0\right)}{\Delta \mathrm{t}_0} \tag{A.1.1}$$

$$\mathrm{P}^* = \frac{(1-\phi)\,\mathrm{V_{tot}}\left(c_i^{\mathrm{out}} - c_i^0\right)}{\Delta \mathrm{t}^*} \tag{A.1.2}$$

Similar expressions were also defined for when transfer time, $\mathrm{t_T}$, is accounted for in the formulation. These expressions are distinguished by use of the overbar

$$\overline{\mathrm{P}} = \frac{\mathrm{V_{tot}}\left(c_i^{\mathrm{out}} - c_i^0\right)}{\left(\Delta \mathrm{t}_0 + \mathrm{t_T}\right)} \tag{A.1.3}$$

$$\overline{\mathrm{P}^*} = \frac{(1-\phi)\,\mathrm{V_{tot}}\left(c_i^{\mathrm{out}} - c_i^*\right)}{\left(\Delta \mathrm{t}^* + \mathrm{t}_\mathrm{T}^*\right)} \tag{A.1.4}$$

We would like to derive the expression used in section 3.5.1 by eq 3.5.1. We start by first dividing eq A.1.4 by eq A.1.3

$$\begin{aligned}\frac{\overline{\mathrm{P}^*}}{\overline{\mathrm{P}}} &= \frac{(1-\phi)\,\mathrm{V_{tot}}\left(c_i^{\mathrm{out}} - c_i^*\right)}{\left(\Delta \mathrm{t}^* + \mathrm{t}_\mathrm{T}^*\right)} \times \frac{\left(\Delta \mathrm{t}_0 + \mathrm{t_T}\right)}{\mathrm{V_{tot}}\left(c_i^{\mathrm{out}} - c_i^0\right)} \\ &= (1-\phi)\left(\frac{c_i^{\mathrm{out}} - c_i^*}{c_i^{\mathrm{out}} - c_i^0}\right)\left(\frac{\Delta \mathrm{t}_0 + \mathrm{t_T}}{\Delta \mathrm{t}^* + \mathrm{t}_\mathrm{T}^*}\right)\end{aligned}$$

Substitution of eq A.1.1 and eq A.1.2 into the above expression then gives after rearrangement:

$$\frac{\overline{\mathrm{P}^*}}{\overline{\mathrm{P}}} = \left(\frac{\mathrm{P}^*\Delta \mathrm{t}^*}{\mathrm{P}\Delta \mathrm{t}_0}\right)\left(\frac{\Delta \mathrm{t}_0 + \mathrm{t_T}}{\Delta \mathrm{t}^* + \mathrm{t}_\mathrm{T}^*}\right)$$

$$= \left(\frac{\mathrm{P}^*}{\mathrm{P}}\right)\left(1+\frac{\mathrm{t_T}}{\Delta \mathrm{t}_0}\right) / \left(1+\frac{\mathrm{t}^*_\mathrm{T}}{\Delta \mathrm{t}^*}\right)$$

We now introduce the transfer rate r, with units of [volume/time]. For a typical standard batch, it is possible to transfer a full volume $\mathrm{V_{tot}}$ in a time of $\mathrm{t_T} = \mathrm{V_{tot}}/r$. Similarly, for typical batch performed using partial emptying and filling, the associated transfer time is thus $\mathrm{t}^*_\mathrm{T} = (1-\phi)\,\mathrm{V_{tot}}/r$. Substitution of the transfer time expressions into the above equation gives

$$\frac{\overline{\mathrm{P}^*}}{\overline{\mathrm{P}}} = \left(\frac{\mathrm{P}^*}{\mathrm{P}}\right)\left[1+\frac{\mathrm{V_{tot}}}{r\Delta \mathrm{t}_0}\right] / \left[1+\frac{(1-\phi)\,\mathrm{V_{tot}}}{r\Delta \mathrm{t}^*}\right]$$

which upon simplification gives

$$\frac{\overline{\mathrm{P}^*}}{\overline{\mathrm{P}}} = \left(\frac{\mathrm{P}^*}{\mathrm{P}}\right)\xi \tag{A.1.5}$$

where

$$\xi = \left[\frac{r}{\mathrm{V_{tot}}}+\frac{1}{\Delta \mathrm{t}_0}\right] / \left[\frac{r}{\mathrm{V_{tot}}}+\frac{(1-\phi)}{\Delta \mathrm{t}^*}\right]$$

This expression may be used an indication for transfer time could affect the benefit gained by partial emptying and filling and associated retained fraction.

Appendix B

Bounding hyperplanes

B.1 Worked example for rotated bounding hyperplanes algorithm

We begin by specification of the system. The van de Vusse reaction scheme and associated kinetics is a commonly used example in AR research, and as a result, the system is well understood. This will allow for comparison between the construction obtained by the method and that suggested by theory. The reaction is given by

$$\begin{array}{ccccc} \mathrm{A} & \underset{k_2}{\overset{k_1}{\rightleftharpoons}} & \mathrm{B} & \overset{k_3}{\rightarrow} & \mathrm{C} \\ & 2\mathrm{A} & \underset{k_4}{\rightarrow} & \mathrm{D} & \end{array} \tag{B.1.1}$$

This is a three dimensional problem: the system involves three independent reactions involving four components. Several variations of the above kinetics exist which all result in different ARs. We present here only the simplest scenario. That is, a 2D irreversible system with mass action kinetics given by the following constants: $k_1 = 1.0$, $k_2 = 0.0$, $k_3 = 1.0$ and $k_4 = 20.0$, such that

$$\mathbf{r}(\mathbf{C}) = \begin{bmatrix} -k_1 c_\mathrm{A} - 2k_4 c_\mathrm{A}^2 \\ k_1 c_\mathrm{A} - k_3 c_\mathrm{B} \\ k_3 c_\mathrm{B} \\ k_4 c_\mathrm{A}^2 \end{bmatrix} \tag{B.1.2}$$

It is further specified that there is a single feed stream containing pure A. The feed concentration is then given by the vector $\mathbf{C_f} = [1,\, 0,\, 0,\, 0]^\mathrm{T}$.

It is known that in order to construct the AR, a CSTR followed by a PFR to equilibrium is required. Using this arrangement, no other achievable concentration may be obtained through reaction and mixing alone. We will now show that the algorithm of rotating bounding hyperplanes produces a region which closely agrees with the above arrangement.

The process of hyperplane rotations, tangency checking and region exclusion is a rather tedious exercise if done without automation, and as a result, we shall only demonstrate the first iteration of the process here. The procedure begins by construction of the stoichiometric subspace S. We have already noted that the dimension of S is three, indicating that the fourth component is not independent and may be computed from the remaining three species by mass balance. Since our concern here is for the construction of a 2D region, we shall only be interested with concentrations residing in the $c_{\mathrm{A}} - c_{\mathrm{B}}$ plane in concentration space. The feed vector is therefore truncated giving $\mathbf{C_f} = [1,\, 0]^{\mathrm{T}}$. Non-negativity constraints on component A and B require that the first two constraints be of the form

$$\begin{aligned} c_{\mathrm{A}} &\geq 0 \\ c_{\mathrm{B}} &\geq 0 \end{aligned}$$

The normal vectors associated with these hyperplanes are then given by $H_1 = \left\{\mathbf{C} \in \mathbb{R}^2 : \mathbf{n}_1^{\mathrm{T}}\mathbf{C} \geq 0\right\}$ and $H_2 = \left\{\mathbf{C} \in \mathbb{R}^2 : \mathbf{n}_2^{\mathrm{T}}\mathbf{C} \geq 0\right\}$ where

$$\mathbf{n}_1 = \begin{bmatrix} 1 \\ 0 \end{bmatrix} \qquad\qquad \mathbf{n}_2 = \begin{bmatrix} 0 \\ 1 \end{bmatrix}$$

Both of the hyperplanes pass through the origin. The third and final constraint is given by $c_{\mathrm{A}} + c_{\mathrm{B}} \geq 1$ which, when written with respect to its hyperplane normal, gives

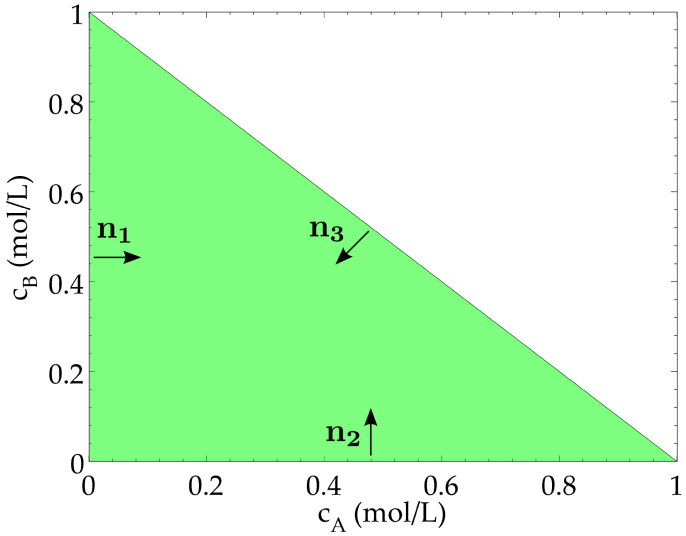
$$\mathbf{n_3} = \frac{1}{\sqrt{2}} \begin{bmatrix} -1 \\ 1 \end{bmatrix}$$

Alternatively, S may be computed with the methods described in appendix B.2 below. The region produced by these constraints results in the convex polytope shown in Figure B.1.1a.

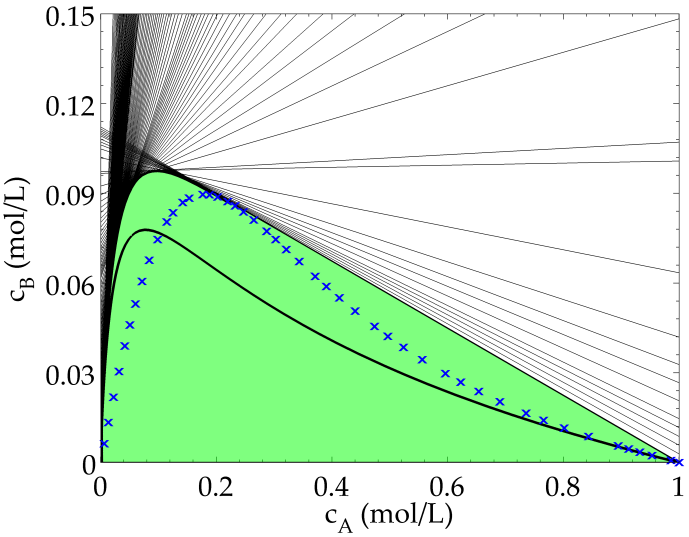
Next, the particular hyperplane passing through the feed point $\mathbf{C_f}$ is identified. Note that two such hyperplanes satisfy this condition. These are H_2 and H_3 respectively. H_2 is a plane that contains both the feed concentration and the equilibrium concentration $[0,\, 0]^{\mathrm{T}}$. As a result, it is impossible to rotate H_2 in a manner that does not exclude one of these two points after the rotation and therefore H_3 is chosen as the first hyperplane to undergo rotation. The first round of infeasible region elimination may now begin. The standard rotation matrix $\mathbf{R} \in \mathbb{R}^n$ is given by

$$\mathbf{R}\,(\theta) = \begin{bmatrix} \cos(\theta) & -\sin(\theta) \\ \sin(\theta) & \cos(\theta) \end{bmatrix}$$

When $\mathbf{R}$ is multiplied by a vector $\mathbf{x}$, the resulting product $\mathbf{Rx}$ is vector $\mathbf{x}$ rotated by an angle θ in an anticlockwise direction. A small angle $\delta\theta$ is specified through which the hyperplane normal is rotated about. This ultimately determines a range



(a) Stoichiometric subspace for 2D van de Vusse kinetics. All concentrations achievable through stoichiometry reside within the shaded region.



(b) AR for van de Vusse kinetics using rotated bounding hyperplanes. The CSTR locus (×) and PFR trajectory (solid line) from the feed point have also been drawn.

Figure B.1.1: 2D van de Vusse constructions

of concentrations swept out by the rotated hyperplane. The value of $\delta\theta$ is arbitrary, although it clear that the value specified will dictate the accuracy with which the final AR is constructed. A trade-off between construction accuracy and construction time must therefore be established – for smaller values of $\delta\theta$ chosen, the associated hyperplane will bind tighter to the AR boundary. In practice, a value of approximately $\delta\theta = 0.001$ radians has been found to be an adequate trade-off between construction accuracy and computational effort. As a result, this value will be used in the current example. The first rotation step may now begin. Application of the rotation matrix to the normal of the H_3 results in the following

$$\begin{aligned}
\mathbf{n_3}^* &= \mathbf{R}\left(\delta\theta\right) \cdot \mathbf{n_3} \\
&= \frac{1}{\sqrt{2}} \begin{bmatrix} \cos\left(0.001\right) & -\sin\left(0.001\right) \\ \sin\left(0.001\right) & \cos\left(0.001\right) \end{bmatrix} \begin{bmatrix} -1 \\ -1 \end{bmatrix} \\
&= \begin{bmatrix} -0.7064 \\ -0.7078 \end{bmatrix}
\end{aligned}$$

Once the hyperplane has been orientated into its new position, points residing on the plane must be checked to determine whether rate vectors are tangent to the plane. If so, then by the hyperplane tangency condition we have found a valid achievable concentration. The subspace spanned by H_3 is discretised into a distinct set of concentrations and then the associated rate vectors at these points are evaluated. This is done as follows. It is clear that concentrations residing on H_3 may be expressed as

$$\mathbf{n_3^{*T}}(\mathbf{C} - \mathbf{C_f}) = n_{3\mathrm{A}} c_{\mathrm{A}} + n_{3\mathrm{B}} c_{\mathrm{B}} = \gamma_3 \tag{B.1.3}$$

where $\gamma = \mathbf{n_3^{*T}}\mathbf{C_f} = n_{3\mathrm{A}} c_{\mathrm{A}}^0 + n_{3\mathrm{B}} c_{\mathrm{B}}^0$. Since at each rotation we know the values of $\mathbf{n_3^*}$, we seek the value of only two unknowns. In order to solve for a valid concentration residing on H_3, it may be tempting to specify one value for either c_{A} or c_{B} and solve for the other – this could be accomplished by generating a grid of M values between 0 and 1 for c_{A} say, then the corresponding M coordinates for c_{B} which lie on the hyperplane may be found by eq B.1.3. This method has two limitations however:

1. If hyperplanes are parallel to the any of the axes, then it is impossible to solve for a concentration by generating a grid in the other axis. For example, we cannot solve for a y position by generating a grid of x points if the hyperplane is parallel to the y-axis (with hyperplane normal given by $\mathbf{n} = [0,\, 1]^{\mathrm{T}}$). A check for the hyperplane orientation is first required then.

2. By generating a grid of points along a particular axis, it is generally not guaranteed that the spacing between the points on the plane will be even for other hyperplanes with different orientations – for planes orientated closely to the y-axis, the spacing between points on the plane will be significantly larger than for planes closely orientated to the x-axis for example.

This method is also cumbersome to program. As a result, discretising points on the plane is performed rather by first computing the basis vectors that are orthogonal to the hyperplane normal (i.e. computing a basis for the subspace spanned by the plane). This method works for all dimensions and all normal orientations. A grid of points can be generated that span the hyperplane using linear combinations of the orthogonal vectors instead. In addition to this, if a method such as QR decomposition is employed when computing this basis, the associated basis vectors are orthogonal to one another and scaled to unity. This ensures that linear combinations of the basis vectors generate points that are evenly spaced on the plane irrespective of the orientation of the plane itself in space.

The evaluation of rate vectors may now proceed. In order for the elimination process to work, we consider only those points lying on H_3 that are contained in the current region defined the list of bounding constraints. This is done by screening the generated points on H_3 and testing for validity. A concentration $\mathbf{C}$ is considered valid if it satisfies all the constraints posed by the current list of bounding hyperplanes. For our example, the initial list of constraints is given by S

$$\begin{aligned} \mathbf{n_1}^{\mathrm{T}}\mathbf{C} &\geq 0 \\ \mathbf{n_2}^{\mathrm{T}}\mathbf{C} &\geq 0 \\ \mathbf{n_3^*}^{\mathrm{T}}\mathbf{C} &\geq \gamma_3 \end{aligned}$$

which when written in matrix form gives

$$\begin{bmatrix} 1 & 0 \\ 0 & 1 \\ -0.7064 & -0.7078 \end{bmatrix} \begin{bmatrix} c_{\mathrm{A}} \\ c_{\mathrm{B}} \end{bmatrix} \geq \begin{bmatrix} 0 \\ 0 \\ -0.7064 \end{bmatrix}$$

There is an additional consideration. Since points are evaluated at discretised steps, there also exists the possibility of over rotating the plane and skipping tangent rate vectors. Hence, a check for both tangent rate vectors and those vectors that point out of H_3 (rate vector which form an obtuse angle with $\mathbf{n_3}^*$) must be performed. With this in mind, the stopping criteria for the current round of rotation is when

$$\mathbf{n_3^*}^{\mathrm{T}}\mathbf{r} \leq 0$$

At each rotation, the hyperplane is discretised into M distinct and valid points. For each of the M points considered, the associated rate vector is computed and the above tangency test is applied. If it is found that none of the M points satisfy the tangency condition, then the current loop and ends and the hyperplane is rotated by another increment of $\delta\theta$. If, however, it is found that a point within the current list of M points is tangent, then we have found a new attainable point with which we can start the next round of rotation. In this case, the hyperplane is rotated back

to its previous orientation by the angle $-\delta\theta$ and the concentration where tangency occurs is also recorded.

When H_3 is unrotated by $-\delta\theta$, the vector $(\mathbf{C} - \mathbf{C_f})$ is rotated by the same amount to ensure that the tangent point found still lies on the plane when rotated back to its previous orientation. This marks the end of the current round of eliminations. We find that under the given system, H_3 is rotated by a total angle of ~0.42 radians before a valid tangent point is found. The new point is added to the existing list of extreme points, in this case only $\mathbf{C_f}$, and the associated hyperplane is also added to the current list of bounding hyperplanes. The new extreme point found now acts the feed vector for the next elimination round. The results of the construction are given by Figure B.1.1b. Also included in the figure is the PFR-CSTR arrangement, suggested by theory, required to generate the AR. We find that there is good agreement between the construction and the theory in this example.

Now that the details of the method have been discussed, we are in a better position to describe the method in a more general way. At the start of an arbitrary stage of construction, the k-th say, k extreme points forming the partial boundary of the AR have been found. In addition to this, k new bounding hyperplanes have been added to the d original hyperplanes in the list, and a new extreme point has been identified about which the k-th rotation may commence. To start the next round of elimination, we introduce a new hyperplane having exactly the same orientation as the last hyperplane added, the k-th, and pre-multiply the normal to the plane, $\mathbf{n}_{k+d}$, by $\mathbf{R}$ and initiate the next loop of rotations. Points on the plane are discretised and checked for tangency and continue in this manner until a new tangent point is found. We follow the unrotation rule discussed above and repeat the process for the (k+1)th stage of elimination. These steps are repeated until an equilibrium point is identified. This marks the end of construction. Viewed in this way, the construction process begins at the feed point and gradually steps along the AR boundary approximating it facet by facet. The constructions of various ARs are given in section 4.4 together with comparisons with the original bounding hyperplanes method.

B.2 Constructing the stoichiometric subspace

We denote by S the stoichiometric subspace of a reactive system. S is is used to form an upper bound on the AR and is therefore the basis of outside-in algorithms. The determination of S requires that we find all the hyperplanes that bound the feasible region.

In general, we have a n component system. The first k species are reactants, whereas the remaining $(n - k)$ species are products. For multiple reactions, it is also assumed that there are, in general, d reactions that take place. Expressing the

reactions in terms of all components then gives:

$$\begin{aligned} r_1 : \nu_1 c_1 + \ldots + \nu_{1k} c_k &\rightleftharpoons \nu_{1(k+1)} c_{k+1} + \ldots + \nu_{1n} c_n \quad \text{(reaction 1)} \\ &\vdots \\ r_d : \nu_d c_1 + \ldots + \nu_{dk} c_k &\rightleftharpoons \nu_{d(k+1)} c_{k+1} + \ldots + \nu_{dn} c_n \quad \text{(reaction d)} \end{aligned}$$

or more compactly

$$r_i = \sum_{i=1}^{d} \nu_{ij} c_j \qquad \text{where } j = 1 \ldots n$$

where ν_{ij} is the stoichiometric coefficient belonging to component j for reaction i in the system. Note that it irrelevant, for our needs, whether the reactions are written with respect to products or reactants. It also does not make a difference whether the reactions are considered strictly forward or reversible (as shall bee seen below). The feed point is also given here as the n dimensional column vector:

$$\mathbf{C_f} = \begin{bmatrix} c_1^0 & c_2^0 & \cdots & c_n^0 \end{bmatrix}^{\mathrm{T}}$$

From the system of reactions, we can thus form the *stoichiometric coefficient matrix* $\mathbf{A}$ containing the reaction coefficients of each component in all reactions

$$\mathbf{A} = \begin{bmatrix} \nu_{11} & \cdots & \nu_{d1} \\ \vdots & \ddots & \vdots \\ \nu_{1n} & \cdots & \nu_{dn} \end{bmatrix}$$

In general, $\mathbf{A}$ has size $n \times d$. The stoichiometric subspace is therefore the space spanned by the columns in $\mathbf{A}$. S may be formed in general by computing the hyperplanes that bound the space. The normals of these planes must be orthogonal to the space and hence the normals must be orthogonal to the columns of $\mathbf{A}$ by definition. This gives us a method of computing the normals belonging to the bounding hyperplanes for S. All points orthogonal to $\mathbf{A}$ can be expressed by the following expression

$$\mathbf{A}^{\mathrm{T}}\mathbf{C} = \mathbf{0}$$

It is clear then that we wish to find the null space of $\mathbf{A}^{\mathrm{T}}$. We call this the matrix $\mathbf{N}$ and define it as $\mathbf{N} = \mathrm{null}\left(\mathbf{A}^{\mathrm{T}}\right)$. If $\mathbf{A}$ has r linearly independent rows, then its rank is r. This indicates that there are r linearly independent reactions occurring in the system. If we have d reactions, and all of them are independent, then $r = d$. It follows that if $\mathbf{A}$ has rank r, then the null space of $\mathbf{A}^{\mathrm{T}}$ must have rank of $(n - r)$. Thus $\mathbf{N}$ must have n rows and $(n - r)$ columns.

$$\mathbf{N} = \begin{bmatrix} \mathbf{n}_1 & \mathbf{n}_2 & \cdots & \mathbf{n}_{n-r} \end{bmatrix}$$

where $\mathbf{n}_i$ is a column of $\mathbf{N}$. The $(n-r)$ columns thus span the null space of $\mathbf{A}^{\mathrm{T}}$, and therefore each $\mathbf{n}_i$ in $\mathbf{N}$ represents a hyperplane normal that bounds S. For hyperplanes stoichiometrically compatible with the feed, these planes must pass through the feed point $\mathbf{C_f}$. Therefore, each column in $\mathbf{N}$ is required to satisfy the relation:

$$\mathbf{n}_i^{\mathrm{T}} (\mathbf{C} - \mathbf{C_f}) = \mathbf{0}$$

or in matrix form

$$\mathbf{N}^{\mathrm{T}} (\mathbf{C} - \mathbf{C_f}) = \mathbf{0}$$

Notice that this is identical in form to the hyperplane expression given by eq 4.2.1. Note further that eq 4.2.1 is also an equality. There is a difference however. Matrix $\mathbf{N}$ has dimension n, which is generally must larger than the dimension that we wish to view the AR in (for constructions in concentration space only, the dimension is usually chosen to coincide with the rank of $\mathbf{A}$).

In order to convert the hyperplane expression from an equality to an inequality expression, we remove the components that we are not interested in. In concept this is simple – the components that are not of interest are removed from the expression with the sign of the terms determining whether the left hand side is less than or greater than zero. In practice however, we cannot guarantee that the elements in $\mathbf{N}^{\mathrm{T}}$ are non-zero, and so it is difficult to determine whether the hyperplane normals are correct once they have been projected into the subspace that we are interested in constructing the AR in.

In order to ensure that no information is lost when the expressions are converted in inequalities, we perform elementary row operations on $\mathbf{N}^{\mathrm{T}}$ to 'clean' the entries in $\mathbf{N}^{\mathrm{T}}$. This ensures that the components that are removed are strictly non-negative. This is done in practice by pre-multiplying $\mathbf{N}^{\mathrm{T}}$ with a matrix $\mathbf{G}$.

$$\mathbf{G}^{-1}\mathbf{N}^{\mathrm{T}} (\mathbf{C} - \mathbf{C_f}) = \mathbf{0}$$

Where $\mathbf{G}$ contains the rows corresponding to the components that we wish to *remove* from our system. The size of $\mathbf{G}$ is $(n-r)\times(n-r)$. It is square and must be invertible. In general, this produces a matrix $\mathbf{F} = \mathbf{G}^{-1}\mathbf{N}^{\mathrm{T}}$ with the columns in $\mathbf{F}$ associated with the discarded components being reduced to the identity matrix. The remaining r columns corresponding to the required hyperplane normal entries.

The r rows in $\mathbf{F}$ together with the n non-negativity constraints for each component in the system, define the set of hyperplanes that bound S.

B.2.1 Example: Methane steam reforming

In order to assist understanding of this procedure, a worked example using methane steam reforming is given. A simplified reaction is shown by the following system

$$\begin{aligned} CH_4 + H_2O &\rightleftharpoons CO + 3H_2 \\ CO + H_2O &\rightleftharpoons CO_2 + H_2 \end{aligned}$$

Both reactions are assumed to be reversible, and so we write both the forward and reverse reactions for the stoichiometric subspace $\mathbf{A}$.

$$\mathbf{A} = \begin{bmatrix} -1 & 1 & 0 & 0 \\ -1 & 1 & -1 & 1 \\ 1 & -1 & -1 & 1 \\ 3 & -3 & 1 & -1 \\ 0 & 0 & 1 & -1 \end{bmatrix}$$

We denote row 1 to be CH_4, 2 for H_2O, 3 for CO, 4 for H_2 and 5 for CO_2. We also specify the feed point to be $\mathbf{C_f} = [1, 1, 1, 0, 0]^{\mathrm{T}}$. Since columns 2 and 4 are linear combinations of columns 1 and 3 respectively, the rank of $\mathbf{A}$ is 2. There are two linearly independent reactions for the methane steam reforming system, and so the AR for this is two dimensional. Computation of $\mathbf{N}$ is then given by:

$$\begin{aligned} \mathbf{N} &= \operatorname{null}\left(\mathbf{A}^{\mathrm{T}}\right) \\ &= \begin{bmatrix} 0.83767 & 0.25280 & -0.36309 \\ 0.37263 & -0.31499 & 0.71100 \\ 0.013661 & 0.66008 & -0.0032395 \\ 0.39888 & -0.24075 & 0.11705 \\ -0.012588 & 0.58584 & 0.59071 \end{bmatrix} \end{aligned}$$

The specific output given above has been obtained from the `null()` function in MATLAB. Picking three components to discard will allow for the proper determination of the hyperplane normals of the remaining two desired components. For this example, we wish to compute the S in $CH_4 - CO$ space (rows 1 and 3 in $\mathbf{N}$). Consequently rows 2, 4 and 5 must be used to form the pre-multiplier matrix $\mathbf{G}$. This results in the following

$$\mathbf{N}^{\mathrm{T}} = \begin{bmatrix} \mathbf{n}_1 & \mathbf{n}_2 & \mathbf{n}_3 & \mathbf{n}_4 & \mathbf{n}_5 \end{bmatrix}$$

and

$$\mathbf{G} = \begin{bmatrix} \mathbf{n}_2 & \mathbf{n}_4 & \mathbf{n}_5 \end{bmatrix}$$

$$= \begin{bmatrix} 0.37263 & 0.39888 & -0.012588 \\ -0.31499 & -0.24075 & 0.58584 \\ 0.71100 & 0.11705 & 0.59071 \end{bmatrix}$$

The rank of $\mathbf{G}$ is 3 and is invertible. Matrix $\mathbf{F}$ can therefore be determined

$$\begin{aligned} \mathbf{F} &= \mathbf{G}^{-1}\mathbf{N}^{\mathrm{T}} \\ &= \begin{bmatrix} -2 & 1 & -1 & 0 & 0 \\ 4 & 0 & 1 & 1 & 0 \\ 1 & 0 & 1 & 0 & 1 \end{bmatrix} \end{aligned}$$

Notice that $\mathbf{G}$ achieves the desired result: columns 2, 4 and 5 of $\mathbf{F}$ form the identity matrix. The components for H_2O, H_2 and CO_2 are thus scaled to unity, they are positive, and isolated for each hyperplane equation. $\mathbf{F}$ can therefore be used to determine the hyperplane normals

$$\begin{aligned} \mathbf{F}\left(\mathbf{C} - \mathbf{C_f}\right) &= \mathbf{0} \\ \mathbf{FC} &= \mathbf{FC_f} \end{aligned}$$

Writing out the hyperplane expressions produces the following result

$$\begin{bmatrix} -2 & 1 & -1 & 0 & 0 \\ 4 & 0 & 1 & 1 & 0 \\ 1 & 0 & 1 & 0 & 1 \end{bmatrix} \begin{bmatrix} c_{\mathrm{CH_4}} \\ c_{\mathrm{H_2O}} \\ c_{\mathrm{CO}} \\ c_{\mathrm{H_2}} \\ c_{\mathrm{CO_2}} \end{bmatrix} = \begin{bmatrix} -2 & 1 & -1 & 0 & 0 \\ 4 & 0 & 1 & 1 & 0 \\ 1 & 0 & 1 & 0 & 1 \end{bmatrix} \begin{bmatrix} 1 \\ 1 \\ 1 \\ 0 \\ 0 \end{bmatrix}$$

or when expressed in terms of explicit equations

$$\begin{aligned} 2c_{\mathrm{CH_4}} + 1c_{\mathrm{H_2O}} - 1c_{\mathrm{CO}} &= -2 \\ 4c_{\mathrm{CH_4}} + 1c_{\mathrm{CO}} + 1c_{\mathrm{H_2}} &= 5 \\ 1c_{\mathrm{CH_4}} + 1c_{\mathrm{CO}} + 1c_{\mathrm{CO_2}} &= 2 \end{aligned}$$

Eliminating the undesired components (H_2O, H_2 and CO_2) thus gives the required inequalities

$$\begin{aligned} 2c_{\mathrm{CH_4}} - 1c_{\mathrm{CO}} &\leq -2 \\ 4c_{\mathrm{CH_4}} + 1c_{\mathrm{CO}} &\leq 5 \\ 1c_{\mathrm{CH_4}} + 1c_{\mathrm{CO}} &\leq 2 \end{aligned}$$

In addition to the 5 non-negativity constraints required for each component

$$c_{\mathrm{CH_4}} \geq 0$$

$$c_{\mathrm{H_2O}} \geq 0$$
$$c_{\mathrm{CO}} \geq 0$$
$$c_{\mathrm{H_2}} \geq 0$$
$$c_{\mathrm{CO_2}} \geq 0$$

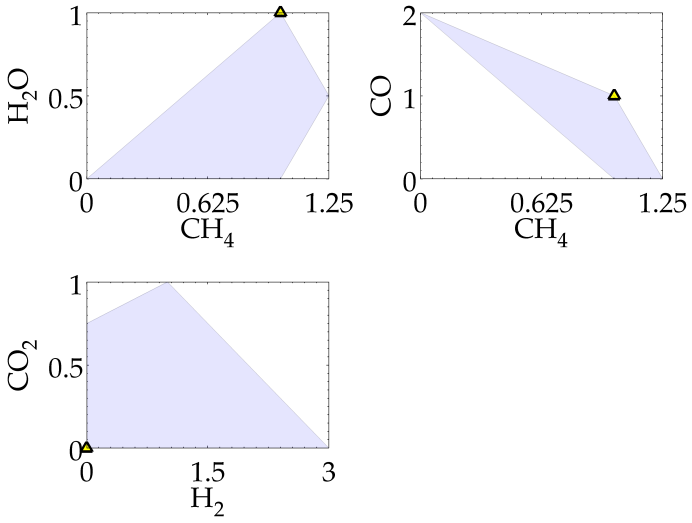
only CH_4 and CO are of interest to us. These are also expressed as hyperplanes passing through the origin

$$\mathbf{n}_{\mathrm{CH_4}} = \begin{bmatrix} 1 \\ 0 \end{bmatrix} \qquad \mathbf{n}_{\mathrm{CO}} = \begin{bmatrix} 0 \\ 1 \end{bmatrix}$$

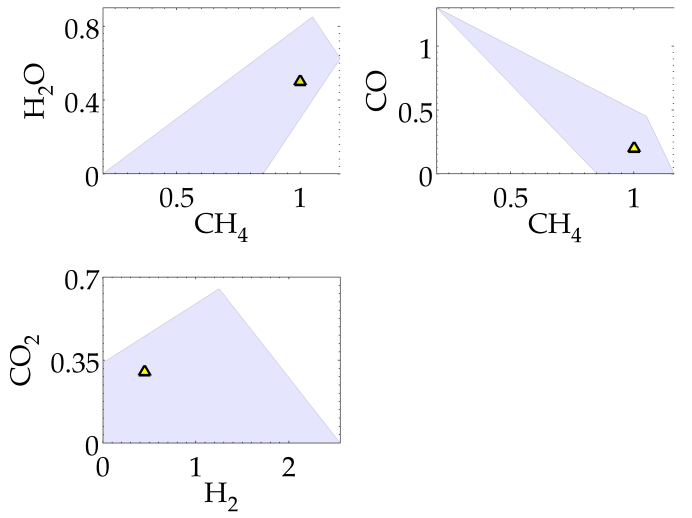
This gives the full set of bounding hyperplanes that define the stoichiometric subspace S:

$$S : \begin{bmatrix} 1 & 0 \\ 0 & 1 \\ -2 & 1 \\ -4 & -1 \\ -1 & -1 \end{bmatrix} \begin{bmatrix} c_{\mathrm{CH_4}} \\ c_{\mathrm{CO}} \end{bmatrix} \geq \begin{bmatrix} 0 \\ 0 \\ 2 \\ -5 \\ -2 \end{bmatrix}$$

A vertex enumeration algorithm can then be used to compute the vertices of the stoichiometric subspace. S has rank 2 and therefore it is a 2-dimensional subspace residing in a 5 component concentration space. It is possible to project S into different component spaces by performing the same procedure for different component pairs. Figure B.2.1 shows the results obtained from the stoichiometric subspace calculation taken for different component pairs in the steam reforming example. Note that the associated regions all appear to have different shapes, however all regions belong to the same stoichiometric subspace. In Figure B.2.1b, we repeat the stoichiometric subspace calculation for a different feed point ($\mathbf{C_f} = [1, 0.5, 0.2, 0.45, 0.3]^{\mathrm{T}}$). Notice how the shape of the stoichiometric subspace changes by specification of a different feed point. In this instance, the position of the feed point is inside the stoichiometric subspace. In general, there is no requirement that the feed lie on the boundary of S.



(a) Stoichiometric subspace for $\mathbf{C_f} = [1, 1, 1, 0, 0]^{\mathrm{T}}$



(b) Stoichiometric subspace for $\mathbf{C_f} = [1, 0.5, 0.2, 0.45, 0.3]^{\mathrm{T}}$

Figure B.2.1: Stoichiometric subspace for the steam reforming system projected onto different component spaces: $CH_4 - H_2O$ (top left), $CH_4 - CO$ (top right) and $H_2 - CO_2$ (bottom left). The feed point is displayed as a filled triangle.